

**CONTRIBUTION OF  
ANGIOTENSIN CONVERTING ENZYME  
TO  
ANGIOTENSIN RECEPTOR BLOCKER  
INDUCED ANGIO-OEDEMA**

Inaugural dissertation

for the attainment of the doctoral degree  
in the Faculty of Mathematics and Natural Sciences  
at the Heinrich Heine University Düsseldorf

presented by

**Ehsan Fahimi**

from Tehran

Düsseldorf, August 2021

From the institute for Pharmacology and Clinical Pharmacology  
at the Heinrich Heine University Düsseldorf

Published by permission of the  
Faculty of Mathematics and Natural Sciences at  
Heinrich Heine University Düsseldorf

Supervisor: Prof. Dr. Georg Kojda  
Co-supervisor: Prof. Dr. Holger Stark

Date of the oral examination: 14/12/2021

*To Gilda,  
for all her love and tireless support.*



## Table of Contents

<b>ABBREVIATIONS .....</b>	<b>3</b>
<b>1. INTRODUCTION .....</b>	<b>5</b>
<b>1.1. ANGIO-OEDEMA .....</b>	<b>5</b>
1.1.1. CLASSIFICATION OF ANGIO-OEDEMA WITHOUT URTICARIA.....	6
1.1.2. EPIDEMIOLOGY .....	10
1.1.3. DIAGNOSIS AND TREATMENT .....	12
<b>1.2. KALLIKREIN-KININ SYSTEM .....</b>	<b>14</b>
1.2.1. KININ FORMATION .....	15
1.2.2. KININ DEGRADATION .....	19
1.2.3. KININ RECEPTORS.....	20
<b>1.3. RENIN-ANGIOTENSIN-ALDOSTERONE SYSTEM .....</b>	<b>23</b>
1.3.1. ANGIOTENSIN CONVERTING ENZYME .....	25
1.3.2. ANGIOTENSIN II RECEPTORS.....	29
<b>1.4. AIM OF THE STUDY .....</b>	<b>35</b>
<b>2. MATERIALS AND METHODS .....</b>	<b>36</b>
<b>2.1. BUFFERS AND SOLUTIONS .....</b>	<b>36</b>
<b>2.2. CELL CULTURE.....</b>	<b>39</b>
<b>2.3. LABORATORY MICE.....</b>	<b>40</b>
2.3.1. AT2 DEFICIENT MOUSE (AT2 <sup>-/-</sup> ) .....	40
2.3.2. GENOTYPING .....	41
2.3.3. ANAESTHESIA AND EUTHANASIA PROCEDURES.....	43
2.3.4. DRUG ADMINISTRATION .....	44
2.3.5. BLOOD COLLECTION AND ORGAN HARVESTING.....	44
<b>2.4. BRADFORD'S PROTEIN ASSAY .....</b>	<b>46</b>
<b>2.5. TAIL-CUFF SYSTEM .....</b>	<b>46</b>
<b>2.6. MODIFIED MILES ASSAY .....</b>	<b>48</b>
<b>2.7. ORGAN BATH STUDIES.....</b>	<b>49</b>
<b>2.8. ENZYME-LINKED IMMUNOSORBENT ASSAYS .....</b>	<b>51</b>
<b>2.9. FLUORESCENCE DETECTION USING MAGNETIC BEADS .....</b>	<b>55</b>
<b>2.10. ACE ACTIVITY ASSAY IN PLASMA AND TISSUE LYSATES.....</b>	<b>57</b>
<b>2.11. WESTERN BLOTTING .....</b>	<b>59</b>
<b>2.12. TWO-PHOTON EXCITATION MICROSCOPY .....</b>	<b>61</b>
<b>2.13. 'A BRADYKININ IN SKIN EDEMA TRIAL' (ABRASE) .....</b>	<b>64</b>
<b>2.14. DATA ANALYSIS.....</b>	<b>65</b>
<b>3. RESULTS.....</b>	<b>66</b>
<b>3.1. PHARMACOLOGIC EVALUATION OF COMPOUND 21 .....</b>	<b>66</b>

## Table of Contents

3.1.1. SYNTHESIS OF COMPOUND 21 .....	66
3.1.2. FUNCTIONAL STUDIES IN ISOLATED AORTIC RINGS.....	68
3.1.3. EFFECT OF AT2 ACTIVATION ON AORTIC RINGS.....	69
<b>3.2. AT2 ACTIVATION IN BRADYKININ-INDUCED EXTRAVASATION.....</b>	<b>71</b>
<b>3.3. BLOOD PRESSURE AND HEART RATE MEASUREMENTS.....</b>	<b>76</b>
<b>3.4. EXTRAVASATION DETECTED BY TWO-PHOTON EXCITATION MICROSCOPY .....</b>	<b>78</b>
<b>3.5. EFFECT OF AT2 ACTIVATION ON ACE ACTIVITY .....</b>	<b>81</b>
3.5.1. ACE ACTIVITY IN ENDOTHELIAL CELLS.....	81
3.5.2. ACE ACTIVITY IN LUNG LYSATES AND PLASMA OF MICE.....	82
<b>3.6. EFFECT OF AT2 ACTIVATION ON ACE PROTEIN CONTENT .....</b>	<b>86</b>
3.6.1. ACE CONTENT IN INCUBATED LUNG FRAGMENTS BY WESTERN BLOT ANALYSIS .....	86
3.6.2. ACE CONTENT IN PLASMA AND LUNGS BY WESTERN BLOT ANALYSIS.....	88
3.6.3. ACE CONTENT IN PLASMA BY ELISA .....	88
3.6.4. ACE CONTENT IN PLASMA BY DYNABEADS® .....	91
<b>3.7. EFFECT OF AT2 ACTIVATION ON PLASMA ANGIOTENSIN .....</b>	<b>93</b>
<b>3.8. CYCLOOXYGENASE ACTIVITY IN BRADYKININ-INDUCED SKIN OEDEMA .....</b>	<b>95</b>
3.8.1. EFFECT OF UNSPECIFIC CYCLOOXYGENASE INHIBITION ON EXTRAVASATION.....	95
3.8.2. RESULTS OF 'A BRADYKININ IN SKIN OEDEMA TRIAL' (ABRASE).....	96
<b>4. DISCUSSION.....</b>	<b>101</b>
<b>4.1. PHARMACOLOGIC EVALUATION OF C21 .....</b>	<b>102</b>
<b>4.2. AT2 ACTIVATION IN BRADYKININ-INDUCED EXTRAVASATION.....</b>	<b>105</b>
<b>4.3. BLOOD PRESSURE AND HEART RATE MEASUREMENTS.....</b>	<b>107</b>
<b>4.4. EXTRAVASATION DETECTED BY TWO-PHOTON EXCITATION MICROSCOPY .....</b>	<b>111</b>
<b>4.5. EFFECT OF AT2 ACTIVATION ON ACE ACTIVITY .....</b>	<b>114</b>
<b>4.6. EFFECT OF AT2 ACTIVATION ON ACE PROTEIN CONTENT .....</b>	<b>117</b>
<b>4.7. EFFECT OF AT2 ACTIVATION ON PLASMA ANGIOTENSIN .....</b>	<b>121</b>
<b>4.8. CYCLOOXYGENASE ACTIVITY IN BRADYKININ-INDUCED SKIN OEDEMA .....</b>	<b>122</b>
<b>5. SUMMARY .....</b>	<b>127</b>
5.1. GRAPHICAL ABSTRACT.....	127
5.2. ABSTRACT (ENGLISH VERSION).....	128
5.3. ABSTRACT (GERMAN VERSION).....	130
<b>6. BIBLIOGRAPHY.....</b>	<b>133</b>
<b>PUBLICATIONS .....</b>	<b>152</b>
<b>FUNDING AND ACKNOWLEDGEMENT.....</b>	<b>155</b>
<b>DECLARATION OF AUTHORSHIP .....</b>	<b>156</b>

## **Abbreviations**

AAE	Acquired angio-oedema
ABRASE	A Bradykinin in Skin Edema Trial
AC	Adenylate cyclase
ACE	Angiotensin I-converting enzyme, kininase II
ACE-2	Homolog of ACE
AEBSF	4-(2-Aminoethyl)benzenesulfonyl fluoride
Ang I	Angiotensin I
Ang II	Angiotensin II
APP	Aminopeptidase P
ARB	Angiotensin II receptor type 1 blocker
AT1	Angiotensin II receptor type 1
AT1a/b	AT1 subtypes found in rodents
AT2	Angiotensin II receptor type 2
AT2 <sup>-y</sup>	Male hemizygous AT2 knockout mouse
AT23/25	PCR primers targeting the coding sequence of AT2
ATP	Adenosine triphosphate
ATRAP	AT1 receptor-associated protein
AVAs	Arterio-venous anastomoses
AVMA	American Veterinary Medical Association
B1	Bradykinin receptor type 1
B2	Bradykinin receptor type 2
C1, C2, C4	Proteins of the complement system
C1-INH	C1-esterase inhibitor
C21	Compound 21
cAMP	Cyclic adenosine monophosphate
cGMP	Cyclic guanosine monophosphate
COVID-19	Coronavirus disease of the year 2019
COX	Cyclooxygenase
CPN	Carboxypeptidase N, kininase I
DAG	Diacylglycerol
DPP4	Dipeptidyl peptidase-4
EDTA	Ethylenediaminetetraacetic acid
EGF	Epidermal growth factor
EGTA	Ethylene glycol-bis(2-aminoethylether)-N,N,N',N'-tetraacetic acid
ELISA	Enzyme-linked immunosorbent assay
eNOS	Endothelial nitric oxide synthase
ER	Endoplasmic reticulum
ERK	Extracellular signal-regulated kinase
FAPGG	N-[3-(2-Furyl)acryloyl]-Phe-Gly-Gly
FITC-dextran	Fluorescein isothiocyanate-dextran
FXII	Hagemann factor, coagulation factor XII
gACE	Germinal isoenzyme of ACE
GPCR	G protein-coupled receptor
GTP	Guanosine triphosphate
HAE	Hereditary angio-oedema
HAIWG	Hereditary Angioedema International Working Group
HDMEC	Human dermal microvascular endothelial cell
HFrEF	Heart failure with reduced left ventricular ejection fraction
HMWK	High molecular weight kininogen
HPLC	High-performance liquid chromatography
HUVECs	Human umbilical vein endothelial cells
IAE	Idiopathic angio-oedema
IgE	Immunoglobulin E

IP <sub>3</sub>	Inositol 1,4,5-trisphosphate
IP <sub>3</sub> R	IP <sub>3</sub> -receptor
KCl	Potassium chloride
kDa	Kilodalton
KHB	Krebs-Hepes buffer
KKS	Kallikrein-kinin system
LANUV	Ethics committee of the district government Düsseldorf
LMWK	Low molecular weight kininogen
MAPK	Mitogen-activated protein kinase
MASP	Mannan-binding lectin-serine protease
MLC	Myosin light chain
MLCK	Myosin light chain kinase
NaCl	Sodium chloride
NADPH	Nicotinamide adenine dinucleotide phosphate
NeoPVU	PCR primer targeting the neomycin cassette within the coding sequence of AT2
NEP	Neutral endopeptidase, neprilysin
NO	Nitric oxide
NSAIDs	Non-steroidal anti-inflammatory drugs
PAE	Pseudo-allergic angio-oedema
PAGE	Polyacrylamide gel electrophoresis
PBS	Phosphate-buffered saline
PCR	Polymerase chain reaction
pD <sub>2</sub>	Negative decadic logarithm of effector concentration producing the half-maximal effect
PIC	Protease inhibitor cocktail
PIP <sub>2</sub>	Phosphatidylinositol-4,5-bisphosphate
PKC	Protein kinase C
PLA2	Phospholipase A2
PLC	Phospholipase C
PMSF	Phenylmethanesulfonylfluoride
PRCP	Prolylcarboxypeptidase
RAAS	Renin-angiotensin-aldosterone system
RAE	RAAS-blocker-induced angio-oedema
ROS	Reactive oxygen species
sACE	Somatic isoenzyme of ACE
SARS-CoV-2	severe acute respiratory syndrome coronavirus type 2.
SBP	Systolic blood pressure
SD	Standard deviation
SDS	Sodium dodecyl sulfate
SDS-PAGE	Sodium dodecyl sulfate-polyacrylamide gel electrophoresis
SEM	Standard error of the mean
sGC	Soluble guanylate cyclase
SHG	Second-harmonic generation
SHP-1	A protein tyrosine phosphatase
STEMI	ST-segment elevation myocardial infarction
STV-HRP	Streptavidin covalently bound to horseradish peroxidase
TE	Tris-EDTA
TMB	3,3',5,5'-Tetramethyl[1,1'-biphenyl]-4,4'-diamine
TPEM	Two-photon excitation microscopy
Tris	Tris(hydroxymethyl)aminomethane
ZnCl <sub>2</sub>	Zinc chloride

# 1. Introduction

## 1.1. Angio-oedema

The term “angio-oedema” is derived from the Greek words *angeîon* and *oîdēma*, meaning “vessel” and “swelling”. In the medical context, this describes a condition in which fluid accumulates in the interstitial tissue (oedema formation) due to excessive leakage of plasma from the supplying blood vessels (extravasation). For centuries, the symptoms of angio-oedema have been reported in the literature. But it was not until 1982 that the German physician Heinrich Irenaeus Quincke succeeded in clearly distinguishing non-allergic angio-oedema from other similar clinical pictures such as urticaria, when describing the symptoms. Henceforth, the term Quincke's oedema has been used to describe the facial symptoms of angio-oedema. The genetic predisposition, that causes the inherited form of angio-oedema, was first discovered by Sir William Osler in 1888 when he observed a family with the symptoms of Quincke's oedema over five generations. Significantly later, in 1963, Donaldson and Evans established a relationship between C1-esterase inhibitor (C1-INH) deficiency and angio-oedema attacks [Reshef, Kidon & Leibovich, 2016]. However, angio-oedema does not only develop as a result of rare genetic disorders. To date, numerous aetiologies for the development of angio-oedema have been described, which generally involve either mast cell degranulation and release of various mediators such as histamine and prostaglandins, elevated bradykinin levels, or still unknown underlying mechanisms. On the one hand, angio-oedema due to mast cell degranulation is more common during exposure to an allergen and usually histamine-mediated. On the other hand, bradykinin-mediated angio-oedema often occurs as an adverse drug reaction, which is prominently observed among cardiovascular drugs such as Angiotensin I-converting enzyme (ACE) inhibitors [Maurer & Magerl, 2021]. Less common among the bradykinin-mediated types are hereditary angio-oedema (HAE) and acquired angio-oedema (AAE) with C1-INH deficiency being the primary cause [Aygoren-Pursun et al., 2018]. The clinical manifestation of non-allergic angio-oedema is a recurrent, short-lived, acute, non-pitting oedematous swelling of the subcutis and/or submucosa. In general, such oedemas may manifest across the face, lips, tongue, and upper respiratory tract, and in some cases, the extremities, genitalia, as well as visceral organs. Notably, oedema formation in the upper aerodigestive tract is a hallmark of ACE inhibitor-induced angio-oedema [Montinaro & Cicardi, 2020]. Especially if the swelling obstructs the airway, e.g., due to laryngeal oedema, it is likely that the patient will suffocate unless appropriate emergency medical treatment is provided (**Figure 1-1**). In routine clinical practice, the diagnosis and treatment of angio-oedema

has remained challenging and often inadequately managed. According to current knowledge, histamine or bradykinin are considered the most potent of the various vasoactive mediators that are crucially involved in the development of angio-oedema. Both mediators are capable of increasing vascular permeability within the affected tissue beyond a physiological level, which may promote increased fluid extravasation and eventually oedema formation [Bas et al., 2007; Reshef, Kidon & Leibovich, 2016].



**Figure 1-1:** The left picture shows an Angiotensin I-converting enzyme (ACE) inhibitor-induced angio-oedema affecting the cheek of an elderly man. The right picture shows a more severe case in an elderly woman who was intubated and admitted to the emergency department due to airway obstruction caused by tongue-base oedema. Images reprinted with kind permission from [Bas & Kojda, 2008].

### 1.1.1. Classification of angio-oedema without urticaria

In clinical practice, angio-oedema that occurs without signs of urticaria (primary angio-oedema) can be roughly divided into an allergic or a non-allergic form. This classification is based on the inflammatory mediator often involved, i.e., histamine or bradykinin. According to a consensus paper of the Hereditary Angioedema International Working Group (HAIWG) from the year 2014, angio-oedema without urticaria is classified into the rare genetic type, i.e. HAE, and non-hereditary (non-HAE) variants [Cicardi et al., 2014]. The different forms of angio-oedema that occur without urticaria are briefly outlined below (**Figure 1-2**). This study addresses a specific type of non-allergic non-HAE that occurs due to a side effect of certain cardiovascular drugs that interfere with the Renin-Angiotensin-Aldosterone System (RAAS), e.g., Angiotensin II receptor type 1 (AT1) blockers (ARBs).

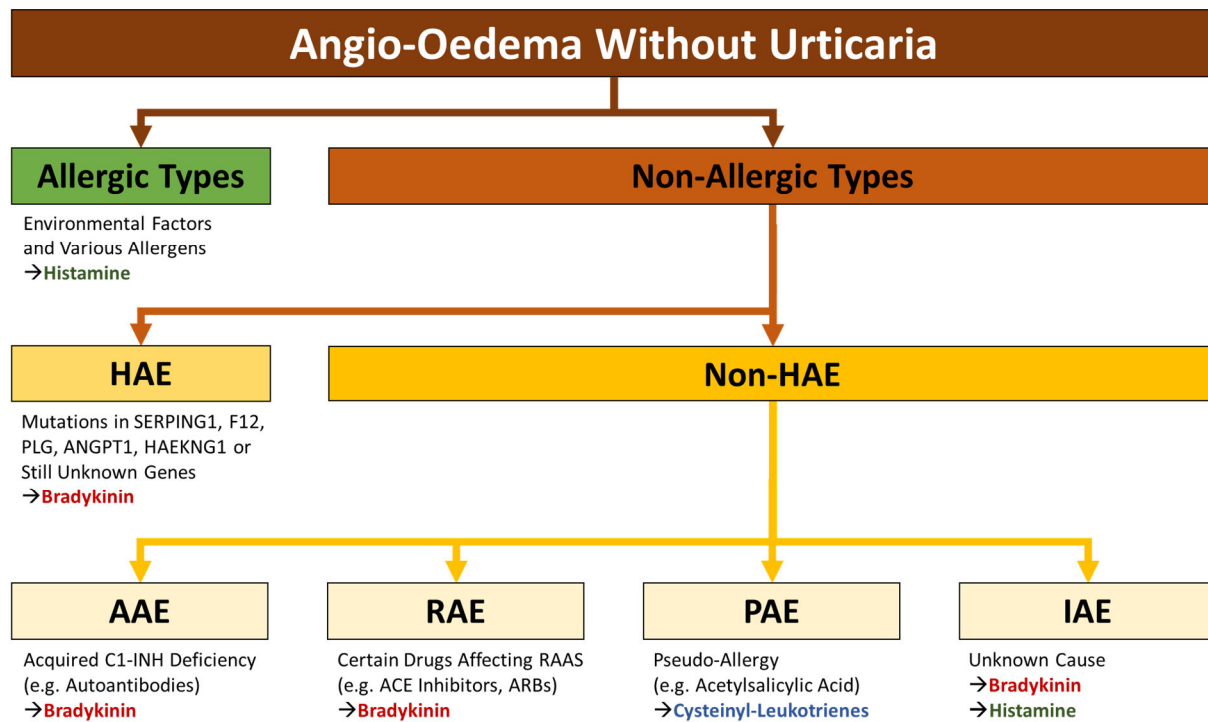


**Figure 1-2:** Angio-oedema without urticaria may be triggered by an allergic reaction in which histamine acts as the main mediator. Non-allergic angio-oedema is often bradykinin-mediated and arises from a variety of causes that may be hereditary (HAE) or non-hereditary (non-HAE). In HAE, mutations in genes encoding specific proteins involved in the metabolism of bradykinin lead to its unrestrained production. The category of non-HAE includes acquired angio-oedema (AAE), renin-angiotensin-aldosterone system blocker-induced angio-oedema (RAE), pseudo-allergic angio-oedema (PAE), and idiopathic angio-oedema (IAE). AAE develops due to C1-esterase inhibitor (C1-INH) consumption, while RAE is commonly induced as an adverse drug reaction to Angiotensin I-converting enzyme (ACE) inhibitors or Angiotensin II receptor type 1 blockers (ARBs). A typical example of PAE is an adverse drug reaction to acetylsalicylic acid characterized by increased formation of cysteinyl-leukotrienes as inflammatory mediators due to inhibition of alternative metabolic pathways for the precursor arachidonic acid. All other unknown variants are classified as IAE with bradykinin or histamine being the most common inflammatory mediators.

**Allergic angio-oedema** The allergic forms of angio-oedema are typically type 1 reactions involving the release of immunoglobulin E (IgE) in response to food, drugs (e.g., opiates) or environmental factors (e.g., insect bites). During this process, mast cells and basophils release inflammatory mediators, especially histamine [Memon & Tiwari, 2020]. Depending on the vascular bed and the severity of the event, histamine acts as the main mediator on endothelial histamine receptors and induces vasodilation and hyperpermeability, which may eventually lead to excessive vascular leakage and oedema formation [Nagy et al., 2008].

**Non-allergic types of angio-oedema** The non-allergic forms of angio-oedema are usually triggered by overproduction and/or reduced degradation of bradykinin. These types of angio-oedema may develop due to a rare genetic disorder, be the result of lymphoproliferative disorders, autoimmune diseases, malignant tumours, infections, or an adverse reaction to certain medications. In addition to HAE and AAE, this category includes RAAS-blocker-induced angio-oedema (RAE), pseudo-allergic angio-oedema (PAE) as well as idiopathic angio-oedema (IAE) in cases with unknown cause [Bas et al., 2007].

**Hereditary angio-oedema** The inherited form of non-allergic angio-oedema is a rare autosomal dominant genetic disorder in which affected metabolic pathways are dysregulated in favour of excessive production of the inflammatory mediator bradykinin. The most common variant involves a regulatory protein of the contact activation, complement and coagulation system, namely C1-INH, which acts as a brake on certain reactions. HAE is divided into three distinct types, HAE due to low C1-INH levels (HAE type-1, approximately 85% of cases), HAE caused by defective C1-INH (HAE type-2, approximately 15% of cases), and HAE despite the presence of regular C1-INH protein (HAE-nl-C1-INH) [Betschel et al., 2019]. While in HAE type-1 and type-2 usually the gene SERPING1 that codes for C1-INH is mutated, for HAE-nl-C1-INH various gene mutations have been identified. There are currently five subtypes of HAE-nl-C1-INH depending on the underlying mutation. In HAE-FXII, the mutation occurs in the F12 gene that codes for the Hagemann factor (also: coagulation factor XII, FXII). HAE-PLG is caused by mutations in the PLG gene, which codes for plasminogen. HAE-ANGPT1 is triggered by mutations in ANGPT1 gene which codes for angiopoietin-1. In cases where a mutation affects the KNG1-gene coding for kininogen 1, HAE-KNG1 may develop. Finally, all other types of HAE-nl-C1-INH with unknown gene mutation as the cause, are referred to as HAE-U. Regardless from which type of HAE a patient suffers, angio-oedema develops due to the uncontrolled production of the kinin bradykinin, which increases vascular permeability and eventually leads to an angio-oedema attack [Busse et al., 2021].

**Acquired angio-oedema** In AAE deficiency of C1-INH occurs without a mutation in the SERPING1 gene. In over 90% of these patients, the onset is beyond the age of 40 and is often associated with lymphoproliferative and autoimmune disorders. Thus, C1-INH is either consumed by malignant lymphoid tissue (AAE type-1) or neutralized by autoantibodies (AAE type-2) thereby causing C1-INH deficiency [Wu et al., 2016].

**Renin-angiotensin-aldosterone system blocker-induced angio-oedema** Among RAE, ACE inhibitor-induced angio-oedema is the most common. It is known that the underlying pathomechanism involves the inhibition of ACE, the key enzyme implicated in the degradation of bradykinin [Bas et al., 2007]. According to the consensus paper of the HAIWG from 2014, non-allergic angio-oedema induced by ACE inhibitors is defined as a distinct group [Cicardi et al., 2014]. In contrast, a classification under the term RAE comprises all drugs that interact with the RAAS and are known to induce a non-allergic bradykinin-induced angio-oedema attack. Thus, not only ACE inhibitors fall into this category, but also ARBs and the renin-inhibitor aliskiren [Montinaro & Cicardi, 2020]. Apart from ACE inhibitors, it is still unclear how ARBs or aliskiren may increase bradykinin levels and trigger an angio-oedema attack. In particular, ARB-induced angio-oedema is the focus of this thesis and will be discussed in more detail. Moreover, there are other drugs that may trigger a bradykinin-induced angio-oedema attack, including sacubitril, an inhibitor of neutral endopeptidase (NEP, also: neprilysin), or alteplase, a plasminogen activator [Bas et al., 2015b]. However, these drugs do not interfere with the RAAS but with the kallikrein-kinin system (KKS), which is tightly linked to the metabolism of bradykinin [Lerch, 2012].

**Pseudo-allergic angio-oedema** Certain adverse drug reactions may cause an angio-oedema attack, that is neither due to an allergic reaction nor bradykinin-induced. A prime example of a drug that may cause PAE is aspirin. This drug belongs to the group of non-steroidal anti-inflammatory drugs (NSAIDs). The pseudo-allergic response to aspirin is thought to be due to inhibition of cyclooxygenase (COX), causing an increase in the supply of its substrate, i.e., arachidonic acid, to the alternative metabolic pathway involved in the formation of cysteinyl-leukotrienes [Morwood et al., 2005].

**Idiopathic angio-oedema** Cases in which all of the above-mentioned causes can be ruled out are referred to as IAE. If the treatment with antihistamines is effective, IAE is considered to be histamine-induced. Otherwise, IAE is assumed to be bradykinin-induced. Moreover, it is possible that pathomechanisms involving other inflammatory mediators also play a role [Long, Koyfman & Gottlieb, 2019].

### 1.1.2. Epidemiology

It is estimated that HAE affects between 1 in 10,000 and 1 in 50,000 people worldwide [Long, Koyfman & Gottlieb, 2019; Zanichelli et al., 2016]. Nevertheless, the majority of cases with bradykinin-induced angio-oedema are caused by drugs and are not related to a genetic disorder. In this context, ACE inhibitor-induced angio-oedema is the most common within the category of RAE [Montinaro & Cicardi, 2020]. Likewise, although with less frequency, ARBs, aliskiren as well as other drug classes such as Dipeptidyl peptidase-4 (DPP4) inhibitors [Brown et al., 2009; White et al., 2010] and neprilysin inhibitors are associated with bradykinin-induced angio-oedema [Bas et al., 2015b]. According to the German Drug Report from 2019, inhibitors of RAAS accounted for approximately 60% of the prescription volume related to antihypertensive therapy. In this regard, for ACE inhibitors and ARBs, overall prescriptions in terms of defined daily doses steadily increased from 2010 to 2019 [Weber & Anlauf, 2020]. Considering that this is an annual trend on the rise, with ACE inhibitors and ARBs being top-performers of that statistic, it is expected that cases of drug-induced angio-oedema might also continue to increase. Certainly, this scenario applies to the global situation, given that these classes of drugs have long proven their efficacy for cardiovascular disorders in clinical trials and are therefore recommended in various international clinical practice guidelines:

ACE inhibitors or ARBs are used to reduce morbidity and mortality in patients with essential hypertension [Unger et al., 2020] and heart failure with reduced left ventricular ejection fraction (HFrEF) [Ponikowski et al., 2016]. Although randomized clinical trials have failed to show a benefit in the treatment of patients suffering from heart failure with preserved ejection fraction, still those RAAS blockers may be safely used to treat a comorbidity such as essential hypertension [Kjeldsen et al., 2020]. Likewise, patients affected by high blood pressure with comorbidities such as peripheral arterial disease or atherosclerotic renal artery disease benefit from the medication with ACE inhibitors or ARBs [Aboyans et al., 2018]. Similar benefits apply to patients with chronic coronary syndrome if they suffer from concomitant conditions such as hypertension, HFrEF, high-risk diabetes, chronic kidney disease, or if they are at high risk for cardiovascular events [Knuuti et al., 2020]. In the event of acute coronary syndrome and provided that the previously mentioned comorbidities are present, these classes of RAAS inhibitors are recommended within the first 24 hours after a ST-segment elevation myocardial infarction (STEMI) [Ibanez et al., 2018] and for long-term management after a non-STEMI [Collet et al., 2021].

ACE inhibitors are generally well tolerated, yet adverse drug reactions occur that may interfere with further therapy. In patients receiving ACE inhibitors, the most commonly reported adverse drug reaction is persistent dry cough (88.2%), followed by symptomatic hypotension (4.1%), angio-oedema or anaphylaxis (1.3%), and renal dysfunction (1%) [Yusuf et al., 2008a]. To overcome such adverse effects while maintaining inhibition of RAAS, physicians may switch their patients to ARBs, but some risk remains with regard to the development or recurrence of angio-oedema and the persistent dry cough. Indeed, clinical trials such as the VALIANT, the HOPE, and the ONTARGET have shown angio-oedema to occur with a frequency of approximately 0.3% to 0.5% under captopril/ramipril and 0.1% to 0.25% under the therapy with telmisartan/valsartan [Pfeffer et al., 2003; Yusuf et al., 2000; Yusuf et al., 2008b]. Interestingly, the PARADIGM-HF study evaluating the efficacy of the novel drug combination of valsartan and the neprilysin inhibitor sacubitril (Entresto<sup>®</sup>), that is currently approved for the treatment of symptomatic HFrEF, revealed a risk of angio-oedema comparable to that of the ACE inhibitor enalapril [McMurray et al., 2014]. In a meta-analysis of 40 clinical trials, the incidence of angio-oedema was found to be significantly higher for ACE inhibitors (0.30%) than for ARBs (0.11%), but patients suffering from heart failure were generally at higher risk for developing ACE inhibitor-induced (1.8-fold) or ARB-induced (2.8-fold) angio-oedema [Makani et al., 2012]. Generally, the risk of developing angio-oedema may be increased by ethnicity, female gender, as well as smoking, pre-existing allergies, or use of immunosuppressants [Woodard-Grice et al., 2010]. In particular, patients of African descent are at higher risk of developing ACE inhibitor-induced angio-oedema [Brown et al., 1996; Gainer et al., 1996; Gibbs, Lip & Beevers, 1999]. Data from an observational cohort study of 267,612 patients on ACE inhibitor therapy found that about half of patients who did not discontinue their ACE inhibitor therapy despite a first episode of angio-oedema, were 137 to 158 times more likely to relapse than those who never experienced an onset of angio-oedema [Mahmoudpour et al., 2015]. The time period for the occurrence of angio-oedema following initial therapy with an ACE inhibitor or ARB, ranges from the first day of use to several years, but roughly two-thirds of angio-oedema induced by ACE inhibitors occur within the first three months of use [Sachs et al., 2018]. The reasons for such variability in the timing of occurrence are unknown, but this fact may complicate the detection of angio-oedema associated with the triggering drug.

### 1.1.3. Diagnosis and treatment

In everyday clinical practice, the emergency treatment of an angio-oedema patient is based on a pragmatic approach that usually considers the main mediators involved, that is histamine or bradykinin, and focuses on the necessary immediate interventions to save the patient's life. Most cases of angio-oedema encountered in the emergency department are histamine-mediated rather than bradykinin-mediated and have a fulminant course. In comparison, bradykinin-mediated angio-oedema preferentially affects sites on the face and oropharynx, progresses slowly without pruritus or erythema, and in severe cases lasts significantly longer than 24 hours. Accordingly, the initial therapeutic approach is the same as for circulatory shock due to anaphylaxis and consists of epinephrine, antihistamines and steroids. However, these drugs may be less effective in bradykinin-induced angio-oedema and depending on the location of the oedema, surgical intervention may be required, e.g., to restore the airway patency if suffocation is imminent [Long, Koyfman & Gottlieb, 2019].

**DAMSEL protocol** A reliable and timely diagnosis of the causative mediator is essential for effective treatment of an angio-oedema attack and to avoid surgical airway opening which is followed by further intensive care measures. To this end, the DAMSEL protocol was developed to diagnose patients suffering from bradykinin-induced angio-oedema at an earlier stage and accordingly treat them more effectively [Lenschow et al., 2018]. Using the DAMSEL protocol, a score is calculated for patients with angio-oedema of the head and neck regions, based on parameters such as patient age (age  $\geq 65$  years), presence of dyspnoea, lack of pruritus or erythema, ongoing ACE inhibitor or ARB therapy, presence of laryngeal oedema, and lack of response to glucocorticoids. Each applicable parameter scores one point, with non-response to glucocorticoids scoring twice. If the total score is at least three points, bradykinin-mediated angio-oedema is more likely to be the case and treatment with C1-INH or the B2 receptor antagonist icatibant is recommended.

**Laboratory parameter for ACE inhibitor-induced angio-oedema** In RAE, discontinuation of the triggering drug is the most obvious step [Bas et al., 2007]. Nevertheless, despite discontinuation of the triggering drug, patients may experience recurrent angio-oedema episodes, as observed in a follow-up study involving 111 patients who had already suffered from ACE inhibitor induced angio-oedema [Beltrami et al., 2011]. Because of the short plasma half-life of bradykinin and the increase of its synthesis by contact activation during venous puncture, its quantification as a biomarker for risk assessment regarding ACE inhibitor-induced angio-oedema is less feasible [Saameli & Eskes, 1962].

It is already known that bradykinin stimulates through its receptor the activation of phospholipase A2 (PLA2) which in turn hydrolyses membrane phospholipids and releases arachidonic acid. This increases the formation of prostaglandins, which are paracrine and autocrine mediators with a short half-life [Leeb-Lundberg et al., 2005]. The degradation product of prostaglandin I2, that is 6-keto-prostaglandin F1 $\alpha$  (6-keto-PGF1 $\alpha$ ), has a significantly longer plasma half-life and seems to reflect increased bradykinin levels, as shown in a study with a small number of patients [Bas, Storck & Strassen, 2017]. Still, further studies are needed to implement 6-keto-PGF1 $\alpha$  as a reliable parameter for the assessment of ACE inhibitor-induced angio-oedema in clinical practice.

**Differential diagnosis of bradykinin-induced angio-oedema** If angio-oedema occurs in recurrent episodes over several months despite discontinuation of the eliciting drug, a different pathogenesis should be considered. Regarding HAE, initial clues arise from family history as well as oedema development in locations other than the head and neck region such as the intestinal tract, which is characterized by abdominal pain during the angio-oedema attack. Typically, patients with HAE experience their first attack between childhood and puberty [Christiansen et al., 2016]. Laboratory diagnostics can clarify whether a patient suffers from HAE, as well as provide information about its type. For the diagnosis of HAE due to C1-INH deficiency, the serum complement component 4 (C4) concentration is first determined. Normal C4 levels during an angio-oedema attack may rule out HAE, whereas reduced C4 levels may indicate HAE. Additional measurement of C1-INH levels as well as the determination of C1-INH functionality is needed to confirm HAE and its type. In HAE type-1, C1-INH level and function are usually below 50% of normal, whereas in HAE type-2, only the functional level is below 50% of normal. Patients at an age atypical for the initial onset of angio-oedema (age >40 years) may require additional screening for AAE. For instance, 80% of cases with acquired C1-INH deficiency, complement component 1q (C1q) levels are also decreased. In case HAE type-1 and type-2 are ruled out and there is uncertainty about AAE, genetic testing can be used to identify the respective HAE-nl-C1-INH variants [Busse et al., 2021].

**Treatment options** For the on-demand treatment of an acute HAE attack, there are currently several options. These are based on inhibition of bradykinin synthesis, either by substitution of plasma-derived (Berinert<sup>®</sup> and Cynrize<sup>®</sup>) or recombinant (Ruconest<sup>®</sup>) C1-INH or by inhibition of kallikrein through ecallantide (Kalbitor<sup>®</sup>), and inhibition of B2 through icatibant (Firazyr<sup>®</sup>). Patients may self-administer all of these medications at home, with the exception of ecallantide, if they have received appropriate training. At this time, ecallantide is only approved in the US for the treatment of an acute HAE attack and should always be administered by a healthcare professional due to the risk of an anaphylactic reaction [Caballero, 2021]. In contrast, for ACE inhibitor-induced angio-oedema, there is currently no consensus on the best pharmacological treatment. Despite the limited evidence for efficacy, icatibant, ecallantide and C1-INH substitution are used off-label [Long, Koyfman & Gottlieb, 2019; Montinaro & Cicardi, 2020].

## 1.2. Kallikrein-kinin system

The most common causes of non-allergic angio-oedema are HAE, AAE and RAE. For the latter case, ACE inhibitors and ARBs, which are used to treat lifestyle diseases such as high blood pressure, heart failure and diabetes, play an important role. All cases have an excess of the inflammatory mediator bradykinin and the resulting over-activation of its receptors in common. Excess bradykinin results from either overproduction or decreased degradation. While the formation of bradykinin takes place within the Kallikrein-kinin system (KKS), whose metabolic pathways overlap with those of the intrinsic coagulation and complement cascade, its degradation is primarily controlled by ACE and neprilysin [Campbell, 2018; Long, Koyfman & Gottlieb, 2019]. Therefore, certain pathological changes within those metabolic pathways may also affect bradykinin metabolism. For instance, low plasma concentration of aminopeptidase P (APP), which is involved in the catabolism of bradykinin, has been suggested as a pre-disposing factor for ACE inhibitor-induced angio-oedema [Adam et al., 2002; Ali et al., 2019]. Likewise, a mutation affecting the ACE gene may cause an overall decrease in ACE activity by causing increased detachment of ACE from the cell membrane, which is accompanied by a decrease in catalytic activity [Persu et al., 2013].

**Role of kinins** In 1949, the Brazilian research team led by Rocha e Silva made an interesting discovery while studying the physiological effects of the snake venom extracted from the pit viper *Bothrops jararaca*: upon incubation with that snake venom, the globulin fraction obtained from dog plasma reduced the contraction of isolated guinea pig ileum, which was an effect not directly related to the venom itself [Rocha, Beraldo & Rosenfeld, 1949]. This discovery describes the first known effect of bradykinin related to the regulation of vascular tone. At that time, the snake venom was thought to have a bradykinin-potentiating effect, as patients bitten by *Bothrops jararaca* developed a severe reduction in blood pressure. It was only years later that this effect was attributed to the inhibition of an important enzyme that breaks down bradykinin, namely ACE [Ferreira, 1965]. Based on the ACE inhibiting peptide sequence derived from the venom of *Bothrops jararaca*, captopril was developed as a first-in-class orally available ACE inhibitor. To this day, this drug and newer derivatives are still used for the treatment of high blood pressure [Ondetti, Rubin & Cushman, 1977]. Meanwhile, bradykinin has been shown to be involved not only in the regulation of the vascular tone, but also in various other physiological processes such as inflammation, nociception and vascular permeability [Leeb-Lundberg et al., 2005].

### 1.2.1. Kinin formation

Unlike the inflammatory mediator histamine, which is synthesised from the amino acid histidine, kinins such as bradykinin or Lys-bradykinin (kallidin) are oligopeptides, released by specific serin proteases (kallikreins) from liver-derived kininogens, i.e., low molecular weight kininogen (LMWK) and high molecular weight kininogen (HMWK). There exist two different pathways by which kinins are produced, the main route involves plasma kallikrein and the other involves tissue kallikrein. Both variants are secreted into the bloodstream as inactive precursors. While tissue kallikrein is synthesized in a variety of tissues and secretory organs, plasma kallikrein is mainly produced in the liver and can be detected comparatively at higher concentrations in plasma [Koumandou & Scorilas, 2013]. Pre-kallikrein and HMWK circulate in the plasma as a complex and may bind to the surface of endothelial cells at an endothelial membrane multiprotein-receptor complex [Moreau et al., 2005]. When initiated by the zymogen FXII, activated plasma kallikrein cleaves HMWK to release bradykinin. Similarly, tissue kallikrein cleaves LMWK or, with lower affinity, HMWK to release kallidin (**Figure 1-3**).

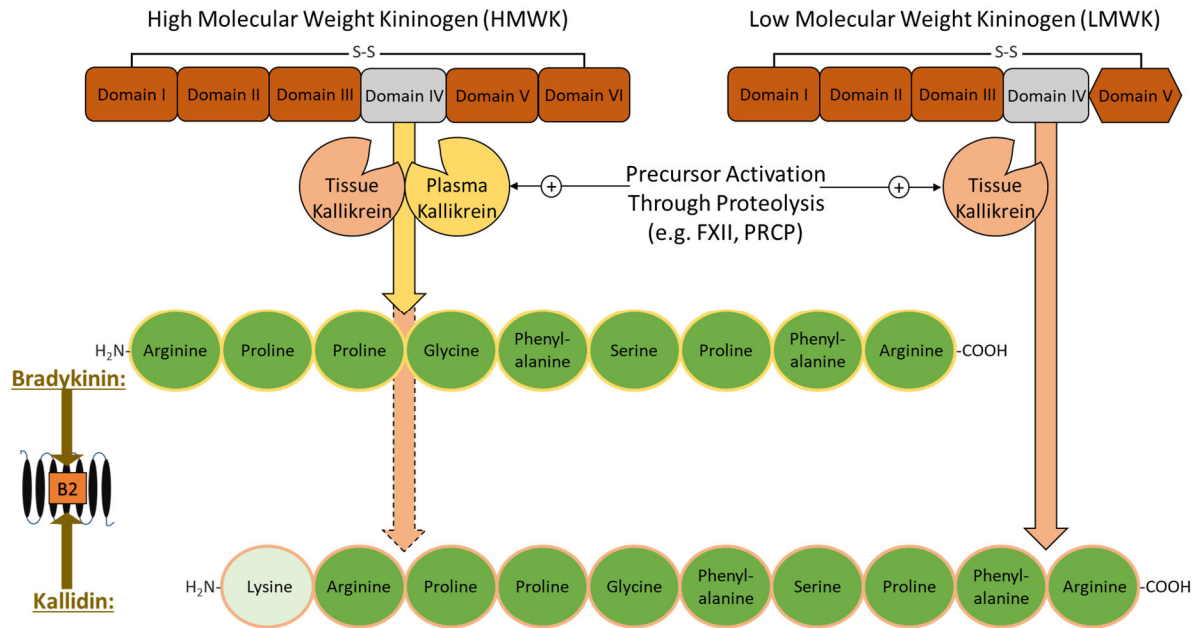


**Figure 1-3:** Plasma kallikrein as well as tissue kallikrein exist as inactive enzymes (precursors) until they are activated by proteolytic cleavage that involves other enzymes such as Hagemann factor (FXII) or prolylcarboxypeptidase (PRCP). Upon activation, tissue-derived kallikrein cleaves lys-bradykinin (kallidin) from protein domain IV of high molecular weight kininogen (HMWK) or low molecular weight kininogen (LMWK). Similarly, plasma-derived kallikrein releases bradykinin exclusively from HMWK. Bradykinin and kallidin exert their physiological effects preferentially through the bradykinin receptor type 2 (B<sub>2</sub>).

Moreover, kallikrein also activates FXII (positive feedback) as well as induces the formation of plasmin, which in turn induces fibrinolysis and to some extent may additionally activate FXII. Interestingly, some degradation products of FXII (FXII-fragments) may also activate pre-kallikrein and thus stimulate further bradykinin formation through kallikrein [Maurer et al., 2011]. Likewise, in-vitro cell studies involving endothelial cells have shown that endothelial cell-derived prolylcarboxypeptidase (PRCP) is capable of directly promoting bradykinin formation through kallikrein [Shariat-Madar, Mahdi & Schmaier, 2002]. Bradykinin and kallidin are considered to be the native products of the KKS, acting as ligands of the same kinin receptor type. Furthermore, degradation products exist, each with different affinities for the respective kinin receptor subtype [Leeb-Lundberg et al., 2005].

**Role of C1-INH in bradykinin-formation** Patients with C1-INH deficiency or dysfunction may suffer from HAE, which is caused by a mutation within the SERPING1 gene, or AAE, in which C1-INH is depleted, e.g., due to an autoimmune disease (refer to: 1.1.1). The plasma protein C1-INH belongs to the serine protease inhibitor (serpin) family and is critically involved in down-regulating the activity of complement system proteins, which include C1r, C1s, and mannan-binding lectin-serine protease (MASP). Moreover, C1-INH is involved in the inhibition of FXII, plasma kallikrein, and plasmin, limiting the activity of the contact activation system and plasmin-induced fibrinolysis [Hofman et al., 2016]. When C1-INH is deficient or dysfunctional, there is an unrestrained interaction between these signalling pathways which can amplify each other beyond physiological levels. In particular, activation of plasma kallikrein by FXII within a self-amplification loop may lead to bradykinin overproduction and subsequently to bradykinin-induced angio-oedema [Caballero, 2021]. Additionally, hormonal changes can also exert an influence. For instance, oestrogens may increase FXII levels as well as decrease C1-INH and ACE levels, whereas androgens may increase APP and C1-INH levels [Zeerleder & Levi, 2016]. Of note, although the degradation of bradykinin by APP also occurs as one of the alternative pathways, the main pathway of degradation involves ACE and neprilysin. Consequently, treatment of patients who suffer from HAE with ACE inhibitors or the novel drug combining valsartan and sacubitril may further increase the risk of an angio-oedema attack.

**Complement system** Being part of the innate and adaptive immune system, the complement system contains more than 30 proteins and has, among other things, the task of marking targets for phagocytosis as well as initiating cell lysis. Relevant signalling pathways are, on the one hand, the classical pathway, which is initiated by antigen-antibody complexes and leads to the formation of the C1 complex, on the other hand, the lectin pathway, which is initiated upon surface contact with pathogens and leads to the activation of MASP. Downstream the cascade, if not interrupted by C1-INH, the complement proteins C1, C2 and C4 are generated and consumed (**Figure 1-4**). This event may not be directly responsible for bradykinin formation, but if C1-INH is already in short supply during an infection, it may be further mobilized for the complement pathway and consequently not made available to other processes crucial for the regulation of bradykinin production [Davis, 2008; Sarma & Ward, 2011].

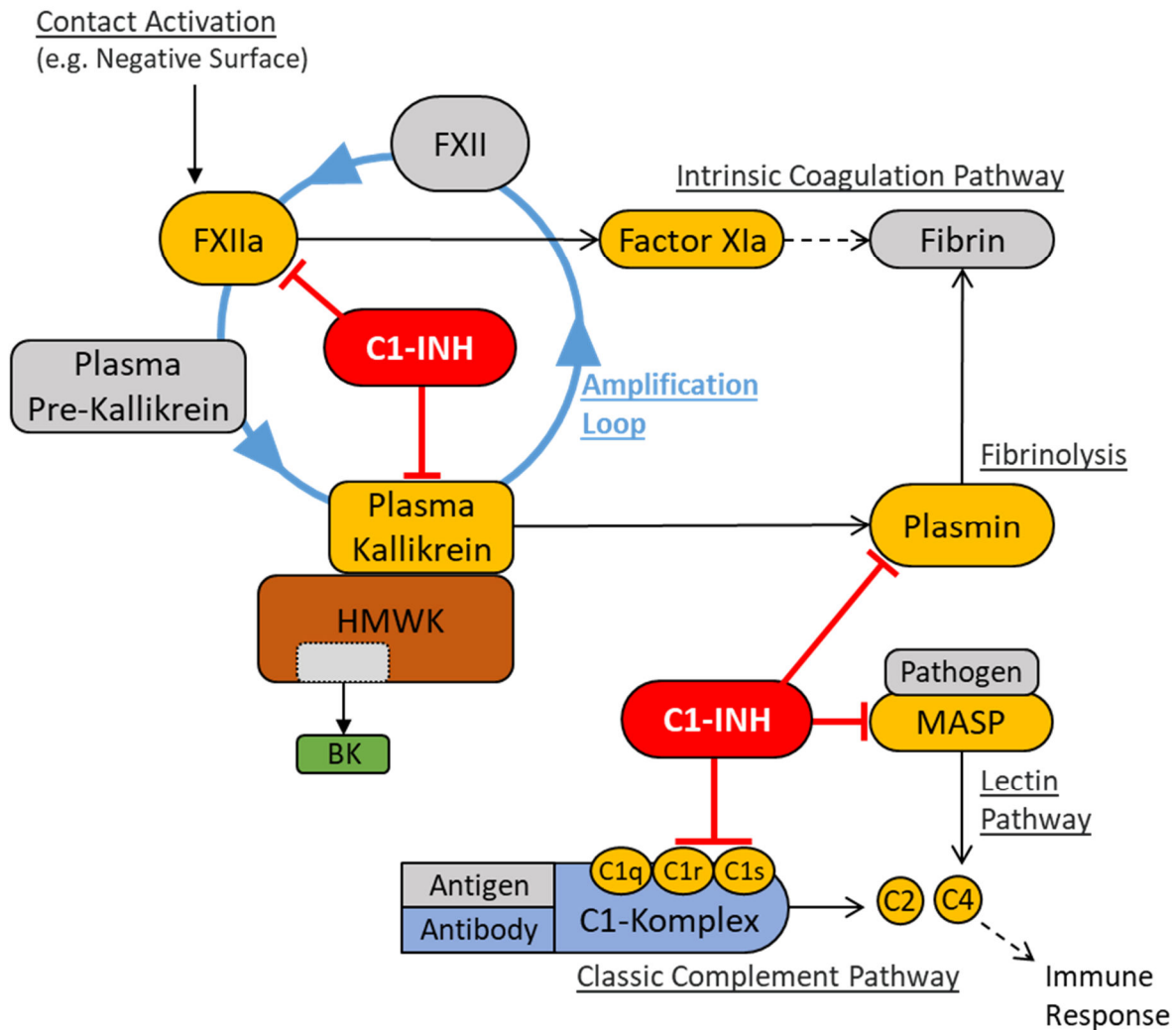


**Figure 1-4:** The regulatory action of C1-esterase inhibitor (C1-INH) on various physiological pathways related to the formation of bradykinin, the complement system, blood coagulation, and fibrinolysis. C1-INH is capable of interrupting the amplification loop of the contact activation through inhibition of activated Hagemann factor (FXIIa) preventing the generation of plasma kallikrein. Furthermore, plasma kallikrein is directly inhibited by C1-INH preventing further cleavage of bradykinin (BK) from high molecular weight kininogen (HMWK). The inhibition of FXIIa also prevents the activity of the intrinsic coagulation pathway, which would progress through activated factor XI (factor XIa). Thus, downstream the cascade, fibrin cross-linking does not occur. In addition, C1-INH limits fibrinolysis by inhibiting plasmin formation from its precursor. Moreover, the inhibition of the complement cascade targeting the complement system proteins C1r and C1s or Mannan-binding lectin-serine protease (MASP) attenuates the downstream immune response of respective pathways.

### 1.2.2. Kinin degradation

Once the peptides bradykinin and kallidin are formed they may exert their biological activity through bradykinin receptors, that is preferentially the bradykinin receptor type 2 (B2). However, these kinins are subject to rapid enzymatic degradation by kininases, hence the half-life is relatively short, typically less than 30 seconds [Saameli & Eskes, 1962]. Several types of kininases found in various tissues and bodily fluids are involved in the degradation of kinins. These include, in addition to ACE and neprilysin, APP, carboxypeptidase N (CPN, also: kininase I), and dipeptidyl peptidase-4 (DPP4) [Hamid et al., 2020]. Bradykinin and kallidin may lose one or more peptide components by proteolytic cleavage, depending on the enzyme involved, which may either produce an inactive peptide or change the receptor preference (Figure 1-5).

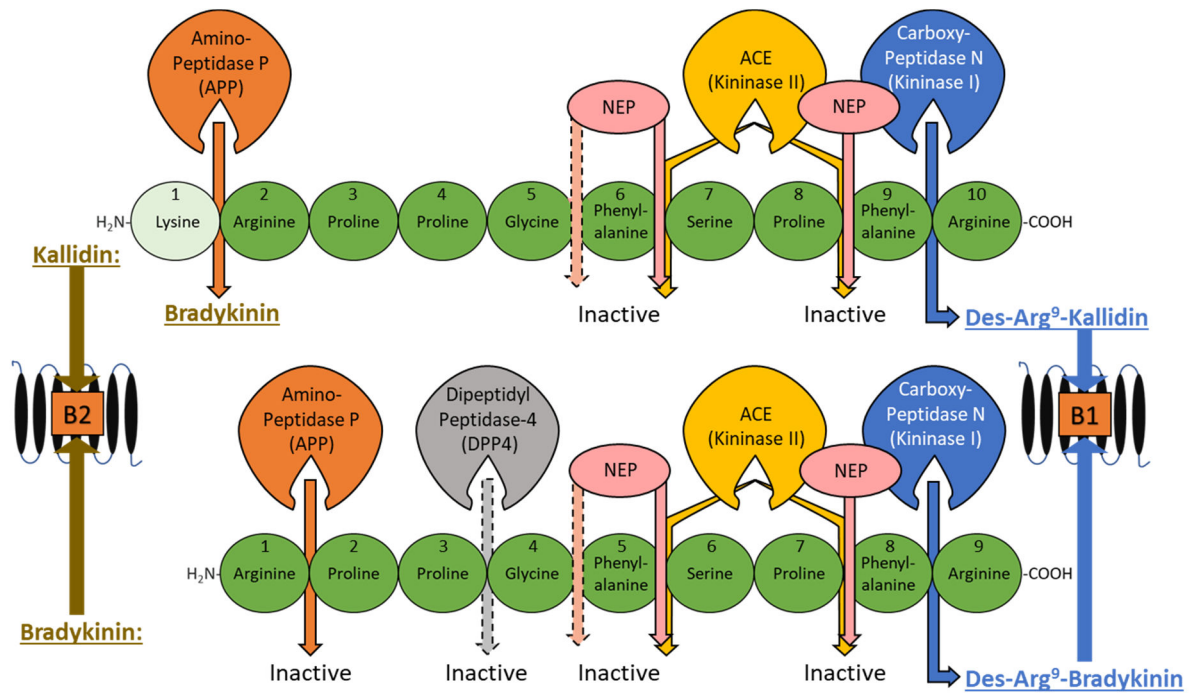


**Figure 1-5:** The sites of enzymatic degradation of the kinins, kallidin (top) and bradykinin (bottom) by various physiological enzymes. The enzyme aminopeptidase P (APP) cleaves kallidin into bradykinin, both of which exert their biological activity mainly through the bradykinin receptor type 2 (B2). In contrast, carboxypeptidase (CPN, kininase I) produces des-arg<sup>9</sup>-bradykinin as well as des-arg<sup>9</sup>-kallidin which preferentially bind to bradykinin receptor type 1 (B1). Bradykinin may be inactivated by APP and then further degraded by dipeptidyl peptidase-4 (DPP4). In addition, bradykinin or kallidin may be sequentially degraded from the C-terminal end by angiotensin I-converting enzyme (ACE, kininase II) or neutral endopeptidase (NEP, neprilysin), leading to biologically inactive products. The additional cleavage site between glycine and phenylalanine was observed after prolonged incubation in-vitro and is more likely implicated in the inactivation of des-Arg<sup>9</sup>-bradykinin [Moreau et al., 2005].

For instance, affinity is shifted toward the bradykinin receptor type 1 (B1) when CPN cleaves the carboxyl-terminal arginine from either bradykinin or kallidin to yield the corresponding des-arginine peptides. In contrast, the cleavage products of the other enzymes are biologically inactive, with the exception of APP, which converts kallidin into bradykinin by cleaving the amino-terminal lysine. The inactivation of kinins may occur non-specifically by neprilysin and DPP4, but the main pathway of inactivation remains dominated by the proteolytic activity of ACE [Campbell, 2003], which sequentially cleaves the carboxyl-terminal dipeptides, i.e., phenylalanine-arginine and serine-proline [Sheikh & Kaplan, 1989].

### 1.2.3. Kinin receptors

Depending on the type of tissue, the action of kinins is associated with vasodilatation, vascular hyperpermeability, inflammatory processes, and pain [Leeb-Lundberg et al., 2005]. These effects are mediated by kinin receptors B1 and B2, localized on cell surfaces. Both receptors are proteins with seven transmembrane domains belonging to the superfamily of G protein-coupled receptors (GPCRs) and share a sequence homology of 36% [Menke et al., 1994]. B2 is constitutively expressed in a variety of tissues and plays an important role during acute inflammation. In contrast, expression of B1 in healthy tissue is low, but increased during injury and chronic inflammation, e.g. due to the accumulation of its agonist des-Arg<sup>9</sup>-bradykinin [Couture et al., 2001]. A randomized clinical trial has provided evidence that overactivation of B2 plays an important role during angio-oedema attacks triggered by cardiovascular drugs such as ACE inhibitors [Bas et al., 2015b]. Similarly, B2 activation is thought to be involved in angio-oedema induced by ARBs such as losartan [Campbell, Krum & Esler, 2005], DPP4 inhibitors such as vildagliptin [Brown et al., 2009], and/or neprilysin inhibitors such as sacubitril [Bas et al., 2015b].

**Signalling pathways** Upon activation of the kinin receptors B1 and B2, which are GPCRs mainly coupled to the Gq/11 protein alpha subunit (Gq), phospholipase C (PLC) is activated. The latter hydrolyses phosphatidylinositol-4,5-bisphosphate (PIP<sub>2</sub>) present in the plasma membrane, producing inositol-1,4,5-trisphosphate (IP<sub>3</sub>) and diacylglycerol (DAG). IP<sub>3</sub> binds to its receptor and enables the release of Ca<sup>2+</sup> from the endoplasmic reticulum into the cytosol, whereas still membrane bound DAG recruits and activates protein kinase C (PKC) from the cytoplasm, which is involved in multiple phosphorylation cascades. Phosphorylation of target proteins, in conjunction with Ca<sup>2+</sup> promotes the activation of PLA<sub>2</sub> and thus the formation of arachidonic acid [Moreau et al., 2005].

Furthermore,  $\text{Ca}^{2+}$  binding to calmodulin, which can activate other proteins such as myosin light chain (MLC) kinase (MLCK), initiates endothelial cell retraction, breaking down intercellular junctions and increasing endothelial permeability [Vandenbroucke et al., 2008]. Calmodulin is also capable of activating endothelial nitric oxide synthase (eNOS), an enzyme that synthesizes nitric oxide (NO) from L-arginine. When NO diffuses into neighbouring smooth muscle cells, it activates soluble guanylate cyclase (sGC), that converts guanosine triphosphate (GTP) into 3',5'-cyclic guanosine monophosphate (cGMP). In addition, paracrine mediators are synthesized from arachidonic acid, such as prostacyclin ( $\text{PGI}_2$ ), which can activate adenylyate cyclase (AC) in smooth muscle cells by stimulating its GPCR (**Figure 1-6**). Then, AC converts adenosine triphosphate (ATP) into 3',5'-cyclic adenosine monophosphate (cAMP) [Leeb-Lundberg et al., 2005; Marceau et al., 2020]. Typically, in the absence of vascular endothelium, contraction in smooth muscle occurs through an increase in intracellular  $\text{Ca}^{2+}$  concentration, which binds to calmodulin and causes activation of MLCK. In turn, phosphorylated MLC binds actin to form phosphorylated actomyosin, initiating the cross-bridge cycle [Kuo & Ehrlich, 2015]. In contrast, increasing concentrations of cGMP and cAMP mediated by endothelial NO and endothelial  $\text{PGI}_2$ , respectively, lead to a decrease in intracellular  $\text{Ca}^{2+}$  levels and thus to an attenuation of vascular smooth muscle cell contraction. The latter is achieved by activating specific protein kinases, e.g., cAMP-dependent protein kinase A (PKA) or cGMP-dependent protein kinase G (PKG) with downstream functional modulation of key proteins (e.g., ion channels and  $\text{Ca}^{2+}$  pumps) that control intracellular levels of  $\text{Ca}^{2+}$  [Morgado et al., 2012].

**Formation of eicosanoids in B2 mediated angio-oedema** From arachidonic acid, bioactive eicosanoids are generated through various metabolic pathways that are initiated by cyclooxygenases (COX), lipoxygenases (LOX), or cytochrome P450 (CYP). The corresponding subclasses of eicosanoids are COX-derived prostanoids, LOX-derived leukotrienes, or CYP-derived hydroxy or epoxy metabolites, which among other things contribute to the regulation of vascular permeability and tonus, inflammatory processes, as well as the immune response [Calder, 2020]. From a pathological point of view, the involvement of eicosanoids such as prostaglandins plays an important role in certain forms of allergies, autoimmune diseases and presumably during bradykinin-induced angio-oedema attacks [Gholamreza-Fahimi et al., 2020].

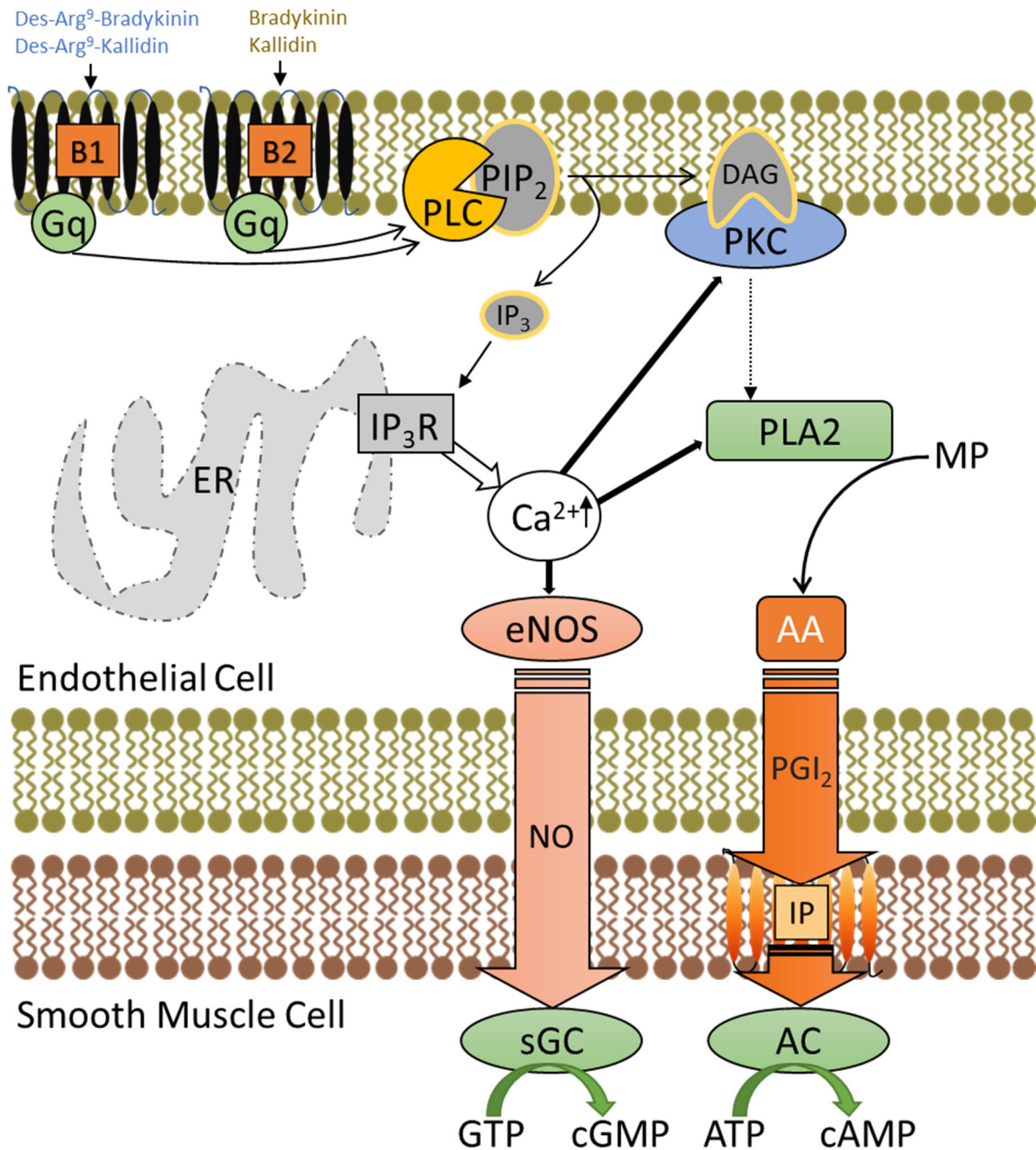


**Figure 1-6:** The signalling pathways of the Gq/11 protein alpha subunit (Gq) coupled bradykinin receptor type 1 (B1) and type 2 (B2) leading to smooth muscle relaxation. Arachidonic acid (AA); adenylate cyclase (AC); adenosine triphosphate (ATP); cyclic adenosine monophosphate (cAMP); cyclic guanosine monophosphate (cGMP); diacylglycerol (DAG); endothelial nitric oxide (eNOS); endoplasmic reticulum (ER); guanosine triphosphate (GTP); prostacyclin receptor (IP); inositol 1,4,5-trisphosphate (IP<sub>3</sub>); IP<sub>3</sub>-receptor (IP<sub>3</sub>R); membrane phospholipid (MP); nitric oxide (NO); prostacyclin (PGI<sub>2</sub>); phosphatidylinositol-4,5-bisphosphat (PIP<sub>2</sub>); protein kinase C (PKC); phospholipase A2 (PLA2); Phospholipase C (PLC); soluble guanylate cyclase (sGC).

### 1.3. Renin-angiotensin-aldosterone system

The first description of the RAAS dates back to the 19th century, with Tigerstedt and Bergman discovering a substance in adrenal extracts they named renin, which was capable of significantly increasing arterial blood pressure when injected into the circulation [Tigerstedt & Bergman, 1898]. Several years later, it was found that renin does not directly affect blood pressure, but rather releases a specific peptide mediator from a precursor protein called angiotensinogen. Based on this, Skeggs et al. reported on a decapeptide called angiotensin I (Ang I), released by renin prior to conversion into angiotensin II (Ang II). The latter was identified as the peptide hormone responsible for increasing blood pressure [Skeggs et al., 1976]. Later, the pulmonary circulation was found to be crucially involved in the conversion of Ang I into Ang II [Ng & Vane, 1968]. Shortly thereafter, the involvement of ACE in both Ang I conversion and kinin inactivation was revealed, establishing for the first time a connection between RAAS and KKS [Yang, Erdos & Levin, 1970].

**Systemic regulation** According to the traditional view, that describes the systemic function of RAAS, the enzyme cascade starts with angiotensinogen. The latter is a protein consisting of 452 amino acids, which is mainly synthesized in the liver and secreted into the systemic circulation. Within the juxtaglomerular apparatus of the kidney, granular cells (juxtaglomerular cells) synthesize and store renin. These cells secrete renin either upon stimulation of  $\beta$ -adrenergic receptors, in the presence of decreased renal blood flow as detected by stretch receptors in the vessel walls, or by stimulation from cells of the macula densa, which respond to decreased sodium levels in the distal convoluted tubule [Sparks et al., 2014]. While renin cleaves Ang I from circulating angiotensinogen, ACE converts Ang I into Ang II. The latter activates AT1 receptors to restore fluid balance and normal blood pressure. In addition, activation of AT1 receptors in the juxtaglomerular apparatus also limits the release of renin, forming a negative feedback loop that prevents excessive activation of the RAAS [Patel et al., 2017]. From a pathophysiological perspective, AT1 mediates further effects that may be responsible for deleterious changes in various end-organs [Schmieder et al., 2007]. Based on this understanding, the intervention with ACE inhibitors or ARBs is not only intended to lower blood pressure, but also to provide end-organ protection, which is in line with the current clinical evidence [Forrester et al., 2018]. In addition, the inhibition of ACE also increases bradykinin levels by blocking bradykinin degradation (**Figure 1-7**). This is a therapeutically desirable effect that significantly contributes to the blood pressure reducing activity of ACE inhibitors in hypertensive patients [Gainer et al., 1998].

diss

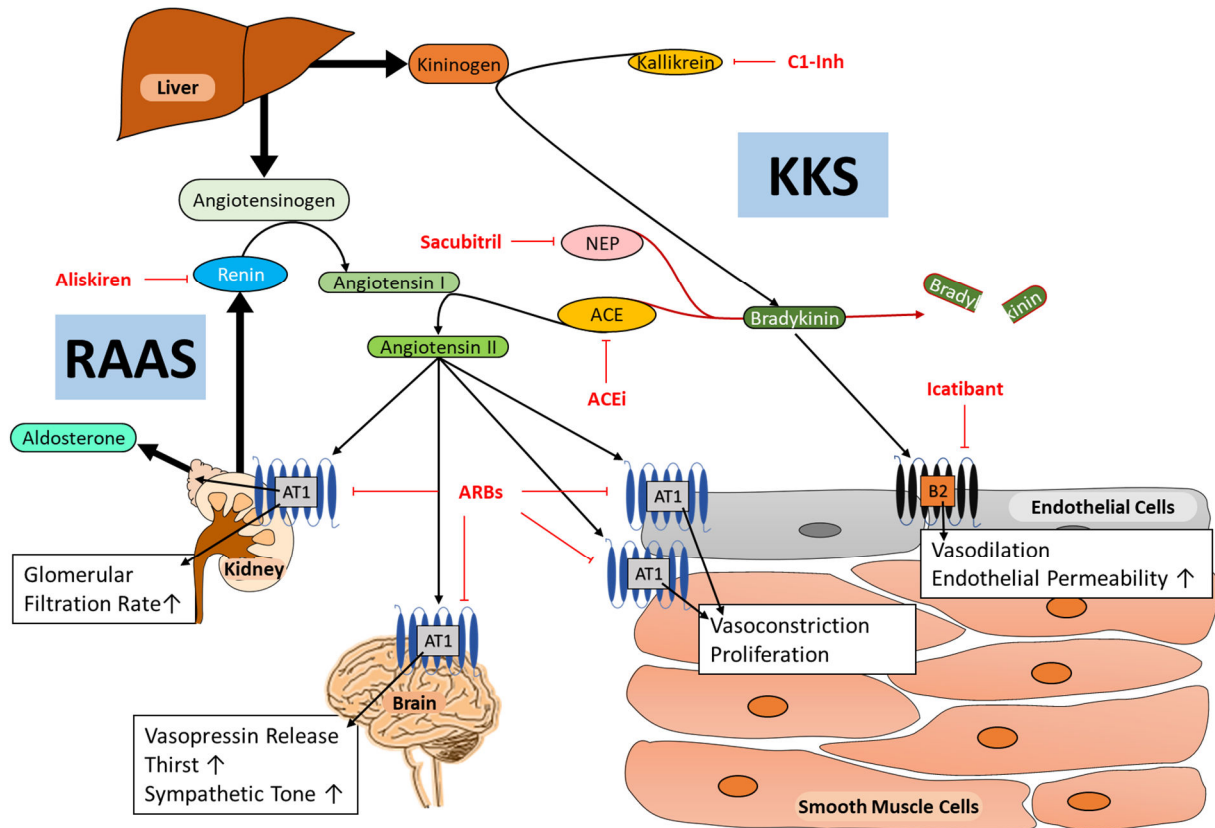


**Figure 1-7:** Illustration of the classical view of the renin-angiotensin-aldosterone system (RAAS) and its connection with the kallikrein-kinin system (KKS). The liver synthesizes and releases the proteins angiotensinogen and kininogen into the systemic circulation. Renin, released from the kidney, cleaves angiotensin I from angiotensinogen. Angiotensin I-converting enzyme (ACE) converts angiotensin I to angiotensin II, which acts through AT1 and mediates multiple effects in various tissues and organs. These effects include an increase in glomerular filtration rate, release of aldosterone from the adrenal gland, release of vasopressin from the hypothalamus, central effects such as thirst and increased sympathetic tone, along with vasoconstriction and increased proliferation in affected tissues. While kallikrein cleaves kininogen to release bradykinin, that mediates vasodilation and increased vascular permeability through the bradykinin receptor type 2 (B2), ACE and neutral endopeptidase (NEP, neprilysin) exert their kininase activity to break down bradykinin into inactive fragments, finally resulting in the formation of Bradykinin (1-5). Therapeutic intervention at various sites of the RAAS and KKS can be achieved with the renin inhibitor aliskiren, ACE inhibitors (ACEi), the neprilysin inhibitor sacubitril, AT1 blockers (ARBs), as well as with icatibant to block B2 or with C1 inhibitors (C1-INH) to limit the activity of kallikrein.

**Local RAAS** Originally, the RAAS was thought to be limited to the regulation of systemic blood pressure and salt-fluid balance, but with increasing understanding and the discovery of new components and interacting signalling pathways, this view has been challenged. Thus, the

concept of a local RAAS that functions as a paracrine regulator in different tissues independent of circulating RAAS components emerged. For example, due to the blood-brain barrier, the majority of brain regions are isolated from the circulating components related to systemic RAAS. Nevertheless, there is evidence suggesting that a central and independent RAAS is involved in the regulation of cognition-related processes in these regions [Jackson et al., 2018]. Similarly, in the human skin all components of the RAAS have been detected [Steckelings et al., 2004]. Thus, most organs, such as the kidney, the heart or the brain, are not only involved in the systemic RAAS, but also have an independently operating local RAAS that regulates cell survival and differentiation as well as inflammatory processes at the cellular level.

### 1.3.1. Angiotensin converting enzyme

In humans, ACE is a ubiquitously expressed, highly glycosylated transmembrane protein which belongs to the protein family of metalloproteinases and dipeptidyl carboxypeptidases. To date, two isoenzymes and one protein homolog of ACE have been described. The isoenzymes are called somatic ACE (sACE) and germinal ACE (gACE). While sACE can be detected in a variety of tissues and bodily fluids, gACE is expressed only in testes and is particularly involved in male fertility. Both ACE isoform are coded by the same gene, however unlike gACE, sACE possesses two homologous interconnected domains (C- and N-domain), with each domain having its own active site. Towards the carboxyl-terminal end, which protrudes into the cytoplasm, all ACE variants have a transmembrane domain that enables anchoring into the cell membrane. Commonly, sACE is often found attached to the surface of endothelial cells, epithelial cells, as well as macrophages and dendritic cells [Guang et al., 2012].

**Soluble ACE** The soluble form of ACE can be detected within the circulation and various bodily fluids. ACE circulating within the blood is mainly released from the pulmonary vasculature, which has an up to 10-fold higher expression rate for ACE when compared to the microcapillaries of the systemic circulation [Danilov et al., 2016]. Furthermore, the process of ACE entering the circulation as a soluble form is called shedding, and for sACE it involves losing the catalytic activity of the C-domain [Iwata & H. Greenberg, 2011]. In the same healthy individual, circulating ACE levels do not vary significantly between multiple measurements. However, when compared, large differences can occur from one individual to another [Beneteau et al., 1986]. Such large differences may correlate with both age and sex or insertion/deletion polymorphism in the ACE gene. In addition, certain diseases such as sarcoidosis may lead to elevated levels of circulating ACE [Lopez-Sublet et al., 2018].

According to published literature, an as yet unknown membrane-bound protease is thought to cleave ACE from the cell surface. Likewise, several cellular proteins, such as PKC and calmodulin have been suggested to interact with ACE and thereby regulate the process of shedding [Iwata & H. Greenberg, 2011].

**Discovery of the ACE homolog** Historically, but also due to its importance as a therapeutic target in cardiovascular diseases, ACE typically refers to sACE. However, in the year 2000, a homolog of sACE (ACE-2) was discovered [Donoghue et al., 2000; Tipnis et al., 2000]. As a consequence, since then further discrimination is made between ACE from the traditional RAAS, i.e., sACE and ACE-2, which is associated with a counter-regulatory axis of RAAS (see below, **Figure 1-8**).

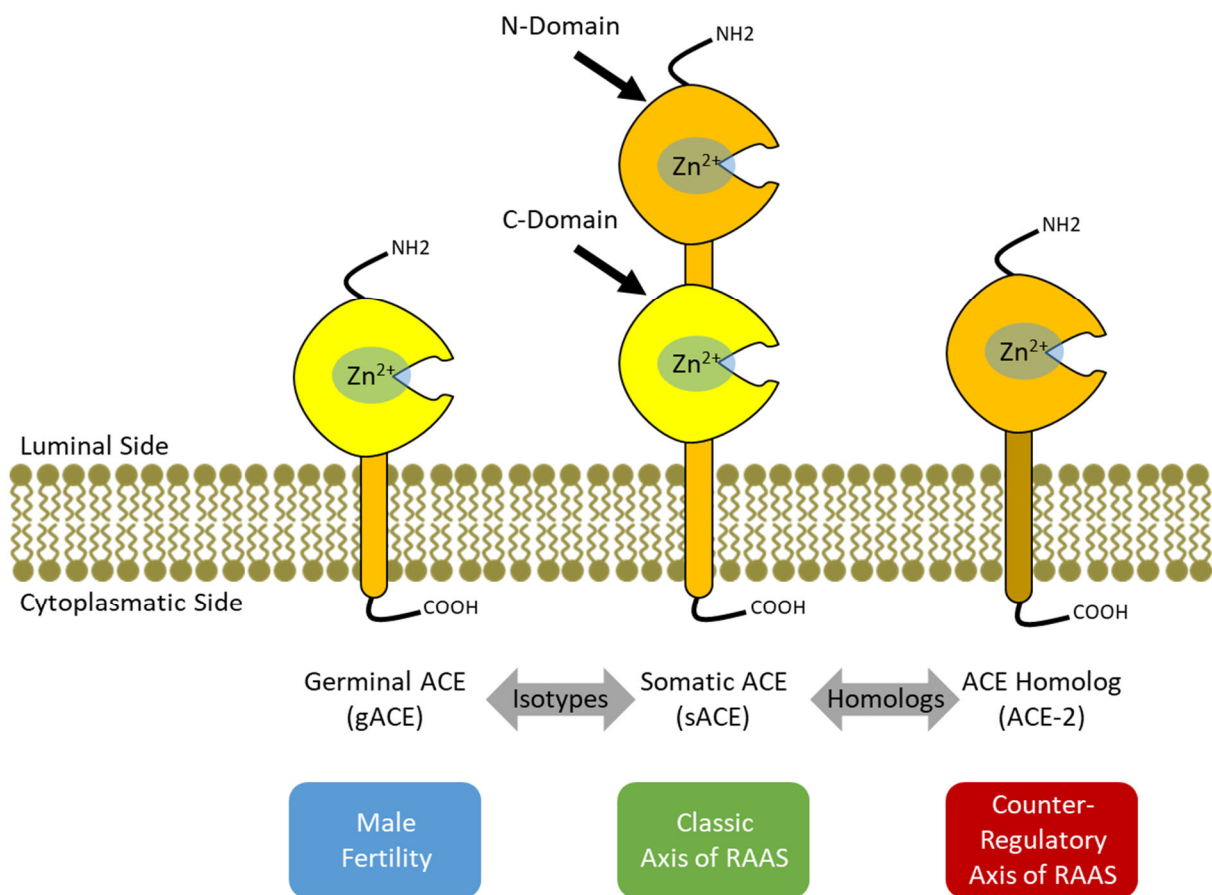


**Figure 1-8:** Schematic representation of membrane anchored angiotensin I-converting enzyme (ACE) variants. Apart from the widespread somatic variant (sACE), ACE also exists in a germinal (gACE) and a homologous (ACE-2) form. While ACE-2 counteracts sACE in its function within the renin-angiotensin-aldosterone system (RAAS), gACE is implicated in male fertility. In comparison, only sACE possesses two domains (C- and N-domain), each with a zinc-dependent active site. Homologous domains between the different ACE variants are marked by the same colour.

**Catalytic domains** The two sACE domains have a sequence identity of over 60% and sequence similarity of up to 80% within their catalytic site, yet they have different biophysical and biochemical properties. For instance, the N-domain is far more resistant to both heat and hydrolysis than the C-domain and both domains are similarly efficient in degrading bradykinin [Georgiadis et al., 2003; Sturrock, Danilov & Riordan, 1997]. In general, the affinity of ACE for bradykinin is higher than that for Ang I, however, other peptides such as substance P or hypothalamic proteins may also be cleaved [Jaspard, Wei & Alhenc-Gelas, 1993]. Between the ACE variants, domain homology is quite variable. Specifically, the C-domain of sACE and the single domain of gACE share high sequence identity, but this is not surprising since both isozymes are coded by the same gene on chromosome 17, though different exons are involved during transcription. In contrast, there is less homology between the N-domain of sACE and the single domain of ACE-2, reaching up to 40% sequence identity, since a different gene located on chromosome X codes for ACE-2 [Riordan, 2003; Tipnis et al., 2000].

**Counter-regulatory axis** Unlike sACE, ACE-2 exhibits monoamidyl carboxypeptidase activity, in other words, only one amino acid is cleaved from the carboxyl-terminal end of its substrate. Bradykinin cannot be cleaved by ACE-2, whereas Ang I is converted into Ang 1-9 through cleavage of leucine. Furthermore, ACE-2 converts Ang II into Angiotensin 1-7 through the carboxyl-terminal cleavage of phenylalanine (**Figure 1-9**), but unlike Ang 1-9, only Ang 1-7 is biologically active and mediates its vasodilator and antiproliferative effects through the Mas receptor [Oudit & Penninger, 2011]. Moreover, common ACE inhibitors such as captopril, lisinopril, or enalapril fail to inhibit ACE-2 [Tipnis et al., 2000]. Especially since 2019, ACE-2 research has gained momentum due to the global outbreak of the coronavirus disease (COVID-19) caused by severe acute respiratory syndrome coronavirus 2 (SARS-CoV-2). It has been proposed that SARS-CoV-2 utilizes ACE-2 as the point of entry into host cells and thereby possibly impairs the counterregulatory pathway of RAAS. Thus, during the course of infection with SARS-CoV-2, a disturbed balance between ACE and ACE-2 may trigger the various symptoms that could be related to the RAAS and its overactivation by the ACE/Ang II axis [Wiese, Allwood & Zemlin, 2020].

**ACE/Ang II axis** In particular, the ACE/Ang II axis plays an important role within the regulatory hormonal systems of RAAS and KKS. As such, the influence of ACE extends to long-term (month to years) cardiac and vascular remodelling processes as well as short-term (hours) adjustments in hemodynamic processes and in the control of renal fluid and salt retention [Navar, 2014]. ACE produces these effects mainly through formation or inactivation of vasoactive peptides, by cleaving a carboxyl-terminal dipeptide sequence from

the precursor peptide Ang I to yield Ang II (**Figure 1-9**), as well as by degrading kinins such as bradykinin and kallidin into inactive peptides (**Figure 1-5**). Moreover, other signalling peptides such as substance P, neurotensin, dynorphin A and enkephalin that play a role in pain perception and inflammation may also be degraded by ACE [Lopez-Sublet et al., 2018]. Ang II and kinins are potent physiological peptide hormones whose dysregulation by ACE may be a cause of cardiovascular disease [Harrison & Acharya, 2014]. The pathophysiological effects mediated by Ang II are particularly associated with vascular and cardiac remodelling processes that may lead to or exacerbate cardiovascular diseases such as hypertension and heart failure. Although the number of these diseases has steadily declined over the decades, cardiovascular events are still responsible for about 40% of all deaths in Germany [Schmitz et al., 2012]. With increasing knowledge about RAAS and its contribution to cardiovascular diseases, the demand for pharmacological approaches to intervene in this system has increased.

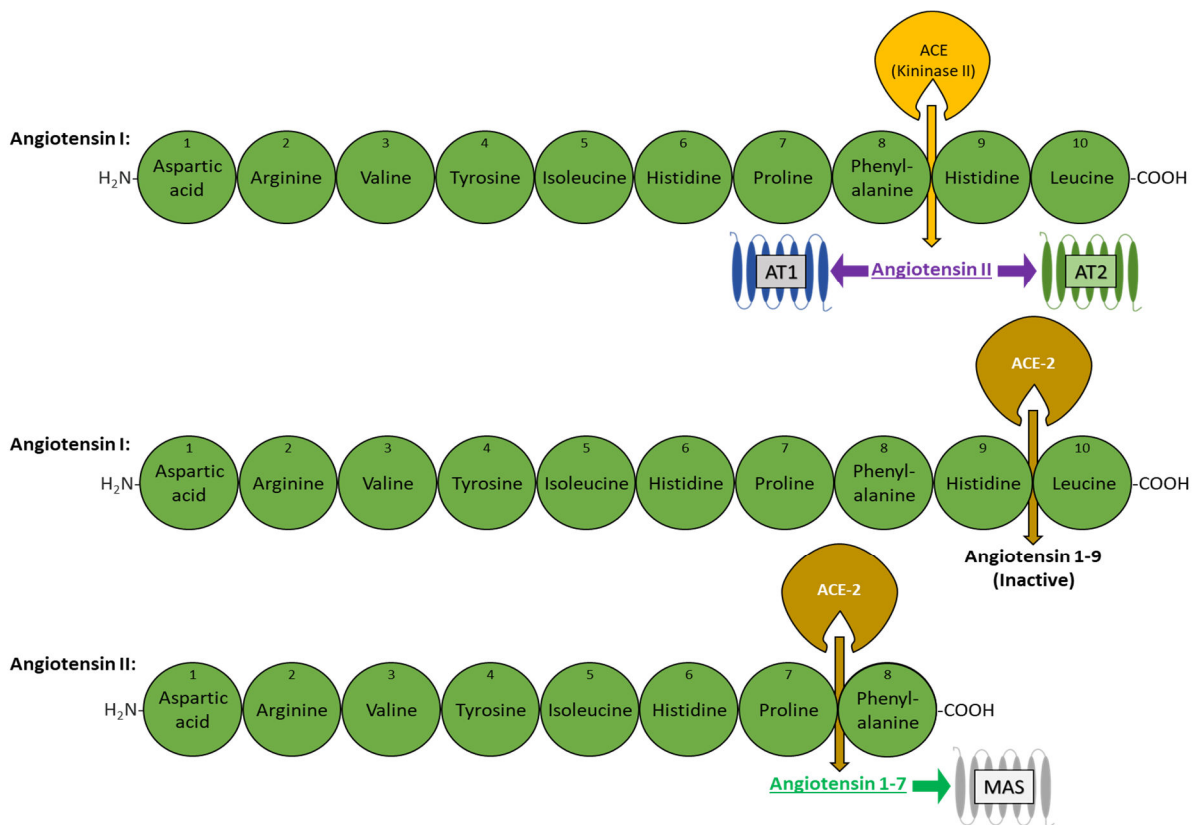


**Figure 1-9:** Angiotensin I-converting enzyme (ACE, also: kininase II) cleaves a carboxyl-terminal dipeptide sequence from the decapeptide precursor angiotensin I (top) to obtain the octapeptide angiotensin II (bottom), which exerts its biological effects through angiotensin II receptor type 1 (AT1) and type 2 (AT2). The ACE homolog (ACE-2) cleaves one amino acid at the carboxyl-terminal end of angiotensin I (middle) or angiotensin II (bottom) to produce angiotensin 1-9 or angiotensin 1-7, respectively. The latter cleavage product is biologically active and exerts its effects through the Mas receptor (MAS).

### 1.3.2. Angiotensin II receptors

The effects of Ang II are mediated by its two receptors angiotensin II receptor type 1 (AT1) and type 2 (AT2). Both receptors are GPCRs with seven transmembrane domains and share approximately 34% sequence homology. In humans, the gene encoding AT1 is located on chromosome 3, whereas the gene encoding AT2 is located on chromosome X. Angiotensin receptors are expressed in wide variety of tissues and organs, including endothelial cells, vascular smooth muscle cells (VSMC), the heart, brain and kidney. Similarly, AT2 receptors are ubiquitously detectable with a strikingly high expression level during prenatal development as well as under inflammatory conditions. However, AT2 expression decreases markedly after birth and remains at a low level in healthy tissue when compared to AT1. For this reason, AT1 is thought to be more important for physiological processes in adulthood, and AT2 is thought to be more important for fetal and early childhood development, and thereafter comes back into play during pathological processes [de Gasparo et al., 2000]. Interestingly, two isoforms of AT1 exist in rodents, which are termed AT1a and AT1b. These receptor subtypes show high homology (>92%) with human AT1, are expressed to varying degrees in different tissues and functionally indistinguishable. While AT1a has been detected in tissues of the vasculature, heart, kidney, lung, liver, and the brain, the AT1b receptor is more abundant in the adrenal gland and in certain regions of the central nervous system where it is involved in the cognitive functions [Cosarderehlioglu et al., 2020; Yamasaki et al., 2020].

**AT1 signalling** To date, research has largely focused on the AT1 receptor, for which multiple signalling pathways have been described. These signalling pathways are partially complex and may overlap with other intracellular signalling cascades responsible for various short- and long-term effects at the cellular level. In the following, a rough overview of the diverse signal transduction pathways of AT1 will be given, that may explain both the physiological and deleterious effects of the classic RAAS (**Figure 1-10**). By increasing intracellular calcium or inhibiting cAMP formation, most of these signalling pathways act on the contractile apparatus of smooth muscle cells, and cause short-term constriction. At the same time, phosphorylation cascades, the formation of certain eicosanoids, and transcriptional events mediate mid- to long-term effects, such as inflammation and remodelling processes within the affected tissue [Dinh et al., 2001]. Activation of AT1 by Ang II triggers specific signalling cascades that may vary depending on tissue type and coupled G-alpha subunit, i.e., Gq, Gi/o, G12, and G13 [de Gasparo et al., 2000]. For instance, vasoconstriction and remodelling processes are commonly associated with the activation of Gq-coupled AT1 receptors. The coupling of AT1

to G12/13 subunits is associated with the regulation of cell mortality, whereas Gi/o coupled AT1 receptors are known to mediate the production of NO and prostaglandins. Moreover, AT1 is implicated in complex signalling processes of the mitogen-activated protein kinase (MAPK) family, e.g., PKC-dependent transactivation of the epidermal growth factor (EGF) receptor [Forrester et al., 2016]. Activation of the EGF receptor was further shown to be implicated in the production of vascular nicotinamide adenine dinucleotide phosphate (NADPH) oxidase-derived reactive oxygen species (ROS), that play a significant role in cell proliferation and regulation of vascular tone [Seshiah et al., 2002]. Strikingly, AT1 is capable of activating signalling pathways that are independent of G-proteins. For example, direct activation of  $\beta$ -arrestin has been described, which among other cellular events is associated with receptor desensitization, uncoupling of G-proteins, and receptor recycling [Shukla, Xiao & Lefkowitz, 2011]. Similarly, in vascular smooth muscle cells, a direct interaction of the AT1 receptor-associated protein (ATRAP) with the carboxyl-terminus of AT1 was found to promote receptor internalization [Cui et al., 2000]. Other direct interactions with proteins may also involve the non-receptor tyrosine kinase Janus kinase 2 (JAK2) [Ali et al., 1997] and the cell-growth factor PLC- $\gamma$ 1 [Venema et al., 1998]. Furthermore, the AT1 receptor may interact with other receptors to form functional heterodimers. One such case is the interaction between AT1 and  $\beta$ -adrenergic receptors resulting in constitutive activation of the affected receptors [Barki-Harrington, Luttrell & Rockman, 2003]. While an enhancement of Gq- and Gi/o-mediated signalling was observed in the case of heterodimerization involving AT1 and B2 [AbdAlla, Lother & Quitterer, 2000], an inhibitory effect on AT1 signalling was observed in heterodimers composed of AT1 and Mas or AT1 and AT2 [AbdAlla et al., 2001; Kostenis et al., 2005]. It is thought that, depending on the organ and receptors involved, heterodimerisation may play an important role in pathological processes, such as heterodimerisation between AT1 and the adrenergic  $\alpha$ -1D receptor in the development of pre-eclampsia [Gonzalez-Hernandez Mde et al., 2010].

**AT2 Signalling** The Ang II/AT2 axis, similar to the Ang1-7/Mas axis, is thought to have a protective function that counteracts the effects of the Ang II/AT1 axis. As such, AT2 signalling has been associated with smooth muscle relaxation and various beneficial impacts on the cardiovascular system, including antihypertensive, anti-proliferative, and anti-inflammatory effects. However, the underlying molecular mechanisms remain poorly understood [Berk, 2003; Patel et al., 2020]. It has already been described that AT2 couples to Gi/o, however the typically related second messenger cAMP was not found to be decreased [Hansen et al., 2000].

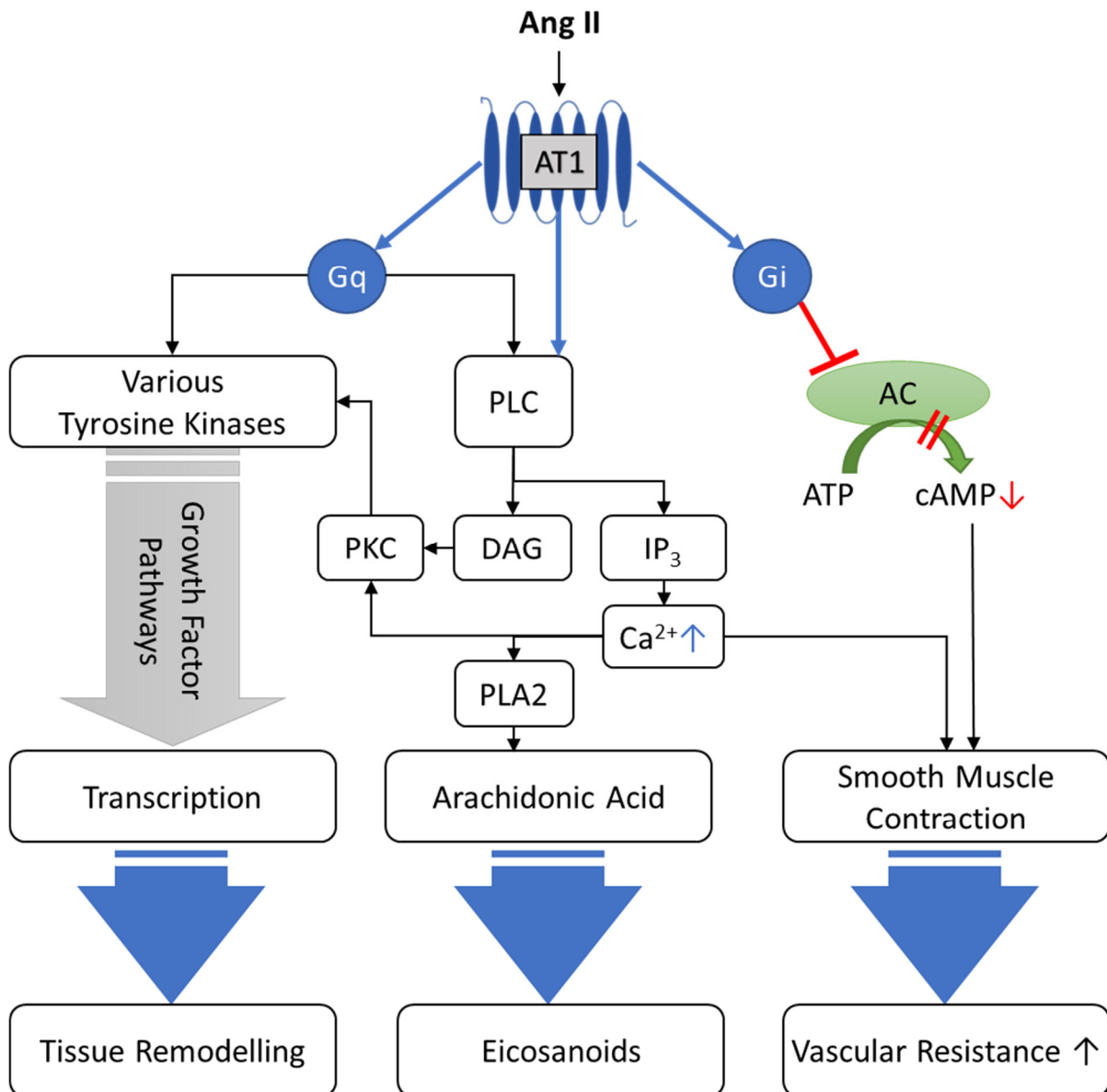


**Figure 1-10:** A simplified representation of the Angiotensin II (Ang II) receptor type 1 (AT1) signal transduction pathways. Once activated, the AT1 receptor can interact either through Gq/11 alpha subunit (Gq), Gi/o alpha subunit (Gi) or directly with proteins such as phospholipase C (PLC) and initiate various signalling cascades associated with tissue remodelling processes, the formation of eicosanoids, and vasoconstriction. Adenylate cyclase (AC); adenosine triphosphate (ATP); cyclic adenosine monophosphate (cAMP); diacylglycerol (DAG); inositol 1,4,5-trisphosphate (IP<sub>3</sub>); protein kinase C (PKC); phospholipase A2 (PLA2).

AT1 and AT2 are structurally different in terms of the third intracellular loop and the carboxyl-terminal end. These structures are particularly important for the recruitment of the Gi/o protein. Although AT2 is classified as a GPCR, it does not utilize the signalling mechanisms typically associated with it. In general, activation of a GPCR leads to a characteristic conformational rearrangement of its transmembrane domains, a process that

facilitates the recruitment of an associated G protein. Yet upon activation, the conformational change of AT2 apparently leads to steric hindrance, which further impedes recruitment of the G protein [Zhang et al., 2017]. For instance, AT2 was shown to activate the protein tyrosine phosphatase SHP-1 without involvement of the Gi/o protein [Feng, Sun & Douglas, 2002], which was associated with inhibition of cell growth in neuronal cells [Li et al., 2007]. Several other phosphatases have been identified to be involved in the anti-proliferative and pro-apoptotic effects of AT2. In cultured rat pheochromocytoma cells with high AT2 expression, activation of AT2 induces apoptosis through MAPK phosphatase-1 inhibiting the cell survival factor Bcl-2 [Horiuchi et al., 1997], and depending on the expression level, AT2 has been shown to induce ligand-independent apoptosis in fibroblasts, epithelial cells, and VSMC, which is mediated through constitutive activation of p38 MAPK and cysteine aspartic protease-3 pathways [Miura, Karnik & Saku, 2005]. Moreover, AT2 activation induces the serine-threonine phosphatase PP2A, which delays opening rectifying K<sup>+</sup>-channels of neuronal cells, leading to hyperpolarization of plasma membranes with subsequent suppression of cellular activities that would be stimulated by depolarization [Huang, Richards & Summers, 1995]. Nevertheless, this atypical GPCR participates in several intracellular signalling pathways, that in part may inhibit AT1 signalling (**Figure 1-11**). For instance, the activation of an inhibitory pathway through protein tyrosine phosphatases (e.g., SHP-1) interrupts the cascade of extracellular signal-regulated kinases (ERKs) that are crucial for cellular processes such as growth and division. On top of that, AT2 is capable of inducing vasodilation through activation of the NO-cGMP system. This occurs indirectly either by promoting the formation of bradykinin, which then activates B2, or by heterodimerization with the latter, which also leads to its activation. Alternatively, AT2 may also directly activate eNOS and thus promote the formation of NO, which in turn leads to vasodilation in smooth muscle cells [Azushima et al., 2020]. In addition, AT2 signalling may influence local inflammation and cell function through activation of PLA2 and subsequent formation of arachidonic acid. Apart from the downstream generation of various eicosanoids that act as paracrine and autocrine mediators [Calder, 2020], the sodium/bicarbonate symporter is activated in cardiac tissues, regulating the intracellular pH within cardiomyocytes through alkalinization. This is an important process for cellular homeostasis, particularly after myocardial infarction [Kohout & Rogers, 1995; Sandmann et al., 2001].

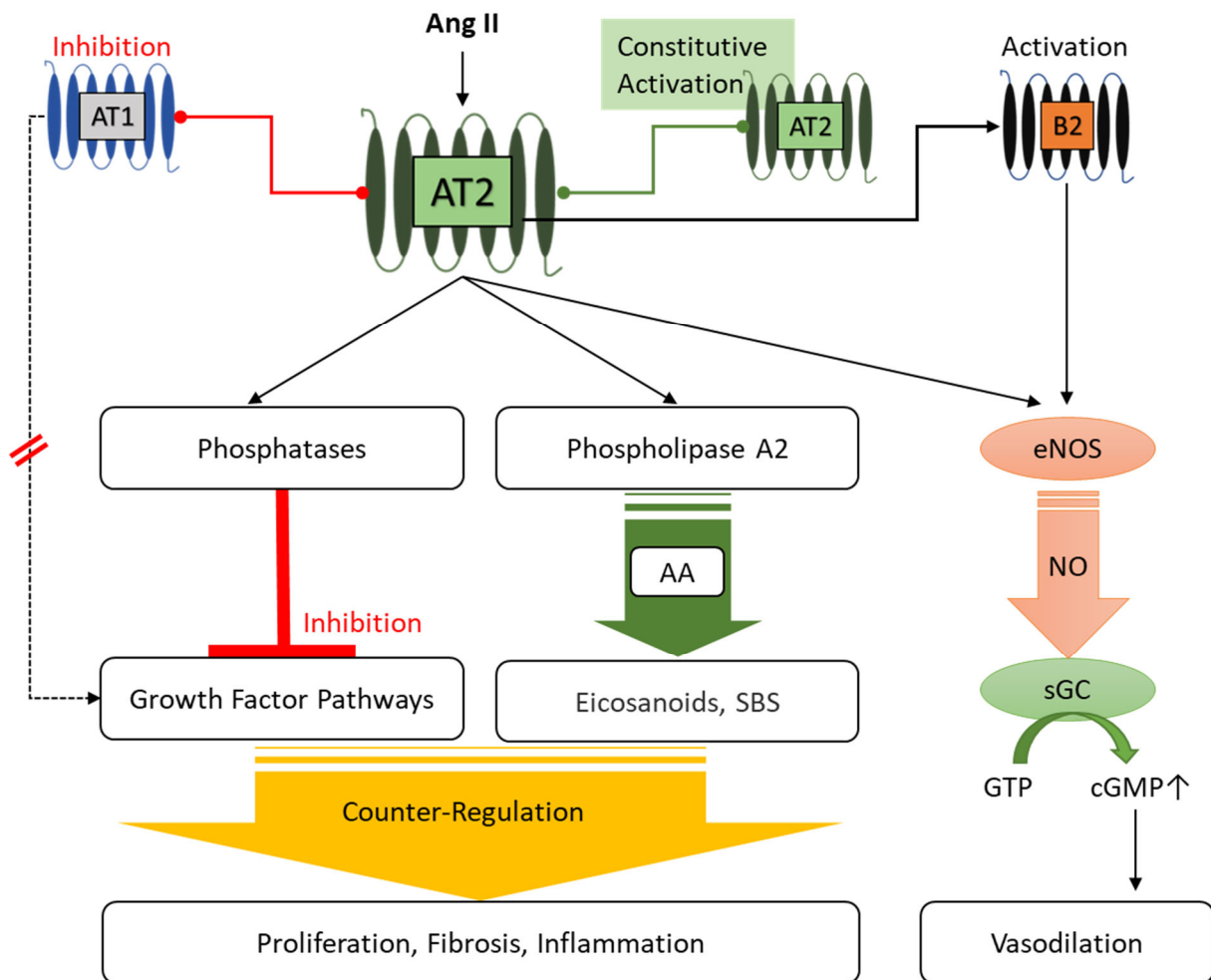


**Figure 1-11:** A short representation of the Angiotensin II (Ang II) receptor type 2 (AT2) signal transduction pathways. AT2 may form functional dimers with other receptors such as Ang II receptor type 1 (AT1), AT2, or bradykinin receptor type 2 (B2), thereby either antagonizing AT1, constitutively activating AT2, or triggering B2 activation. Binding of Ang II to AT2 may initiate distinct signalling pathways. While phosphatases intervene in growth factor pathways, phospholipase A2 releases arachidonic acid (AA) from membrane lipids. Downstream, various paracrine and autocrine active eicosanoids are synthesized, while in cardiac tissues sodium/bicarbonate symporters (SBS) are activated for pH regulation. These mechanisms are responsible for the antiproliferative, anti-fibrotic and anti-inflammatory effects of AT2. In addition to indirect B2 activation, AT2 is also capable of inducing vasodilation through direct activation of endothelial nitric oxide (eNOS). Nitric oxide (NO) generated by eNOS activates soluble guanylate cyclase (sGC) which in turn converts guanosine triphosphate (GTP) into cyclic guanosine monophosphate (cGMP). The increase in cGMP causes relaxation in smooth muscle cells.

Another characteristic of AT2 is its ability to dimerize with other receptors, including B2, Mas, AT1 or another AT2 receptor. While heterodimerization with AT1 antagonizes the latter [AbdAlla et al., 2001], homodimerization with another AT2 results in constitutive activation of AT2 [Miura, Karnik & Saku, 2005]. Similarly, heterodimer formation between the AT2 and Mas receptors, both of which mediate similar effects, constitutively activates the respective receptors [Leonhardt et al., 2017], and in the case of dimerization between AT2 with B2 there is an enhanced formation of NO and cGMP [Abadir et al., 2006].

Remarkably, overall ACE activity in mice deficient of AT2 is significantly increased [Hunley et al., 2000], whereas in cultured human endothelial cells, AT2 stimulation leads to a reduction of ACE activity to approximately half of the basal level [Dao et al., 2016]. These findings indicate that AT2 is involved in modulation of ACE activity, which may involve shedding of membrane-bound ACE [Iwata & H. Greenberg, 2011; Parkin, Turner & Hooper, 2004]. Taken together, the AT2 signalling pathway is thought to have protective effects on various organs and the cardiovascular system that are rather in contrast to the effects of AT1. However, due to the predominance of the AT1/Ang II axis, some effects of AT2, such as blood pressure reduction, are likely to be negligible [McFall, Nicklin & Work, 2020].

## 1.4. Aim of the study

Non-allergic angio-oedema is caused by swelling of mucosal and submucosal tissue at various sites and can be potentially life-threatening when manifested as a laryngeal oedema. Based on the underlying molecular mechanism, non-allergic angio-oedema can be divided into different subtypes. In the majority of cases, the involvement of bradykinin and the overactivation of its receptor has been shown to be critical for the development of non-allergic angio-oedema [Bas et al., 2007].

Often, when patients cannot tolerate ACE inhibitors, they are switched to ARBs, albeit a certain risk of developing angio-oedema remains [Sica & Black, 2002]. It is widely accepted that ACE inhibitors may increase the risk of angio-oedema due to impaired bradykinin degradation [Nussberger et al., 1998; Pellacani, Brunner & Nussberger, 1994]. Furthermore, clinical trials with the B2 blocker icatibant in patients under ACE inhibitor therapy demonstrated that B2 activation contributes to both blood pressure reduction [Gainer et al., 1998] and the development of angio-oedema [Bas et al., 2015a]. In contrast, the underlying pathophysiology of ARB-induced angio-oedema is less well understood and there is no rationale for a potentially effective treatment. Nevertheless, there is evidence from a clinical trial suggesting that the ARB losartan increases bradykinin levels in hypertensive patients due to reduced bradykinin degradation [Campbell, Krum & Esler, 2005]. Current evidence suggests that treatment with the ARBs likely leads to increased AT2 activation due to elevated Ang II levels. The downstream signalling might inhibit ACE-mediated bradykinin degradation [Dao et al., 2016; Hunley et al., 2000], leading to increased bradykinin concentrations along with enhanced stimulation of B2 which might be a factor triggering angio-oedema.

The aim of this project is to shed some light on the still unknown pathomechanism of ARB-induced angio-oedema. Focus is placed on the following research questions, which are discussed in conjunction with the findings from conducted experiments and the current state of research:

**Does activation of AT2 receptor contribute to non-allergic bradykinin-induced angio-oedema, in particular ARB-induced angio-oedema?**

**Is the AT2 receptor capable of modulating ACE activity?**

**What role might COX metabolites play in B2-mediated extravasation?**

## 2. Materials and Methods

### 2.1. Buffers and solutions

Chemicals and solvents, unless stated otherwise, were purchased from the companies Carl Roth (Karlsruhe, Germany), Merck (Darmstadt, Germany) or Sigma-Aldrich (Munich, Germany). All aqueous solutions, e.g., buffers, were made using double distilled water from the lab's water still (GFL, Burgwedel, Germany).

#### **Assay buffer for ACE activity, pH 8.3**

300 mM	NaCl,
0.1 mM	ZnCl <sub>2</sub> ,
2.3 mM	FAPGG,
50 mM	Tris.

#### **Bead buffer, pH 7.4**

0.1%	bovine serum albumin,
2 mM	sodium citrate diluted,
dissolved in phosphate-buffered saline.	

#### **Blood-sampling buffer, pH 4.5**

67 mM	citric acid,
100 mM	trisodium citrate,
400 µg/ml	hexadimethrine bromide,
263 µM	leupeptin,
20 mM	AEBSF,
2.0 mg/ml	soybean trypsin inhibitor,
100 mM	benzamidine,
30 I.E.	heparin.

#### **Bradford reagent, for protein quantification**

0.02%	Coomassie Blue G-250,
10%	phosphoric acid,
5%	ethanol.

#### **Bromophenol blue solution**

0.005%	bromophenol blue,
30%	glycerol.

#### **Cell lysis buffer**

10 µM	ZnCl <sub>2</sub> ,
200 µM	PMSF,
0.1%	Triton X-100.

**Krebs-Hepes buffer (KHB), for organ preparations**

99.0 mM	NaCl,
4.69 mM	KCl,
1.87 mM	CaCl <sub>2</sub> ,
1.20 mM	MgSO <sub>4</sub> ,
25.0 mM	NaHCO <sub>3</sub> ,
1.03 mM	K <sub>2</sub> HPO <sub>4</sub> ,
20.0 mM	Na-Hepes,
11.1 mM	D-glucose.

**Laemmli buffer (two-fold), pH 6.8**

4%	SDS,
20%	Glycerol,
10%	2-Mercaptoethanol,
0.004%	Bromophenol blue,
125 mM	Tris.

**Organ bath buffer (modified Krebs-Henseleit buffer), pH 7.4**

118.07 mM	NaCl,
4.70 mM	KCl,
1.60 mM	CaCl <sub>2</sub> ,
1.18 mM	MgSO <sub>4</sub> ,
25.0 mM	NaHCO <sub>3</sub> ,
1.18 mM	K <sub>2</sub> HPO <sub>4</sub> ,
5.55 mM	D-glucose,

Continuous aeration by Carbogen (5% carbon dioxide and 95% oxygen) for pH adjustment.

**Phosphate-buffered saline (PBS), pH 7.4**

140 mM	NaCl,
2.7 mM	KCl,
10 mM	Na <sub>2</sub> HPO <sub>4</sub> ,
1.8 mM	KH <sub>2</sub> PO <sub>4</sub> .

**Protease inhibitor cocktail (PIC)**

1.5 mM	E-64,
1 mM	pepstatin A,
2 mM	leupeptin,
5 mM	bestatin,
80 mM	aprotinin,
100 mM	AEBSF.

**Separation-gel buffer (four-fold), pH 8.8**

0.4%	SDS,
1.5 M	Tris.

**Stacking-gel buffer (four-fold), pH 6.8**

0.4%	SDS,
500 mM	Tris.

**TAE buffer, pH 8.0**

40 mM	Tris,
0.1%	acetic acid,
10 mM	EDTA.

**Tail lysis buffer, pH 8.0**

50 mM Tris,  
100 mM EDTA,  
100 mM NaCl,  
1% SDS.

**Tank-buffer for SDS-PAGE (ten-fold)**

1% SDS,  
250 mM Tris,  
1.90 M Glycine.

**TE-buffer, pH 8.0**

10 mM Tris,  
1 mM EDTA.

**Tissue-lysis buffer, pH 7.6**

50 mM Tris,  
1 mM EDTA,  
1 mM EGTA,  
150 mM NaCl,  
25 mM glycerol 2-phosphate,  
1 mM PMSF  
1% Triton X-100,  
addition of 50  $\mu$ l protease inhibitor cocktail for each gram of tissue.

**Transfer-buffer for western blot (ten-fold)**

250 mM Tris,  
1.9 M Glycine,  
20% Methanol.

**Trypsin/EDTA solution for cell dissociation, pH 8.0**

40 mM Tris,  
0.1% acetic acid,  
10 mM EDTA.

**Vehicle solution, pH 7.4**

0.5% Methylcellulose  
0.2% Tween 80  
Diluted in phosphate-buffered saline.

## 2.2. Cell culture

For in-vitro studies, human dermal microvascular endothelial cells (HDMECs) were obtained from Promo Cell (Heidelberg, Germany). These primary cells were isolated from the breast skin of a 47-year-old female Caucasian donor.

**Cell culture maintenance and sub-culturing** Endothelial cells were seeded following the manufacturer's instruction and kept in an incubator operated at 37°C and 5% carbon dioxide, receiving endothelial cell growth medium MV (Promo Cell, Heidelberg, Germany) which contained fetal calf serum (5%), endothelial cell growth supplement (0.4%), epidermal growth factor (0.01%), heparin (9%) and hydrocortisone (0.1%). Cells were allowed to adhere to the cell culture flask until the next day and the growth medium was then changed to remove non-adherent cells. Fresh supplement was provided every second or third day, depending on microscopic observations and growth performance. Cells were sub-cultured once confluency exceeded 80%. For this, cells were washed with calcium- and magnesium-free phosphate-buffered saline (Thermo Fisher, Wesel, Germany) then dissociated using Trypsin/EDTA solution. After counting the cells using a counting chamber, the appropriate size and number of flasks for reseeding in fresh growth medium was calculated.

**Cell incubation and lysate preparation** Sub-cultures of passage numbers five to ten with a confluence of more than 80% were incubated in phenol red- and serum-free basal medium (Promo Cell, Heidelberg, Germany) with the addition of various pharmacological substances at a final concentration of 100 µM for 1 hour (**Table 2-1**).

Substance	Target protein	Action
Captopril	ACE	Inhibition
Telmisartan	AT1	Inhibition
Compound 21	AT2	Activation
PD123319	AT2	Inhibition

**Table 2-1:** Substances and their pharmacological targets used for cell incubations.

Following the incubation procedure, the cells were washed with phosphate-buffered saline (PBS), then covered with chilled cell lysis buffer and scraped with a cell spatula. The cell suspension obtained was transferred to test tubes and stored on ice. Afterwards, the samples were shock frozen in liquid nitrogen and homogenized in a cold room by sonification. Finally, cell debris was removed in a further step by centrifugation (13000xg) for 15 minutes.

## 2.3. Laboratory mice

All animal experiments described in this work have been approved by the ethics committee of the district government (LANUV) in Düsseldorf (reference number: 81-02.04.2018.A354 and 84-02.04.2016.A114) and are in accordance to article 8 of the German Animal Welfare Act (“Tierschutzgesetz”) in its version of 20th November, 2019. For experimental use, inbred laboratory mouse strains such as C57BL/6 and FVB/N were purchased from the rodent breeding company Janvier Labs (Le Genest-Saint-Isle, France) and delivered to the local animal facility (ZETT, UKD Düsseldorf, Germany), where also the colony of the AT2 knockout mouse was housed and bred. Keeping and breeding conditions were in positive pressured rooms operated at 20°C with a 55±5% relative humidity and circadian lighting control. Mice were regularly supervised by veterinarians and received standard mouse chow as well as acidified drinking water (pH 3) ad libitum. Only male mice between 10 and 12 weeks of age with a bodyweight between 20 and 25 grams were used for the experiments. Additionally, imported mice were given at least one week to acclimatise to their new environment before being included in an experiment. Female mice were excluded from all experiments to avoid the effects of the oestrous cycle.

### 2.3.1. AT2 deficient mouse (AT2<sup>-y</sup>)

In rodents and humans, the AT2 gene is located on chromosome X and codes for the AT2 receptor. Human and murine AT2 share a high sequence homology of over 90% [Lazard et al., 1994]. The disruption of the coding sequence for AT2 and the generation of the AT2 knockout mouse to study the function of AT2 have already been described [Hein et al., 1995; Ichiki et al., 1995]. A chimeric mouse was created from mouse embryonic stem cells (derived from 129/Sv mice) with disrupted AT2 gene. The gene disruption was achieved using a targeting vector containing the neomycin resistance gene for positive selection and a suicide gene for negative selection. Eventually, the offspring with desired recombination event had their AT2 coding sequence in Exon 3 disrupted through insertion of the neomycin-resistance gene. These Knockout mice were bred from a cross of 129/S0v and FVB/N strains backcrossed to FVB/N for at least ten generations. The colony was further maintained by breeding between homozygous female (-/-) and hemizygous male (-/y) knockout mice. Only the male hemizygous (-/y) AT2 knockout (AT2<sup>-y</sup>) was used for experiments and male FVB/N were used for control experiments.

Moreover, an additional strain was generated with the genetic background changed to C57BL/6 by backcrossing the AT2<sup>-y</sup> to C57BL/6J mice for at least ten generations. While initial experiments with FVB/N mice using the Miles assay technique proved unsuitable, this new background allowed comparative studies with C57BL/6 mice.

### 2.3.2. Genotyping

For successful breeding as well as identification of the appropriate genotype for research studies, a genotyping method was required. Genomic mouse DNA was obtained by collecting distal tail tissue from 3 weeks old supposedly AT2 deficient mice, then related DNA-sequence was extracted and amplified utilizing the polymerase chain reaction (PCR) method. The result was visualized through gel electrophoresis.

The following protocol for DNA extraction from tail tissue was applied:

1. Overnight digestion at 60°C in 750 µl tail lysis buffer containing proteinase K (0.5 µl/ml; Qiagen, Hilden, Germany).
2. Addition of 6 M NaCl, shaking for 20 times, then incubation on ice for 10 minutes.
3. Centrifugation step (16,000xg at 4°C for 15 minutes).
4. Supernatant is incubated with chilled ethanol at -20°C for 30 minutes.
5. Centrifugation step (16,000xg at 4°C for 30 minutes).
6. sample is inverted and allowed to air dry on the laboratory bench, then the pellet is resuspended in 80 µl TE buffer and dissolved overnight.
7. Detection of DNA content at 260 nm wavelength with Biophotometer® (Eppendorf, Hamburg, Germany) and subsequent determination of DNA purity, i.e., the ratio of the absorbance at 260 nm divided by the reading at 280 nm. For DNA samples, a ratio of approximately 1.8 is accepted as pure.
8. If not for immediate use, samples are stored at -20°C.

PCR was carried out using a universal Taq PCR Master Mix Kit (Qiagen, Hilden, Germany) and three primers, as described below (**Table 2-2**).

Primer	Orientation	Primer sequence	Binding sequence
AT23	Reverse	5'- GAACTACATAAGATGCTTGCCAGG -3'	Coding sequence (CDS) for AT2
AT25	Forward	5'- CCACCAGCAGAAACATTACC -3'	
NeoPVU	Forward	5'- GGCAGCGCGGCTATCGTGG -3'	Neomycin cassette within CDS of AT2

**Table 2-2:** Selected primers with their sequences and DNA binding sequences for PCR.

Following thermocycler conditions were applied for PCR:

1. Initial denaturation at 95°C for 3 minutes.
2. Denaturation at 94°C for 1 minute and 10 seconds.
3. Annealing at 60°C for 1 minute and 15 seconds.
4. Elongation at 72°C for 1 minute and 7 seconds.
5. Repetition of steps 2 to 4 for 35 times
6. Final elongation at 72°C for 5 minutes.
7. Cooling down to 4°C until further processing of samples.

To separate and evaluate DNA-samples, agarose gel electrophoresis was performed. Briefly, a 2% agarose gel was cast by heating agarose powder in TAE buffer until completely dissolved, with the addition of GelRed™ (10.000x stock; Biotium Inc., Hayward, CA, USA) for gel-staining. PCR samples and a 100 bp DNA ladder (Thermo Fisher, Schwerte, Germany) were stained 1:1 with bromophenol blue solution (0.005% bromophenol blue and 30% glycerol dissolved in distilled water) and each loaded into the gel's pre-cast wells. Then Electrophoresis was started inside a Bio-Rad chamber (Bio-Rad, Munich, Germany) with the gel immersed in TAE buffer and an electric potential of 90 voltage applied for 30 min.

The separated DNA was visualised under UV light and matched against a DNA standard as well as positive and negative controls from previous genotyping. Amplification products from the primers AT23 and AT25 delivered a band at 500 bp while those from AT23 and NeopVU showed a band at 700 bp (**Table 2-3**).

Genotypes	Amplification products (approximates)
homozygous female (-/-)	700 bp
hemizygous male (-/y)	700 bp
heterozygous female (-/+)	500 bp and 700 bp
wildtype (+/+)	500 bp

**Table 2-3:** The genotypes of the AT2 knockout mouse and corresponding amplification products, expressed as the number of base pairs (bp).

### 2.3.3. Anaesthesia and euthanasia procedures

In mice, anaesthesia was induced by intraperitoneal co-injection of ketamine and xylazine (100:5 mg/kg bodyweight), which lasted approximately 60 minutes and was sufficient for all related in-vivo experimental procedures described in this work.

Mice were euthanized either before organ extraction or at the end of an in-vivo experiment. The procedures chosen for euthanasia were the most humane methods recommended by the American Veterinary Medical Association (AVMA) guidelines for the euthanasia of animals. Nevertheless, it was also necessary to choose a method that was compatible with the experimental requirements. For instance, cervical dislocation as a euthanasia method would not be suitable for extracting an intact aorta, but it was used for mice under anaesthesia. For this, the base of the mouse's skull was held down with a steel rod while the tail was rapidly pulled, which caused death by displacement of the cervical vertebrae. The alternative euthanasia method consisted of placing the mouse in a small gassing chamber and gradually replacing the air inside with carbon dioxide. Using this method, death occurred within two minutes due to respiratory arrest. The latter method was especially used for organ harvesting. In each case, death was confirmed by the absence of the corneal reflex.

### 2.3.4. Drug administration

Substances were administered locally by intradermal injection into the dorsal skin or systemically either by intraperitoneal injection or by tail vein access using a special catheter (**Figure 2-1**).

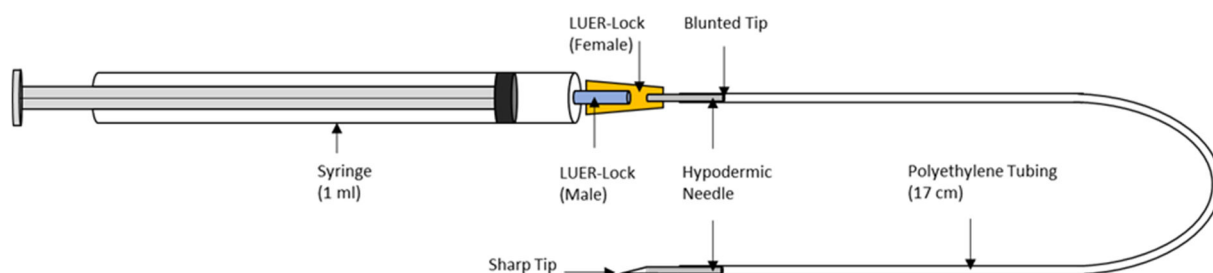


**Figure 2-1:** Schematic drawing of a self-built catheter for tail vein access.

The special catheter was built from a 1 ml syringe (Omnifix<sup>®</sup>-F.), two hypodermic needles (26 G, 0.45 mm x 12 mm, B. Braun, Melsungen, Germany) and a polyethylene tubing with an inner diameter of 0.38 mm (PORTEX<sup>®</sup>, Smiths Medical, Grasbrunn, Germany). Using forceps, the first hypodermic needle was bent apart from its LUER-lock while the second was clipped at the tip, then both were connected using a 17 cm long polyethylene tubing. This construct was mounted on a 1 ml syringe after being loaded with the appropriate volume. The dead volume of all components was calculated and taken into account in all applications.

### 2.3.5. Blood collection and organ harvesting

Mice were sacrificed prior to blood withdrawal or organ extraction with carbon dioxide and then attached to a thick Styrofoam plate using pins. The fur was sanitized with ethanol (70%) and the chest cavity cut open to expose the heart and the lungs.

**Preparation of plasma** The right ventricular was punctured for blood collection using a 0.45 x 12 mm needle attached to a 1 ml syringe that contained 80  $\mu$ l blood-sampling buffer [Suffritti et al., 2014]. A total of 800  $\mu$ l blood was collected through this method. The blood sample was gently inverted a few times and transferred into a chilled tube. To obtain the plasma fraction, the corpuscular fraction was spun down at 1000xg and the supernatant was subsequently spun down at 13,000xg to discard any remaining insoluble fractions. Plasma samples were kept on ice or frozen for later analysis.

**Irrigation of the circulatory system** After blood collection and prior to organ extraction, circulating blood was diluted with 10 ml chilled Krebs-Hepes buffer (KHB) to reduce clotting and blood content in all organs. For this the inferior vena cava was severed and KHB gradually injected into the left ventricular. The excess of circulating volume was ejected through the severed vena cava inferior and aspirated by a suction pump.

**Organ extraction** After irrigating the circulatory system, lung lobes were separated from their pulmonary arteries and briefly washed in KHB and transferred into test tubes for snap freezing. The heart was removed by cutting the remaining connecting vessels, which exposed the thoracic aorta (**Figure 2-2**). Finally, the thoracic aorta was excised successively with curved scissors starting from the aortic arch along the spine to slightly below the diaphragm. Special care was required when handling the aorta as overstretching and damage to the aorta resulted in poor functionality or loss of endothelium. Isolated organs were used either for functional organ bath studies or in incubation experiments to perform further biochemical analysis.

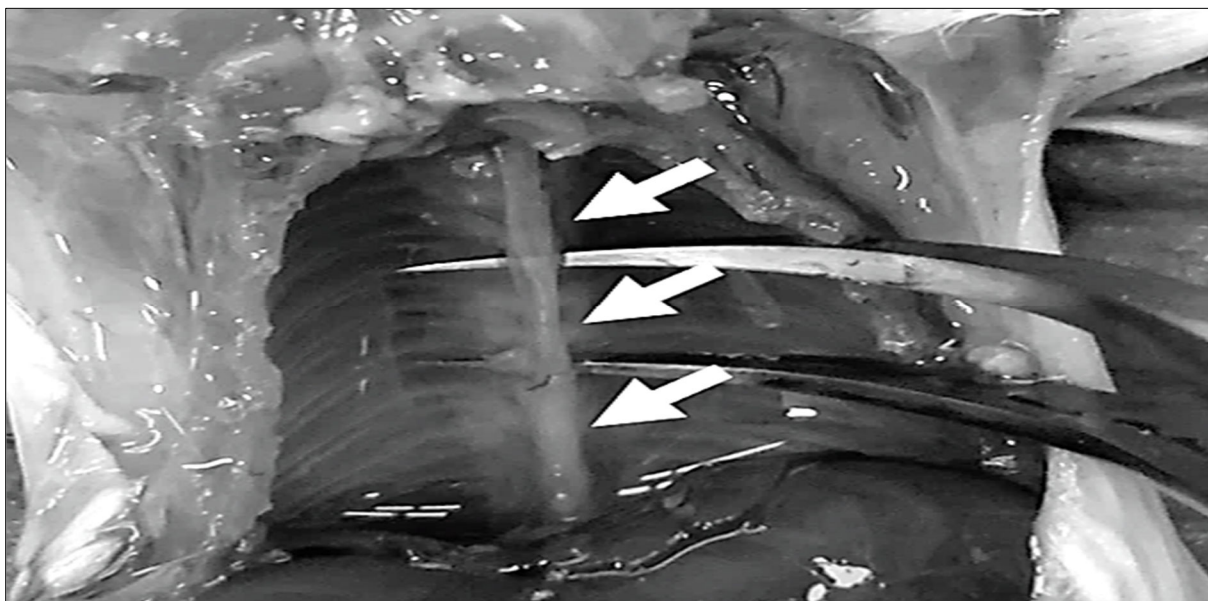


**Figure 2-2:** The thoracic aorta of a mouse (arrow markings).

**Preparation of organ lysates** At all stages of preparation, the samples were either chilled on ice or processed in a cold room. The sample of a snap-frozen organ was ground between two stainless steel plates, while the upper plate was slowly rotated and struck with a hammer at different positions. Then, the obtained powder was suspended in chilled tissue-lysis buffer and further processed in a Potter-Elvehjem Homogeniser. The yielded suspension was sonicated for 15 minutes and centrifuged at 13000xg for another 15 minutes. Lastly, the supernatant was aliquoted and stored at -80°C if no further analytical processing, e.g., Bradford assay, was scheduled.

## 2.4. Bradford's protein assay

Proteins concentrations from organ lysates and plasma samples were determined using the Bradford protein assay, named after Marion M. Bradford who developed this method [Bradford, 1976]. This assay is based on the dye Coomassie Brilliant Blue G-250 (Bio-Rad, Munich, Germany) that interacts with carboxyl groups of proteins and forms a protein-dye complex stabilizing its charged ionic form. In the process, a hypochromic shift from 470 nm to 595 nm is observed, whereby the reddish-brown hue of the dye shifts to a bluish hue. Hereby, a spectrometric quantification of a sample's total protein is made possible, since the increase in absorbance at 595 nm is directly proportional to the concentration of the dye-protein complexes formed. However, this linear relationship between absorbance and concentration is only valid within a certain concentration range as determined by a standard curve. Therefore, for each set of measurements, a calibration curve was prepared from standard protein solutions of bovine serum albumin (Sigma Aldrich, Munich, Germany) diluted in 5 mM Tris at pH 7.6, which yielded concentrations ranging from 10 µg/ml to 140 µg/ml. In addition, a dilution series was prepared for each sample with unknown protein concentration to ensure a measurement within the linear range of the calibration curve. Next, a mixture of 100 µl sample solution and 400 µl Bradford reagent was transferred to a polystyrene semi-microcuvette (Sarstedt, Nuremberg, Germany) and allowed to react for five minutes at room temperature. The absorption was measured at 595 nm using a spectrometer (DU 640 Spectrophotometer, Beckman, Krefeld, Germany).

## 2.5. Tail-cuff system

The tail-cuff system is a validated non-invasive method for measuring systolic blood pressure (SBP) and heart rate in conscious mice [Krege et al., 1995]. Based on the principle of the photoplethysmogram, a computer-assisted tail-cuff system (BP-2000 Blood Pressure Analysis System, Visitech Systems, Apex, USA) was used to collect data from four mice simultaneously. For the measurements, mice were placed on a heated plate (37°C) and secured by special tunnel-shaped holders while the tail was passed through an inflatable cuff and held in position with medical tape. Then a continuous beam of light was sent through a tail segment to a photoresistor, which relayed changes in blood volume distending the tail artery as photoelectric signals to the computer (**Figure 2-3**).

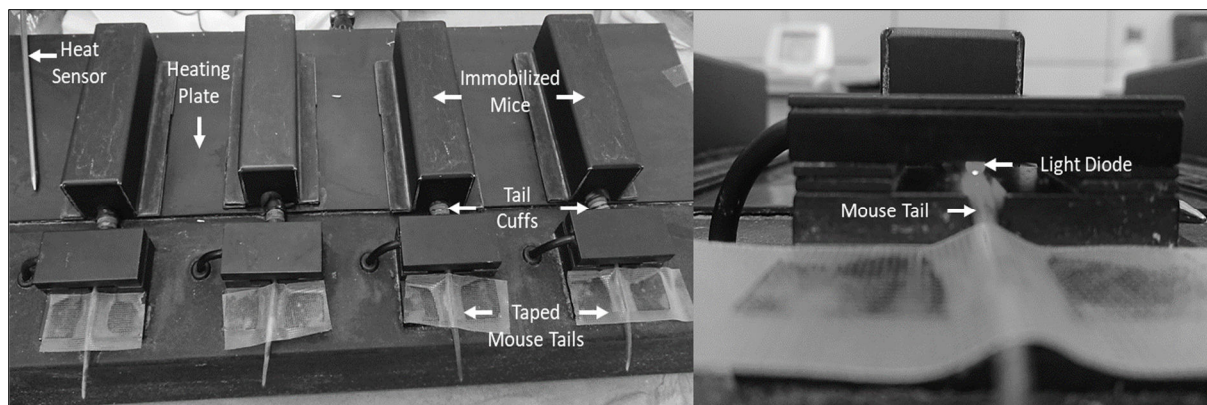


**Figure 2-3:** Blood pressure and heart rate measurements by the tail-cuff system. The left picture shows four mice secured by special tunnel-like holders. The right image shows a close-up of a fixed mouse tail between the light source and the photoresistor.

These photoelectric signals were represented by the software as oscillating waveforms, with each peak resulting from one cardiac cycle. For each measurement, i.e., for the duration of a waveform cycle, the tail-cuff was automatically inflated to cut off blood flow at the measurement site, resulting in disappearance of arterial pressure and reduction of amplitudes to approximately 10% of the initial value, respectively. During tail-cuff deflation, the first appearance of the pressure wave was detected as SBP. Based on ten waveform cycle measurements, SBP was calculated, while the heart rate was calculated based on the number of peaks per minute. All measurements were taken daily during the active phase of the animals over a period of ten days. The first seven days were the adjustment phase, whereas only the results of the last three days were used for the evaluation.

A day's measurement lasted approximately 30 minutes for each mouse and consisted of 30 waveform cycles. For the final evaluation, SBP was calculated as the mean value from the last 3 days of the experiment, i.e., the mean value from 90 waveform cycles. For pharmacological treatment, mice received the corresponding substances through the intraperitoneal route one hour prior to the measurements. Injections were either a vehicle solution containing 0.5% methylcellulose and 0.2% Tween 80 dissolved in PBS, compound 21 (C21, 0.5 mg/kg bodyweight), telmisartan (10 mg/kg bodyweight) or the combination of the latter two.

## 2.6. Modified Miles assay

The Miles assay as a method to study the vascular permeability in the skin of guinea pigs was originally developed by Miles and Miles [Miles & Miles, 1952]. In this modified version, the blue-coloured dye Evans blue is used that would bind to albumin when injected by intravenous route. Under physiologic conditions Evans blue barely leaves the vascular lumen, but under pathological conditions or induced extravasation by certain substances, the endothelial barrier may be disrupted, making it permeable to larger proteins such as albumin. During the experiments, extravasation was induced by local intradermal injection of histamine, bradykinin, or labradimil, a proteolytically stable analogue of bradykinin [Shimuta et al., 1999]. Subsequently, the degree of induced extravasation of albumin-bound Evans blue as a response to pharmacological treatment was quantified within local extravasates using a spectrometer.

The modified Miles assay was performed in anesthetized mice that received Evans blue dye (Sigma Aldrich, Munich, Germany) at a concentration of 30 mg/kg bodyweight through a tail vein access using a special catheter (**Figure 2-1**). After 20 minutes, the depilated dorsal skin received at different sites 30  $\mu$ l intradermal injections of either bradykinin, labradimil or histamine (2 nmoles each) as well as vehicle, i.e., PBS, which served as control. Within 30 minutes, systemically circulating Evans blue dye gradually extravasated at the injection sites. Hereafter, the mouse was sacrificed by cervical dislocation and its dorsal skin excised. Then extravasates were punched out using a circular punch cutter. After the specimen's weight was determined, its dye content was extracted in 1 ml dimethylformamide overnight at 57°C. Following centrifugation at maximum speed the dye solution was cleared of insoluble residues and quantified at 620 nm by a spectrometer (DU 640 Spectrophotometer, Beckman, Krefeld, Germany). A calibration curve for Evans blue solved in dimethylformamide was created by two-fold serial dilutions starting at 30  $\mu$ g/ml (**Figure 2-4**).

Extrapolated concentrations were normalized to the weight of their corresponding excised specimens and calculated as fold increase of extravasation as compared to vehicle injection. To study the effect of AT<sub>2</sub> on bradykinin-induced extravasation, half an hour prior to the Miles assays, C57BL/6 were either treated with the AT<sub>2</sub> agonist C21, the AT<sub>2</sub> antagonist PD123319 or the combination of the latter two or C21 combined with icatibant (0.5 mg/kg bodyweight each) as well as vehicle solution which was composed of 0.5% methylcellulose and 0.2% Tween-80 dissolved in PBS.

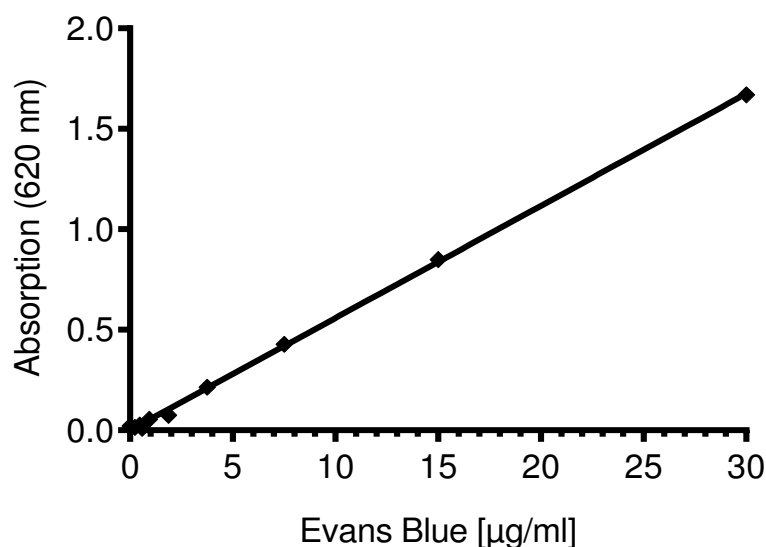


**Figure 2-4:** Standard curve for quantifying Evans blue concentration in specimens.

## 2.7. Organ bath studies

**Incubation of lung segments** The lung lobes were harvested from mice and cut into fragments measuring approximately 0.5 cm in diameter. These fragments were washed and incubated in presence or absence of 100  $\mu\text{M}$  C21 while submerged in carbogen gassed and pre-heated ( $37^\circ\text{C}$ ) organ bath buffer. After a period of 30 minutes the supernatant was taken and the remaining lung fragments homogenized following the protocol for organ lysate preparation.

**Wire myography of mouse aortic rings** The contractile response of isolated resistance vessels measured by wire myograph was pioneered by [Mulvany & Halpern, 1976]. Using this principle, vascular reactivity of aortic rings in response to various substances was determined. First, the mouse thoracic aorta was freshly harvested and freed from residual blood, surrounding fat, and connective tissue. Then approximately two 5 mm ring segments were separated from the aorta and each threaded in horizontal position between two triangular tungsten wires. The first wire was attached to a hook at the bottom and the second was attached to a polyester thread at the top which in turn was connected to a force transducer (Ametek, Rochester, USA). Signals from the force transducer were amplified and sent to a chart recorder (SE-120; ABB, Mannheim, Germany). Wires holding the aorta were immersed in 10 ml of organ bath buffer in a double-walled glass chamber jacketed with temperature-controlled water. Moreover, the temperature was set at  $37^\circ\text{C}$  and carbogen (95% oxygen and 5% carbon dioxide) continuously

supplied to maintain a pH of 7.4 (**Figure 2-5**). This way, a total of four chambers were operated simultaneously. The mounted vessels were stretched to a resting force of 9.81 mN and allowed to equilibrate to a stable baseline for 30 minutes with the buffer being replaced every 10 minutes. To test the viability of the aortic segments, i.e., the maximum contractile response to stimuli, a saturated KCl solution was added to a final concentration of 100 mM. In a receptor independent manner, potassium induced in high concentrations depolarization of smooth muscle cell membrane which in consequence opened voltage-gated calcium channels and increased the extracellular calcium influx, finally activating the contractile apparatus. After three consecutive washings with the organ buffer solution, a second KCl response curve was recorded. With the integrity of the smooth muscle cells intact, next the integrity of the endothelial layer was confirmed. At first, a concentration response curve to phenylephrine with cumulative concentrations from  $10^{-9}$  to  $10^{-5}$  M was recorded. The contractile response induced by phenylephrine was independent of the endothelium but mediated by  $\alpha_1$ -adrenergic receptors leading to increased calcium influx and further activation of the contractile machinery. After the washing phase, again phenylephrine was added to a final concentration of the half-maximum contractile response which usually ranged from 0.1 to 0.2  $\mu$ M. The phenylephrine-induced contraction was then gradually counteracted by acetylcholine with rising cumulative concentrations reaching from  $10^{-9}$  to  $10^{-5}$  M. Acetylcholine-induced relaxation was exclusively dependent on NO release from endothelial NO synthase, that is, the more intact the endothelial layer, the more the aorta relaxed toward baseline with increasing acetylcholine concentration added to the organ bath. An aortic preparation was defined as endothelium-intact if acetylcholine was able to relax phenylephrine-induced tension to one-fifth or less. In contrast, pre-contracted aortic rings with response less than 10% to acetylcholine were defined as denuded of their endothelium layer. This feature was only achieved after rubbing the inner lumen of aortic segments against a thin wire for a few times. After determination of the endothelium status and a washing phase, again the aortic rings were pre-contracted by phenylephrine and exposed to cumulative concentrations of C21 ranging from  $10^{-9}$  to  $10^{-5}$  M.

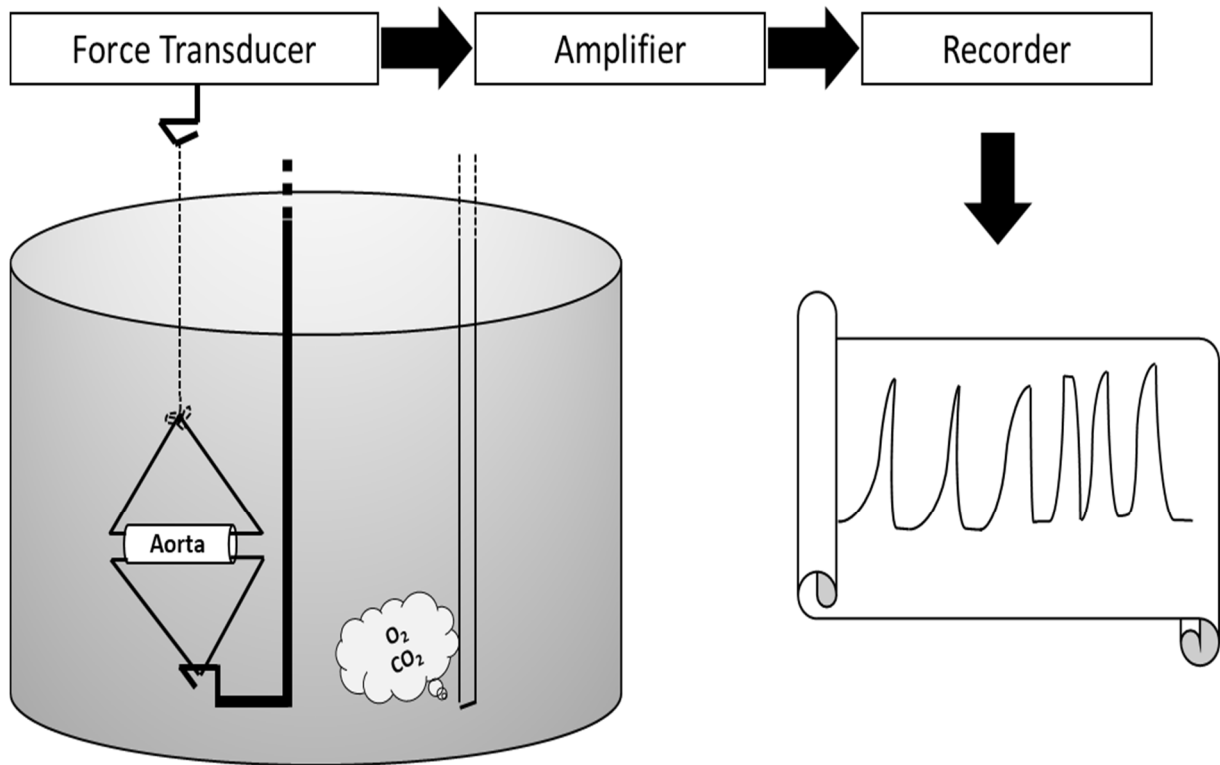


**Figure 2-5:** A schematic illustration of the wire myograph.

## 2.8. Enzyme-linked Immunosorbent Assays

The first immunoassay sensitive enough to measure the concentration of substances in samples implicated radiolabelled molecules in the process of antibody-antigen complex formation and subsequent detection by a gamma counter [Wide, Axen & Porath, 1967]. Depending on the concentration, the targeted antigen displaced its radiolabelled counterpart and reduced the gamma signal. Further developments in this field improved practicality and safety by using enzyme reactions that allowed detection in the visible electromagnetic spectrum [Engvall & Perlmann, 1971]. Since then, laboratories have been using different variations of commercially available enzyme-linked immunosorbent assays (ELISA) to quantify their desired antigens.

**Murine plasma ACE by sandwich ELISA** ACE protein levels in mouse plasma samples were quantified using the commercially available RayBio<sup>®</sup> Mouse ACE ELISA kit (Antibodies-online, Aachen, Germany), employing the sandwich ELISA technique (**Figure 2-6**). In accordance with the manufacturer's protocol, the incubation steps were performed with gentle shaking at room temperature. In-between the steps, a washing procedure with the kit's own buffer was carried out. Briefly, 100  $\mu$ l of ACE standard solutions as well as diluted plasma samples (1:1000) were pipetted into wells of a microplate pre-coated with ACE targeting

antibodies and allowed to incubate for 2.5 hours. After a washing phase, 100 µl solution of biotinylated detection antibodies raised against ACE was added to respective wells for another hour of incubation. For the next step, 100 µl of a solution containing streptavidin covalently bound to horseradish peroxidase (STV-HRP) was added. During 45 minutes of incubation, the biotinylated detection antibody was linked with STV-HRP. The last incubation step was initiated by transferring the chromogenic substrate 3,3',5,5'-Tetramethyl[1,1'-biphenyl]-4,4'-diamine (TMB) into corresponding wells. As TMB was gradually oxidized by the enzyme HRP the solution turned blue. This reaction was stopped after 30 minutes with 50 µl sulfuric acid (0.2 M) which turned the solution yellow and allowed spectrometric detection at 450 nm using Synergy™ Mx Microplate Reader (BioTek, Bad Friedrichshall, Germany).

**Plasma angiotensin I and II by competitive ELISA** The decapeptide Ang I and the octapeptide Ang II were each quantified in mouse plasma utilizing the commercially available kits ab136934-Angiotensin I ELISA Kit (abcam, Berlin, Germany) and RAB0010-Angiotensin II EIA Kit (Sigma Aldrich, Munich, Germany). Both kits applied the principle of the competitive ELISA (**Figure 2-7**). All incubation steps and washing procedures were performed according to the manufacturer's instructions. For the first incubation step, an antibody solution targeting the desired antigen, i.e., Ang I or Ang II, was pipetted into corresponding wells of a microplate, pre-coated with the suitable capture antibody. Next, standard concentration solutions as well as diluted plasma samples (1:2) were spiked with a known concentration of a biotin-labelled target antigen and added to the corresponding wells of the microplate. Within a defined incubation time, target antigen and its biotin labelled counterpart competed for the same capture antibody's binding site. In consequence, the higher the concentration of the target antigen was, the more its biotinylated version was displaced. From this step onwards, the procedure was similar to the sandwich ELISA. STV-HRP was added to form a non-covalent bond with biotin. Subsequently, a coloured oxidation product was formed by immobilised HRP when TMB was added. This reaction was stopped by acidification with sulfuric acid, which simultaneously allowed spectrometric detection at 450 nm. The concentration derived from the standard curve was inversely proportional to the concentration of the target antigen in the samples.

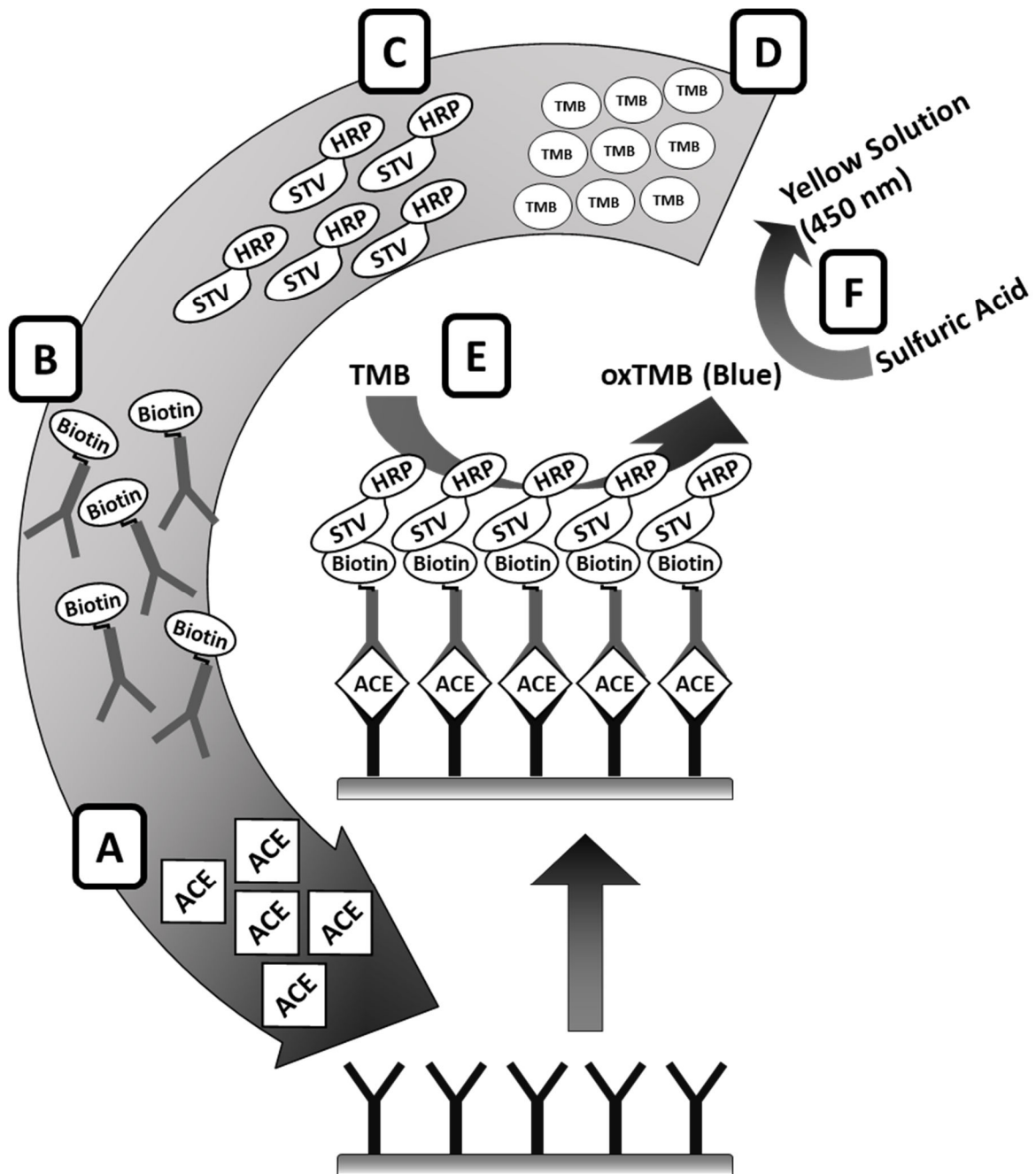


**Figure 2-6:** A sandwich ELISA visualized step by step: (A) ACE proteins from a sample bind to specific capture antibodies on coated wells of a microplate. (B) Then a biotin-conjugated detection antibody directed against ACE is added to form a sandwich complex. (C) The addition of streptavidin-horseradish peroxidase (STV-HRP), which binds to biotin, provides the detection antibody with peroxidase capability. (D-E) In the presence of 3,3',5,5'-Tetramethyl[1,1'-biphenyl]-4,4'-diamine (TMB), HRP oxidizes TMB (oxTMB) and tints the solution blue. (F) The catalytic reaction is stopped by acidification using sulfuric acid (0.2 M), which turns the solution yellow. Finally, ACE is quantified at 450 nm using a microplate reader.

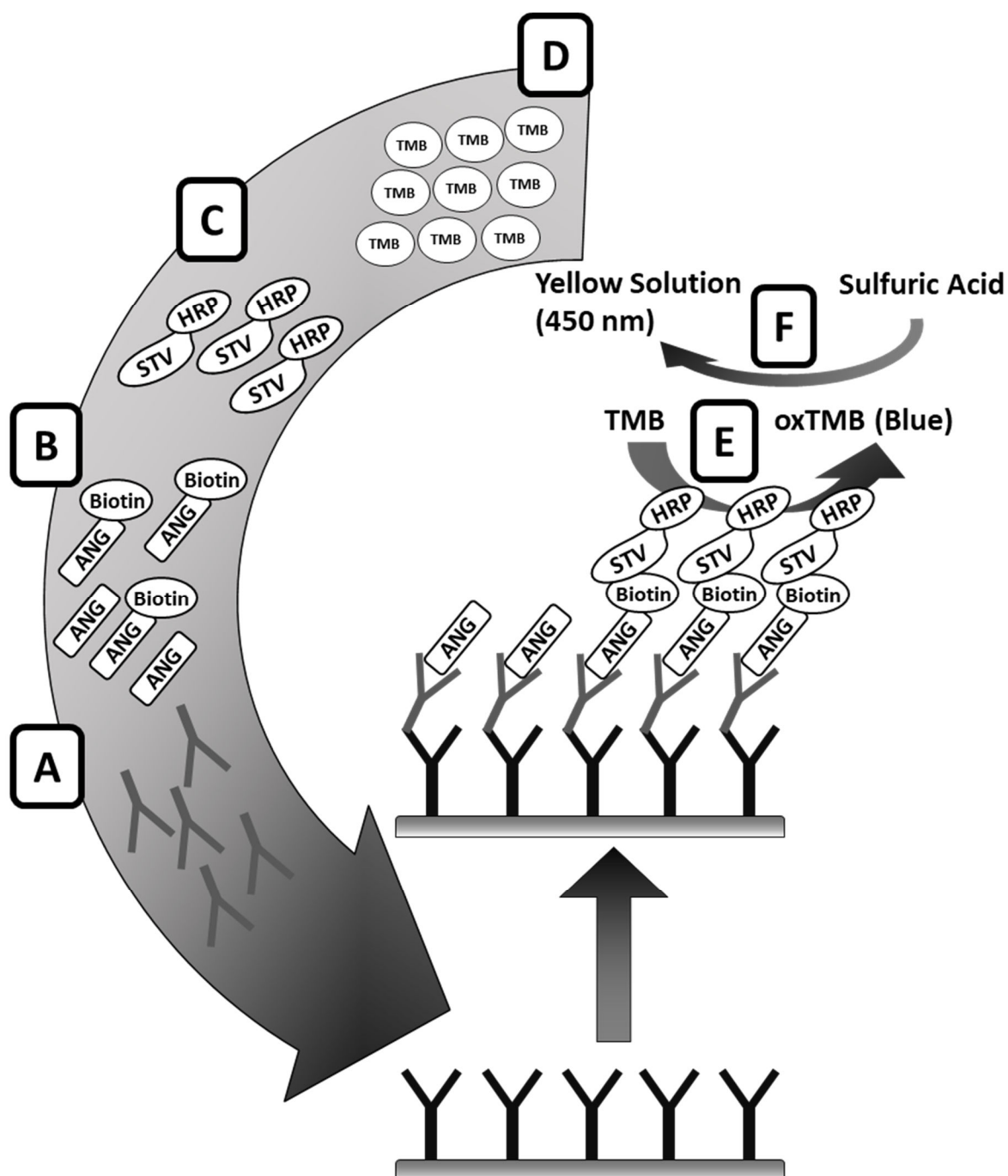


**Figure 2-7:** The principle of a competitive ELISA:(A) The microplate is coated with immobilized antibodies directed against a second antibody. The latter, which directed against a desired antigen, i.e., angiotensin (ANG) I or II, is added so that it is captured by the first antibody. (B) A sample containing an unknown concentration of ANG is spiked with biotin-conjugated ANG and allowed to react with the second antibody. Both ANG and its biotin-conjugated counterpart compete for the same antibody's binding site. (C) Antibody-bound biotinylated ANG gains catalytic capability by linkage to streptavidin-horseradish peroxidase (STV-HRP). (D) In the presence of 3,3',5,5'-Tetramethyl[1,1'-biphenyl]-4,4'-diamine (TMB) (E) HRP turns the solution blue through formation of oxidized TMB (oxTMB). (F) This reaction is stopped by lowering the pH with sulfuric acid (0.2 M) turning the solution yellow. Finally, absorption is measured by a microplate reader at 450 nm.

## 2.9. Fluorescence detection using magnetic beads

Uniform microbeads were originally developed by the Norwegian professor John Ungestad in 1976 and are still used today in various fields of research. In particular, the use of magnetizable microbeads linked to a specific antibody provided an innovative method for the isolation and quantification of a desired protein, e.g., ACE, from liquid samples such as plasma. For this purpose, uniform (2.8  $\mu\text{m}$ ) magnetizable polystyrene beads conjugated to a secondary antibody raised against rabbit IgG (Dynabeads™ M-280 Sheep Anti-Rabbit IgG, Thermo Fisher, Darmstadt, Germany) were used in combination with two monoclonal primary antibodies raised against ACE, i.e., mouse anti-ACE (sc-23908, Santa Cruz Biotechnology, Heidelberg, Germany) and rabbit anti-ACE (ab75762, Abcam, Berlin, Germany) to capture ACE in plasma samples. Subsequently, ACE was quantified by fluorescence detection in the near-infrared spectrum using secondary, i.e., IRDye 800 CW donkey anti-mouse IgG and IRDye 800 CW goat anti-rabbit IgG (LI-COR, Bad Homburg, Germany).

During the preliminary tests, appropriate dilutions of antibodies and plasma samples were determined. To enable comparison between samples, first the grade at which the beads would be saturated with ACE had to be identified and the suitable total protein determined. Plasma samples diluted to 80  $\mu\text{g}/\text{ml}$  total protein, i.e., below the saturation threshold, were found to be suitable for quantitative ACE assay (**Figure 2-8**).

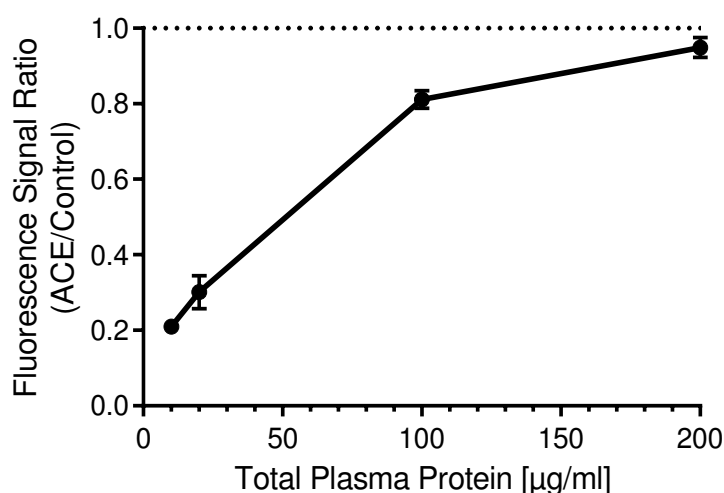


**Figure 2-8:** The fluorescence signal from ACE as compared to the corresponding loading control is detected at various total plasma protein concentrations ranging from 10 to 200  $\mu\text{g}/\text{ml}$  on Dynabeads™ using an infrared microplate imager. At 200  $\mu\text{g}/\text{ml}$  total plasma protein, the beads are almost saturated with ACE proteins (n=3 each).

**Established protocol for ACE detection** For the first preparation step, Dynabeads™ were washed according to the manufacturer's protocol with bead buffer, which was composed of PBS containing 0.1% bovine serum albumin, 2 mM sodium citrate, with pH adjusted to 7.4. In addition, the total protein content of the plasma samples was determined using the Bradford protein assay to subsequently prepare the appropriate dilution, which was at 80 µg/ml total protein. Generally, after each incubation step, the solutions containing beads were resuspended and washed three times in bead buffer using a magnetic sample rack (DynaMag™, Thermo Fisher, Schwerte, Germany). The first two incubation steps were performed in parallel, for one hour each. While to the suspension containing  $10^7$  beads the rabbit anti-ACE antibody (1:50) was added, diluted plasma samples were incubated with the mouse anti-ACE antibody (1:100). For the next step, the diluted plasma samples were transferred to the washed beads to form a sandwich-antibody-complex with ACE within one hour of incubation. Afterwards, the secondary antibodies raised against goat and mouse IgG (each diluted at 1:5000) were added for another hour of incubation. Finally, fluorescence intensity was detected using the Odyssey® Infrared Imager (LI-COR GmbH, Bad Homburg, Germany) on a microplate with  $10^6$  beads suspended in 200 µl for each well. The fluorescent signal emitted by the secondary antibody bound to rabbit IgG represented the maximum coupling capacity to ACE, i.e., the loading control, whereas the fluorescent signal emitted by the secondary antibody bound to mouse IgG represented the sandwiched ACE only (**Figure 2-9**). Beads conjugated with rabbit IgG served as both positive and negative controls, whereas unconjugated beads served as background. After subtraction of background, the ratio of ACE signal to the corresponding loading control was formed.

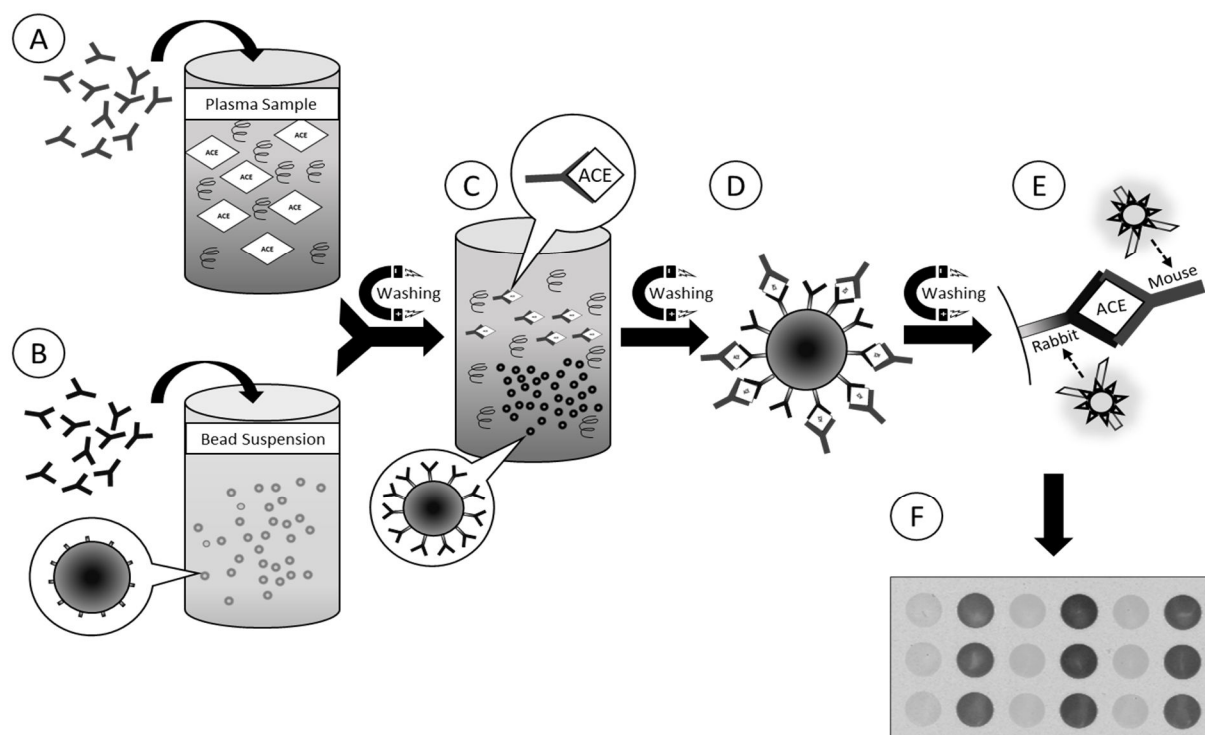


**Figure 2-9:** Using microbeads and specific antibodies, ACE is bound within the plasma sample through several incubation and washing steps to be quantified by fluorescence detection on a microplate. (A) Mouse antibodies directed against ACE are added to the plasma sample. (B) Simultaneously, rabbit antibodies raised against ACE are added to the magnetic beads with covalent-bound antibodies on their surface directed against rabbit IgG. After one hour of incubation, the beads are washed using a magnetic sample rack and then (C) resuspended in the plasma sample for an additional hour of incubation. (D) Sandwich-antibody-complexes with ACE are established and separated through the washing procedure. (E) The complex is conjugated with infrared-dye labelled antibodies either raised against rabbit or mouse IgG and (F) detected on a microplate using an infrared microplate imager.

## 2.10. ACE activity assay in plasma and tissue lysates

The catalytic activity of ACE was determined in mouse plasma and lung lysates as well as human endothelial cell lysates by a kinetic spectrometric assay based on continuous N-[3-(2-Furyl)acryloyl]-Phe-Gly-Gly (FAPGG) degradation [Holmquist, Bunning & Riordan, 1979]. Utilizing the absorption maximum at 340 nm, the degradation of FAPGG by ACE was recorded over time using a microplate reader (Synergy™ Mx Microplate Reader, BioTek, Bad Friedrichshall, Germany) and subsequently the catalytic activity of ACE derived from standard curves. While samples were prepared as described before, the lysis buffer was modified to maintain the catalytic activity of ACE, i.e., the buffer contained PIC and was composed of 150 mM NaCl, 1% Triton X-100, 1 mM PMSF and 50 mM Tris buffer with pH

adjusted to 8. Sample volumes of 50  $\mu\text{l}$  were loaded into the wells of a 96-well microplate along with 150  $\mu\text{l}$  of the assay buffer which consisted of 300 mM NaCl, 0.1 mM  $\text{ZnCl}_2$ , 2.3 mM FAPGG and 50 mM Tris with pH adjusted to 8.3. The addition of 100  $\mu\text{M}$  captopril served as a control, and for the background sample FAPGG was excluded. As for the standard curve, 50  $\mu\text{l}$  standard ACE solutions (rabbit lung ACE, Sigma Aldrich, Munich, Germany) ranging in catalytic activity from 0 to 20 mU/ml were prepared. All steps up to this point were performed on ice, then the final mixture was equilibrated by continuously shaking the microplate and heating to 37°C. Next, the decrease in absorption at 340 nm was recorded over 45 minutes (**Figure 2-10**). The ACE activity of a sample was calculated using a formula (**Equation 2-1**) that incorporated the data from the standard calibration curves (**Figure 2-11**) as well as the sample's total protein content.

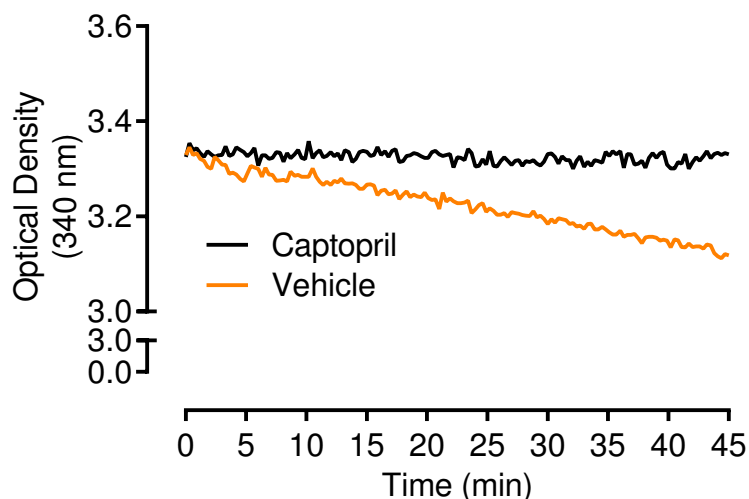


**Figure 2-10:** ACE activity measured over the course of 45 minutes in plasma samples of C57BL/6. In the presence of the ACE inhibitor captopril, hydrolysis of FAPGG is inhibited.

$$\text{ACE Activity} = \frac{V_s/V_m \times m_s}{m_c [\text{mU}^{-1}]}$$

$V_s$  : Volume of Sample [ $\mu\text{l}$ ]       $m_s$  : Slope of Sample [ $\text{mU}^{-1}$ ]  
 $V_m$  : Volume Measured [ $\mu\text{l}$ ]       $m_c$  : Slope of Calibration curve

**Equation 2-1:** The formula for calculating ACE activity.

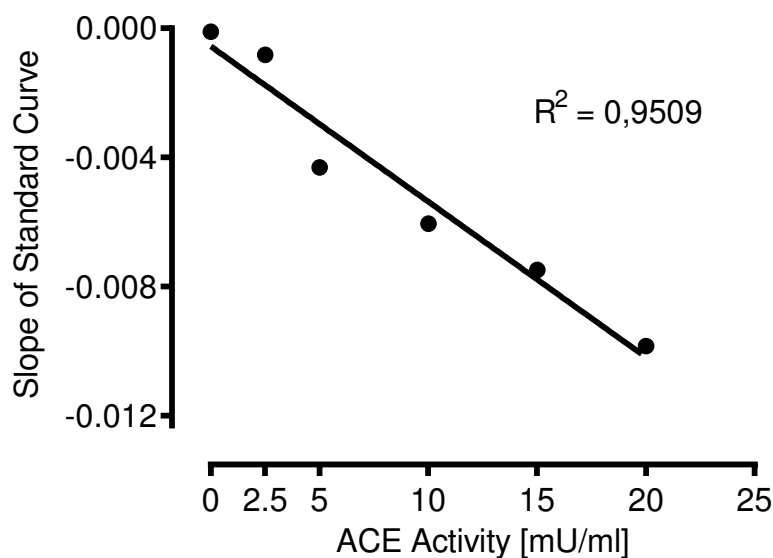


**Figure 2-11:** The example of an interpolated calibration curve obtained from the plotted slopes of corresponding standard solutions with defined ACE activity in the range of 0 to 20 mU/ml.

## 2.11. Western blotting

As a method to study protein expression, the western blot technique was first introduced in 1979 by Towbin who separated proteins through polyacrylamide gel electrophoresis (PAGE) and transferred them to nitrocellulose membranes to perform on-membrane immunodetection [Towbin, Staehelin & Gordon, 1979]. The equipment used for all procedures described in this section, from gel casting to blotting were the Mini-PROTEAN® Tetra Vertical Electrophoresis System and the Mini Trans-Blot® Module as well as the PowerPac™ HC Power Supply (Bio-Rad Laboratories, Feldkirchen, Germany).

**Preparation of samples** In 1970, Laemmli published the sodium dodecyl sulfate-polyacrylamide gel electrophoresis (SDS-PAGE) as a technique for efficient separation of proteins [Laemmli, 1970]. First, samples were diluted in equal parts with Laemmli buffer which was composed of 4% SDS, 20% glycerol, 10% 2-mercaptoethanol, and 0.004% bromophenol blue dissolved in 0.125 M Tris with pH adjusted to 6.8. Then the dilutions were heated for five minutes at 95°C for denaturation. During this process, SDS reduced the proteins to their linear primary structure and applied a negative charge to them, thereby leading to different charge-to-mass ratios among the proteins. Thus, once exposed to an electric field, the proteins could be separated by size while passing through a porous gel.

**Preparation of polyacrylamide gels** A polyacrylamide gel is a three-dimensional network of pores created through linear polyacrylamide polymerization and crosslinking to bis-acrylamide monomers. The pore size of the gel matrix affects the separation efficiency of proteins in a sample and can be influenced by the ratio of acrylamide to bis-acrylamide. For instance, increasing the polyacrylamide chain length and the degree of crosslinking would restrain the movement of larger proteins due to smaller pores. For SDS-PAGE, a discontinuous gel composed of a stacking-zone with big pores (4.5% acrylamide/bis-acrylamide 37.5:1) and a separation-zone with small pores (7.5% to 12% acrylamide/bis-acrylamide 37.5:1) was polymerized using solutions with corresponding buffers (stacking-gel buffer or separation-gel buffer) in conjunction with a free radical-generation-system consisting of 0.6 µg/ml tetramethyl ethylenediamine and 0.8 µg/ml ammonium persulfate. When the proteins were exposed to an electric field, the stacking zone enhanced the sieving effect since all proteins were "lined up" by mass before passing through the separating gel.

**Separation of proteins** Vertical electrophoresis took place in a tank filled with tank-buffer with two gels fixated by an electrode assembly while being submerged in parallel position. Samples were loaded with 20 to 80 µg of total protein accompanied by 2 µl of molecular PageRuler™ (Thermo Fisher, Schwerte, Germany) into the appropriate wells. For the stacking period, 90 volts were applied and at a later stage, when the samples migrated to the separation zone, the voltage was increased to 150 volts. The Separation of the proteins was terminated once the bromophenol blue front had run off the gel.

**Transfer onto a membrane** With SDS-PAGE completed, a transfer-sandwich was prepared for wet electroblotting. Briefly, the gel was attached to a nitrocellulose membrane (Immobilon-NC Membrane, Merck Millipore, Darmstadt, Germany) and enclosed by sponges and filter papers. The transfer-sandwich was inserted into a blotting chamber filled with transfer-buffer to perform electrophoresis at 90 volts for 90 minutes.

**Immunodetection** Blotted nitrocellulose membranes were first blocked with Odyssey® Blocking Buffer (LI-COR GmbH, Bad Homburg, Germany) following the manufacturer's instructions. Then the membrane was incubated with a primary antibody targeting a specific antigen overnight in a cold room (**Table 2-4**).

Cat#	Clonality	Target	Host	Dilution	Peer-Reviewed in
ab75762 (Abcam)	Mono	ACE	Rabbit	1:200 - 1:500	[Yang et al., 2016; Zhou et al., 2015]
A2066 (Sigma)	Poly	$\beta$ -actin	Rabbit	1:10,000 - 1:25,000	[Lira et al., 2017; Yousif et al., 2014]

**Table 2-4:** Primary antibodies used for immunodetection.

On the next day, the membrane was incubated with the infrared dye-coupled secondary antibody IRDye 800 CW goat anti-rabbit IgG or IRDye 680RD goat anti-rabbit IgG (1:10,000, LI-COR GmbH, Bad Homburg, Germany) raised against the host antigen of the primary antibody. Finally, the Odyssey<sup>®</sup> Infrared Imager (LI-COR GmbH, Bad Homburg, Germany) was used to scan for signals on the nitrocellulose membrane while the software Image Studio<sup>™</sup> Lite Ver 5.2 (LI-COR GmbH, Bad Homburg, Germany) was utilized for quantification.

## 2.12. Two-photon excitation microscopy

Two-photon excitation microscopy (TPEM) is an imaging system that allows the visualization of living tissue through excitation of fluorophore molecules. The practical use of TPEM was first described in 1994 by [Denk et al., 1994]. Compared with confocal microscopy which has limitations visualizing thick specimens, TPEM allows visualization of deep tissue layers up to 100  $\mu$ m depth with relatively high signal-to-noise and low phototoxicity. This type of microscopy exploits the optical phenomenon of second-harmonic generation (SHG): a femtosecond-laser fires two photons successively with half the energy needed to excite a fluorophore into a nonlinear transmission medium, e.g., subcutaneous tissue. These photons eventually meet and match their phases to produce a new photon with the energy needed to excite the target fluorophore. With the effect of SHG, lower energy is needed for excitation of fluorophores and as a consequence less tissue damage occurs and light scattering is reduced. For TPEM, Olympus FV1000MPE (Tokyo, Japan) equipped with a 25X, NA1.05 water dipping objective and a femtosecond-pulsed, mode-locked MaiTai DeepSee Ti:Sapphire laser (Spectra-Physics, Mountain View, CA, USA) was used to visualize the fluorescent-dye labelled microvasculature in murine earlobes. The mouse was anesthetized for the entire procedure, positioned under the objective of the microscope and received injections of two different fluorophores through a tail vein catheter (**Figure 2-1**). The first fluorophore injected was a 250 kDa Fluorescein isothiocyanate-dextran (FITC-dextran, anionic charge, Sigma Aldrich,

Munich, Germany) which remained in the vascular lumen due to its size and allowed adjustment and focusing of the microscope (**Figure 2-12**).

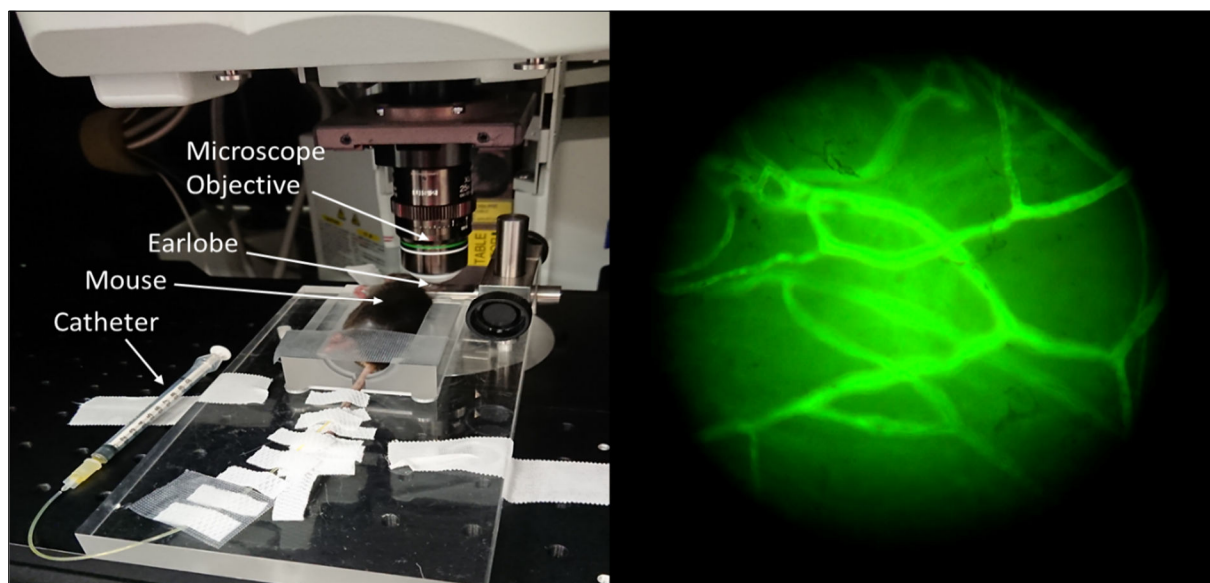


**Figure 2-12:** The left image shows an anesthetized mouse placed under the microscope objective after receiving the 250 kDa dextran-conjugated fluorophore through a tail vein catheter. The right image displays an image of microvessels in a 200  $\mu\text{m}$  deep tissue layer of the earlobe, as observed through the microscope's eyepiece during excitation of the 250 kDa fluorophore by two-photon excitation technique.

After a suitable scan area was determined, the second fluorophore (Alexa Fluor<sup>®</sup> 594, anionic charge, 10 kDa, Thermo Fisher, Wesel, Germany) was injected through the catheter. This fluorophore was capable of gradually leaving the vessel lumen due to its small size. For better differentiation, the 250 kDa fluorophore was rendered in green while the 10 kDa fluorophore was rendered in red (**Figure 2-13**). In a similar approach another dextran-conjugated fluorophore with 70 kDa (Dextran Texas Red<sup>™</sup> 595, neutral charge; Thermo Fisher, Wesel, Germany) was used. Each recording took approximately 45 minutes to complete, with two frames generated every minute. Each frame was composed of eight parts taken from sequentially scanned 3- $\mu\text{m}$ -thick tissue sections at different depths. At the end, a three-dimensional cubic image was reconstructed for each frame and analysed by the software Imaris (Bitplane, Zürich, Switzerland). The software was capable of identifying the vascular space using the signal from the 250 kDa fluorophore, which remained in the vascular lumen throughout the recording. From this, it was then possible to perform calculations for the 10 kDa fluorophore, which, in contrast to the 250 kDa fluorophore, gradually lost intensity in the same defined vascular space (**Figure 2-14**).

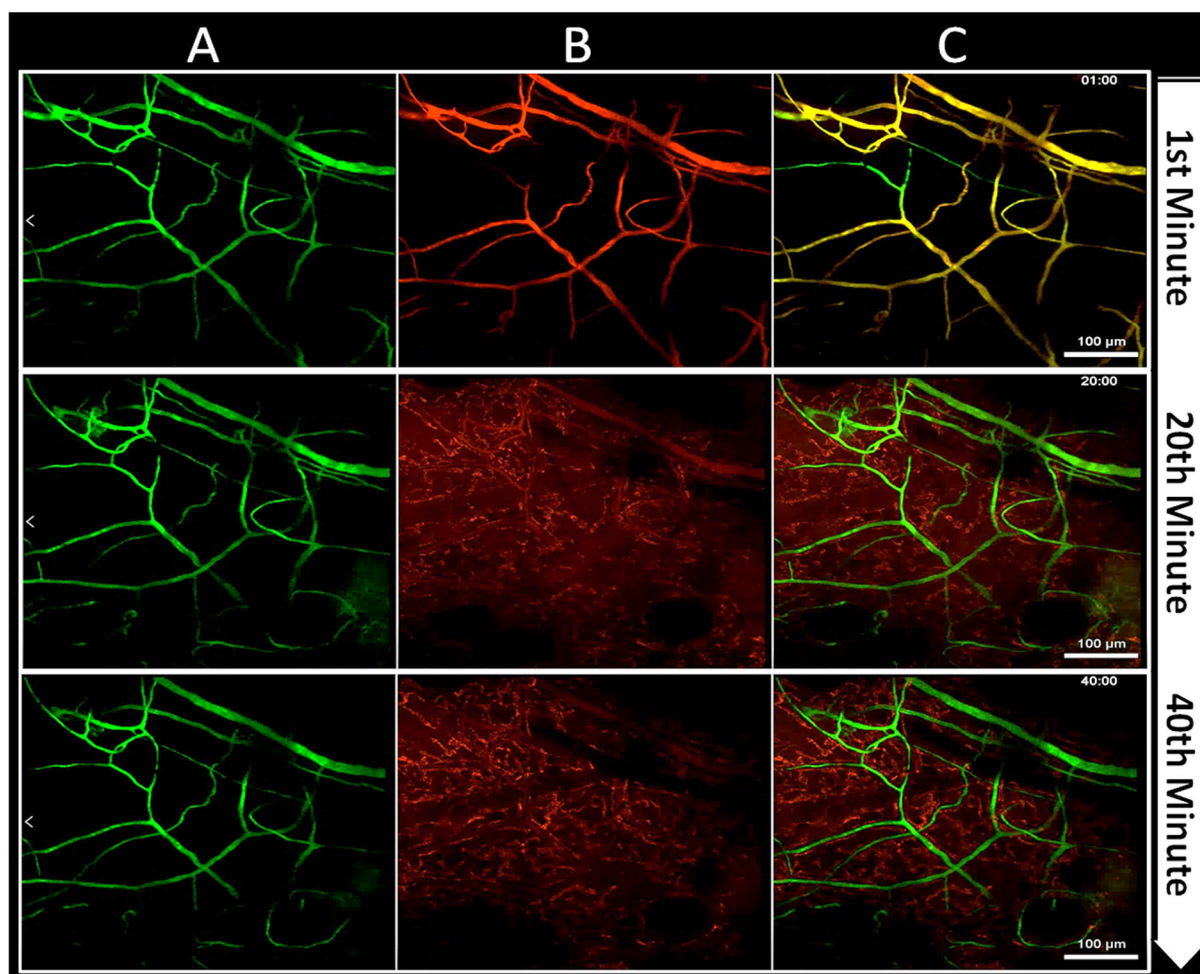


**Figure 2-13:** Images from microvessels within the earlobe of a mouse taken by two-photon excitation microscopy at a depth of 200  $\mu\text{m}$ , that show the distribution of fluorophores at chosen time points, i.e., at the 1st, 20th, and 40th minute. After injection of the (A) green color-coded 250 kDa and the (B) red color-coded 10 kDa fluorophore dyes, only the latter gradually leaves the vascular lumen and is completely accumulated inside extravascular space at the 40th minute. (C) The overlay shows the inability of the 250 kDa fluorophore to leave the vascular lumen in contrast to the 10 kDa fluorophore which over time tints the interstitial space red.

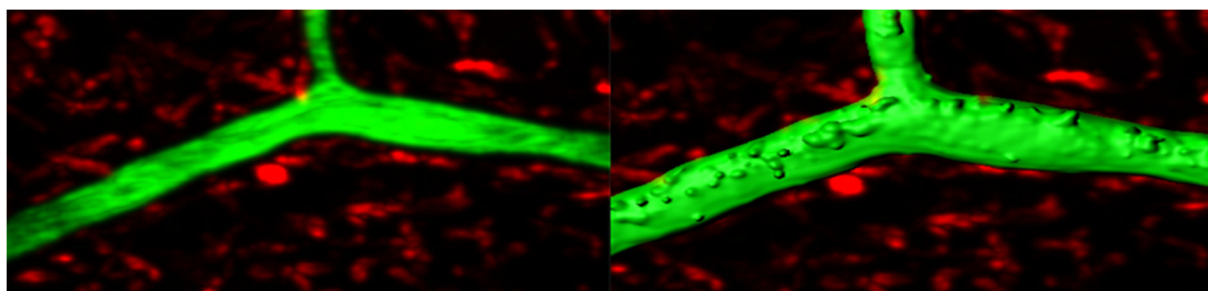


**Figure 2-14:** Software-assisted identification of pixels generated from fluorophore signals. Left: Native image of a vessel. Right: Masking of the vessel space dominated by the 250 kDa fluorophore signal.

### 2.13. ‘A Bradykinin in Skin Edema Trial’ (ABRASE)

In a translational research approach to the Miles assays and to investigate the role of prostaglandin synthesis during the formation of bradykinin-induced oedema in the human skin, a clinical trial was conducted. For this, volunteers took nonsteroidal anti-inflammatory drugs and intradermal injections of bradykinin solutions into their ventral forearm skin.

**Design of study** The clinical study entitled “A Bradykinin in Skin Edema Trial (ABRASE)” was approved by the medical faculty’s ethics commission of the Heinrich-Heine University (study number issued in the medical faculty’s clinical trial register: 2015-11-4583; ethics committee vote number: 5339R). ABRASE was carried out at three different locations in Germany involving the Institute of Pharmacology and Clinical Pharmacology, University Hospital Düsseldorf; the Department of Oto-Rhino-Laryngology, Head and Neck Surgery, Ulm University Medical Centre; and the Otorhinolaryngology Department, University Hospital Rechts der Isar, Technical University, Munich. Each volunteer was briefed and had to sign an informed consent prior to enrolment. Included were healthy adult Caucasian or Arabic volunteers of either sex with the ability to consent, no history of chronic disease and with intact skin at the anterior forearm. Exclusion criteria were acute or chronic medical conditions, especially atopic dermatitis, a history of allergies, chronic inflammation and the use of anti-inflammatory drugs within the last seven days, chronic medication (except oral contraceptives), pregnant or breastfeeding women, and any contraindications to ibuprofen. A total of 38 healthy human volunteers of both sexes were enrolled at three centres. One participant from the centre in Düsseldorf was excluded by the ROUT test (calculated with Graph Pad Prism 6) and one participant from the centre in Ulm was excluded after enrolment due to withdrawal of informed consent. The intervention study consisted of two days. On the first day, the subjects received intradermal injections of 18.9 nmol bradykinin along with vehicle solution as control into the skin of the anterior forearm. To assess bradykinin-induced extravasation, the expansion of wheals at the injection sites was measured over 120 minutes at defined time points. After a rest period of 180 minutes, volunteers were administered a 600 mg ibuprofen tablet (IbuHEXAL<sup>®</sup>, Hexal AG, Holzkirchen, Germany) and had to wait another 60 minutes. Then, bradykinin was injected again at another site and the resulting wheal was measured over 120 minutes. The same procedure was repeated on another day, but this time a COX-1 selective inhibitor was used.

**Preparation of solutions** Commercially available saline solutions (Fresenius Kabi Deutschland GmbH, Bad Homburg, Germany) were used for control injections as well as for

the preparation of 1 mg/ml bradykinin acetate solutions. All preparation steps were carried out under aseptic working conditions under a laminar flow cabin. To this end, the prepared solutions were filtered (Minisart™ NML syringe filter, 0.2 µm, Sartorius, Göttingen, Germany) and transferred into sterile Save-Lock tubes (Eppendorf, Hamburg, Germany). Then the solutions were snap frozen in liquid nitrogen to be stored at -80°C and shipped on dry ice to the study centres in Munich and Ulm. For intradermal injection, Hamilton™ syringes (1705 LT Syr, DURATEC GmbH, Hockenheim, Germany) were used which were autoclaved at 121°C for 20 minutes prior to use. With an attached hypodermic needle (Sterican®, 30G 0.30 x 12 mm) syringes were loaded with either 20 µl saline or bradykinin solution.

**Injection and measurement procedure** Throughout the experiment, the volunteers remained comfortably seated at a table in a well-tempered room (21-23°C) with the posterior side of a selected forearm placed on a medical pad (MoliNea S, Paul Hartmann AG, Heidenheim, Germany). The forearm was disinfected with antiseptic solution (Kodan® tincture forte colourless, Schülke & Mayr GmbH, Norderstedt, Germany) and allowed to dry. Then two distinct sites of the skin were selected for the injection of 20 µl bradykinin solution and vehicle solution respectively. For a successfully executed intradermal injection, the needle was inserted at an angle of approximately 15 degrees with the bevel completely immersed in the skin tissue. Next, the injection volume inside the syringe was displaced by slowly pushing the plunger. The emerging wheal at the injection site was recognised as a palpable skin elevation, whose dimensions were determined with a Vernier calliper at defined points in time, i.e., 5, 10, 20, 30, 60, 90 and 120 min after the performed injection. The size of a wheal was determined by its largest (LE) and smallest (SE) expansion. From these values the average diameter ( $d=(LE+SE)/2$ ) as well as the perimeter ( $p=\pi d$ ) and the wheal's total area ( $A=\pi d^2/4$ ) was calculated. The maximal wheal size was defined as the highest calculated value of the wheal's total area within the measured time frame.

## 2.14. Data analysis

Experimental data are expressed as mean ± standard error of the mean (SEM) of the number of individual samples (n) and analysed using the computer program GraphPad Prism (V6.07, La Jolla, CA, USA). The unpaired t-test was used for the comparison of two independent samples. One exception was the analysis of the ABRASE data, for which Wilcoxon matched-pairs signed rank test (paired t-test) was carried out. For comparisons between three or more samples, analysis of variance with pairwise comparisons using Tukey's post-hoc test was performed. Statistical significance was considered for  $P<0.05$ .

### 3. **Results**

Currently, there is no reliable method to directly quantify bradykinin that plays a central role in non-allergic angio-oedema. It is challenging to quantify bradykinin concentrations in an accurate and reproducible manner. For example, when puncturing a vein to take blood, the contact activation system is triggered by the Hagemann factor, which would artificially promote bradykinin formation [Schmaier, 2016]. Apart from its low abundance and extremely short half-life of several seconds, bradykinin is difficult to protect from enzymatic degradation in the presence of circulating proteases, which besides ACE include neprilysin, APP and CPN [Cyr et al., 2001; Murphey et al., 2000]. Moreover, local bradykinin concentration in the oedematous tissue can be much higher than in the systemic circulation, thus the site of blood collection should be chosen with consideration [Nussberger et al., 1999]. Because of these confounding factors, a suitable method for direct quantification of bradykinin concentration remains an unmet need, particularly in the clinical setting for diagnosis of non-allergic angio-oedema. Therefore, different experimental approaches and parameters were chosen to investigate a putative contribution of AT<sub>2</sub> to non-allergic angio-oedema. Moreover, the clinical study ABRASE was initiated to explore the role of COX in the development of local bradykinin-induced wheals in the skin of humans.

#### 3.1. **Pharmacologic evaluation of compound 21**

##### 3.1.1. **Synthesis of compound 21**

Since early AT<sub>2</sub> research, the peptide agonist CGP42112 has become well established and still has the highest affinity among existing AT<sub>2</sub> agonists [Bosnyak et al., 2011], although concentration-dependent antagonistic activity has also been reported [Stoll et al., 1995]. Apart from this, the peptide structure limits its usefulness for in-vivo experiments, since peptides tend to be rapidly degraded by enzymes and therefore have poor bioavailability. This has changed with the development and synthesis of the first selective non-peptide AT<sub>2</sub> agonist C21, which demonstrated oral bioavailability of up to 30% and an estimated half-life of 4 h in rats [Wan et al., 2004]. Yet, this substance was not commercially available in the early stages of this research project, so it was necessary to collaborate with the local Institute of Pharmaceutical and Medicinal Chemistry, which carried out the synthesis of C21 according to the published protocol, thus providing the main tool for this work (**Figure 3-1**). After the synthesis, the raw

product was further purified by flash column chromatography. Then, the final product was identified by HPLC analysis with a purity of 96.7% (**Figure 3-2**).

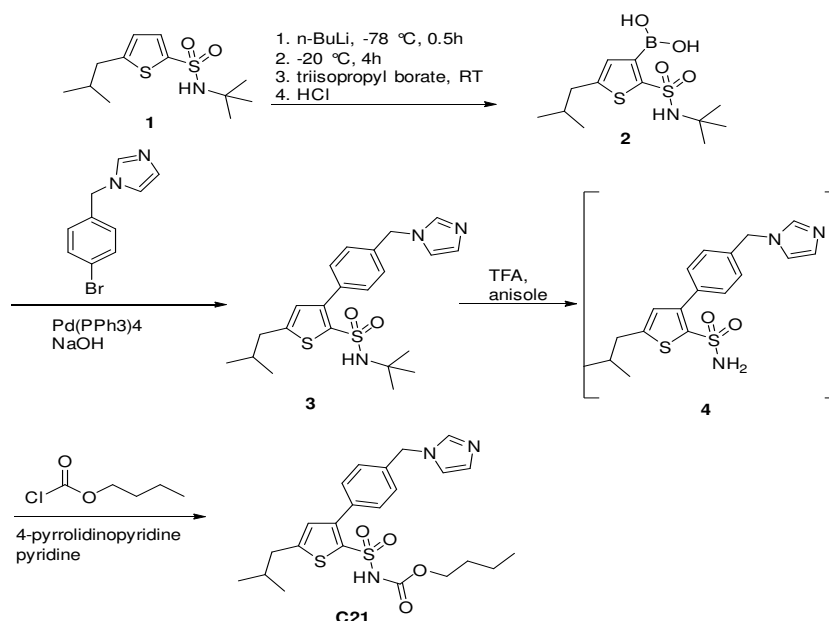


**Figure 3-1:** Scheme of the chemical synthesis of compound 21 (C21). N-(tert-butyl)-5-isobutylthiophene-2-sulfonamide (**1**) is converted into the corresponding boronic acid (**2**). The subsequent Suzuki cross-coupling reaction of (**2**) with 1-(4-bromobenzyl)-1H-imidazole provides the key intermediate (**3**). Deprotection by treatment with TFA furnishes the primary sulfonamide (**4**) which is directly treated with butyl chloroformate in pyridine in the presence of 4-pyrrolidinopyridine as catalyst to yield C21.

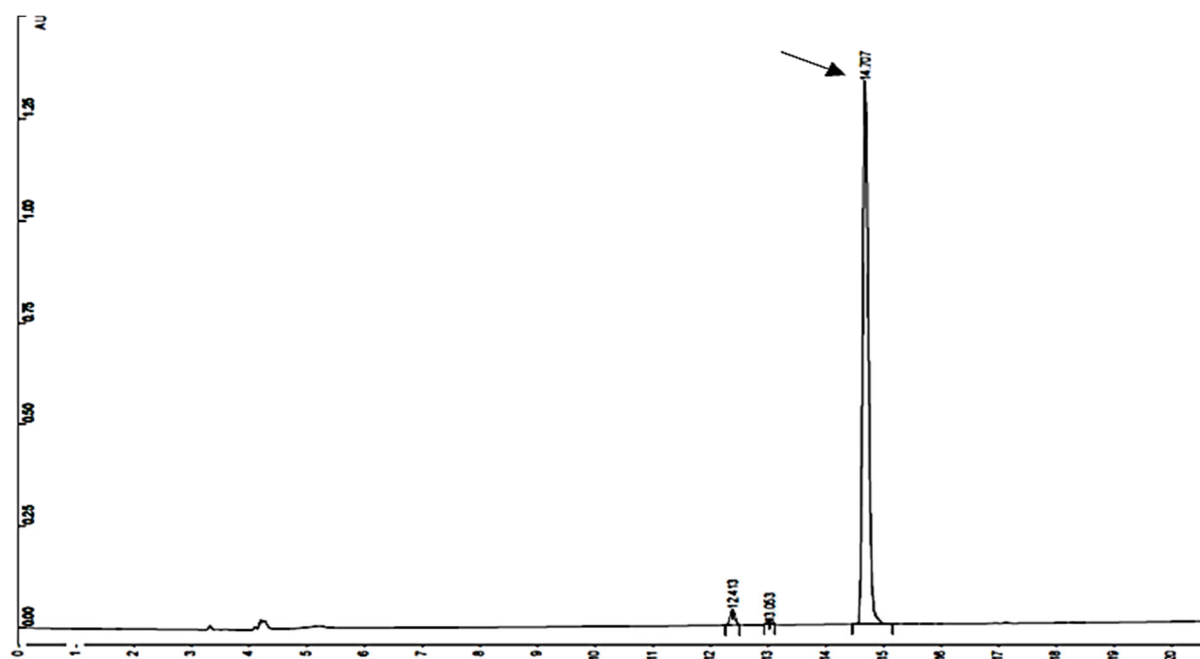


**Figure 3-2:** HPLC chromatogram of compound 21, with the arrow marking the corresponding peak.

### 3.1.2. Functional studies in isolated aortic rings

The thoracic aorta extracted from the mouse strains C57BL/6, FVB/N and AT2<sup>-/-</sup> was functionally examined using the organ bath apparatus. First, the pressor response of the aortic ring to cumulative concentrations of phenylephrine ranging from 10<sup>-9</sup> to 10<sup>-5</sup> M was assessed. For comparison of the efficacy, the negative common logarithm of the effector concentration producing the half-maximal effect (pD<sub>2</sub>) was used. Comparing the three mouse strains, the pD<sub>2</sub> values of phenylephrine for C57BL/6 (5.88±0.05), FVB/N (5.81±0.07) and AT2<sup>-/-</sup> (5.89±0.05) were not statistically significant (P=0.3514, Two-way analysis of variance, **Figure 3-3**).

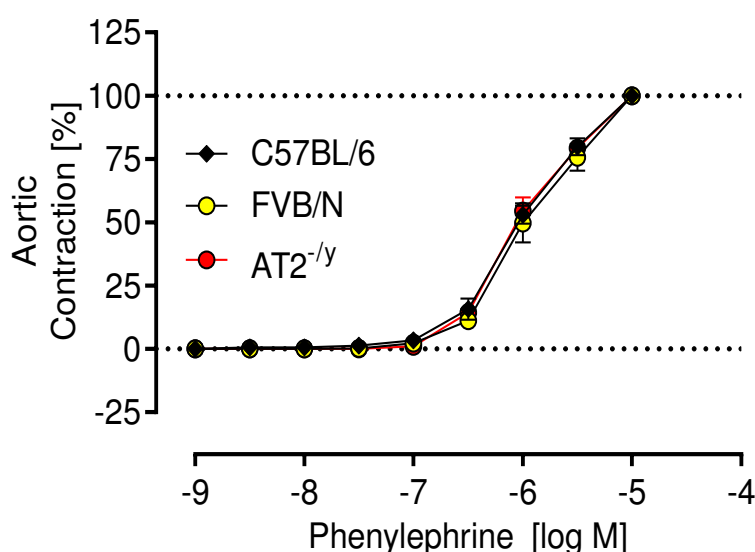


**Figure 3-3:** Results of the organ bath experiment to investigate the vasoconstrictive effect of phenylephrine on rings of the thoracic aorta, extracted from the mouse strains C57BL/6, FVB/N and AT2<sup>-/-</sup>. Aortic rings are challenged with increasing phenylephrine concentrations, starting at 10<sup>-9</sup> M up to a maximal effector concentration reaching 10<sup>-5</sup> M. However, there is no significant difference between the mouse strains when comparing the graphs (n=6 each, P=0.3514, Two-way ANOVA). Concentration-effect curves are recorded under 9.81 mN of resting tension.

The endothelial function of the aortic segments, i.e., the ability to induce relaxation by NO formation, was determined by increasing acetylcholine concentrations in the range of 10<sup>-9</sup> to 10<sup>-5</sup> M, at half-maximal contractile response to phenylephrine. The resulting concentration response curve to acetylcholine obtained from the aortic rings of FVB/N (pD<sub>2</sub> 6.67±0.09) showed a leftward shift as compared to the concentration response curves from aortic rings of C57BL/6 (pD<sub>2</sub> 6.31±0.13) and AT2<sup>-/-</sup> (pD<sub>2</sub> 6.52±0.12), suggesting a strain

dependent variation (\* $P < 0.006$  vs. FVB/N, Tukey's post-hoc test following Two-way analysis of variance, **Figure 3-4**).

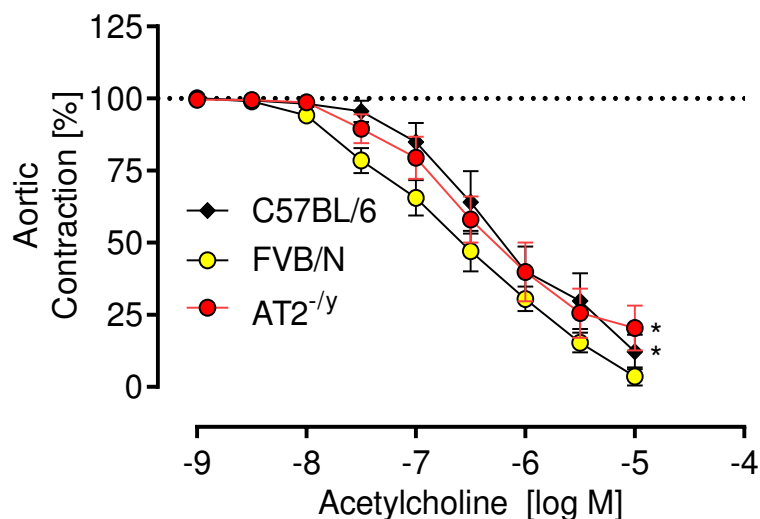


**Figure 3-4:** The vasodilator effect of acetylcholine on phenylephrine pre-contracted ( $10^{-7}$  M) mouse aortic rings with intact endothelium. Aortic segments relax in response to cumulative concentrations of acetylcholine reaching from  $10^{-9}$  to  $10^{-5}$  M and show a significant leftward shift of the curve in FVB/N as compared to AT2<sup>-/-</sup> and C57BL/6 (n=6 each,  $P=0.0006$ , Two-way ANOVA, \* $P < 0.006$  vs. FVB/N, Tukey's multiple comparison test).

In summary, aortic function at C57BL/6, FVB/N and AT2<sup>-/-</sup> is comparable in terms of contractile response to phenylephrine. Remarkably, the endothelium-dependent vasodilator response to acetylcholine is slightly stronger in FVB/N in comparison to the other strains. These findings allow further comparative organ bath studies in view of C21 and the effect of AT2 activation on a conductance vessel such as thoracic aorta.

### 3.1.3. Effect of AT2 activation on aortic rings

To validate the agonistic activity and selectivity of C21 towards AT2, phenylephrine pre-contracted aortic segments of C57BL/6, FVB/N and AT2<sup>-/-</sup> were challenged with increasing concentrations of C21. Aortic rings of C57BL/6 ( $pD_2$   $6.18 \pm 0.19$ ) and FVB/N ( $pD_2$   $6.67 \pm 0.18$ ) having an intact endothelium, relaxed at increasing concentrations of C21 reaching from  $10^{-9}$  to  $10^{-5}$  M, but as expected there was no relaxation in aortic rings of AT2<sup>-/-</sup> with lack of

AT2 (\*P<0.0001 vs. AT2<sup>-/-</sup>, Tukey's post-hoc test following Two-way analysis of variance, **Figure 3-5**).

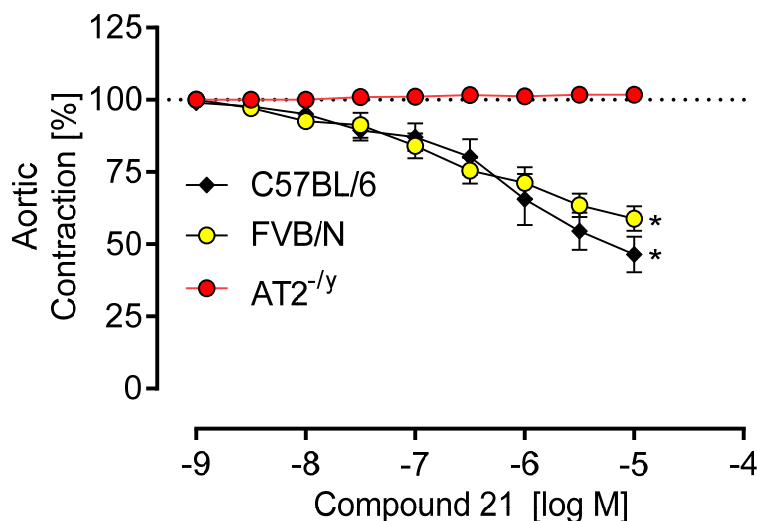


**Figure 3-5:** Cumulative concentration-response curves to compound 21 in phenylephrine ( $10^{-7}$  M) pre-contracted mouse thoracic aortic rings with intact endothelium. Compound 21 induces relaxation in aortic rings of C57BL/6 and FVB/N. In contrast, there is no effect in aortic rings of AT2<sup>-/-</sup> which indicates specificity of compound 21 for AT2 (n=6 each, P=0.0001, Two-way ANOVA, \*P<0.0001 vs. AT2<sup>-/-</sup>, Tukey's multiple comparison test).

While acetylcholine-induced vasorelaxation is dependent on endothelium-derived NO, endothelial dependence of C21-induced vasorelaxation still had to be confirmed. Thus, the aortic rings of C57BL/6 were stripped of their endothelium and the result confirmed by the missing response to acetylcholine. Then the denuded aortic rings were challenged with rising concentrations of C21 reaching from  $10^{-9}$  to  $10^{-5}$  M, however no statistically significant effect was produced (P=0.5116, Two-way analysis of variance, **Figure 3-6**). This part of the experiment provides evidence for an endothelium-dependent vasodilator effect produced by C21 in aortic rings of mice. Overall, organ bath experiments demonstrated that C21 is capable of inducing endothelium-dependent and AT2-mediated relaxation of aortic rings pre-contracted with phenylephrine. Accordingly, the stimulation of AT2 with the selective AT2 agonist C21 represents a valid pharmacological tool for further investigations.

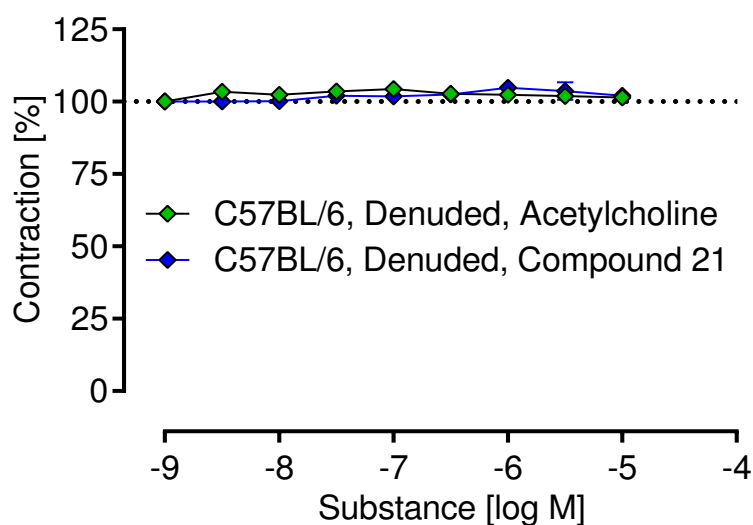


**Figure 3-6:** Denuded aortic ring segments of C57BL/6 after pre-contraction with phenylephrine ( $10^{-7}$  M) are subsequently challenged with accumulating concentrations of acetylcholine and compound 21 (both reaching from  $10^{-9}$  to  $10^{-5}$  M). The denudation of the aorta's endothelium is verified through the lack of response to the endothelium-dependent relaxation induced by acetylcholine. Similarly, the subsequent challenge with compound 21 does not produce vasorelaxation (n=6 each,  $P=0.5116$ , Two-way ANOVA).

### 3.2. AT2 activation in bradykinin-induced extravasation

In non-allergic bradykinin-induced angio-oedema, the endothelial barrier is disrupted due to B2 overactivation, resulting in increased plasma extravasation accompanied with a swelling of the skin, mucosa and submucosa. The Miles assay is a suitable instrument for quantifying dermal extravasation in the skin of laboratory animals. In this experiment, the role of AT2 in bradykinin-induced angio-oedema was investigated in the skin of C57BL/6 mice. For this purpose, the mice were treated half an hour prior to the Miles assay with either C21 (0.5 mg/kg bodyweight), C21 in combination with PD123319 (0.5 mg/kg bodyweight), or C21 in combination with icatibant (0.5 mg/kg bodyweight). The control group included mice that were pre-treated with vehicle solution. Dermal extravasation developed in the dorsal skin of mice in response to the intradermal injection of either bradykinin, labradimil or histamine (2 nmol each). The additional intradermal injection of vehicle solution served as control. Over the course of 30 minutes, the previously injected albumin-bound dye Evans blue continuously accumulated at the injection sites along with the extravasates.

The extravasations were then cut out of the skin to extract the accumulated dye for further quantification using a spectrometer. In the following, extravasation is expressed as the fold increase in Evans blue concentration as compared to vehicle. Compared to vehicle, treatment with C21 significantly increased dermal extravasation induced by bradykinin from  $3.9 \pm 0.22$ -fold to  $4.7 \pm 0.15$ -fold of vehicle ( $*P < 0.05$  vs. control, Tukey's post-hoc test following One-way analysis of variance), but extravasation induced by labradimil, that is a proteolytic stable bradykinin analogue, was not significantly increased (from  $4.0 \pm 0.14$ -fold to  $4.1 \pm 0.20$ -fold of vehicle). As anticipated, there was no significant increase in histamine-induced extravasation in the treatment group receiving C21 (from  $4.0 \pm 0.14$ -fold to  $4.1 \pm 0.16$ -fold of the vehicle, **Figure 3-7**). The difference between bradykinin-induced and labradimil-induced extravasation could be related to reduced degradation of bradykinin, but not of labradimil, which is metabolically more stable because of its non-peptide structure [Shimuta et al., 1999].

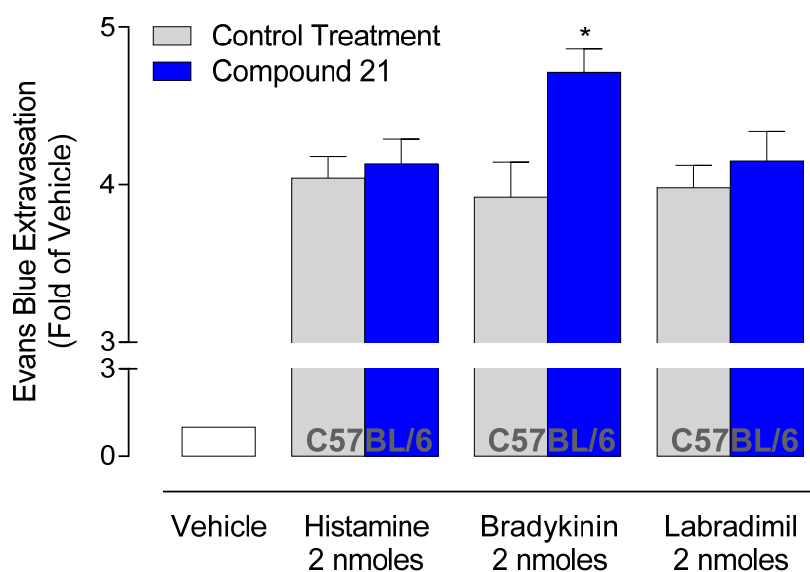


**Figure 3-7:** Results from the Miles assay to evaluate bradykinin-induced plasma extravasation in the dorsal skin of C57BL/6 mice. Pre-treatment with compound 21 (0.5 mg/kg bodyweight) significantly increased dermal extravasation from  $3.9 \pm 0.2$ -fold to  $4.7 \pm 0.2$ -fold of vehicle. In striking contrast, extravasation induced by the synthetic B2 agonist labradimil, which cannot be hydrolysed by ACE is not affected ( $n=12$  each,  $P < 0.0001$ , One-way ANOVA,  $*P < 0.05$  vs. control, Tukey's multiple comparison test). Vehicle denotes physiologic buffer solution.

To test whether the observed effect of increased bradykinin-induced dermal extravasation can be attributed to the AT2 signalling pathway, mice were pre-treated with C21 in combination with the AT2 antagonist PD123319. In this experiment, no significant effect on bradykinin-induced extravasation was produced, since PD123319 inhibited the effect of C21 ( $P < 0.0001$ , One-way analysis of variance, **Figure 3-8**). Apparently, the enhancing effect of C21 on bradykinin-induced extravasation in the dorsal skin of C57BL/6 is triggered by stimulation of AT2. To confirm this finding, the Miles assay was also performed on genetically modified C57BL/6 lacking the AT2 receptor. In those AT2 knockout mice, treatment with C21 had no additional effect on bradykinin-induced extravasation, confirming that the enhancing effect on bradykinin-induced extravasation previously observed in C57BL/6 is indeed mediated by AT2 ( $P < 0.0001$ , One-way analysis of variance, **Figure 3-9**).

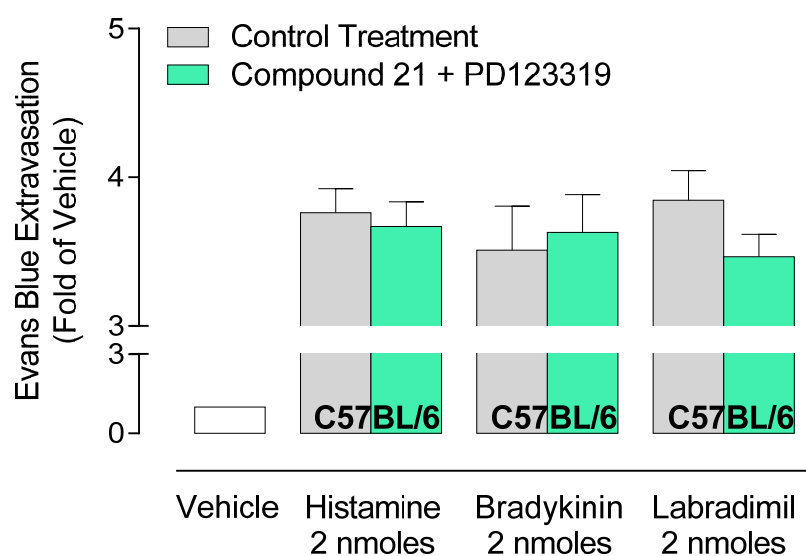


**Figure 3-8:** Results from the Miles assay to test the AT2 dependence of increased bradykinin-induced extravasation following treatment of C57BL/6 with compound 21. Treatment of C57BL/6 with PD123319 in addition to compound 21 (0.5 mg/kg bodyweight each) has no significant effect on bradykinin-induced or labradimil-induced extravasation as compared to control treatment. Similarly, histamine-induced extravasation is not affected in any treatment group ( $n=5$  each,  $P < 0.0001$ , One-way ANOVA). Vehicle denotes physiologic buffer solution.

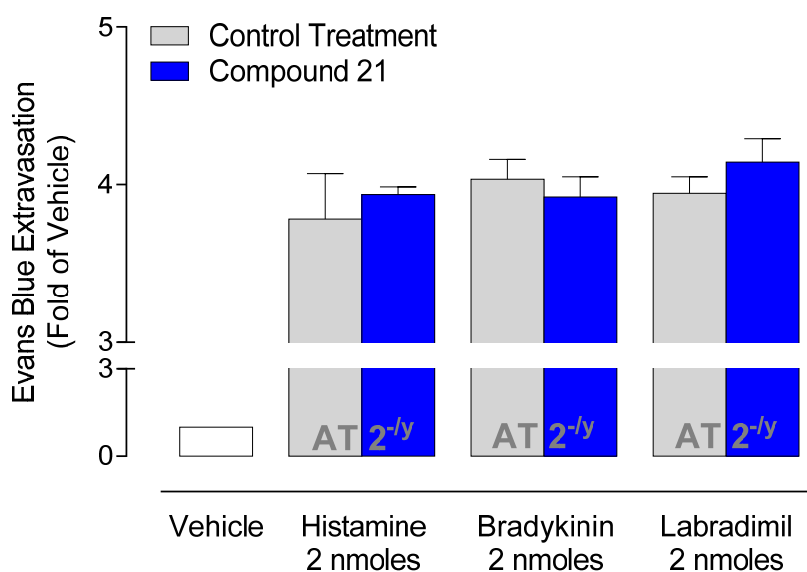


**Figure 3-9:** Results from the Miles assay to test the AT<sub>2</sub> dependence of increased bradykinin-induced extravasation following treatment of genetically modified C57BL/6 lacking AT<sub>2</sub> (AT<sub>2</sub><sup>-/-</sup>) with compound 21. AT<sub>2</sub><sup>-/-</sup> mice pre-treated with compound 21 (0.5 mg/kg bodyweight) show no effect regarding bradykinin-induced or labradimil-induced extravasation as compared to control treatment. Similarly, histamine-induced extravasation is not affected in any treatment group (n=5 each, P<0.0001, One-way ANOVA). Vehicle denotes physiologic buffer solution.

While it is known that intradermal injection of bradykinin and subsequent overactivation of B<sub>2</sub> is responsible for extravasation in the skin, it remains unclear whether the enhancing effect of C21 is also mediated by B<sub>2</sub> activation. To clarify this, an additional experiment was performed in which mice were pre-treated with the B<sub>2</sub> antagonist icatibant in addition to C21. The treatment with icatibant strongly and significantly reduced bradykinin-induced extravasation from 3.5±0.29-fold to 1.8±0.28-fold of vehicle. Likewise, the combined treatment with C21 and icatibant (C21/ICA) significantly reduced bradykinin-induced extravasation to 2.0±0.13-fold of vehicle. A similarly significant effect was observed in labradimil-induced extravasation in the group treated with icatibant (2.3±0.13-fold of vehicle) and in the treatment group receiving the combination of C21 and icatibant (1.79±0.22-fold of vehicle; \*P<0.001 vs. control, Tukey's post-hoc test following One-way analysis of variance). As anticipated, no effect on histamine-induced extravasation was observed (**Figure 3-10**). These findings suggest the need for B<sub>2</sub> activation to enhance bradykinin-induced extravasation in the skin of mice after AT<sub>2</sub> activation by C21.

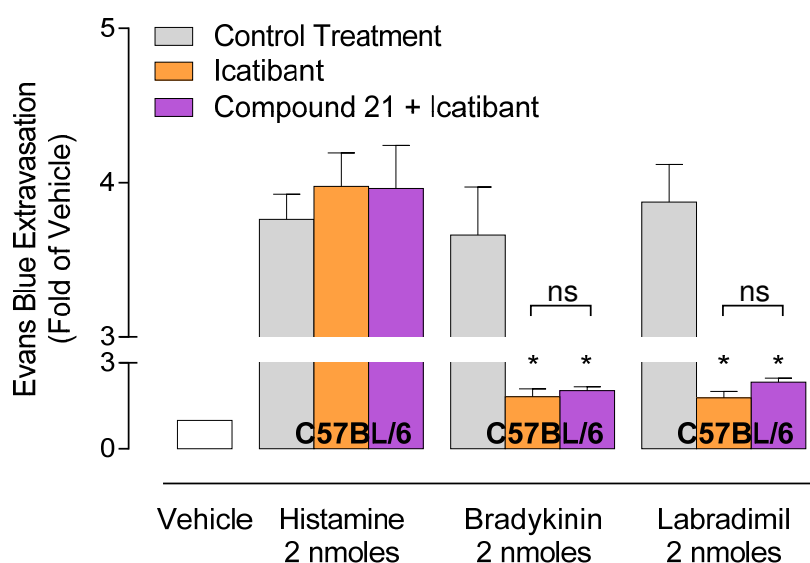


**Figure 3-10:** Results from the Miles assays to evaluate the role of B2 in the enhanced bradykinin-induced extravasation, following AT2 activation. The effect of compound 21 on extravasation is dependent on B2 since icatibant, the selective B2 antagonist, reduces extravasation despite of treatment with compound 21 in a significant and similar manner as compared to non-treatment (n=5 each,  $P < 0.0001$ , One-way ANOVA,  $*P < 0.001$  vs. control, Tukey's multiple comparison test). Icatibant does not affect histamine-induced extravasation; vehicle denotes physiologic buffer solution.

The Miles assay is a suitable tool to assess induced extravasation in the skin of mice, as these experiments involving C21 revealed: AT2 activation by pre-treatment with C21 increased vascular permeability and enhanced the bradykinin-induced extravasation of the albumin-bound dye Evans blue. This effect was abolished by PD123139 indicating its dependence on AT2 activation. Inhibition of B2 by icatibant revealed that B2 activation is crucial for the effect of C21, which enhances bradykinin-induced extravasation in the skin of mice. However, C21 did not affect labradimil-induced extravasation. Considering the higher stability and half-life of labradimil but the lower affinity towards B2 in comparison to bradykinin, there might be a decreased elimination of bradykinin, e.g., reduced enzymatic degradation by ACE as an explanation. In conclusion, AT2 activation increases in a B2 dependent manner the dermal extravasation in the skin of mice, this effect might be accountable to a decreased degradation of bradykinin.

### 3.3. Blood pressure and heart rate measurements

In organ bath studies, C21 produced an endothelium-dependent and AT<sub>2</sub>-mediated relaxation of pre-contracted mouse aortic rings, and in Miles assays, mice pre-treated with C21 showed an increased bradykinin-induced dermal extravasation. These findings put forward the question whether C21 might also influence central blood flow and affect skin perfusion. In spontaneously hypertensive rats it was shown that C21 alone did not have an effect on blood pressure, however simultaneous blockade of the AT<sub>1</sub> receptor revealed a depressor effect which was abolished by PD123319 [Bosnyak et al., 2010], suggesting that C21 does not affect skin perfusion. A similar approach was chosen in normotensive C57BL/6 mice to investigate a possible contribution of AT<sub>2</sub> activation to blood pressure. Those mice received daily bolus injections of C21 (0.5 mg/kg bodyweight), telmisartan (10 mg/kg bodyweight), or both, and their SBP and heart rate were determined using the tail-cuff system. While C21 (123.3±3.23 mmHg) alone had no significant effect on SBP of C57BL/6, treatment with telmisartan significantly lowered SBP from 118±1.76 mmHg (baseline value) to 98.1±1.82 mmHg. Similarly, combined treatment with telmisartan and C21 significantly reduced the SBP to 104.1±1.44 mmHg (\*P<0.001 vs. baseline, Tukey's multiple comparison test following One-way analysis of variance), but the difference between the latter treatment groups was not statistically significant (**Figure 3-11**).

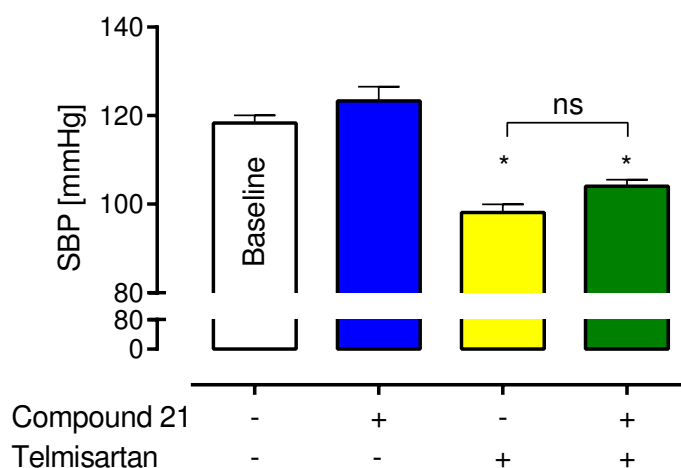


**Figure 3-11:** Systolic blood pressure (SBP) of awake C57BL/6 mice after daily treatment schedules, measured with an automated tail-cuff system. Compared to the baseline value, compound 21 (0.5 mg/kg bodyweight) does not affect SBP. The treatment with telmisartan (10 mg/kg bodyweight) and combined treatment with telmisartan and compound 21 results in a significantly reduction of SBP, but there is no significant difference between those treatment groups (n=8 each, P<0.0001, One-way ANOVA, \*P<0.001 vs. baseline, Tukey's multiple comparison test).

Given that stress is correlated with heart rate and may impact blood pressure, the heart rate was also monitored during each tail-cuff session to evaluate the level of stress. The data from this experiment were considered reliable as long as the mean heart rate of each treatment group was below 600 beats per minute, which was achieved after a one-week adaptation phase. The measurements revealed no significant differences between the treatment groups ( $P=0.1753$ , One-way analysis of variance, **Figure 3-12**).

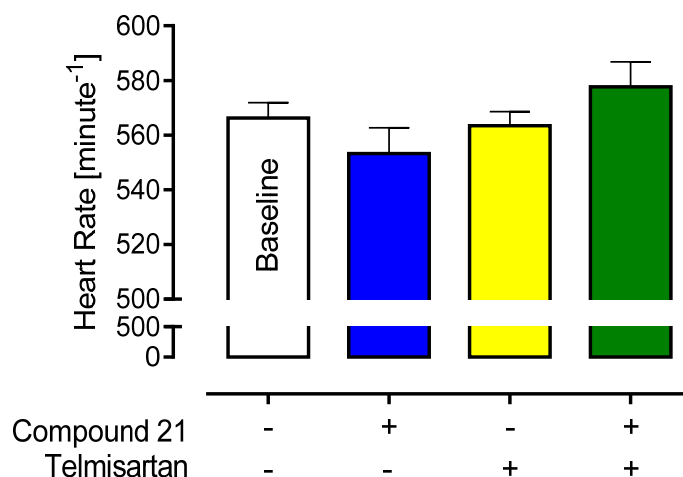


**Figure 3-12:** Heart rates of C57BL/6 during blood pressure measurements. Despite treatment with compound 21 (0.5 mg/kg bodyweight), telmisartan (10 mg/kg bodyweight) or the combination of both, the measured heart rates do not differ across treatment groups. The data shown are the mean values calculated from the last three days of measurement ( $n=8$  each,  $P=0.1753$ , One-way ANOVA).

In conclusion, treatment of C57BL/6 with C21 did not reveal any effect on SBP, nor was there any additional effect when those mice were treated with telmisartan in addition to C21, as no difference was found in comparison to the treatment with telmisartan alone. It is likely that AT2 activation has no effect on skeletal muscle arterioles that determine blood pressure, but an influence on vasomotion of the small dermal blood vessels cannot be excluded, considering the increased bradykinin-induced extravasation in the preceding Miles assay experiment. It should also be taken into account that when systemic blood pressure drops below a certain level, the skin is not perfused properly with blood and it would be difficult to detect extravasation even if provoked. The effect of systemic arterial blood pressure on skin perfusion was previously observed in mice that received high doses of the ACE inhibitor moexipril, which significantly diminished bradykinin-induced and histamine-induced dermal extravasations [Bisha et al., 2018].

### 3.4. Extravasation detected by two-photon excitation microscopy

TPEM was established as a complementary visual detection method to the Miles assay for the in-vivo assessment of extravasation. Although the Miles assay is useful to study the effect of permeabilizing mediators in the skin of mice, it does not reveal whether the albumin-binding dye Evans blue is predominantly distributed in the interstitial or intravascular space. Furthermore, extravasation can only be quantified at the injection site and at a specific time, usually after 20 to 30 minutes and after excision of the affected tissue followed by elution of the dye overnight. Consequently, the Miles assay only detects locally stimulated extravasation, but does not allow quantification of endothelial permeability of dermal blood vessels under non-inflammatory conditions, nor does it provide information on physiological plasma circulation or extravasation. These limitations were overcome by the TPEM using two different fluorescent dyes of different molecular weight: the dye of higher molecular weight would remain inside the vascular lumen while the dye of lower molecular weight would leave the vascular lumen over time and accumulate inside the interstitial space. This method was successfully used to visualize dermal blood vessels in the earlobes of mice and to monitor the barrier function of those vessels over time. Previous results from two-photon excitation microscopy showed that physiologic extravasation in mice was not affected by overexpression of B2 receptors or despite systemic inhibition of B2 by icatibant or treatment with the ACE inhibitor moexipril [Bisha et al., 2018], suggesting that B2 activity may be negligible during physiological plasma extravasation. A more profound activation of B2 would be of interest to study the barrier function of dermal blood vessels during the pathological state which is present in bradykinin-induced oedema.

Thus, anesthetized C57BL/6 mice received intravenous injections of a 250 kDa fluorescence-labelled dextran to enable visualization of the microvasculature inside one of the earlobes as well as a 10 kDa fluorescence-labelled dextran to detect extravasation over a period of 45 minutes. To induce extravasation, the treatment group received 30 minutes prior to recordings an intraperitoneal bolus injection of the B2 agonist labradimil (20 mg/kg bodyweight) while the control group received vehicle solution, i.e., PBS. As anticipated, because of its size, the 250 kDa dye remained in the vascular lumen throughout the entire recording session, which allowed continuous visualisation of the small dermal vessels inside the earlobe. Contrary, the 10 kDa dye gradually left the vascular lumen over the 45 minutes. Against expectations, treatment with labradimil had no effect on physiological extravasation, as no significant difference was found when compared to control treatment

( $P < 0.0001$ , Two-way analysis of variance). Although a delayed extravasation with slower onset of maximum was observed within the first 20 minutes, this could be associated with reduced systemic blood pressure, possibly induced by overactivation of B2 (**Figure 3-13**).

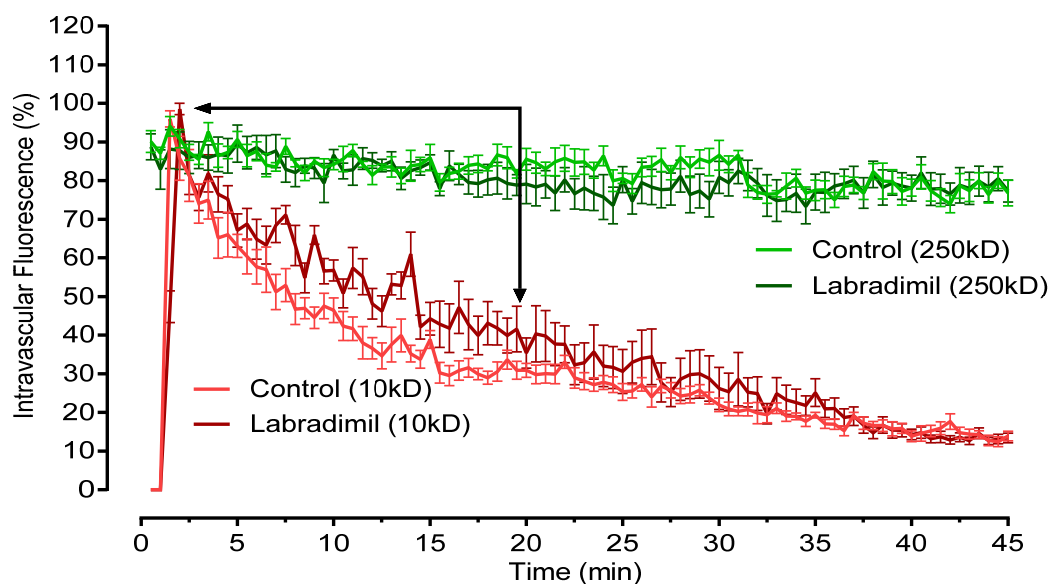


**Figure 3-13:** Processed two-photon excitation microscopy imaging data of small dermal blood vessels in the ear of anaesthetized C57BL/6. Mice in the control group are treated with vehicle, while the other group is treated with labradimil (20 mg/kg bodyweight). Recordings show the 10 kDa probe but not the 250 kDa probe leaving the vascular lumen spontaneously over the period of 45 minutes. Treatment with labradimil does not significantly change the rate of extravasation when compared to vehicle treatment, but a small trend of delayed extravasation with slower onset of maximum (arrow marks) is observed ( $n=6$ , for each time point,  $P < 0.0001$ , Two-way ANOVA).

After injection, the 10 kDa probe extravasated continuously until there was almost no vascular fluorescence measurable. Considering the size of the 10 kDa dextran, it is roughly comparable to the size of a small globular blood protein such as myoglobin which under physiologic conditions easily leaves the vascular lumen (Koskelo, Kekki and Wager (1967)). This might also explain why there was no significant increase in the velocity or quantity of the 10 kDa dye's extravasation despite the treatment with labradimil. As for larger proteins such as albumin (~68 kDa) extravasation only occurs in small amounts, but under pathologic conditions, i.e., the formation of oedema, albumin is found among other larger proteins in exudates of oedematous tissue. In light of this result, a new approach was chosen in which the 10 kDa dextran dye was replaced by a 70 kDa dextran dye. The latter corresponds approximately to the molecular weight

of albumin. However, this approach also proved to be ineffective because unlike the result obtained with the 10 kDa dye, the 70 kDa dye did not leave the vessel lumen. Consequently, there was no significant difference between the control and the treatment group ( $P=0.0335$ , Two-way analysis of variance, **Figure 3-14**).

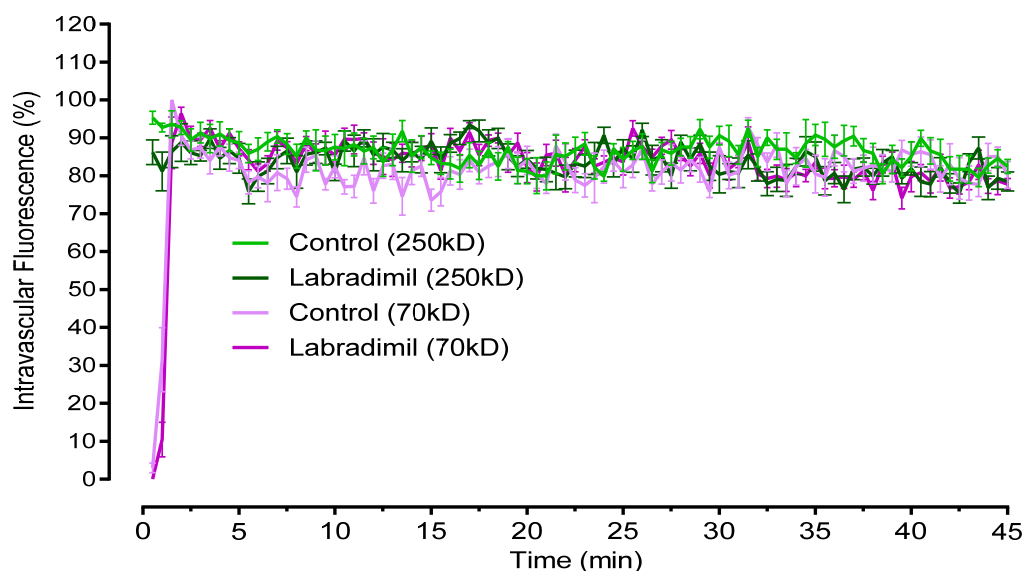


**Figure 3-14:** Processed two-photon excitation microscopy imaging data of small dermal blood vessels in the ear of anaesthetized C57BL/6. In both treatment groups, the 70 kDa and the 250 kDa probe display similar characteristics and do not leave the vascular lumen during the period of 45 minutes ( $n=6$  for each time point,  $P=0.0335$ , Two-way ANOVA).

In summary, the TPTEM is a suitable in-vivo instrument to evaluate physiologic extravasation in small blood vessels over time. The treatment of mice with labradimil to induce extravasation and the use of the 10 kDa dextran dye to assess a possible impairment of the endothelial barrier showed no significant differences compared to the control treatment. Changing the size of the dye to 70 kDa did not lead to the desired result either, quite the contrary, because the fluorescence signal did not leave the vascular lumen until the end of recording. On the one hand, if there is an actual increase in endothelial permeability, the 10 kDa dextran could be considered too low in molecular weight to detect a difference. On the other hand, the 70 kDa dye resembles albumin only in its molecular weight, otherwise there is no similarity with the folded structure of that protein. A new approach might be the use of a spherical instead of a linear probe, e.g., the use of a fluorescent conjugate of albumin.

### 3.5. Effect of AT2 activation on ACE activity

#### 3.5.1. ACE activity in endothelial cells

Results from the Miles assay showed an increased bradykinin-induced but not labradimil-induced extravasation in the skin of mice which assumedly is connected to a reduced enzymatic degradation. To evaluate a possible effect of AT2 signalling on the activity of ACE which is the key enzyme in degradation of bradykinin, homogenates of HDMECs were incubated with related substances and assayed for the catalytic activity of ACE. For comparative purposes, ACE activity data from human umbilical vein endothelial cells (HUVECs) were kindly provided by the local institute's research group, parts of which have already been published [Dao et al., 2016]. For the ACE activity assay in HUVECs incubations were performed with either PD123319, Ang II in combination with telmisartan or PD123319 in addition to that combination. Also, incubations with vehicle solution were performed which served as control. Results of ACE activity assay in homogenates of HUVECs showed that incubation with telmisartan and Ang II significantly reduced ACE activity to  $46.9\pm 4.4\%$  as compared to vehicle (\* $P < 0.05$  vs. vehicle, Tukey's post-hoc test following One-way analysis of variance), and this effect was abolished in the presence of PD123319. Of note, PD123319 alone did not have an effect on ACE activity (**Figure 3-15**). In HUVECs, under concurrent inhibition of AT1, the AT2 was targeted by its substrate Ang II which resulted in a decrease of ACE activity.

In analogy to the experiments with HUVECs, for the preparation of the ACE activity assay in HDMECs, incubations were performed with either PD123319, C21, the combination of C21 and PD123319 or captopril, with vehicle solution used for control incubations. Incubation of HDMECs with the selective AT2 agonist C21 resulted in a significant reduction of ACE activity to  $51.0\pm 2.8\%$  as compared to vehicle. PD123319 alone had no effect on ACE activity, but was capable of abolishing the effect of C21. Incubation with captopril almost completely inhibited ACE activity (\* $P < 0.05$  vs. vehicle, Tukey's post-hoc test following One-way analysis of variance, **Figure 3-15**). In summary, two different approaches, one based on indirect stimulation of AT2 by combined incubation with telmisartan and Ang II and the other based on direct stimulation of AT2 by incubation with C21, led to a similar result. Furthermore, the reduction in ACE activity was abolished by PD123319, suggesting that this effect is dependent on AT2. Furthermore, the specificity of the ACE activity assay was confirmed after incubation with captopril, which almost completely inhibited ACE activity.

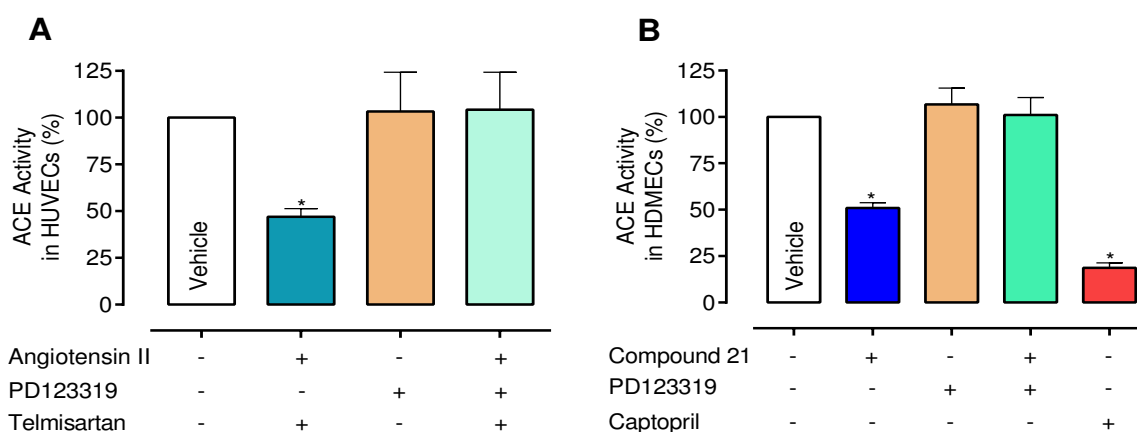


**Figure 3-15:** The results from the ACE activity assay performed with human endothelial cell lysates. **(A)** Co-incubation of HUVECs for three hours with angiotensin II and telmisartan significantly reduces ACE activity as compared to vehicle, this effect is abolished by PD123319. (n=5 each, P=0.0154, One-way ANOVA, \*P<0.05 vs. vehicle, Tukey's multiple comparison test). **(B)** When HDMECs are incubated with the AT2 agonist compound 21, a significant reduction in ACE activity is observed within one hour. PD123319 alone does not have an effect on ACE activity but blocks the effect produced by compound 21. Captopril almost abolishes ACE activity which validates the assay's selectivity for ACE (n=6 each, P<0.0001, One-way ANOVA, \*P<0.05 vs. vehicle, Tukey's multiple comparison test). In both cell line incubation with PD123319 alone does not have an effect on ACE activity. The above substances were used for incubation at a concentration of 100  $\mu$ M.

### 3.5.2. ACE activity in lung lysates and plasma of mice

Results from incubation experiments with endothelial cells indicate that there is a link between AT2 activation and reduction of ACE activity. Therefore, an in-vivo approach was chosen to further investigate ACE activity in lung lysates and plasma of C57BL/6. For this purpose, those mice were pre-treated for one hour with either captopril (10 mg/kg bodyweight), telmisartan (10 mg/kg bodyweight), C21 (0.5 mg/kg bodyweight), the combination of C21 plus telmisartan or C21 plus PD123319 (0.5 mg/kg bodyweight). Moreover, the treatment with vehicle solution served as control. Next, blood and lungs were collected and processed according to the protocol for measuring ACE activity. Data of the ACE activity assay on lung lysates did not reveal a significant difference in ACE activity in any treatment group as compared to control. Still, there was a trend of reduced ACE activity after treatment with telmisartan comparable to that of the treatment groups C21/PD123319 and C21/telmisartan. Captopril, which confirmed the specificity of the assay, significantly reduced ACE activity to  $6.7 \pm 0.7\%$  as compared to control treatment (\*P<0.0001 vs. other conditions, Tukey's post-hoc test following One-way analysis of variance, **Figure 3-16**).

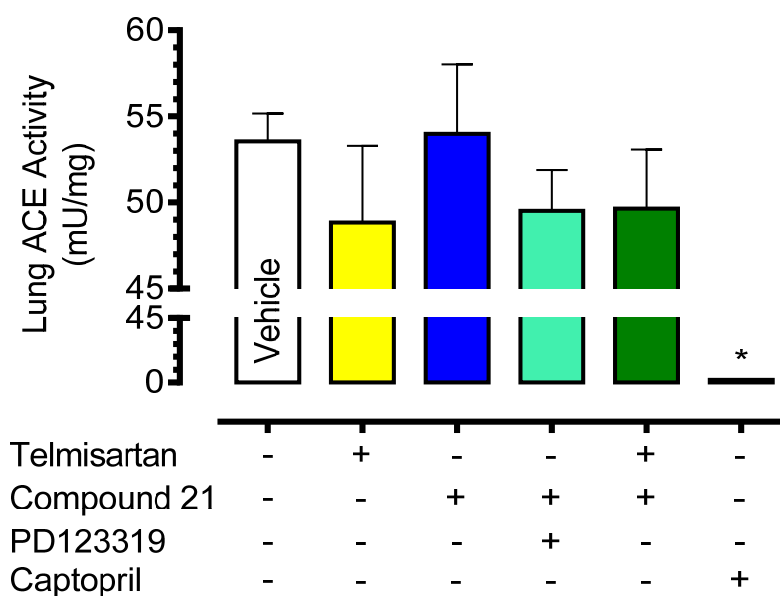


**Figure 3-16:** The results from the ACE activity assay performed with lung lysates of C57BL/6. The One-hour treatment with either telmisartan (10 mg/kg bodyweight), compound 21 (0.5 mg/kg bodyweight), the combination compound 21 plus telmisartan or compound 21 plus PD123319 (0.5 mg/kg bodyweight) shows no statistically significant change in the ACE activity of lung lysates as compared to vehicle treatment. Captopril (10 mg/kg bodyweight) almost abolishes ACE activity which shows the assay's specificity for ACE (n=6 each,  $P < 0.0001$ , One-way ANOVA,  $*P < 0.0001$  vs. other conditions, Tukey's multiple comparison test).

Similar results were obtained from plasma samples that showed no significant differences in ACE activity among the treatment groups. The specificity of the assay was again confirmed by strong inhibition of ACE with captopril, reducing the measured ACE activity to  $6.7 \pm 0.4\%$  as compared to control treatment ( $*P < 0.0001$ , Tukey's post-hoc test following One-way analysis of variance, **Figure 3-17**).

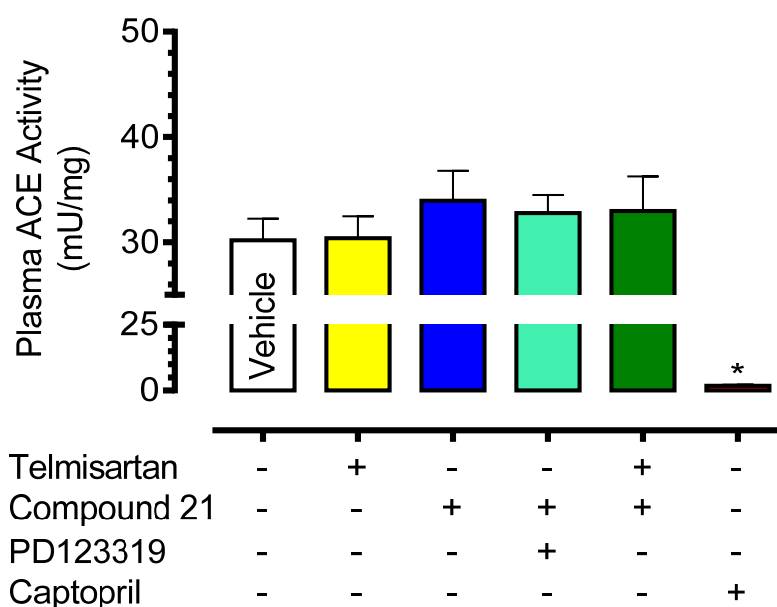


**Figure 3-17:** The results of the ACE activity assay performed with plasma samples taken from C57BL/6. Blood samples are collected after a one-hour treatment with either telmisartan (10 mg/kg bodyweight), compound 21 (0.5 mg/kg bodyweight), the combination C21 plus telmisartan or C21 plus PD123319 (0.5 mg/kg bodyweight). The assay reveals no statistically significant change in ACE activity in those treatment group as compared to vehicle treatment. Captopril (10 mg/kg bodyweight) almost abolishes ACE activity which shows the assay's specificity for ACE (n=6 each,  $P < 0.0001$ , One-way ANOVA,  $*P < 0.0001$  vs. other conditions, Tukey's multiple comparison test).

The lack of an effect produced by AT2 activation in-vivo might be attributed to the generally high elimination rate of drugs in mice. This can lead to poor effective plasma concentrations as well as short-lived effects of C21. Accordingly, the dose of C21 was increased to 1.0 mg/kg bodyweight and the time of treatment was reduced to 30 minutes. Interestingly, the plasma samples of those mice had a significant increase of plasma ACE activity to  $129.9 \pm 13.6\%$  as compared to vehicle treatment ( $*P = 0.0131$  vs. vehicle, unpaired t-test, **Figure 3-18**). One explanation for this result could be an increased concentration of circulating ACE, possibly induced by AT2 activation. Unfortunately, no significant change in ACE activity was found in lung lysates ( $P = 0.9083$  vs. vehicle, unpaired t-test, **Figure 3-19**).

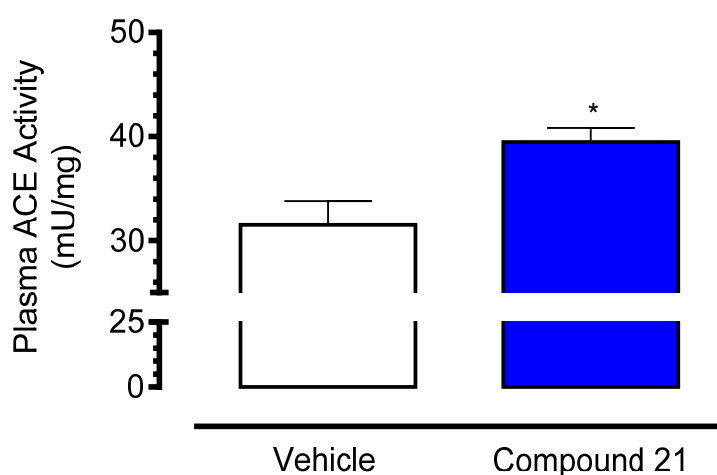


**Figure 3-18:** The results of the ACE activity assay performed with plasma samples taken from C57BL/6. In plasma of those mice, ACE activity is significantly increased after 30 minutes treatment with compound 21 (1.0 mg/kg bodyweight) in comparison with vehicle (n=6 each, \*P=0.0131 vs. vehicle, calculated using two-tailed unpaired t-test).

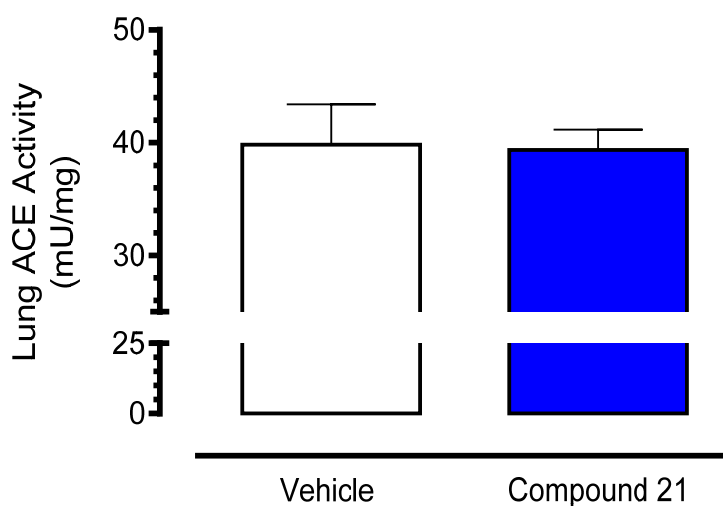


**Figure 3-19:** The results from the ACE activity assay performed with lung lysates of C57BL/6. After 30 minutes of treatment with compound 21 (1.0 mg/kg bodyweight) ACE activity is not significantly affected as compared to vehicle treatment (n=6 each, P=0.9083 vs. vehicle, calculated using two-tailed unpaired t-test).

The in-vitro effects of reduced ACE activity observed in HUVECs and HDMECs by stimulation of AT2 were not reproducible in-vivo with lung and blood samples of C57BL/6 that were pre-treated with C21. However, after increasing the concentration of C21 to 1.0 mg/kg bodyweight, plasma ACE activity was significantly increased after only 30 minutes, whereas in lung lysates there was still no effect. It appears that a higher concentration for C21 is necessary to trigger an effect on ACE activity in-vivo. Based on the hypothesis of an AT2-induced release of cell membrane-bound ACE and the associated increase in systemically circulating ACE, the increase in ACE activity observed in plasma samples could be explained. One might expect a reduction of membrane bound ACE in this process which should have been shown in lung lysates of the affected mice. Although ACE is predominantly expressed in lung capillaries, the effect of the postulated AT2-mediated shedding might not be enough to make a significant reduction in ACE activity detectable.

### **3.6. Effect of AT2 activation on ACE protein content**

#### **3.6.1. ACE content in incubated lung fragments by western blot analysis**

Previous experiments that showed increased ACE activity in plasma but not in lung lysates of mice pre-treated with C21, raise the question how the ACE concentration might be affected. Accordingly, to quantify the effect of AT2 activation on ACE protein content, isolated lung fragments of C57BL/6 were incubated in organ bath buffer containing C21 at a final concentration of 100  $\mu$ M. Incubation in vehicle solution served as a control. Afterwards, ACE protein content was determined by western blot using the supernatant and prepared lung lysates. Incubation with C21 resulted in a slight but not statistically significant decrease in ACE concentration in lung lysate as compared to the control incubation. Conversely, the supernatants of lungs incubated with C21 showed an increase in ACE concentration (\* $P$ <0.05 vs. vehicle, Tukey's post-hoc test following One-way analysis of variance). Also, the difference in ACE content between lysate and supernatant was significant (\* $P$ <0.015 vs. lysate, unpaired t-test, **Figure 3-20**).

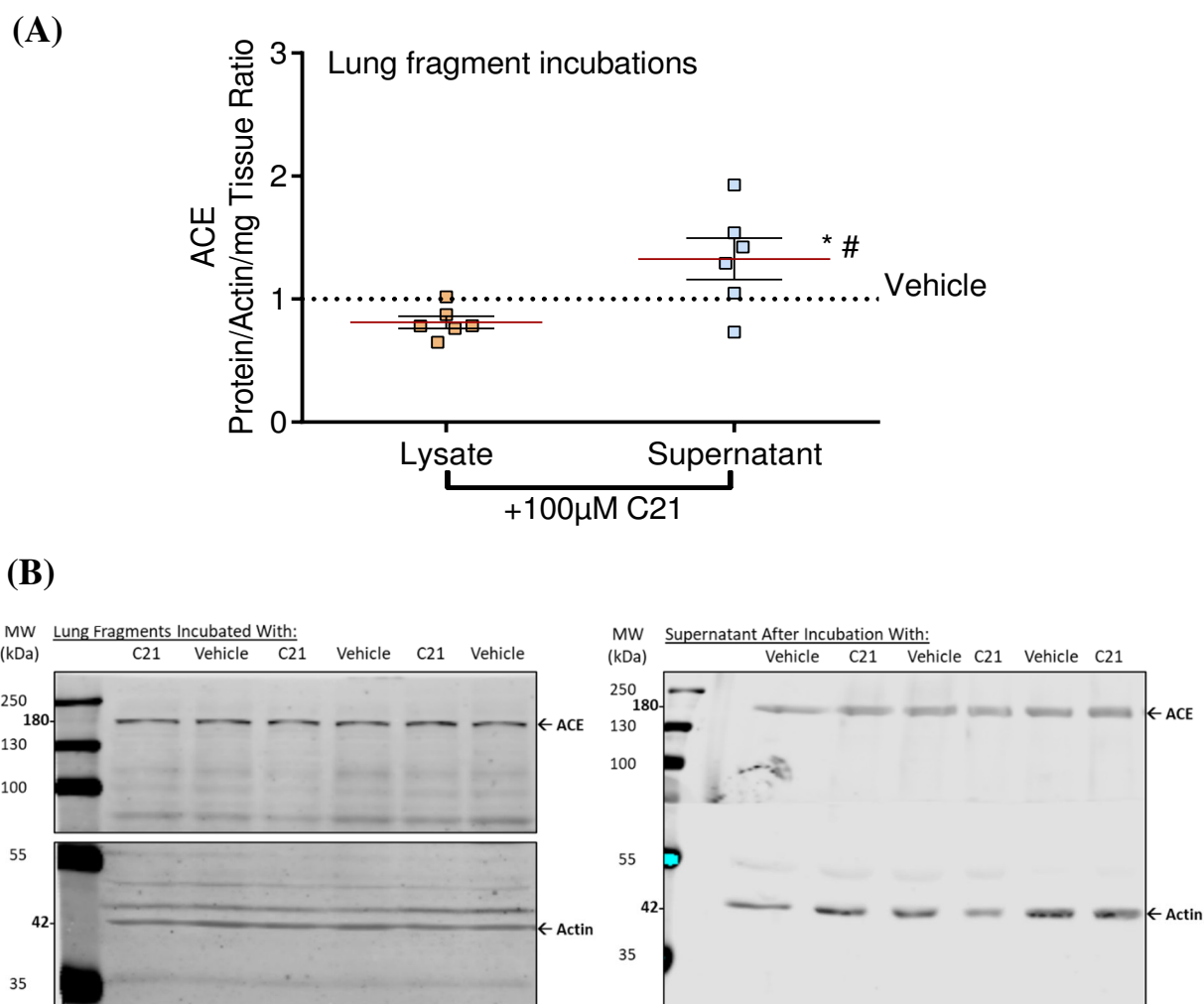


**Figure 3-20:** Results of the quantitative western blot on ACE protein content as determined in lysates of incubated lungs that were collected from C57BL/6. **(A)** Incubation of lungs fragments with compound 21 (C21) for 30 minutes results in a numerical reduction of the ACE protein content in lung lysates to  $0.81 \pm 0.05$ -fold as compared to incubation with vehicle. In contrast, supernatants from lungs incubated with C21 show a statistically significant increase in ACE content to  $1.33 \pm 0.17$ -fold when compared to vehicle. ( $n=6$  each,  $P=0.0046$ , One-way ANOVA,  $*P<0.05$  vs. vehicle, Tukey's multiple comparison test). Also, there is a significant difference in ACE protein content between lysate and supernatant ( $n=6$  each,  $\#P<0.015$  vs. lysate, calculated using two-tailed unpaired t-test). **(B)** The images of western blots showing the detection of ACE and  $\beta$ -actin from lung lysates and supernatants, respectively. These images are shown as an overlay of the signals detected at 700 nm and 800 nm, whereby the  $\beta$ -actin signal is only detectable at 800 nm.

Western blot analyses on the incubation experiments with C21 showed a trend towards decreasing ACE protein content in lung lysates, while ACE protein content was significantly increased in supernatants. This correlates with previous findings of increased ACE activity in plasma and unchanged ACE activity in lung lysates.

### 3.6.2. ACE content in plasma and lungs by western blot analysis

The incubation experiment with C21 to evaluate the effect of AT2 activation on lung fragments showed a significant increase in ACE protein content in the supernatant, but also a decrease in ACE protein content in lung lysates, which was not significant. In order to achieve a higher level of evidence for these findings, an in-vivo approach was chosen in which C57BL/6 were pre-treated with either telmisartan (10 mg/kg bodyweight), C21 (0.5 mg/kg bodyweight), telmisartan plus C21 or the latter in combination with PD123319 (0.5 mg/kg bodyweight). The treatment with vehicle solution served as a control. After 30 minutes, those mice were sacrificed and their lungs were extracted and prepared for quantitative western blot analysis to quantify ACE protein content. Results of the western blot analysis yielded a significant decrease in ACE protein content in lung lysates of C57BL/6 pre-treated with C21 ( $0.5 \pm 0.1$ -fold of vehicle), and this was also found in mice co-treated with C21 and telmisartan ( $0.42 \pm 0.1$ -fold of vehicle, \* $P < 0.05$  vs. vehicle, Tukey's post-hoc test following One-way analysis of variance). However, treatment with telmisartan alone had no significant effect on ACE protein content. In addition, the effect of C21 was eliminated by simultaneous treatment with PD123319 (**Figure 3-21**).

The observed reduction of ACE protein content in lung lysates of C57BL/6 after pre-treatment with the AT2 agonist C21, further supports the idea of a shedding mechanism induced by AT2 activation. Unfortunately, western blot analysis for corresponding plasma samples to detect a presumably C21-induced increase in ACE protein content did not yield valid results because of the relatively low plasma concentration of the target protein and possibly also due to methodological limitations.

### 3.6.3. ACE content in plasma by ELISA

Data from lung tissue of mice treated with the AT2 agonist C21 revealed a reduction of ACE protein content, however corresponding plasma samples couldn't be analysed by the same method. Therefore, the ACE protein content was determined by ELISA in plasma samples of C57BL/6, FVB/N and AT2<sup>-/-</sup> that were treated for one hour with either C21 (1.0 mg/kg bodyweight) or vehicle solution. Treatment with C21 did not significantly affect ACE protein content in any treatment group when compared to control. However, when compared to the C57BL/6 strain, the FVB/N strain revealed a significantly lower plasma ACE protein content in the vehicle ( $11.2 \pm 0.36$   $\mu\text{g/ml}$  vs.  $9.3 \pm 0.14$   $\mu\text{g/ml}$ ) and C21 treatment group ( $11.7 \pm 0.43$   $\mu\text{g/ml}$  vs.  $9.9 \pm 0.42$   $\mu\text{g/ml}$ , \* $P < 0.05$  vs. C57BL/6's control, # $P < 0.05$  vs. C57BL/6's compound 21, Tukey's post-hoc test following One-way analysis of variance, **Figure 3-22**).

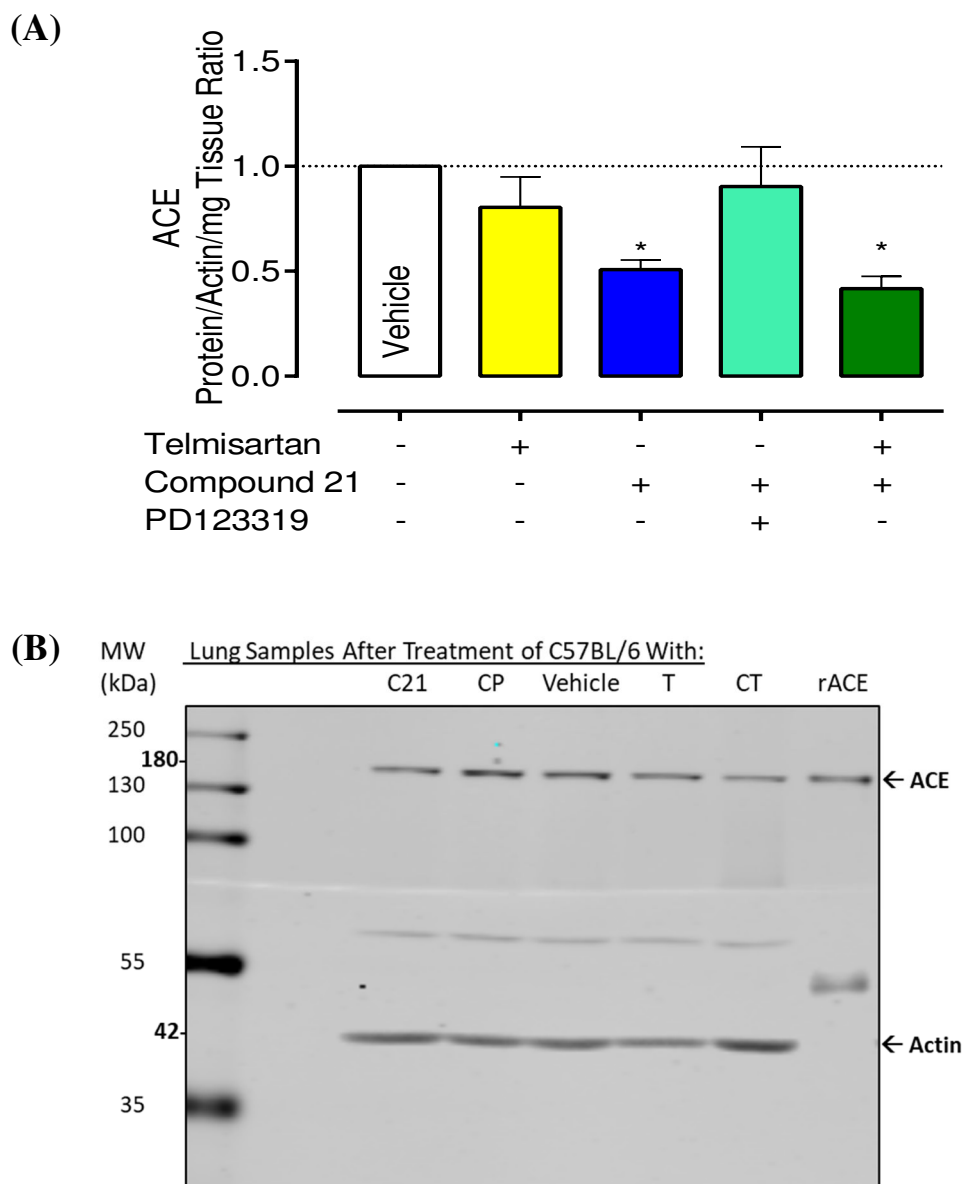


**Figure 3-21:** (A) Results of the quantitative western blot on ACE protein content as determined in lysates of lungs extracted from pre-treated C57BL/6. A 30-minute treatment of those mice with C21 significantly diminishes ACE protein content in lungs as compared to vehicle treatment. Similarly, a significant reduction of ACE protein content is observed after combined treatment with C21 and telmisartan, however telmisartan alone does not have an effect on ACE protein content in lungs. Furthermore, the effect of C21 is eliminated by PD123319 ( $n=6$  each,  $P=0.0035$ , One-way ANOVA,  $*P<0.05$  vs. vehicle, Tukey's multiple comparison test). (B) The image of a western blot showing the detection of ACE and  $\beta$ -actin in lysates that were extracted from the lungs of C57BL/6. Those mice were pre-treated either with vehicle solution (vehicle), telmisartan (T), compound 21 (C21), PD123319 in combination with C21 (CP) or the latter in combination with telmisartan (CT). Rabbit lung ACE (rACE) was used as a positive control. Signals are presented as an overlay of the detection channels 700 nm and 800 nm, but only the  $\beta$ -actin signal is detectable at 800 nm.

Results from the ACE-ELISA did not reveal a significant increase in plasma ACE protein content. Although ACE protein content was decreased in lung lysates of C57BL/6 treated with C21, there was no change of ACE protein concentration in plasma of C57BL/6. It is striking that a significantly lower plasma ACE protein content was found in FVB/N, whereas for AT2<sup>-/-</sup> this was only observed as a trend. While the effect of age and environment can be ruled out due to standardized keeping and age selection, it is most likely that observed disparities between the mouse strains are probably due to genetic background. Similarly, it has already been reported that the differential expression of ACE in people from different ethnic backgrounds may be related to polymorphisms of the ACE gene [Bouzekri et al., 2004; Danilov et al., 2017].

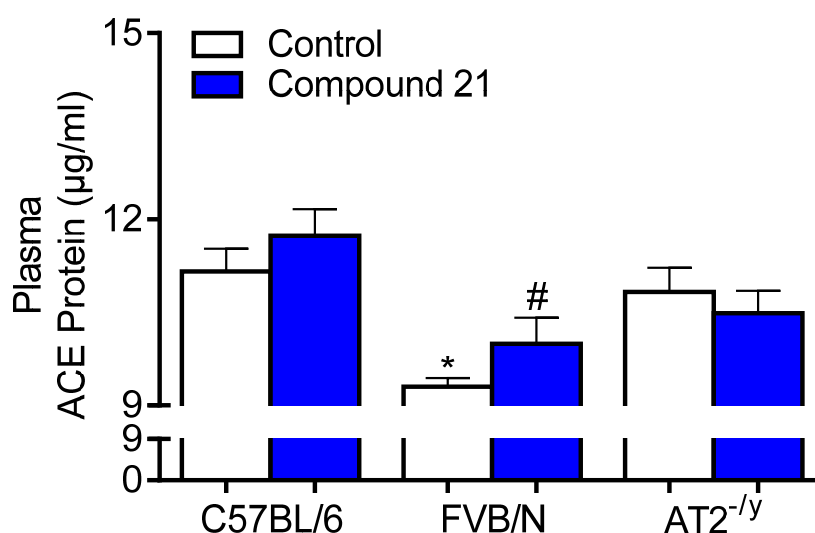


**Figure 3-22:** Plasma ACE protein concentration of C57BL/6, FVB/N and AT2<sup>-/-</sup> after 30 minutes of treatment with compound 21 as measured by ACE-ELISA. In all mouse strains, treatment with compound 21 (1.0 mg/kg bodyweight) does not have a significant effect on plasma ACE concentration as compared to vehicle treatment (control). However, there is a significantly higher ACE protein concentration in plasma of C57BL/6 compared to FVB/N (n=6 each, P=0.001, One-way ANOVA, \*P<0.05 vs. C57BL/6's control, #P<0.05 vs. C57BL/6's compound 21, Tukey's multiple comparison test).

### 3.6.4. ACE content in plasma by Dynabeads®

The plasma ACE protein content was previously not detectable by the western blot method, but it was successfully detected by the ELISA technique. However, those ELISA results did not indicate an increase in ACE protein content that should have been expected after observing a significant decrease in ACE protein content in lung lysates from mice pre-treated with C21 for half an hour. To further confirm this result, an additional immunological method based on magnetizable polystyrene beads (Dynabeads®) was applied to quantify ACE in plasma of mice pre-treated with either vehicle or C21 (1.0 mg/kg bodyweight). Using the Dynabeads®, an antibody-antigen complex was built up in several incubation and purification steps to isolate ACE from diluted plasma samples (80 µg/ml total protein) of C57BL/6, FVB/N and AT2<sup>-/-</sup>. Subsequently, ACE was detected and quantified with fluorophore-conjugated secondary antibodies, one to detect ACE and the other to normalize that fluorescent signal. (**Figure 3-23**). Analysis of the fluorescence signals (**Figure 3-24**) showed no significant difference between the measured plasma samples of the respective mouse strains or treatment groups (P=0.9981, One-way analysis of variance, **Figure 3-25**).

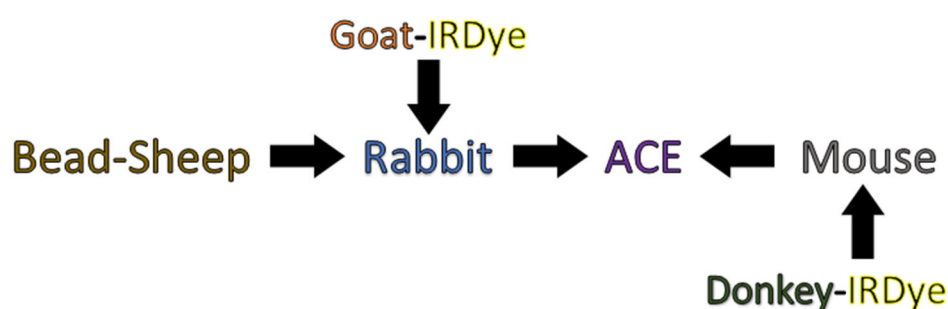


**Figure 3-23:** The principle of using antibody-linked magnetic beads (Dynabeads®) and antibodies to capture and detect ACE from the plasma samples. With each incubation step (arrow), the complex shown is built up in an antibody-antigen interaction: Beads are covalently bound to anti-sheep antibodies (bead-sheep) directed against an anti-rabbit antibody (rabbit), which in turn is directed against ACE. Finally, ACE is flanked by an anti-mouse antibody (mouse). The detection and quantification are based on the fluorescence signal of an infrared dye-conjugated secondary antibody raised against the mouse antibody (donkey-IRDye) normalized to the control signal, which is the fluorescence signal of a second infrared dye-conjugated secondary antibody raised against the rabbit antibody (goat-IRDye).

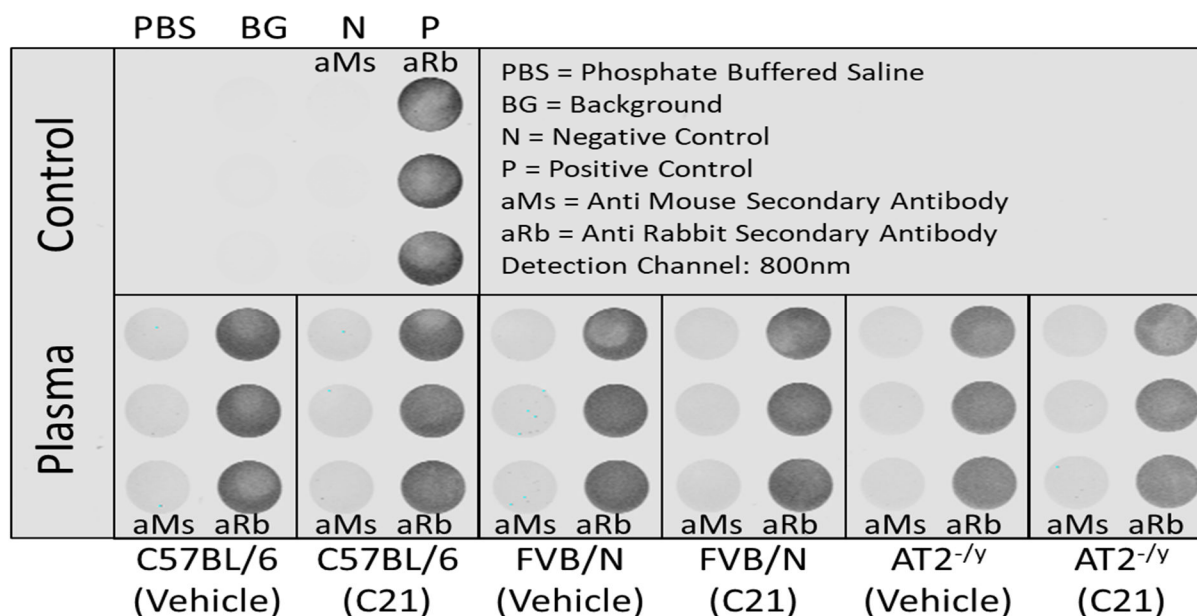


**Figure 3-24:** Imaged fluorescence signals from Dynabeads® on a microplate. Beads are used to isolate ACE from plasma of C57BL/6, FVB/N and AT2<sup>-/-</sup> that were pre-treated with either vehicle or compound 21 (C21, 1.0 mg/kg bodyweight). Fluorescence signals detected at 800nm are emitted from secondary antibodies raised against mouse IgG (aMs) or rabbit IgG (aRb). The signal generated by aMs represents the captured ACE from plasma samples, while the signal generated by aRb represents the saturated signal of the beads to which the signal from aMs is normalized. Rabbit anti-ACE-linked beads are used for controls (N, P), whereas unconjugated beads are used for background (BG).

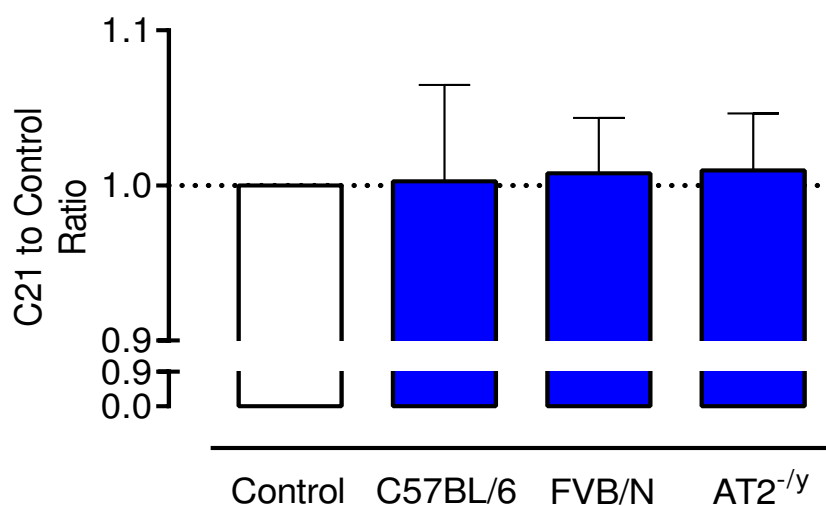


**Figure 3-25:** Normalized ACE fluorescence signals from plasma samples of C57BL/6, FVB/N and AT2<sup>-/-</sup> mice that were pre-treated with either C21 or vehicle (control). Treatment of mice with C21 has no significant effect on ACE plasma levels as compared to control, nor is there a difference between the mouse strains. (n=6 each, P=0.9981, One-way ANOVA).

### 3.7. Effect of AT2 activation on plasma angiotensin

ACE is the main enzyme that breaks down Ang I into Ang II. For further interpretation of prior findings in regards to the C21-induced changes in ACE activity and protein content, plasma levels of Ang I and Ang II were measured using the ELISA technique. In preparation for the assay, the mouse strains C57BL/6, FVB/N and AT2<sup>-y</sup> were pre-treated for one hour prior to blood collection with either vehicle, telmisartan (10 mg/kg bodyweight), C21 (1.0 mg/kg bodyweight) or C21 in combination with telmisartan or PD123319 (1.0 mg/kg bodyweight). ELISA results revealed a significantly higher plasma concentration of Ang I in comparison to Ang II across all strains and treatment groups. The sole treatment of mice with telmisartan, but not with C21 or PD123319, increased plasma levels of Ang I and Ang II slightly. The same effect was also observed after combined treatment with telmisartan and C21, demonstrating the effect of telmisartan, which elevates plasma levels of Ang II by blocking AT1 and thereby decoupling the negative feedback loop of renin (\*P<0.01 vs. angiotensin I, #P<0.001 vs. angiotensin I of Vehicle, PD12319, C21 and C21 plus PD123319, Tukey's post-hoc test following One-way analysis of variance, **Figure 3-26**).

However, after calculating and analysing the ratio of Ang II to Ang I, it was found that there were no differences between the treatment groups of the respective strains, indicating that the physiological balance between Ang I and Ang II was maintained ( $P \geq 0.4681$ , One-way analysis of variance, **Figure 3-27**). In conclusion, the rise of Ang I and Ang II plasma levels after treatment with telmisartan is probably related to the disruption of the renin feedback which leads to higher plasma concentration of the precursor for Ang I, i.e., angiotensinogen. Higher plasma levels of ACE could lead to higher degradation of Ang I and increased levels of circulating Ang II, but this effect was not observed since there were no differences between the treatment groups when the ratio of Ang II to Ang I was calculated. Again, these results do not speak in favour of the ACE shedding hypothesis that might be induced by AT2 activation.

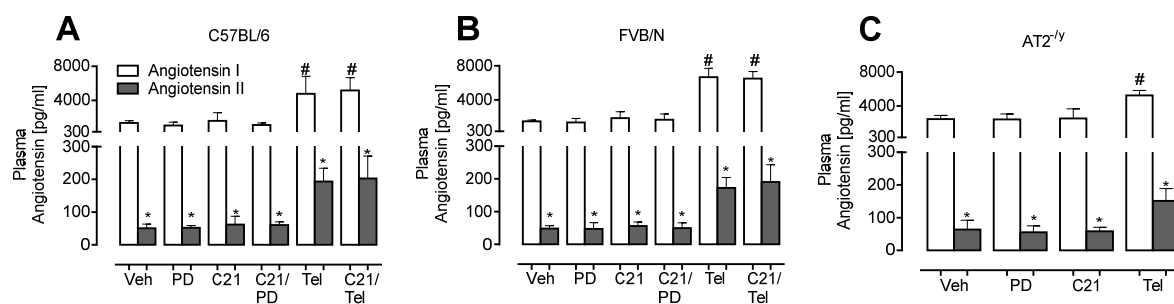


**Figure 3-26:** ELISA test results showing the plasma concentrations of angiotensin I and angiotensin II of C57BL/6, FVB/N and  $AT2^{-ly}$  after pre-treatment with one of the following: vehicle (Veh), PD123319 (PD, 1.0 mg/kg bodyweight), compound 21 (C21, 1.0 mg/kg bodyweight), telmisartan (Tel, 10 mg/kg bodyweight) the combination of C21 plus PD (C21/PD) or C21 plus Tel (C21/Tel). (A-C) In general, the plasma concentration of Angiotensin I is significantly higher compared to Angiotensin II, especially under the effect of telmisartan. The comparison between all treatment groups within each strain reveals no significant difference, except that telmisartan causes an increase in Angiotensin I and Angiotensin II plasma levels due to disruption of the negative renin feedback (for each figure  $n=6$ ,  $P<0.0001$ , One-way ANOVA,  $*P<0.01$  vs. angiotensin I,  $\#P<0.001$  vs. angiotensin I of Veh, PD, C21 and C21/PD, Tukey's multiple comparison test).

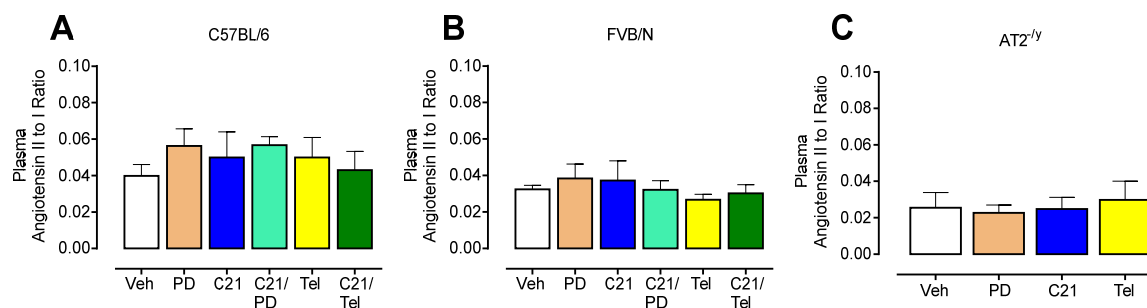


**Figure 3-27:** (A-C) ELISA test results from plasma samples of the mouse strains C57BL/6, FVB/N and  $AT2^{-ly}$ , expressed as the ratio of Angiotensin II to Angiotensin I. Those mice are pre-treated with either vehicle (Veh), PD123319 (PD, 1.0 mg/kg bodyweight), compound 21 (C21, 1.0 mg/kg bodyweight), telmisartan (Tel, 10 mg/kg bodyweight) the combination of C21 plus PD (C21/PD) or C21 plus Tel (C21/Tel). The comparison between the treatment groups of each strain shows no significant difference, which demonstrates that the balance between Angiotensin I and Angiotensin II is maintained under all conditions (for each figure  $n=6$ ,  $P=0.7817$  [figure A],  $P=0.7888$  [figure B],  $P=0.4681$  [figure C], One-way ANOVA).

## 3.8. Cyclooxygenase activity in bradykinin-induced skin oedema

### 3.8.1. Effect of unspecific cyclooxygenase inhibition on extravasation

During non-allergic bradykinin-induced angio-oedema, there is increased activation of endothelial B2 receptors, which are Gq alpha-subunit coupled GPCRs. Subsequent phospholipase C activation leads to the release of intracellular calcium, which in turn activates eNOS, PLA2, and various endothelial hyperpolarizing factors to further release paracrine signals, including NO and prostaglandins [Bas et al., 2007]. Miles assays using either eNOS-deficient mice or C57BL/6 mice pre-treated with an NO synthase inhibitor revealed no difference in the extent of bradykinin-induced extravasation when compared to matched controls [Gholamreza-Fahimi et al., 2020], suggesting that the NO signal in the skin of mice is not important for bradykinin-induced extravasation. On the other hand, it has been reported that local injection of prostaglandin E2 (PGE<sub>2</sub>) can dilate the blood vessels in the ear of mice and increase local blood flow [Omori et al., 2014]. In a similar experiment, the combined intradermal injection of bradykinin and prostacyclin (PGI<sub>2</sub>) in prostacyclin receptor knockout mice showed reduced plasma extravasation when compared to transgenic negative littermates [Murata et al., 1997]. A recently published study showed that bradykinin-induced extravasation in the dorsal skin of mice, especially in B2 overexpressing mice, was significantly reduced after pre-treatment with the non-specific COX inhibitor diclofenac [Bisha et al., 2018]. Accordingly, prostaglandins appear to be important contributors to the development and severity of bradykinin-induced extravasation in the skin of mice, however the role of COX during extravasation remains to be elucidated. Hence, the Miles assay technique was applied in C57BL/6 which were treated with diclofenac (5 mg/kg bodyweight) at two different time points. Mice receiving a post-treatment with diclofenac, i.e., 10 minutes after the corresponding intradermal injections, showed significantly lower bradykinin-induced ( $3.2 \pm 0.18$ -fold of vehicle) and labradimil-induced ( $3.1 \pm 0.11$ -fold of vehicle) extravasation as compared to control treatment which consisted of an intraperitoneal injection of PBS. Likewise, mice pre-treated with diclofenac, i.e., 20 minutes before receiving the corresponding intradermal injections, showed a comparatively greater reduction in bradykinin-induced ( $2.3 \pm 0.28$ -fold of vehicle) and labradimil-induced ( $2.4 \pm 0.25$ -fold of vehicle) extravasation as compared to control treatment. Furthermore, the greater decrease in bradykinin-induced extravasation observed in the pre-treatment group was also significant as compared to the post-treatment group (\* $P < 0.05$  vs. control, # $P < 0.01$  vs. post-treatment, Tukey's post-hoc test following One-way analysis of variance, **Figure 3-28**). These data underline the importance of early COX inhibition

to limit the progression of dermal extravasation in the dorsal skin of mice, but they also show that an already triggered bradykinin-induced extravasation can also be inhibited, albeit the effect is less pronounced since a major part of the extravasation has already occurred.

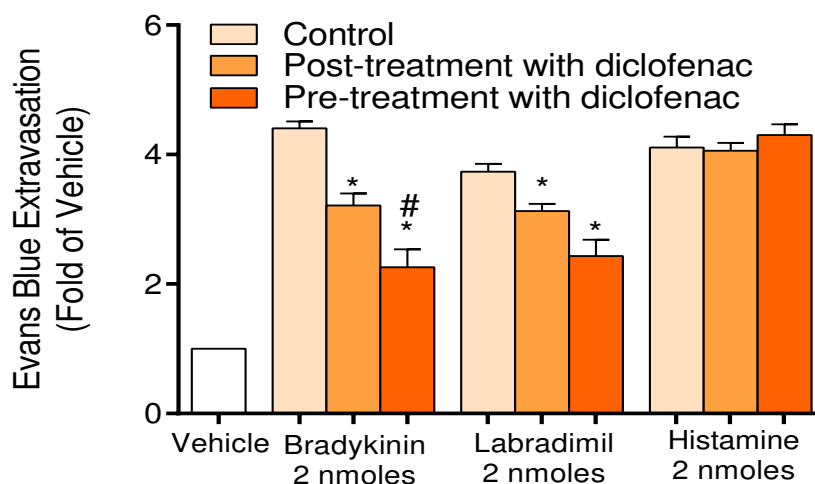


**Figure 3-28:** Results of the Miles assay showing the effects of non-specific COX inhibition on locally induced extravasation in the dorsal skin of C57BL/6. Mice are pre-treated by intraperitoneal injection of diclofenac (5 mg/kg bodyweight) at two different time points, with one group receiving diclofenac 20 minutes before (pre-treatment) and the other group 10 minutes after (post-treatment) intradermal injection of bradykinin, labradimil and histamine at different sites of the dorsal skin. Extravasation is normalized to the effect induced by vehicle injection. In comparison to the control treatment group (left column) extravasation induced by bradykinin and labradimil is significantly reduced in both post-treatment (middle column) and pre-treatment (right column) groups. While mice from the pre-treatment group show a greater reduction in bradykinin and labradimil-induced extravasation, only the bradykinin-induced extravasation is significantly reduced when compared to the corresponding post-treatment group. Of note, diclofenac does not have an effect on histamine-induced extravasation (n=6 each,  $P < 0.0001$ , One-way ANOVA, \* $P < 0.05$  vs. control, # $P < 0.01$  vs. post-treatment, Tukey's multiple comparison test).

### 3.8.2. Results of 'A Bradykinin in Skin Edema Trial' (ABRASE)

In the previous experiments, it was shown in the dorsal skin of mice that bradykinin-induced extravasation was significantly diminished by non-selective COX inhibition. In an attempt to transfer these findings into a clinical context, a multicentre study was conducted: a number of healthy volunteers of both genders received intradermal bradykinin injections and saline control injections into the skin of the forearm (**Figure 3-29**). At defined time points ranging from 5 to

120 minutes, the size of developing wheals was measured. After the 120-minute period, the volunteers took 600 mg of the non-selective COX inhibitor ibuprofen and the measurement procedure described above was repeated. On a different day, the same experiment was repeated with nine volunteers, whereby ibuprofen was exchanged for 60 mg etoricoxib, a more selective inhibitor towards COX-2.

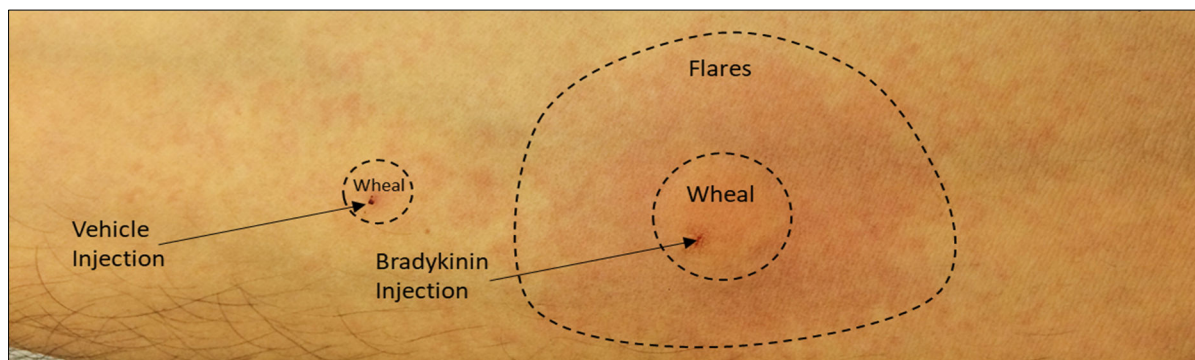


**Figure 3-29:** An example of wheals emerging from intradermal injections of 18.9 nmol bradykinin (right) and vehicle injection with 0.9% saline (left) into the upper ventral forearm of a volunteer. Only palpable wheals are counted during the course of the experiment.

The primary endpoint of the study was the time to complete resolution of the wheals, whereas the secondary endpoint was defined as the change in the mean maximal size of wheals prior to and after the intervention with ibuprofen or etoricoxib. The results presented for ibuprofen involve 29 volunteers from three study centres and cover just a portion of a previously published data set [Gholamreza-Fahimi et al., 2020], while the results for etoricoxib have not yet been published and involve only nine volunteers from one study centre. The outcomes related to the intake of 600 mg ibuprofen showed that the mean time to complete resolution of bradykinin-induced wheals decreased significantly from  $98.3 \pm 4.2$  to  $82.4 \pm 5.0$  minutes ( $*P < 0.0001$  vs. bradykinin, Wilcoxon matched-pairs signed rank test, **Figure 3-30**). In contrast, the study results regarding the intake of 60 mg etoricoxib tablets did not reveal a significant effect on the primary endpoint, suggesting that COX-2 does not play a role in the maintenance of bradykinin-induced dermal extravasation. ( $P > 0.9999$ , Wilcoxon matched-pairs signed rank test, **Figure 3-31**).

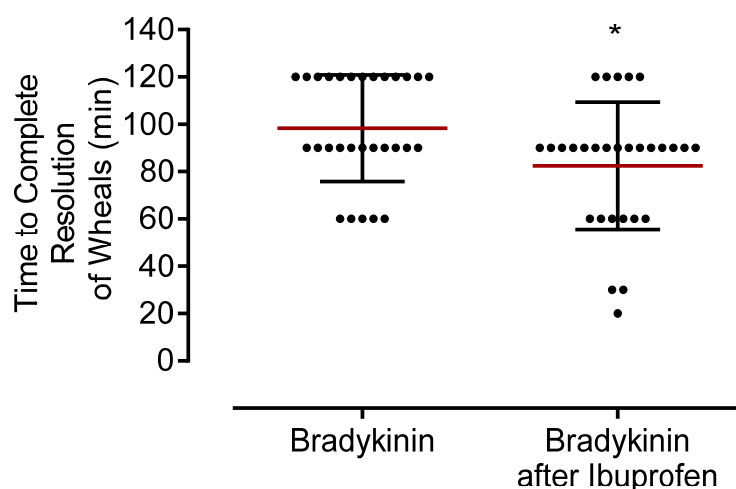


**Figure 3-30:** Partial results of the ABRASE study. After the intake of 600 mg ibuprofen, the primary endpoint of the study, that is the mean time to complete resolution of wheals, is significantly lower when compared to control (n=29 each group, \*P<0.0001 vs. bradykinin, Wilcoxon matched-pairs signed rank test).

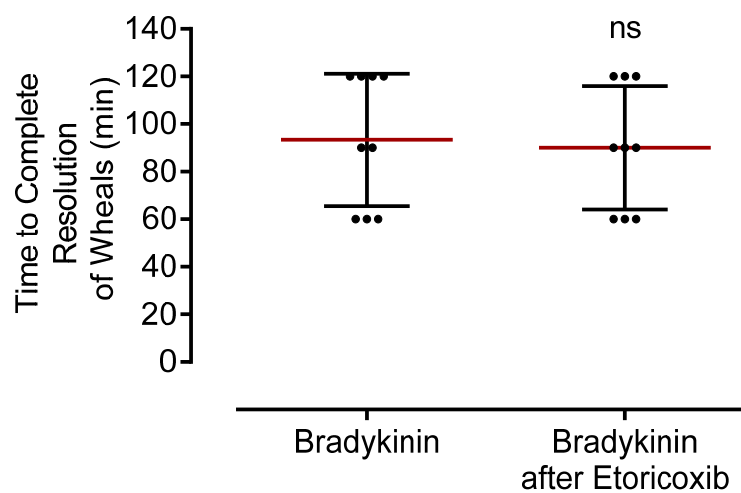


**Figure 3-31:** The effect of 60 mg etoricoxib on bradykinin-induced wheals. Despite treatment with etoricoxib, the mean time to complete resolution is not significantly affected when compared to control (n=9 each, P>0.9999, Wilcoxon matched-pairs signed rank test).

The Data on the secondary endpoint revealed a significant reduction of the mean maximal wheal size after the intake of ibuprofen, from  $420.3 \pm 51.5 \text{ mm}^2$  to  $324.6 \pm 47.4 \text{ mm}^2$  (\*P=0.0014, paired t-test, **Figure 3-32**).

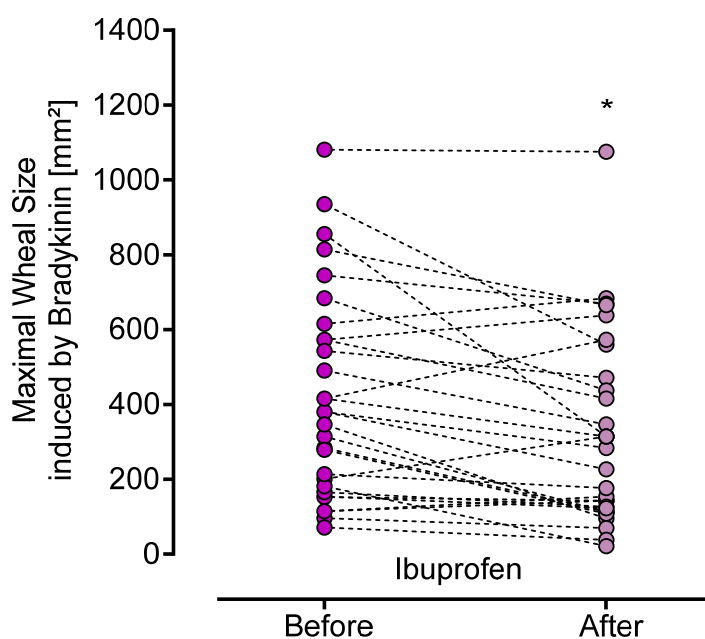


**Figure 3-32:** Illustration of variations in the maximal size of wheals among volunteers prior to and after the intake of 600 mg ibuprofen. These variations are defined as the secondary endpoint of the ABRASE trial. Although there is a large variation in the maximal size of wheals, a significant reduction is observed. This effect is most likely caused by the non-selective COX inhibitor ibuprofen (n=29 each group, \*P=0.0014, calculated using two-tailed paired t-test).

Likewise, a significant reduction of the mean maximal wheal size from  $820.7 \pm 80.4 \text{ mm}^2$  to  $591.9 \pm 48.1 \text{ mm}^2$  was observed after the intake of etoricoxib (\*P=0.0065, paired t-test, **Figure 3-33**). After treatment with ibuprofen, the time to complete resolution of the wheals was significantly reduced, but treatment with etoricoxib had no significant effect, which may suggest that COX-2 is less important in this context. However, the secondary endpoint showed that both, non-specific COX inhibition by ibuprofen and the more COX-2 specific inhibition by etoricoxib were able to significantly reduce the mean maximal size of the wheals. These findings can be explained by a residual activity of etoricoxib toward COX-1. Consequently, it is reasonable to assume that COX-1 plays an important role in the dermal bradykinin-induced extravasation that occurs in human skin.

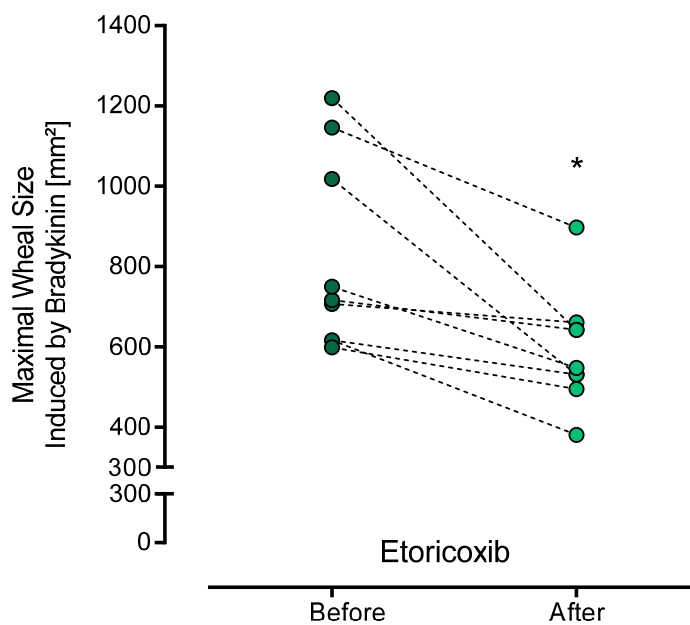


**Figure 3-33:** Illustration of variations in the maximal size of wheals among volunteers prior to and after the intake of 60 mg etoricoxib. These variations are defined as the secondary endpoint of the ABRASE trial. Treatment with etoricoxib, a more selective inhibitor of COX-2, leads to a significant reduction in the maximal size of the wheals as compared to the control (n=9 each group, \*P=0.0065, calculated using two-tailed paired t-test).

## 4. **Discussion**

The pathophysiology of ARB-induced angio-oedema is still poorly understood. It is reasonable to assume an important role for AT<sub>2</sub>, because inhibition of AT<sub>1</sub> by ARBs may favour increased AT<sub>2</sub> activation. There is evidence that AT<sub>2</sub> can modulate ACE activity, e.g., AT<sub>2</sub><sup>-/-</sup> mice have an overall higher ACE activity when compared to wildtype mice [Hunley et al., 2000]. In animal studies, treatment with ARBs promotes an increase of bradykinin and prostaglandins in an AT<sub>2</sub>-dependent manner, reducing infarct size in pigs and blood pressure in hypertensive rats [Gohlke, Pees & Unger, 1998; Jalowy et al., 1998]. Similarly, the results of a study in patients with coronary artery disease that were treated with candesartan suggest a contribution of both bradykinin and NO to the vascular effects of ARBs [Hornig et al., 2003]. Moreover, a case series in patients with ARB-induced angio-oedema who were treated with icatibant implies the involvement of B<sub>2</sub> activation [Strassen et al., 2015]. Thus, ARB-induced angio-oedema is most likely bradykinin-mediated, which is in line with the findings of this work:

In Miles assay experiments, bradykinin-induced extravasation is enhanced under the effect of AT<sub>2</sub> agonist C21. Furthermore, bradykinin degradation might be affected by impaired ACE activity, as observed in endothelial cells after AT<sub>2</sub> stimulation. There is elevated ACE activity in plasma of mice that were pre-treated with C21, suggesting an increased shedding of membrane-bound ACE. Incubation of lung snippets with C21 caused a trend toward decreased ACE content in lung lysates and significantly increased ACE content in the corresponding supernatants. Likewise, lung lysates of mice pre-treated with C21 reveal a reduced ACE protein content. These findings suggest a modulating effect of AT<sub>2</sub> on ACE activity, which might be linked to the phenomenon of ACE shedding. Despite the methodological heterogeneity of the overall experimental data, the majority of observations rather indicate the involvement of AT<sub>2</sub> in bradykinin-induced angio-oedema, which likely involves the release of membrane-bound ACE into the circulation, a process referred to as shedding. During this process, the second catalytic site of ACE is deactivated, thereby reducing its catalytic activity to degrade bradykinin. This might increase the risk of B<sub>2</sub> overactivation which is accompanied with endothelial hyperpermeability and the clinical manifestation of an ARB-induced angio-oedema.

## 4.1. Pharmacologic evaluation of C21

The RAAS and its players are found within the systemic circulation and in various tissue types, where they typically act on blood pressure, hemodynamic, inflammation and tissue remodelling processes. A key player in that system is the peptide-hormone Ang II, which promotes through chronic AT1 activation most of the deleterious effects of RAAS, in particular hypertension, cardiovascular and renal remodelling [Campbell, 1987; Chappell, 2012; Paul, Poyan Mehr & Kreutz, 2006]. In contrast, antihypertensive, antiproliferative, antifibrotic and anti-inflammatory effects are associated with AT2 activation [Carey, 2017]. Human AT1 and AT2 are both GPCRs and share a protein sequence homology of approximately 30% [UniProt, 2019]. AT1 is most abundantly expressed in adults, as opposed to AT2, which is most abundantly expressed in the developing fetus. However, the expression of AT2 is downregulated after birth and only increases again in a pathological state, such as vascular injury [Yamada et al., 1999].

In clinical practice, patients have benefited for many years from medication with AT1 receptor antagonists (e.g., telmisartan) given their prognostic value, especially in the treatment of essential hypertension, chronic heart failure or diabetic nephropathy. By comparison, there exist non-selective AT2 agonists with antagonistic activity towards AT1 (Saralasin and Sarile) and selective AT2 agonists, e.g., CGP-42112 and (4-NH<sub>2</sub>-Phe<sub>6</sub>)-Ang II. However, none of those substances offer any therapeutic benefit due to their unstable peptide structure and so far, their use has been limited to research purposes only [Vasile et al., 2020]. It was not until 2004, with the publication of the first selective non-peptide drug AT2 agonist, known as C21, that current AT2 research moved into the clinical trial phase. At this time the antifibrotic effect of C21 is being evaluated in patients with idiopathic pulmonary fibrosis [McFall, Nicklin & Work, 2020]. C21 has high AT2 affinity ( $K_i=0.4$  nM) with simultaneous low affinity for AT1 ( $K_i>10,000$  nM). This compound was designed to have high oral bioavailability and thus potential clinical utility [Wan et al., 2004], realized by a thienylphenyl core structure with three functional groups consisting of isobutyl, methylene imidazole and butyl sulfonylcarbamate (**Figure 4-1**).

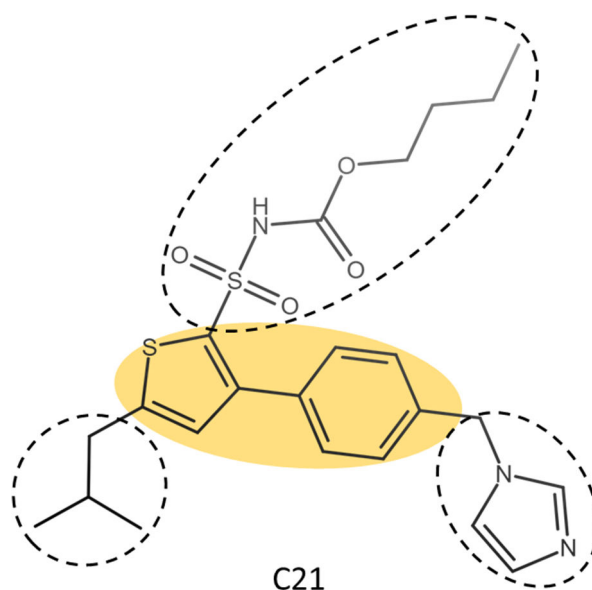


**Figure 4-1:** Structural formula of the small molecule AT2 agonist butyl N-[3-[4-(imidazol-1-ylmethyl)phenyl]-5-(2-methylpropyl)thiophen-2-yl]sulfonylcarbamate, also known as compound 21 (C21). The highlighted part of the structural formula shows the thienylphenyl core structure, while dashed circles mark the lipophilic isobutyl side chain (left), the sulfonyl carbamate group (top), and the imidazole group (right), all of which are essential for the selectivity and agonistic activity of C21.

**Organ bath studies** It is well established that AT2 is expressed alongside AT1 in the thoracic aorta of growing mice, with AT1 expression and its ratio to AT2 increasing with age [Yamada et al., 1999; Yoon et al., 2016]. The isolated organ bath is a physiologically valid model both for characterizing C21 as well as for evaluating the effect of AT2 activation on the contractile response of the mouse thoracic aorta [Gohlke, Pees & Unger, 1998; Katada & Majima, 2002; Matavelli & Siragy, 2015].

To examine strain- and genotype-dependent differences between C57BL/6, FVB/N, and AT2<sup>-y</sup>, corresponding thoracic aortic rings were isolated and challenged with cumulative concentrations of the  $\alpha_1$ -adrenergic receptor agonist phenylephrine. In this experiment, the aortic rings exhibited a similar contractile response across the strains (**Figure 3-3**). However, endothelium-dependent relaxation induced by increasing acetylcholine concentrations at half-maximal contractile response to phenylephrine revealed inter-strain variations. When comparing the aortic ring responses of C57BL/6 and AT2<sup>-y</sup> to that of FVB/N, a significantly stronger relaxation to acetylcholine is observed (**Figure 3-4**). Although the FVB/N strain is more similar to the genetic background of AT2<sup>-y</sup>, the response of the thoracic aorta to acetylcholine is not identical. Otherwise, the thoracic aortas of C57BL/6 and AT2<sup>-y</sup> react to acetylcholine in a similar way. This might be explained by an inter-strain genetic variation

[Keane et al., 2011], which probably affects the NO-cGMP signalling pathway of FVB/N towards the enhanced acetylcholine-mediated vasodilation. When increasing concentrations of C21 were added to the organ bath, it was expected that aortic rings of AT2<sup>-/-</sup> would not relax due to the lack of AT2. In contrast the aortic rings of C57BL/6 and FVB/N responded with relaxation (**Figure 3-5**), suggesting AT2-induced vasorelaxation. It should be noted that the maximum relaxation induced by C21 is less pronounced when compared to that of acetylcholine, which approaches the baseline. In the same way as with acetylcholine, it was assumed that this reaction would depend on the presence of the endothelial layer. To test this, the aortic rings of C57BL/6 were denuded from their endothelium so that no relaxation occurred in the presence of acetylcholine. Likewise, no relaxation occurred when C21 was added to the organ bath, which confirms that an intact endothelium is necessary to induce relaxation in thoracic aortic rings (**Figure 3-6**).

These results are in line with those of a previously published organ bath study in which endothelial-dependent relaxation was observed in pre-contracted mouse thoracic aortas using two different peptide AT2 agonists, CGP-42112 and  $\beta$ -Pro-Ang III [Del Borgo et al., 2015]. In addition, vasodilation induced by those peptides was abolished by the AT2 antagonist PD123319, indicating AT2 dependency. In analogy, C21-induced vasodilation in the aortic rings of AT2<sup>-/-</sup> was no longer observed. A limitation of these experiment is that the NO-cGMP signalling pathway, which is widely accepted to contribute to AT2 activation [Johren, Dendorfer & Dominiak, 2004], was not further elucidated. For instance, in human aortic endothelial cells, AT2 activation by C21 has been reported to result in increased NO release by modulating the phosphorylation state of eNOS [Peluso et al., 2018]. Furthermore, receptor heterodimerization between AT2 and B2 has been discussed, pointing to a BK-NO-cGMP signalling pathway [Abadir et al., 2006]. In contrast, a separate study reported C21-induced relaxation in pre-constricted vessels of human coronary microartery as well as in iliac and mesenteric arteries extracted from rats and mice. The author of this study proposes an AT2-independent mechanism such as the inhibition of calcium transport into cells, since C21-induced relaxation was considered not to be dependent on AT2, the endothelium or the NO-cGMP pathway [Verdonk et al., 2012]. Nevertheless, it should be taken into account that different types of vessels may react distinctly when testing reactivity. Even in the same conduit vessel such as the aorta, there are still differences between the segments in terms of structure, biochemical aspects and developmental origin of the cell types involved [Guo et al., 2006; Karpe et al., 2012], so that depending on whether the thoracic or abdominal segment is examined, the vascular reactivity to substances might also vary. Another important aspect

would be the high micromolar concentration of C21 used, which could promote off-target effects, including AT1 agonism, as already reported for the peptide AT2 agonist CGP-42112 [Macari et al., 1993; Macari et al., 1994].

Taken together, the data obtained from the organ bath experiments are consistent with the literature, since it could be shown that C21-induced vasodilatation in the thoracic aortas of C57BL/6 and FVB/N are endothelium-dependent and due to the lack of relaxation in aortic rings of AT2<sup>-/-</sup> also dependent on AT2 activation. A non-specific effect of C21 can probably be excluded, since sub-micromolar concentrations of C21 were used and similar results were produced by another research group when challenging mouse thoracic aortas with selective peptide AT2 agonists [Del Borgo et al., 2015].

## 4.2. AT2 activation in bradykinin-induced extravasation

The microvasculature is a network of tiny vessels of the arterial, venous and lymphatic system that runs through various organs. It allows the exchange of water, electrolytes, proteins and immune cells, which are essential for maintaining homeostasis and immune surveillance. The ability to control the transition of different substances according to the demands of the respective tissue and without disturbing the physiological balance, plays a decisive role. In this context, straightforward regulatory mechanisms that do not directly affect vascular permeability to substances may include vasodilatation followed by an increased flow rate or the utilization of concentration gradients [Curry & Noll, 2010]. Other types of regulation are less straightforward and involve receptor-mediated opening mechanisms of the endothelial barrier for a transient increase in permeability. Among others, bradykinin and histamine, which act through their respective GPCR's, are known to increase vascular permeability [Wettschureck, Strilic & Offermanns, 2019]. The various types of angio-oedema are eventually induced by unphysiologically increased bradykinin or histamine concentrations [Memon & Tiwari, 2020].

Extravasation mainly occurs in smaller vasculature, especially in capillaries and post-capillary venules and refers both to a passive (spontaneous) and an active process (through gateways and transporters) in which contents of the vascular system cross the endothelial barrier and enter the interstitial compartment. The crossing of the endothelial barrier is dynamically regulated by transcellular (i.e. channels, fenestrations or vesicles) and paracellular (via openings of junctional complexes) transport mechanisms of the endothelium but also depends on the properties of the extravasating substance [Park-Windhol & D'Amore, 2016].

Under physiological conditions, spontaneous extravasation applies to solutes and smaller molecules below 40 kDa, whereas larger proteins such as albumin require active transport through a transcellular pathway, i.e., transcytosis via caveolae. In contrast, under pathological conditions, such as bradykinin-induced extravasation in which endothelial integrity is compromised, albumin and larger plasma proteins (e.g., antibodies and fibrinogen) as well as corpuscular blood components (e.g., leukocytes) can rapidly escape through the paracellular pathways that result from loosened cell-cell junctions of the endothelium. Excessive extravasation due to impaired endothelial barrier function and the inability to drain the extravasated fluid through the lymphatic system in time can lead to oedema formation and inflammation within the affected tissue [Claesson-Welsh, 2015].

During an angio-oedema attack, vascular permeability to albumin is increased, therefore the amount of extravasated albumin can be used as a surrogate parameter to assess vascular hyperpermeability. In 1952, Miles and Miles set the methodological groundwork with the Miles assay to study histamine-induced extravasation of previously injected pontamine sky blue in the skin of guinea pigs [Miles & Miles, 1952]. After the original dye was replaced by Evans blue, which has a strong affinity to albumin, the degree of vascular hyperpermeability could be evaluated based on the increase of extravasated albumin-dye complexes at the investigated site. Over time, this method was further optimised by other scientists and adapted to different organs of mice to evaluate the effect of applied substances on extravasation [Yao et al., 2018]. The modified Miles assay described in this work has already been successfully applied to assess induced vascular hyperpermeability in the dorsal skin of mice in response to different applied substances [Bisha et al., 2018; Gholamreza-Fahimi et al., 2020].

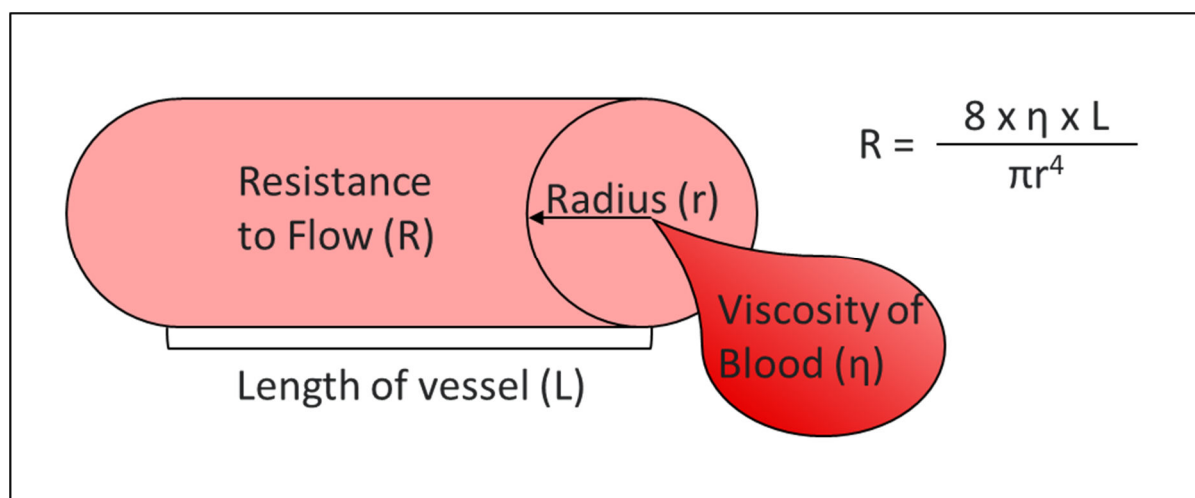
**Extravasation studies (AT2)** To investigate a possible influence of AT2 activation on the endothelial barrier regarding an altered extravasation, C57BL/6 mice received C21 by intraperitoneal route and hyperpermeabilizing substances such as bradykinin, labradimil and histamine intradermally. The results of the Miles assay experiments revealed a significantly increased bradykinin-induced extravasation in mice treated with C21 as compared to control treatment (**Figure 3-7**). Since treatment with C21 produced no effect on histamine-induced extravasation, a histaminergic pathway can probably be excluded. Strikingly, C21 is capable of potentiating bradykinin-induced but not labradimil-induced extravasation, especially considering that labradimil is proteolytically more stable than bradykinin [Shimuta et al., 1999]. A possible explanation could be that although in-vitro affinity studies already reported good selectivity of labradimil towards the B2 receptor, yet in some cases up to 20-fold lower affinity was reported when compared to bradykinin [Emerich et al., 2001]. Taking into account that

bradykinin, unlike labradimil, has the lower proteolytic stability and a stronger affinity to B<sub>2</sub>, increased bradykinin-induced extravasation under treatment with C21 may be associated with a reduced bradykinin degradation. In an additional control experiment the mice were treated with the AT<sub>2</sub> antagonist PD123319 on top of C21. Indeed, the effect of C21 could be linked to AT<sub>2</sub> activation as the increased bradykinin-induced extravasation was eliminated by PD123319 (**Figure 3-8**). Although using a knockout model with mice lacking AT<sub>2</sub> would provide stronger evidence on AT<sub>2</sub> in this process, it was not possible to apply the Miles assay to AT<sub>2</sub><sup>-/-</sup> bred on the FVB/N background. Initial attempts to inject FVB/N mice the Evans blue dye caused a much stronger background signal, resulting in less extravasation upon evaluation, so a comparative study with C57BL/6 mice was not feasible. This also indicates a limitation of the Miles assay, in which the circulating dye must remain significantly lower than the extravasated dye until the end of the experiment. For this reason, the genetic background of AT<sub>2</sub><sup>-/-</sup> was backcrossed to a C57BL/6 substrain. Indeed, the control experiment performed with AT<sub>2</sub><sup>-/-</sup> mice bred on a C57BL/6 background also confirmed the AT<sub>2</sub>-dependent effect of C21, as there was no effect observed after treatment with C21 in the absence of AT<sub>2</sub> (**Figure 3-9**). As a further step, C57BL/6 were also treated with the B<sub>2</sub> antagonist icatibant to demonstrate that the increased extravasation is dependent on B<sub>2</sub> activation. Treatment with Icatibant significantly reduced B<sub>2</sub>-mediated extravasation induced by bradykinin and labradimil, and this was not significantly affected despite concomitant treatment with C21, suggesting that the enhancing effect of C21 on bradykinin-induced extravasation is due to B<sub>2</sub> activation (**Figure 3-10**). In general, it should also be considered that in these kind of experiments, no distinction is made between vascular and interstitial dye at the site of extravasation and thus no information is obtained about which vessel types might be involved [Nagy et al., 2008]. Nevertheless, these Miles assay data demonstrate a bradykinin-enhancing and B<sub>2</sub>-dependent effect of the AT<sub>2</sub> agonist C21, which significantly increases extravasation in skin of mice as compared to control.

### 4.3. Blood pressure and heart rate measurements

The circulatory system can be divided into the systemic and pulmonary circulations. The driving force of this system is blood pressure, which is maintained by the cardiac cycle of filling and emptying, also called diastole and systole. In mammals, peak blood pressure is produced in the systolic phase of the heart, where blood is pumped into the root systemic artery, the aorta. From there, the blood pressure decreases as blood flows into increasingly smaller arterioles, which finally lead into capillary vessels, where the transition into the venous system takes place.

At the same time, the architecture of the arteries changes when moving farther away from the heart and depending on the type of tissue being supplied. An important aspect is the decrease in elasticity (ability to recoil) and increase in compliance (resistance to recoil) further down the arterial tree. In particular, arterioles act as resistance vessels and can influence blood flow to meet the regional needs of tissues. According to Hagen-Poiseuille's law, the flow resistance that is created through the energy dispersed by friction in a blood vessel under laminar flow, is defined by the length of the vessel, the viscosity of the blood and the inverse radius of the vessel to the fourth power (**Equation 4-1**).



**Equation 4-1:** Flow resistance in-vivo, based on the Hagen-Poiseuille equation.

Consequently, in microcirculation, which is dominated by resistance vessels, the blood flow is tightly regulated by altering the radius of the blood vessel. In a nutshell, blood flow to organs and blood pressure are controlled by vascular resistance and cardiac output, with the latter being the product of heart rate and stroke volume (**Figure 4-2**). One important regulatory mechanism related to blood perfusion of the skin is tied to the presence of arterio-venous anastomoses (AVAs), these are connections between small arterial and venous vessels (shunt vessels), which are particularly numerous in certain skin regions as well as in the mucous membranes [Walloe, 2016]. The AVAs function similarly to sphincters; they are densely lined with smooth muscle cells and are impermeable when inactive, but once activated, e.g., by adrenergic stimulation, they allow blood flow. Apart from regulation of blood flow to the organs, this function might be useful to regulate the body temperature, where blood is utilized as a heat conductor. In other words, blood is supplied to the periphery for cooling or centralized to maintain the core temperature. During pathological conditions, such as circulatory shock, this mechanism may also help to divert blood flow from less critical organs, such as the skin, to vital organs, such as

the brain, heart, and nephrons. Accordingly, blood pressure and skin perfusion tend to correlate under non-physiological conditions and are rather independent of each other under physiological conditions. The blood circulatory system consists of intertwined local and systemic processes tightly linked to metabolic demand, myogenic vascular tone, vascular response to shear stress and neuro-humoral regulation, all of which serve to counteract fluctuations in arterial blood pressure and ensure blood flow to the organs [Magder, 2018].

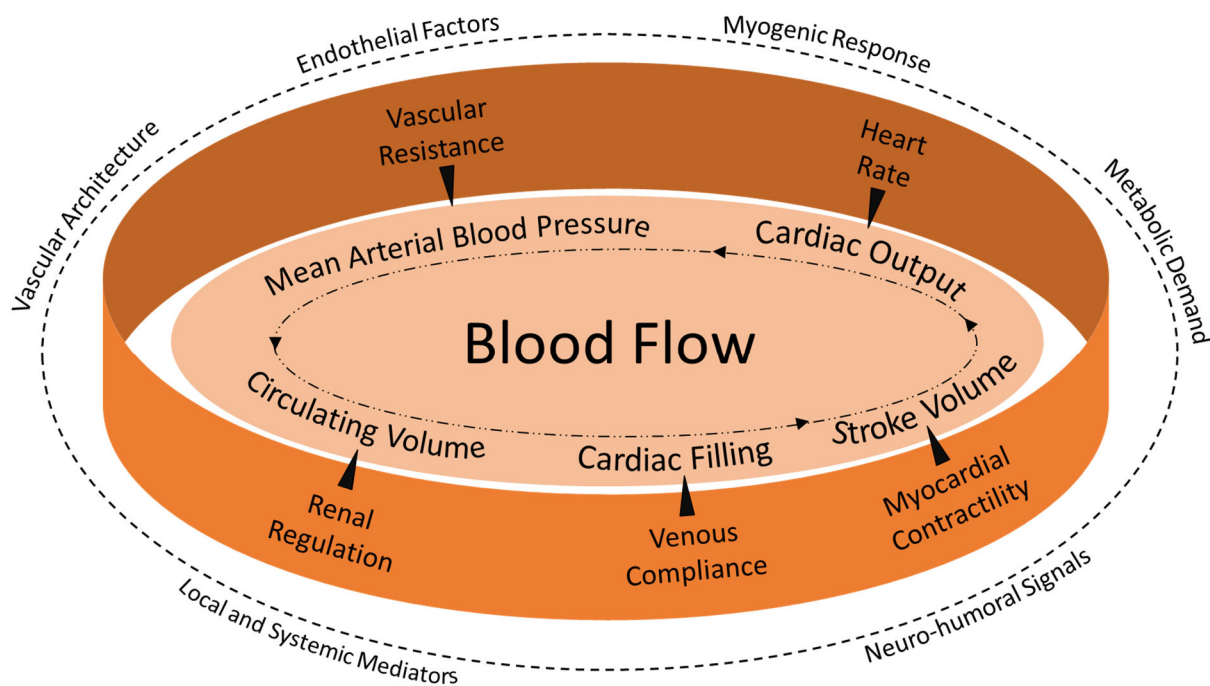


**Figure 4-2:** Schematic representation of various systemic and local determinants that may interact and influence blood flow to a variety of organs.

On the one hand, microcirculatory regulation might involve local vasoconstriction that occurs through a vascular myogenic response to elevated intraluminal pressure. In contrast, local vasodilation might be induced by release of endothelial NO due to increased shear stress. On the other hand, local and systemic circulation is affected by the neuro-humoral activity of both the baroreceptor reflex and the RAAS (**Figure 4-2**). Usually, short-term adaptation to changes in blood pressure and perfusion, as in case of the transition from a lying to an upright position, is controlled by the baroreceptor reflex (orthostatic regulation), while long-term control of blood pressure and arterial tone is controlled by RAAS [Davis, 2012; Stauss, 2007].

The RAAS is ubiquitously active and mediates its classical physiological effects through the Ang II/AT1 axis. As an example, the AT1 signalling pathway mediates the release of aldosterone and vasopressin in addition to direct vasoconstriction, along with renal sodium and water retention as well as an increase in sympathetic tone, ultimately leading to an increase in

blood pressure. Consequently, patients suffering from arterial hypertension due to RAAS overactivation benefit from therapy with AT1 blockers, such as telmisartan, to lower blood pressure and, more importantly, to reduce cardiovascular morbidity and mortality [Sharpe, Jarvis & Goa, 2001]. AT1 blockade has been shown to increase Ang II levels [Campbell, 1996], so it is reasonable to conclude that a shift towards increased AT2 activation may be involved in the cardioprotective effect of AT1 blockers. In this regard, the seemingly dominant role of AT1 in RAAS overshadows the part played by AT2.

The Miles assay experiments with C57BL/6 mice have shown increased bradykinin-induced dermal extravasation due to treatment with C21. Depending on the degree of B2 activation by bradykinin, blood pressure and possibly blood flow to the skin may also be affected. The impact of B2 on blood pressure has been well documented in transgenic animals. When compared to non-transgenic control mice, the tail-cuff-measured SBP is approximately 20 mmHg higher in B2 deficient mice [Madeddu et al., 1999], whereas B2 overexpressing mice have a reduced SBP of approximately 15 mmHg [Bisha et al., 2018]. Using the miles assay technique in mice, the author of the latter study also found that the ACE inhibitor moexipril can enhance bradykinin-induced extravasation at a specific dose, where a lower dose had no effect and a higher dose significantly attenuated extravasation of the skin due to centralization of blood flow. This demonstrates that systemic circulation and local circulation can function independently to some degree. As such, a moderate reduction in blood pressure may be offset by dilatation of the blood vessels in the skin to prevent a change in blood flow.

**The Tail-cuff system** To study the effect of C21, and respectively the effect of AT2 activation on blood pressure, which may contribute to changes in blood flow and subsequently to extravasation itself, C57BL/6 mice received daily treatments with C21 and subsequently SBP and heart rate were measured using the tail-cuff system. Daily intraperitoneal treatments with C21 did not significantly affect SBP as compared to baseline, while treatment with telmisartan significantly reduced SBP, as it was the case with the combined treatment C21/telmisartan ( $104.1 \pm 1.44$  mmHg,  $P < 0.001$  vs. baseline, **Figure 3-11**). Although a small trend could be observed, the additive antihypertensive effect of treatment with C21/telmisartan was not statistically significant. With regard to the measured heart rates, which can be used to assess the stress level of the animals and can also be a variable in blood pressure regulation, there were no noticeable differences between the treatment groups (**Figure 3-12**), indicating that no direct effect of AT2 activation on cardiac output can be expected.

First evidence of a blood pressure regulating function of AT2 was provided by genetically modified mice. When compared to non-transgenic littermates, AT2<sup>-/-</sup> mice develop a more pronounced pressure response to Ang II [Hein et al., 1995; Ichiki et al., 1995], and mice that overexpress AT2, show an attenuated pressure response to Ang II, while concomitant treatment with PD123319 (AT2 antagonist), L-NAME (NOS inhibitor), or icatibant (B2 antagonist) results in approximately the same pressure response as observed in non-transgenic littermates [Tsutsumi et al., 1999]. This study demonstrates a counter-regulatory function of AT2 towards AT1 and also establishes the link between AT2 activation and the BK-NO-cGMP pathway. In stroke-prone spontaneously hypertensive rats, AT2 activation leads to a B2-dependent release of NO which is accompanied by cGMP formation, however with no effect on blood pressure [Gohlke, Pees & Unger, 1998]. A study in which C21 was used to evaluate the effect of AT2 activation in conscious spontaneously hypertensive rats, did not yield a blood pressure lowering effect. Interestingly, under simultaneous AT1 blockade, C21 enhanced the blood pressure lowering effect [Bosnyak et al., 2010]. Additionally, a study with chronic administration of Ang-(1-9) demonstrated an AT2-mediated reduction of SBP in hypertensive rats without the need of simultaneous AT1 blockade [Ocaranza et al., 2014]. To date, no study has reported AT2-mediated blood pressure reduction in conscious normotensive animals, which is probably due to the fact that AT2 is typically upregulated in a pathological condition such as hypertension to counterbalance the AT1-mediated effects to some degree. Since AT1-mediated effects are more pronounced due to tonic activity, vasodilation mediated by AT2 may only be exposed during AT1 blockade [Foulquier, Steckelings & Unger, 2012].

Overall, the data collected from blood pressure measurements suggest that AT2 activation does not have a significant effect on systemic blood pressure, which is consistent with current body of evidence. Although AT2 activation showed no effect on SBP in mice, an effect on the microcirculation, such as enhanced blood flow or increased endothelial permeability, cannot be ruled out.

#### **4.4. Extravasation detected by two-photon excitation microscopy**

The preceding in-vivo findings from local extravasation studies and recorded blood pressure data of C57BL/6 mice receiving C21 indicate that AT2 activation is more likely to have an effect on microcirculation than on macrocirculation. It is therefore more reasonable to investigate changes in small dermal vessels and study a probably altered endothelial barrier function. Although the Miles assay is a useful technique to study the effect of permeabilizing

mediators in-vivo, it is not possible to distinguish between interstitial and intravascular dye present within the tissue sample, nor is it possible to study the progression of extravasation over time in the same animal. Furthermore, it is impossible to study changes of spontaneous extravasation. On the contrary, the non-invasive TPEM enables the differentiation between the intravascular and interstitial compartments through the use of two different fluorescent dyes, thus allowing to monitor the endothelial barrier of smaller dermal blood vessels during a defined time frame. To this end, the TPEM was already adapted when studying the role of B2 in physiological extravasation [Bisha et al., 2018], though the experimental framework for this was originally set out in a publication that evaluated TPEM as a promising technique to study vascular permeability in the ventral ear skin of mice [Egawa et al., 2013]. The latter study demonstrated extravasation of fluorescent dextran-tracers just below the molecular weight of 70 kDa during non-inflammatory conditions and extravasation of dextran-tracers ranging from 70 to 2000 kDa in histamine-induced hyperpermeability.

For the visualization of the vasculature and to determine the site of measurement, the non-extravasating 250 kDa FITC-dextran was chosen, whereas a 10 kDa dextran-tracer was used to visualize the physiological extravasation over time in form of leakage and shifting of the fluorescence signal towards the interstitial space. However, the focus of this experiment was not on physiological extravasation but on B2-mediated extravasation, and the next step would have been to evaluate the effect of AT2 activation by C21 on the microcirculation. To induce B2-mediated extravasation, labradimil was injected by intraperitoneal route at 20 mg/kg bodyweight. A higher dose by intraperitoneal injection or even lower doses by intravenous injection resulted in significantly reduced perfusion at the investigated site with partial interruption of flow, probably due to increased B2-induced vasodilation of upstream arteries and possibly centralization of blood flow. Thus, successful imaging was only possible with the above-mentioned dose of labradimil and by slower systemic exposure via the intraperitoneal application route. Evaluation of the data from the imaging of the microvascular inside the ventral ear of C57BL/6 mice did not reveal any significant differences as compared to control. No increased extravasation for the 250 kDa FITC-dextran during the 45-minute measurement period occurred, despite treatment with labradimil. Similarly, the 10 kDa dextran-tracer showed no significant change in the velocity or quantity of extravasation, but the slower inflow of the dye to the maximum value around the third minute of recording was striking when compared with the control (**Figure 3-13**). Unfortunately, in this experiment, labradimil-induced hyperpermeability could not be demonstrated with the 10 kDa dextran-tracer, since no increased leakage of that tracer could be observed. Interestingly, under the same conditions in which a

70 kDa fluorescent dextran-tracer was used to measure extravasation, no extravasation occurred, in fact, the tracer remained inside the vasculature throughout the recording period (**Figure 3-14**).

There are several possible explanations for these findings. B2-mediated hyperpermeability may not affect basal extravasation of smaller molecules in the 10 kDa range, probably because these molecules can freely cross the endothelial barrier under physiological conditions already. The strikingly late onset of the maximum could be explained by a stronger upstream vasodepressor effect induced by greater B2 activation, which in turn could reduce downstream perfusion in smaller arteries, including those at the site of recording. Another aspect that has been poorly understood but is becoming increasingly important, is the glycocalyx of the endothelial barrier, a gelatinous, negatively charged layer that extends into the vessel lumen and can repel negatively charged molecules, macromolecules larger than 70 kDa as well as cellular components of the blood [Kruger-Genge et al., 2019; Pillinger & Kam, 2017]. Moreover, the net electrical charge of dextran-tracers depends largely on the linked fluorophore and the method of production. For instance, the dextrans used in this work, i.e., the 250 kDa and 10 kDa dextrans, have a negative net charge, whereas the 70 kDa dextran has a neutral net charge. In spite of the neutral net charge of the 70 kDa dextran-tracer, no shift into the interstitial space was detected under B2-mediated hyperpermeability. One reason for this may be the shape of the dextran, which also plays a role, since with increasing molecular weight, the degree of branching and the expansion of the polysaccharide-chains in plasma also increase, which is in contrast with the folded structure of plasma proteins such as albumin. Consequently, the anatomic passages of the endothelial barrier that might be wide open under B2-mediated hyperpermeability, are not accessible to larger dextrans because of their bulkiness. It is remarkable that under histamine-induced hyperpermeability, FITC-dextrans up to a molecular weight of 2000 kDa were reported to leak from the microvasculature within the ventral mouse ear [Egawa et al., 2013], however, this was not the case here for the 250 kDa dextran under B2-mediated hyperpermeability. It is well known that histamine and bradykinin mediate the phosphorylation of eNOS and thus promote the formation of NO. While the NO-cGMP pathway leads to smooth muscle cell relaxation and consequent vasodilation, NO also nitrosylates beta-catenin and thereby disrupts the adherent junctions between endothelial cells [Claesson-Welsh, 2015]. Thus, histamine and bradykinin increase blood flow and permeability through a common mechanism. However, for histamine, it has also been demonstrated to induce the formation of vesiculo-vacuolar organelle, providing an additional transcellular pathway for

extravasation [Feng et al., 1996]. Therefore, when comparing histamine to bradykinin, it is possible that histamine renders the endothelial barrier more permeable to larger molecules.

In summary, it was not possible to establish a control experiment to demonstrate B2-mediated hyperpermeability with either a 10 kDa or a 70 kDa dextran-tracer. As a consequence, in this approach, C21 could not be used to investigate the presumed effect of AT2-mediated hyperpermeability. Further adaptations of the experimental setup will therefore be necessary to address this particular research question. For example, it would be reasonable to use a fluorescent tracer based on albumin. Under physiological conditions, albumin extravasates primarily through the transcellular pathway and therefore increased extravasation would probably be easier to detect during B2-mediated vascular hyperpermeability. Furthermore, it is not clear how histamine-induced extravasation compares with bradykinin-induced extravasation in this experiment, hence a histamine control experiment might be interesting. Finally, the route and method of administration of labradimil might as well be reconsidered, e.g., using an automated infusion pump to push the circulatory system into B2-mediated hyperpermeability in a more controlled manner.

#### **4.5. Effect of AT2 activation on ACE activity**

Within RAAS, ACE plays a crucial role in the regulation of blood pressure, electrolyte balance, and blood volume. This regulation essentially involves the adjustment of steady-state concentrations for certain peptide hormones through proteolytic activity. ACE, also known as kininase II, bears its names most notably for the exopeptidase activity that involves cleavage of a dipeptide from the carboxyl-terminal end of either Ang I or bradykinin and thereby producing Ang II and bradykinin 1-7 respectively. Although ACE is capable of further degrading bradykinin 1-7 to bradykinin 1-5, there exist other enzymes that may catalytically cleave bradykinin or Ang I at different stages of degradation across the corresponding peptide chains. Nevertheless, the major pathways that generate Ang II and degrade bradykinin are dominated by ACE, which is ubiquitously expressed and can be detected in various tissues and fluids. In addition to the above-mentioned ACE variant, which is regarded as sACE, the somatic variant, there is also an isoenzyme, which is exclusively expressed in the male testis, i.e., gACE. Recent research has also uncovered the existence of the homolog protein ACE-2, that acts as a counterpart to the previously known effects of ACE. The counter-regulatory signalling pathway mediated by ACE-2 unfolds its actions through the conversion of Ang II to Angiotensin 1-7

and subsequent activation of its receptor, Mas. This section focuses on the classic RAAS signalling pathway, centred on ACE, which regulates steady-state levels of Ang II and bradykinin [Riordan, 2003; Turner & Hooper, 2002]. There is evidence for interaction between AT2 and B2 as well as the downstream NO/cGMP signalling [Abadir et al., 2006; Gohlke, Pees & Unger, 1998]. Recently, a relationship between AT2 activation and ACE activity has been demonstrated. In mice, it was shown that NO is capable of upregulating AT2 expression, while simultaneously reducing ACE activity. Also, incubation of HUVECs with telmisartan and Ang II revealed a decrease in ACE activity [Dao et al., 2016]. Furthermore, mice lacking AT2 were found to have an overall increased ACE activity [Hunley et al., 2000]. It can thus be concluded that AT2 exerts a modulating effect on ACE activity.

**ACE activity in endothelial cells** To investigate the hypothesis of AT2-mediated inhibition of ACE activity, in-vitro experiments were performed with endothelial cell cultures. Combined treatment with telmisartan and Ang II significantly reduced ACE activity measured in lysates of HUVECs to approximately half of control. This effect was abolished by the addition of PD123319. Likewise, direct stimulation of AT2 using C21 in HDMECs significantly reduced ACE activity as compared with control (**Figure 3-15**). Again, this effect was abolished by PD123319, which strongly suggests AT2 dependency. Moreover, the incubation with captopril performed in HDMECs, but neglected for HUVECs, was to demonstrate the selectivity of the assay for ACE, because other less specific enzymes may also degrade the substrate (FAPGG) and thus confound the results. In contrast to HUVECs, microvascular endothelial cells may be more relevant to the study of angio-oedema in terms of the skin's microcirculation, yet both experiments provided similar results in terms of AT2-mediated reduction of ACE activity. It is up for discussion how ACE activity could be reduced by AT2 activation.

ACE exists primarily in a membrane-bound form, but a soluble form is also detectable in various bodily fluids such as plasma. Though, one important difference arises between the two forms, that is unlike the membrane-bound form, the soluble form of ACE lacks functionality of its second catalytic site, which is related to the loss of membrane anchoring. Indeed, there is evidence for a phenomenon known as shedding, in which ACE is detached from its membrane as a result of proteolytic cleavage by an as yet unknown enzyme [Oppong & Hooper, 1993]. This process probably involves phosphorylation events at the cytoplasmic tail that destabilise the membrane anchoring of ACE and promote its detachment [Chattopadhyay et al., 2005; Kohlstedt et al., 2002]. Thus, one possible explanation for the decreased ACE activity is that AT2 activation might induce shedding of ACE from the endothelial cell membrane. The attempt to determine the ACE activity in the supernatant of the cells unfortunately remained

inconclusive, possibly due to both the low abundance and the dilution effect of the cell culture medium.

**ACE activity in lungs and plasma** An in-vivo approach using mouse lungs and plasma was performed to verify the in-vitro findings of reduced ACE activity that was associated with AT<sub>2</sub> activation. In comparison to vehicle, treatment of C57BL/6 with C21 and appropriate control substances, i.e., telmisartan and PD123319, failed to reveal any changes in ACE activity as determined in the lung lysates. The specificity of the assay was demonstrated by captopril, which markedly inhibited ACE activity (**Figure 3-16**). Moreover, ACE activity was determined in plasma samples collected from those C57BL/6 mice to test the hypothesis of increased ACE shedding, which would possibly manifest as increased ACE activity in the systemic circulation. Against expectations, there was no significant effect on plasma ACE activity after treatment with C21 as compared to mice treated with vehicle (**Figure 3-17**). The dose of C21 used to treat the mice here is the same dose that showed an effect in the Miles assay. Those mice received 0.5 mg/kg bodyweight of C21 half an hour before the Miles assay was performed, which then produced an increase in bradykinin-induced extravasation (**Figure 3-7**). However, for ACE activity determination, following treatment with C21, mice were taken one hour later for determination of ACE activity in lung and plasma.

In general, smaller animals metabolize pharmacological substances faster than larger ones, which also means that the same concentration in a mouse, when administered by bodyweight, is potentially toxic in humans. On this basis, a dose adjustment for C21 was made to 1.0 mg/kg bodyweight, and the time to obtain lung and blood samples for determination of ACE activity was shortened to half an hour. Interestingly, in plasma samples from those mice, these adjustments resulted in a significant increase in ACE activity (**Figure 3-18**). This in-vivo finding supports the hypothesis of AT<sub>2</sub>-induced shedding, since the increased ACE activity in plasma is most likely related to increased ACE concentration, which in turn might be provided through shedding of membrane-bound ACE. Against this assumption, ACE activity measured in lung lysates did not reveal a significantly reduced ACE concentration as compared to vehicle treatment (**Figure 3-19**). Yet, this result is not surprising, taking into account that ACE is most abundantly expressed in the lung and that the systemic effect of AT<sub>2</sub> activation would probably not cause shedding of ACE in large amounts. Assuming that ACE would be released into plasma on a large scale, there would also be a significant decrease in overall ACE activity. In this scenario, a decrease in SBP would occur as a result of decreased Ang II as well as increased bradykinin levels, but this effect was not observed during SBP measurements with the tail-cuffs (**Figure 3-11**). It should be noted that not the plasma ACE (soluble ACE), but membrane-bound

ACE plays the crucial role in maintaining blood pressure, probably because of the second active catalytic site as well as higher concentration on the endothelial cell surface [Kessler et al., 2003]. Thus, although increased ACE activity in plasma of mice receiving C21 may be related to ACE shedding, this effect may be less pronounced to translate into a reduced ACE activity in the lung.

#### 4.6. Effect of AT2 activation on ACE protein content

**Western blot analysis** The ACE activity measured in plasma depends on the concentration of systemically circulating ACE. In turn, this concentration is largely determined by endothelial cells of the capillaries, secreting membrane-bound ACE [Lopez-Sublet et al., 2018]. Thus, supporting evidence for the hypothesis of AT2-mediated shedding of ACE can be obtained from the quantification of ACE. To this end, initial in-vitro data were collected from incubation experiments with lung snippets using the western blot method. This analytical technique was developed specifically for the qualitative and semi-quantitative analysis of proteins and has become a standard procedure since its introduction into biochemistry [Renart, Reiser & Stark, 1979; Towbin, Staehelin & Gordon, 1979].

In simple terms, denatured proteins are separated according to their size by gel-electrophoresis and then targeted with antibodies directed against a specific protein epitope. Next, visualization is accomplished by the addition of a fluorescent-labelled antibody directed against the previous antibody. For the semi-quantitative determination of the target protein, in this case ACE, a particular reference protein is simultaneously targeted, for which a stable expression is expected during the entire course of the experimental procedure, e.g., the house keeping protein  $\beta$ -actin. Under the condition that the total amount of protein present in the samples does not vary excessively or that the fluorescence signal of the target protein is not oversaturated, normalization to the housekeeping protein-signal can be performed and comparative statements about the concentration of the target protein among the samples can be made. The antibodies involved in this experiment have been used in several peer-reviewed publications, in which proteins from mouse tissues were successfully analysed by western blot using those antibodies, in addition to other immunological methods (**Table 2-4**). The incubated lung fragments with their supernatant were analysed by western blot using the rabbit anti-ACE antibody and the corresponding secondary antibody, which yielded a signal for ACE at approximately 180 kDa. After normalization to  $\beta$ -actin, ACE protein levels were decreased for lung fragments incubated with C21 when compared to control, though this effect was not statistically significant.

By contrast, the ACE content in the corresponding supernatant was significantly elevated (**Figure 3-20**). Both membrane-bound ACE in tissue and soluble ACE in supernatant were detected by the same method. Although only a trend of decreasing ACE concentration was detected in the lung snippets, soluble ACE, which could not escape from the lung microvessels, may have masked a more pronounced decrease in ACE content. Nonetheless, this in-vitro experiment provides additional support for AT2-mediated shedding hypothesis.

For the in-vivo approach, C57BL/6 were treated with C21 at a dose of 0.5 mg/kg bodyweight for half an hour and subsequently ACE levels in lung and plasma were analysed by western blot. In addition, mice were also treated with telmisartan (10 mg/kg bodyweight) to assess changes in ACE concentration that may be associated with AT1 inhibition. The ACE content in lungs of C57BL/6 that were treated with telmisartan was not significantly decreased, but a minor trend could be observed when compared to vehicle treatment. Notably, treatment with C21 resulted in a significant reduction of ACE content, which was slightly enhanced by concomitant treatment with telmisartan. Moreover, the effect of C21 was abolished by PD123319, verifying the AT2 dependence of this effect (**Figure 3-21**).

Reduction of ACE content in the lungs as a result of treatment with C21 is in agreement with previous in-vitro findings from lung snippets. Although the decrease in ACE content caused by incubation with C21 was not statistically significant and could only be seen as a trend in lung fragments, a statistically significant and more pronounced decrease in ACE content was found in the in-vivo experiment by treatment of mice with C21. This may be due to the fact that most of the released membrane-bound ACE was distributed into the bloodstream and thus was no longer localized in the lung tissue. Furthermore, systemic washout with buffer solution through injection into the left ventricular to clear organs of excess blood also might have contributed to this effect. Unfortunately, the ACE content in plasma could not be determined by the western blot method. It was not possible to dilute the plasma to a level that would allow the total amount of protein to be suitable for western blotting while still providing sufficient amount of ACE protein for detection. Although there are several commercially available kits capable of removing interfering high abundance proteins such as albumin, in this context it was not feasible to choose such an indirect method for the quantification of ACE [Haudenschild et al., 2014]. During purification, depending on the method used, it cannot be ruled out that ACE may also be removed or chemically altered. In one study, albumin was shown to interact with ACE and was even able to influence its activity [Fagyas et al., 2014]. It is therefore possible that when albumin is removed, some of the ACE protein bound to albumin may also be removed, thus confounding the subsequent quantitative analysis. Therefore, an alternative immunological

method had to be chosen for the quantification of ACE in plasma, which did not require any purification steps of plasma samples.

**ACE-ELISA** Considering the soluble form of ACE present in plasma at a relatively low level next to proteins with high abundance, the only remaining approach was to isolate this protein directly prior to quantification. For this purpose, a commercially available ELISA was used. Unlike the western blot method, which involves all proteins in a sample up to the detection stage, the ELISA method allows exclusion of all non-relevant proteins at an early stage of the application. During ACE-specific ELISA, ACE protein is initially bound to a solid-phase antibody (ACE capturing antibody), whereby soluble ACE is removed from the plasma sample. After several washing steps and the formation of a sandwich complex with an additional enzyme-coupled antibody as well as the subsequent colour reaction, ACE was quantified spectrometrically (**Figure 2-6**). For the ACE-ELISA, in addition to C57BL/6, AT2<sup>-y</sup> and their transgene-negative littermates (FVB/N) were also treated with C21. In this experiment, C21 was administered at 1.0 mg/kg bodyweight for 30 minutes, comparable to the dose that resulted in a statistically significant increase in plasma ACE activity. Contrary to expectations, there was no significant increase in plasmatic ACE levels in any of the mouse strains after treatment with C21, although a slight trend in that direction was observed in C57BL/6 and FVB/N but not in AT2<sup>-y</sup> (**Figure 3-22**). Interestingly, there were differences between the strains, in particular, a significantly lower plasma ACE concentration was measured in FVB/N when compared to C57BL/6. In addition to the fact that the endothelium-dependent vasodilatory response to acetylcholine is stronger in FVB/N (**Figure 3-4**), the lower ACE levels in FVB/N suggest broader differences between the phenotype of C57BL/6 and FVB/N concerning the cardiovascular system and RAAS. Consequently, comparisons between these strains should be made with caution, especially considering that FVB/N is the genetic background of AT2<sup>-y</sup>. With the ELISA technique it was possible to successfully determine ACE from plasma, but the result is not consistent with previous observations, because no significant increase in ACE concentration could be detected, although under the same treatment conditions ACE activity was significantly increased in C57BL/6.

**Dynabeads**<sup>®</sup> To conclusively evaluate this result, the plasma samples were analysed by an additional immunological method. For this method, magnetic beads were used with specific antibodies bound to their surface. These antibodies are thus comparable to the solid-phase antibodies used in an ELISA, with the difference that they are suspended in the plasma sample and thus have more surface area available for binding. After stepwise formation of an ACE sandwich complex by primary Antibodies raised against ACE, this complex was detected using

fluorophore-conjugated secondary antibodies (**Figure 2-9**). Quantification of ACE was based on normalization of the fluorescence signal from bound ACE to the control signal representing all binding sites of the magnetic beads (**Figure 3-23**). During design of the experiment, it was important not to overload the binding sites of the magnetic beads with ACE, otherwise no changes would be detectable. Initial experiments revealed that saturation of binding sites with ACE was reached at 200  $\mu\text{g/ml}$  total plasma protein, so plasma samples were diluted down to 80  $\mu\text{g/ml}$  total protein to avoid excess loading of the beads with ACE (**Figure 2-8**). Despite these efforts, the plasma samples of C57BL/6, FVB/N, and AT2<sup>-/-</sup> assayed with the magnetic beads revealed no change in ACE content as compared to control (**Figure 3-25**), suggesting that plasma ACE concentrations might not be affected by treatment of mice with the AT2 agonist C21. Comparing the approaches of ACE quantification in the plasma of mice, it is noticeable that no connection between AT2 activation and decreased ACE activity was found with the ELISA and the Dynabead<sup>®</sup> method in comparison to the Western blot method. A major difference between the methods is the denatured form of proteins during western blot detection, in which unfolded ACE protein is detected by antibodies. In contrast, during ELISA and also the use of magnetic beads, the soluble form of ACE, which is present in native form alongside other plasma proteins, is captured and detected. Therefore, the native soluble form of ACE may not be quantitatively accessible to the antibodies used, partly due to steric hindrance from folding or interactions with other plasma proteins [Danilov et al., 2016], as in the case of albumin, that could potentially bind to ACE and shield it from antibody binding [Fagyas et al., 2014]. As a prospect for further experiments in this area, it would be advisable to denature the proteins of plasma samples prior to an ELISA or other methods involving antibodies. In summary, for the data on quantification of ACE from mouse lungs and plasma, the hypothesis of AT2-mediated ACE shedding could not be substantiated, since no method on its own was able to show statistically significant reduction of membrane-bound ACE accompanied by an increase in soluble ACE. However, it should also be noted that these experimental approaches only study systemic changes and therefore do not allow conclusions to be drawn about local changes, which may yield different results depending on the vascular bed affected. For example, in the Miles assay, which examines local dermal extravasation in mice, an increase in bradykinin-induced extravasation was measured after treatment with C21, primarily involving the dermal vascular bed.

#### 4.7. Effect of AT<sub>2</sub> activation on plasma angiotensin

**Angiotensin-ELISA** In RAAS, renin breaks down angiotensinogen into Ang I, which in turn is broken down by ACE into Ang II. Hence, it can also be assumed that AT<sub>2</sub>-mediated changes in ACE activity, as previously observed in cells and partly in mice, also influence the level of Ang I and Ang II in the systemic circulation. The shedding of the membrane-bound ACE produces the soluble form of ACE, a process in which the function of the carboxyl-terminal catalytic site is lost. Interestingly, that catalytic site has been shown to be more efficient in cleaving Ang I [Jaspard, Wei & Alhenc-Gelas, 1993], thus a pronounced loss of membrane-bound ACE should also affect the degradation of Ang I to Ang II in the short term. In preparation for this experiment, C57BL/6, FVB/N and AT<sub>2</sub><sup>-/-</sup> were treated with either telmisartan (10 mg/kg bodyweight), C21 (1.0 mg/kg bodyweight) or C21 with either telmisartan or PD123319 (1.0 mg/kg bodyweight). Blood was then collected and plasma samples prepared to determine the concentration of Ang I and Ang II according to the corresponding ELISA protocol. Similar results were found for all strains, with plasma levels of Ang I significantly higher than those of Ang II (**Figure 3-26**).

This ratio in favour of higher Ang I levels, is not surprising, as this has already been reported in the literature [Campbell et al., 1995; Kessler et al., 2005]. There was a striking difference found in all treatment groups receiving telmisartan, because both Ang I and Ang II levels were higher than in the other treatment groups. Yet, this was statistically significant for Ang I only. This finding is not novel and has been reported repeatedly in the literature. Since AT<sub>1</sub> blockers interrupt the AT<sub>1</sub>-mediated negative feedback loop of renin, Ang I is increasingly cleaved from angiotensinogen while simultaneously promoting the formation of Ang II by ACE [Aoki et al., 2010; Campbell, Krum & Esler, 2005; Wagner et al., 1998]. In no case did treatment with C21 produce a change in plasma concentrations of Ang I and Ang II as compared to control. Likewise, the observed effect of telmisartan as described above was not affected by the additional treatment of C21. Furthermore, no significant change was observed in any treatment group with regard to the equilibrium between Ang I and Ang II (**Figure 3-27**). Although these data do not support a change in ACE activity that might be associated with the hypothesis of shedding, it cannot be ruled out that other enzymatic pathways may compensate for altered peptide levels of Ang II and thus mask a decreased ACE activity. For this, it might be useful to measure further degradation products of Ang I and Ang II. On the one hand, Ang I may be cleaved by ACE-2 or neprilysin, giving rise to angiotensin 1-9 and angiotensin 1-7, respectively. On the other hand, Ang II is also processed by ACE-2 or aminopeptidase A,

contributing to the generation of Angiotensin 1-7 and angiotensin A, respectively. Moreover, further cleavage products of those peptides, which may also be biologically active, should also be considered [Paz Ocaranza et al., 2020].

#### **4.8. Cyclooxygenase activity in bradykinin-induced skin oedema**

Basically, angio-oedema can be divided into the allergic and the non-allergic type. The pharmacologic emergency management of an acute angio-oedema attack is challenging because of the difficulty in identifying the underlying pathomechanism and the limited time available for a comprehensive diagnosis. In particular, when the upper airway threatens to be obstructed by progressive swelling, rapid action is required. For this reason, regardless of aetiology, initial pharmacotherapeutic intervention usually consists of antihistamines, corticosteroids, and epinephrine. However, this treatment protocol has shown limited efficacy in patients with hereditary or non-allergic angio-oedema. Although the majority of cases are bradykinin-mediated, there exist cases of unknown aetiology (idiopathic), or in case of pseudo-allergy to aspirin, an increased formation of cysteinyl-leukotrienes is suspected as the cause.

The most common cause appears to be an adverse drug reaction related to several RAAS-inhibitors, most notably ACE inhibitors [Montinaro & Cicardi, 2020]. At this point, the remaining therapeutic options target the bradykinin pathway, which may be substitution therapy with C1-INH, fresh frozen plasma, kallikrein inhibition by ecallantide or B2 inhibition using icatibant [Bas et al., 2007; Swanson & Patel, 2020]. It would seem reasonable to prevent the effects of bradykinin, by blocking B2 using icatibant, however results of several clinical trials on the benefits of icatibant are conflicting [Bas et al., 2015a; Sinert et al., 2017; Straka et al., 2017]. Nevertheless, it should also be considered that the initial pharmacotherapeutic intervention as well as delayed use of icatibant may have masked its benefits. During bradykinin-induced angio-oedema that is hallmarked by B2 overactivation, it is unclear what role downstream signalling pathways play. Endothelial B2 is a Gq alpha coupled receptor, whose stimulation triggers multiple signalling pathways, involving the activation of phospholipase C as well as subsequent IP<sub>3</sub>-dependent release of intracellular calcium, thereby activating eNOS and phospholipaseA2 and D. Thus, NO, prostaglandins, leukotrienes and epoxyeicosatrienoic acids are produced [Kakoki & Smithies, 2009].

**3.8.1. Effect of unspecific cyclooxygenase inhibition on extravasation** The Miles assay experiments performed with C57BL/6 in which eNOS was inhibited by L-NAME or with mice lacking eNOS, no effect of bradykinin or labradimil on skin extravasation was observed as compared with control treatment, suggesting that NO released from small dermal blood vessels of mice does not contribute to B2-mediated extravasation [Gholamreza-Fahimi et al., 2020]. The same method was applied to investigate the role of prostaglandins by non-specific inhibition of both isoforms of cyclooxygenase using diclofenac (5 mg/kg bodyweight). Remarkably, treatment of C57BL/6 with diclofenac showed a significant reduction of dermal extravasation induced by bradykinin and labradimil when compared with vehicle treatment. Interestingly, this effect was less pronounced when diclofenac was administered at the 10th minute of ongoing extravasation (**Figure 3-28**). This finding underscores not only the important role of COX in bradykinin-induced extravasation, but also the importance of early intervention in favour of less marked extravasation. It is also likely that COX plays a less prominent role in the later progression of extravasation. The COX dependency of bradykinin-induced extravasation has been previously described with non-specific COX-inhibitors such as diclofenac [Bisha et al., 2018] and ibuprofen, as well as the more specific COX-1 inhibitor SC560 and the more specific COX-2 inhibitor celecoxib [Gholamreza-Fahimi et al., 2020]. It is quite controversial whether eNOS plays a role in bradykinin-induced extravasation in the skin of mice. In fact, proinflammatory mediators such as vascular endothelial growth factor and platelet-activating factor have been reported to induce hyperpermeability of the microvasculature, which is predominantly mediated by eNOS-derived NO [Duran, Breslin & Sanchez, 2010]. A study in bovine endothelial cells revealed approximately a 50-fold increase in NO production and a 5-fold increase in the production of the prostaglandin PGI<sub>2</sub> following stimulation with vascular endothelial growth factor [He et al., 1999], whereas a different study using porcine aortic endothelial cells found a 30-fold increase in PGI<sub>2</sub> production after stimulation with bradykinin [Takeuchi et al., 2004]. The effect of prostaglandins was also studied in the skin of guinea pigs, where PGE<sub>2</sub> alone could not induce extravasation as potent as bradykinin, but in addition to bradykinin, extravasation was further enhanced [Williams & Morley, 1973]. This effect was also investigated in the skin of rabbits and ascribed to the vasodilatory action of PGE<sub>2</sub> and the subsequent increase in blood flow [Williams & Peck, 1977]. Notably, non-specific COX inhibition by ibuprofen or indomethacin failed to abolish the potentiating effect of PGE<sub>2</sub> on bradykinin-induced extravasation [Rampart & Williams, 1986; Williams & Morley, 1973; Williams & Peck, 1977]. Bradykinin is capable of stimulating the formation of prostaglandins in endothelial cells of different vascular origin [Leeb-Lundberg

et al., 2005] and releases PGE<sub>2</sub> from isolated skin tissue [Sauer et al., 1998]. Experiments with genetically modified mice lacking the PGI<sub>2</sub> receptor revealed reduced dermal extravasation in response to combined intradermal injection of bradykinin and PGI<sub>2</sub> when compared to wildtype mice [Murata et al., 1997]. As a limitation, the authors of that study failed to compare extravasation induced by bradykinin alone to point out the potentiating effect of PGI<sub>2</sub> on bradykinin-induced extravasation in the skin of mice. Nonetheless, these data suggest that prostaglandins have a significant function in plasma extravasation under inflammatory conditions. To date, the role of prostaglandin formation downstream of bradykinin signalling has not been well studied. In this context, the involvement of various prostaglandins and the different prostaglandin receptor subtypes would be of interest, such as the E-, D-, and I-type prostaglandins and the corresponding receptors EP2, EP4, DP1, and IP, which may play a role during bradykinin-induced extravasation in the dermal microvasculature of mice [Hata & Breyer, 2004; Narumiya, Sugimoto & Ushikubi, 1999]. Considering that during B<sub>2</sub> signalling, eNOS-derived NO is rather negligible and COX inhibition by neither ibuprofen nor diclofenac can completely suppress bradykinin-induced extravasation, it is reasonable to assume that additional metabolites of arachidonic acid may be involved. These metabolites may be leukotrienes synthesized by lipoxygenases and/or epoxyeicosatrienoic acids produced by cytochrome P450 2C [Fisslthaler et al., 1999].

**Clinical trial - ABRASE** To verify the findings on the involvement of COX also in humans, the ABRASE trial was conducted. The volunteers received an intradermal injection of bradykinin to create an interstitial reservoir from which bradykinin was released steadily to the small dermal blood vessels located in the ventral forearm. As a result of the local increase of bradykinin, formation of visible and palpable wheals could be observed (**Figure 3-29**). In line with previous clinical studies evaluating the efficacy of icatibant on hereditary [Cicardi et al., 2010] and ACE inhibitor-induced angio-oedema [Bas et al., 2015a], the primary endpoint was defined as time to complete resolution of wheals. This process might involve both the breakdown of bradykinin and the removal of excess fluid through the lymphatic or capillary system [Nagy et al., 2008], whereas clinical studies with Icatibant for the treatment of patients with non-allergic angio-oedema indicate that inhibition of B<sub>2</sub> may also contribute to the resolution of angio-oedema [Bas et al., 2015a; Cicardi et al., 2010]. The partial results of the ABRASE study presented in this thesis show a significant reduction in the mean time to complete resolution of the bradykinin-induced wheal from 98.3±4.2 to 82.4±5.0 minutes in healthy volunteers medicated with 600 mg ibuprofen, a non-selective COX-inhibitor (P<0.0001 vs. control, **Figure 3-30**). In contrast, this effect could not be achieved by the intake

of 60 mg etoricoxib, a more selective COX-2 inhibitor (**Figure 3-31**), suggesting that COX-2 may play a minor role in the development of bradykinin-induced extravasation in human skin. Interestingly, for the secondary endpoint, a significant reduction in mean maximal wheal size was found after the intake of both ibuprofen (**Figure 3-32**) and etoricoxib (**Figure 3-33**). This outcome for volunteers treated with etoricoxib might be attributed to a residual inhibitory activity towards COX-1. Unfortunately, no selective COX-1 inhibitor for the use in humans is available to assess the role of COX-1. Albeit COX-2 is considered to play a major role in vascular endothelial cells, apparently COX-1 activity and in particular the downstream cell-specific synthases, e.g., for PGI<sub>2</sub>, should be taken into account [Capone et al., 2007]. Strikingly, the effect in volunteers treated with a non-selective COX-inhibitor was smaller than in mice. While in adults 600 mg of orally administered ibuprofen is a common dosage for the treatment of pain, fever and inflammation, in mice the dose of the non-specific COX-inhibitors diclofenac and ibuprofen used during the Miles assays is significantly higher in relation to bodyweight. In addition, the active substances were injected intraperitoneally, which is known to result in faster absorption with a shorter time to reach the maximum plasma concentration ( $t_{max}$ ) and a higher maximum plasma concentration ( $c_{max}$ ) as compared to oral administration [Salama et al., 2016], therefore it can be assumed that in mice higher plasma concentrations of COX-inhibitor was present when bradykinin was injected. Moreover, following B2 activation, downstream signalling in small dermal blood vessels of mice may be more dependent on COX than it is in humans. In large blood vessels of mice, such as the aorta, bradykinin has been shown to mediate constriction in a COX-dependent manner following B2 activation [Bisha et al., 2018; Felipe et al., 2007; Khosravani et al., 2015]. By contrast, in humans, continuous infusion of bradykinin into the brachial artery induced vasodilation as well as increased blood flow in the forearm, but when the COX inhibitor aspirin was administered 30 minutes prior to infusion, no effect was observed [Benjamin et al., 1989]. On the other hand, the NOS-inhibitor NG-monomethyl-L-arginine produced a strong inhibition of bradykinin-induced human forearm blood flow [Cockcroft et al., 1994], while NOS did not contribute to bradykinin-induced dermal extravasation in mice. The increased blood flow following bradykinin infusion is largely dependent on vasodilation of resistance vessels, indicating that, bradykinin-induced COX-activation may be of lesser importance in that context. Conversely, the results of the ABRASE study suggest that in small skin vessels of humans, COX activity is significantly involved during bradykinin-induced endothelial hyperpermeability. It is likely that downstream bradykinin signalling in resistance vessels is distinct from dermal microvasculature. Additional research is needed to determine which type of prostaglandin as

well as the corresponding prostaglandin receptor may be involved in the progression of bradykinin-induced dermal extravasation. Moreover, the ABRASE study did not exclude that NOS activity contributes to bradykinin-induced hyperpermeability. In conclusion, the methodology employed here, which focuses on intradermal injection of bradykinin, only covers aspects of the pathophysiology of non-allergic angio-oedema and it is uncertain whether COX activity plays a role in this condition. Still, B2 activation is a crucial step in the development of non-allergic angio-oedema [Bas et al., 2015a; Cicardi et al., 2010] and these data imply that COX activity contributes to bradykinin-induced extravasation in humans.

## 5. Summary

### 5.1. Graphical Abstract

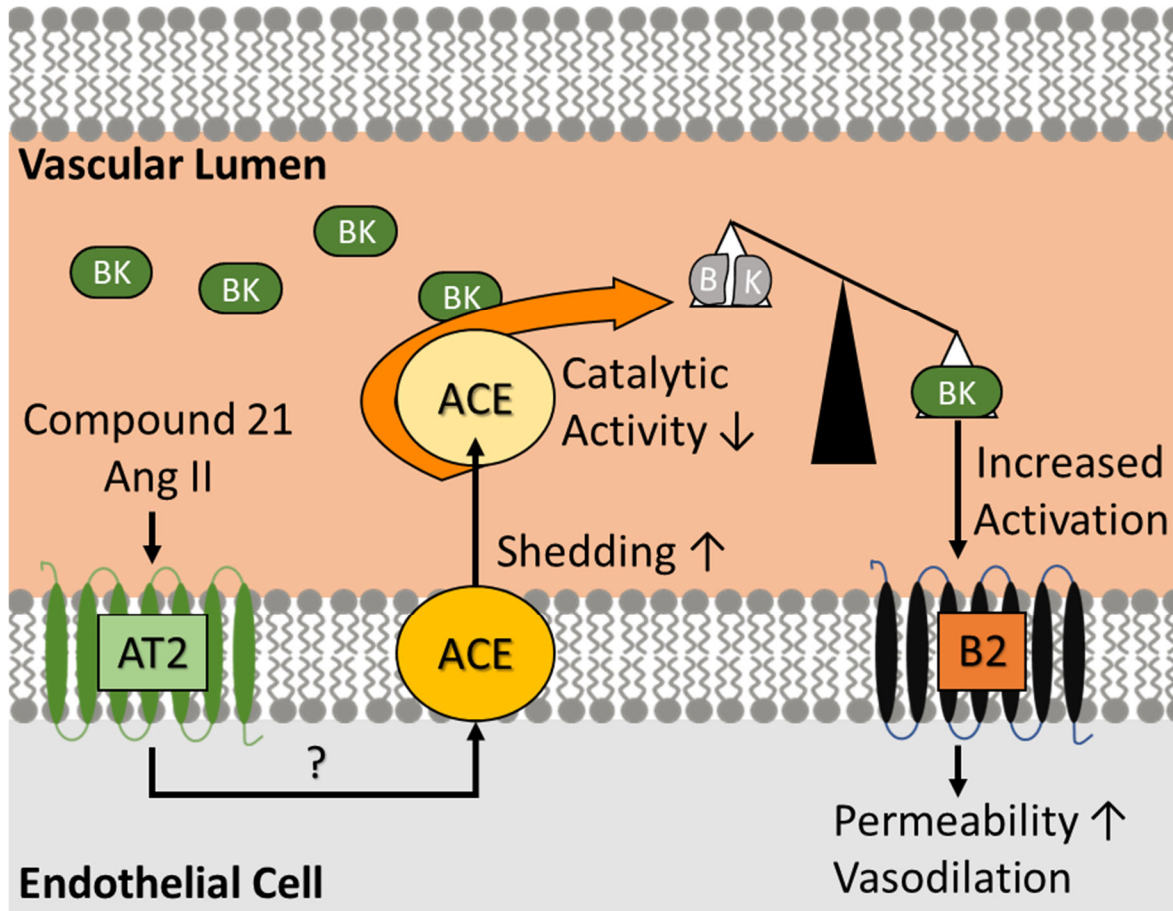


**Figure 5-1:** Graphical representation of a potential impact of angiotensin II receptor type 2 (AT2) signalling on the metabolism of bradykinin (BK). Upon activation of AT2 by its substrate angiotensin II (Ang II) or the selective agonist compound 21, the membrane-bound angiotensin I converting enzyme (ACE) is increasingly released from its membrane-anchorage into the vascular lumen. In this soluble state, the catalytic activity of ACE is diminished, which may impair the degradation of BK. Finally, locally higher steady-state concentrations of BK may lead to overactivation of the bradykinin receptor type 2 (B2), which in turn mediates increased endothelial permeability and vascular smooth muscle dilatation. This may favour the development of non-allergic angio-oedema.

## 5.2. Abstract (English version)

### Objectives

For decades, angiotensin I (Ang I)-converting enzyme (ACE) inhibitors and angiotensin II (Ang II) receptor type 1 (AT1) blockers (ARBs) have been used to treat hypertension and heart failure. A potentially life-threatening side effect of these therapeutics is non-allergic angio-oedema, typically characterized by subcutaneous swelling of the face, oral cavity, and the larynx, which if untreated is likely to develop into airway obstruction. For ACE inhibitors, an impaired degradation of bradykinin and subsequent overactivation of bradykinin receptor type 2 (B2) is thought to be the cause. The pathophysiology of ARB-induced angio-oedema is poorly understood, yet recent evidence suggests a link between increased Ang II receptor type 2 (AT2) stimulation and reduced bradykinin degradation, which calls for further investigations.

### Materials

Mouse aortic rings were used in organ bath studies to characterize the AT2 agonist compound 21 (C21). Since bradykinin is mainly degraded by ACE, C21 was used to investigate a possible effect of AT2 stimulation on ACE activity in human dermal microvascular endothelial cells (HDMEC) as well as in mouse lungs and plasma. Additional immunological approaches were made using those mouse samples to investigate changes in protein levels of ACE, Ang I and Ang II, as each would reflect changes in altered ACE activity. The effect of AT2 activation on bradykinin-induced hyperpermeability was studied in the dorsal skin of mice using the Miles assay technique. To investigate possible effects of AT2 stimulation on the circulatory system of mice, on the one hand blood pressure data were collected and on the other hand the microcirculation within the earlobe was visualized by two-photon excitation microscopy (TPEM). Finally, several animal studies and a multicentre clinical trial were conducted to further explore the signal transduction mechanisms that lead to the increased dermal extravasation caused by bradykinin.

### Results

Initial studies in HDMECs showed a significant reduction in ACE activity induced by the AT2 agonist C21, consistent with a previous experiment in a different endothelial cell line using Ang II and an ARB to stimulate AT2. The in-vivo experiment employing the Miles assay technique, confirmed AT2 activation having an enhancing effect on bradykinin-induced extravasation in the skin of mice. An effect that was absent in mice lacking AT2 or when AT2 was simultaneously blocked by PD123319, indicating reliance on AT2 activation. A correlation between AT2 activation and systolic blood pressure of mice was not detected that could have

affected bradykinin-induced extravasation. However, this does not exclude a direct effect of AT<sub>2</sub> on the dermal microcirculation which requires further optimisation of TP<sub>EM</sub> to clarify. Further approaches to investigate the effect of AT<sub>2</sub> on ACE yielded heterogeneous results. For instance, lung snippets incubated with C21 and assayed for ACE activity revealed a slightly decreased ACE activity, whereas the corresponding supernatants showed a significant increase in ACE activity. In addition, a dose-dependent increase in ACE activity was observed in plasma but not in lung lysates of mice treated with C21. These data on ACE activity suggest a cleavage of membrane-bound ACE into its soluble form, which is also accompanied by some loss of catalytic activity. Interestingly, western blot analysis of ACE protein content in lung lysates of mice previously treated with C21 revealed a significant reduction of ACE protein content. However, further immunological approaches using the ELISA technique and Dynabeads failed to demonstrate increased ACE levels in corresponding plasma samples, possibly due to methodological limitations. Moreover, plasma Ang I and Ang II levels in mice were found to be unaffected by C21 treatment. Additional studies in mice showed that B<sub>2</sub> activation does not involve activation of endothelial nitric oxid synthase but rather activation of cyclooxygenases (COX). The non-selective COX inhibitor diclofenac significantly inhibited bradykinin-induced dermal extravasation. A similar, albeit smaller, effect was observed in human volunteers receiving an intradermal injection of bradykinin after the intake of ibuprofen.

### **Conclusion**

Overall, the data suggest a contribution of AT<sub>2</sub> to non-allergic bradykinin-induced angio-oedema. This is particularly evident from the significantly increased bradykinin-induced extravasation in the skin of mice pre-treated with C21, suggesting a locally impaired bradykinin degradation. Some experimental approaches failed to show systemic effects of AT<sub>2</sub> activation on ACE activity. Presumably, a putative effect was offset by the involvement of different vascular beds, with each having different responses at the local level. However, AT<sub>2</sub> stimulation was also shown to modulate ACE activity both in-vitro and in-vivo, probably through a shedding mechanism in which membrane-bound ACE is converted to a soluble, circulating form with reduced catalytic activity. Given that bradykinin is mainly degraded by ACE, the shedding phenomenon could lead to increased local bradykinin concentrations, eventually resulting in B<sub>2</sub> overactivation and the clinical manifestations of bradykinin-induced angio-oedema. Separate studies investigating the downstream signalling of B<sub>2</sub> demonstrated the contribution of COX activity to bradykinin-induced dermal extravasation in mouse models and in humans. This finding may provide a rationale for pharmacological inhibition of arachidonic acid metabolism, which is the substrate of COX.

### 5.3. Abstract (German version)

#### Zielsetzung

Seit Jahrzehnten werden Angiotensin I (Ang I)-konvertierendes Enzym (ACE)-Inhibitoren und Angiotensin II (Ang II) Rezeptor Typ 1 (AT1)-Blocker (ARBs) zur Behandlung von Bluthochdruck und Herzinsuffizienz eingesetzt. Das nicht-allergische Angioödem ist eine potentiell lebensbedrohliche Nebenwirkung dieser Therapeutika, das durch subkutane Schwellungen des Gesichts, der Mundhöhle und des Kehlkopfes gekennzeichnet ist und sich unbehandelt zu einer Atemwegsobstruktion ausweiten kann. Bei ACE-Hemmern wird ein gestörter Abbau von Bradykinin und eine anschließende Überaktivierung des Bradykinin-Rezeptors Typ 2 (B2) als Ursache vermutet. Hingegen ist über die Pathophysiologie des ARB-induzierten Angioödems nur wenig bekannt. Neuere Erkenntnisse deuten auf einen Zusammenhang zwischen erhöhter Stimulation des Ang II Rezeptors Typ 2 (AT2) und reduziertem Bradykinin-Abbau hin, welches weitere Untersuchungen erfordert.

#### Methoden

Die Aorta der Maus wurden in Organbadstudien verwendet, um den AT2-Agonisten Compound 21 (C21) zu charakterisieren. Da Bradykinin hauptsächlich durch ACE abgebaut wird, wurde C21 verwendet, um einen möglichen Effekt der AT2-Stimulation auf die ACE-Aktivität in humanen dermalen mikrovaskulären Endothelzellen (HDMEC) sowie in der Lunge und im Plasma von Mäusen zu untersuchen. Zusätzliche immunologische Untersuchungen wurden mit diesen Mausproben durchgeführt, um Abweichungen in den Proteinmengen von ACE, Ang I und Ang II zu ermitteln, da diese sich in eine veränderte ACE-Aktivität widerspiegeln würden. Mittels der Miles-Assay-Methode wurde der Effekt der AT2-Aktivierung auf die Bradykinin-induzierte Hyperpermeabilität in der dorsalen Haut von Mäusen untersucht. Um mögliche Effekte der AT2-Stimulation auf das Kreislaufsystem von Mäusen zu ergründen, wurden zum einen Blutdruckdaten erhoben und zum anderen die Mikrozirkulation im Ohrläppchen mittels Zwei-Photonen-Anregungsmikroskopie (TPEM) visualisiert. Des Weiteren wurden mehrere Untersuchungen an Tieren und eine multizentrische klinische Studie durchgeführt, um Mechanismen der Signaltransduktion zu erkunden, die zur vermehrten dermalen Extravasation unter dem Einfluss von Bradykinin führen.

## Ergebnisse

Erste Versuche mit HDMECs zeigten eine signifikante Reduktion der ACE-Aktivität, die durch den AT2-Agonisten C21 induziert wurde, was mit einem früheren Experiment in einer anderen Endothelzelllinie übereinstimmt, bei dem Ang II und ein ARB zur Stimulation von AT2 verwendet wurden. Das In-vivo-Experiment, bei dem die Miles-Assay-Methode eingesetzt wurde, bestätigte, dass die AT2-Aktivierung einen verstärkenden Effekt auf die Bradykinin-induzierte Extravasation in der Haut von Mäusen hat. Dieser Effekt blieb bei Mäusen, denen AT2 fehlte, oder bei gleichzeitiger Blockierung von AT2 durch PD123319 aus, woraus sich eine Abhängigkeit von der AT2-Aktivierung ableiten lässt. Ein Zusammenhang zwischen der AT2-Aktivierung und dem systolischen Blutdruck der Mäuse wurde nicht festgestellt, der die Bradykinin-induzierte Extravasation hätte beeinflussen können. Dies schließt jedoch eine direkte Wirkung von AT2 auf die dermale Mikrozirkulation nicht aus, was zur Klärung eine weitere Optimierung der TPEM erfordert. Andere Ansätze zur Untersuchung der Wirkung von AT2 auf ACE lieferten heterogene Ergebnisse. So zeigten Lungenschnipsel, die mit C21 inkubiert und auf ACE-Aktivität untersucht wurden, eine leicht verminderte ACE-Aktivität, während die entsprechenden Überstände eine signifikante Erhöhung der ACE-Aktivität zeigten. In einem anderen Ansatz, bei dem Mäuse mit C21 behandelt wurden, wurde ein dosisabhängiger Anstieg der ACE-Aktivität im Plasma, aber nicht in den Lysaten der Lunge beobachtet. Diese Daten zur ACE-Aktivität deuten auf eine Spaltung des membrangebundenen ACE in seine lösliche Form hin, die auch mit einem gewissen Verlust an katalytischer Aktivität verbunden ist. Interessanterweise zeigte die Western-Blot-Analyse der Lunge von Mäusen, die zuvor mit C21 behandelt wurden, eine signifikante Reduktion des ACE-Proteinspiegels. Weitere immunologische Ansätze mit der ELISA-Technik und Dynabeads konnten jedoch keine erhöhten ACE-Spiegel in den entsprechenden Plasmaproben nachweisen, was möglicherweise auf methodische Einschränkungen zurückzuführen ist. Außerdem wurde festgestellt, dass die Ang I- und Ang II-Spiegel im Plasma von Mäusen durch die Behandlung mit C21 nicht beeinflusst wurden. Zusätzliche Untersuchungen an Mäusen zeigten, dass die B2-Aktivierung nicht mit der Aktivierung der endothelialen Stickstoffmonoxid-Synthase, sondern mit der Aktivierung von Cyclooxygenasen (COX) einhergeht. Der nicht-selektive Inhibitor Diclofenac hemmte die Bradykinin-induzierte dermale Extravasation signifikant. Ein ähnlicher, wenn auch geringerer Effekt wurde bei Probanden beobachtet, die nach der Einnahme von Ibuprofen eine intradermale Injektion von Bradykinin erhielten.

**Fazit**

Insgesamt legen die experimentellen Daten einen Beitrag von AT2 zum nicht-allergischen Bradykinin-induzierten Angioödem nahe. Insbesondere zeigt sich dies an der signifikant erhöhten Bradykinin-induzierten Extravasation in der Haut von Mäusen, die mit C21 vorbehandelt wurden, was auf einen lokal beeinträchtigten Bradykinin-Abbau hindeutet. Bei einigen experimentellen Ansätzen, die keine systemischen Effekte der AT2-Aktivierung auf die ACE-Aktivität zeigen konnten, kann angenommen werden, dass ein vermeintlicher Effekt durch die Beteiligung verschiedener Gefäßbetten mit jeweils unterschiedlichen Reaktionen auf lokaler Ebene aufgehoben wurde. Allerdings wurde auch gezeigt, dass die AT2-Stimulation die ACE-Aktivität sowohl in-vitro als auch in-vivo moduliert, vermutlich durch einen Shedding-Mechanismus, bei dem membrangebundenes ACE in eine lösliche, zirkulierende Form mit reduzierter katalytischer Aktivität umgewandelt wird. Da Bradykinin hauptsächlich durch ACE abgebaut wird, könnte das Shedding-Phänomen zu erhöhten lokalen Konzentrationen von Bradykinin führen, was schließlich zu einer B2-Überaktivierung und dem klinischen Erscheinungsbild des Bradykinin-induzierten Angioödems führen kann. Separate Studien, die den nachgeschalteten Signalweg von B2 untersuchten, zeigten den Beitrag der COX-Aktivität zur Bradykinin-induzierten dermalen Extravasation in Mausmodellen und beim Menschen. Dieser Befund könnte eine Rationale für die pharmakologische Hemmung des Arachidonsäure-Stoffwechsels liefern, der das Substrat der COX ist.

## 6. Bibliography

Abadir PM, Periasamy A, Carey RM, & Siragy HM (2006). Angiotensin II type 2 receptor-bradykinin B2 receptor functional heterodimerization. *Hypertension* 48: 316-322.

AbdAlla S, Lothar H, Abdel-tawab AM, & Quitterer U (2001). The angiotensin II AT2 receptor is an AT1 receptor antagonist. *J Biol Chem* 276: 39721-39726.

AbdAlla S, Lothar H, & Quitterer U (2000). AT1-receptor heterodimers show enhanced G-protein activation and altered receptor sequestration. *Nature* 407: 94-98.

Aboyans V, Ricco JB, Bartelink MEL, Bjorck M, Brodmann M, Cohnert T, Collet JP, Czerny M, De Carlo M, Debus S, Espinola-Klein C, Kahan T, Kownator S, Mazzolai L, Naylor AR, Roffi M, Rother J, Sprynger M, Tendera M, Tepe G, Venermo M, Vlachopoulos C, Desormais I, & Group ESCSD (2018). 2017 ESC Guidelines on the Diagnosis and Treatment of Peripheral Arterial Diseases, in collaboration with the European Society for Vascular Surgery (ESVS): Document covering atherosclerotic disease of extracranial carotid and vertebral, mesenteric, renal, upper and lower extremity arteries Endorsed by: the European Stroke Organization (ESO) The Task Force for the Diagnosis and Treatment of Peripheral Arterial Diseases of the European Society of Cardiology (ESC) and of the European Society for Vascular Surgery (ESVS). *Eur Heart J* 39: 763-816.

Adam A, Cugno M, Molinaro G, Perez M, Lepage Y, & Agostoni A (2002). Aminopeptidase P in individuals with a history of angio-oedema on ACE inhibitors. *Lancet* 359: 2088-2089.

Ali HA, Lomholt AF, Mahmoudpour SH, Hermanrud T, Bygum A, von Buchwald C, Jakobsen MA, & Rasmussen ER (2019). Genetic susceptibility to angiotensin-converting enzyme-inhibitor induced angioedema: A systematic review and evaluation of methodological approaches. *PLoS One* 14: e0224858.

Ali MS, Sayeski PP, Dirksen LB, Hayzer DJ, Marrero MB, & Bernstein KE (1997). Dependence on the motif YIPP for the physical association of Jak2 kinase with the intracellular carboxyl tail of the angiotensin II AT1 receptor. *J Biol Chem* 272: 23382-23388.

Aoki A, Ogawa T, Sumino H, Kumakura H, Takayama Y, Ichikawa S, & Nitta K (2010). Long-term effects of telmisartan on blood pressure, the renin-angiotensin-aldosterone system, and lipids in hypertensive patients. *Heart Vessels* 25: 195-202.

Aygoren-Pursun E, Magerl M, Maetzel A, & Maurer M (2018). Epidemiology of Bradykinin-mediated angioedema: a systematic investigation of epidemiological studies. *Orphanet J Rare Dis* 13: 73.

Azushima K, Morisawa N, Tamura K, & Nishiyama A (2020). Recent Research Advances in Renin-Angiotensin-Aldosterone System Receptors. *Curr Hypertens Rep* 22: 22.

Barki-Harrington L, Luttrell LM, & Rockman HA (2003). Dual inhibition of beta-adrenergic and angiotensin II receptors by a single antagonist: a functional role for receptor-receptor interaction in vivo. *Circulation* 108: 1611-1618.

- Bas M, Adams V, Suvorava T, Niehues T, Hoffmann TK, & Kojda G (2007). Nonallergic angioedema: role of bradykinin. *Allergy* 62: 842-856.
- Bas M, Greve J, Stelter K, Havel M, Strassen U, Rotter N, Veit J, Schossow B, Hapfelmeier A, Kehl V, Kojda G, & Hoffmann TK (2015a). A randomized trial of icatibant in ACE-inhibitor-induced angioedema. *N Engl J Med* 372: 418-425.
- Bas M, Greve J, Strassen U, Khosravani F, Hoffmann TK, & Kojda G (2015b). Angioedema induced by cardiovascular drugs: new players join old friends. *Allergy* 70: 1196-1200.
- Bas M, & Kojda G (2008). Das nicht allergische Angioödem – Alte und neue Arzneimittel als Auslöser und Therapeutika. *Fortbildungstelegramm Pharmazie* 2: 85-100.
- Bas M, Storck K, & Strassen U (2017). Potential Biomarkers for the Diagnosis of Angiotensin-Converting Enzyme Inhibitor-Induced Angioedema. *ORL J Otorhinolaryngol Relat Spec* 79: 85-92.
- Beltrami L, Zanichelli A, Zingale L, Vacchini R, Carugo S, & Cicardi M (2011). Long-term follow-up of 111 patients with angiotensin-converting enzyme inhibitor-related angioedema. *J Hypertens* 29: 2273-2277.
- Beneteau B, Baudin B, Morgant G, Giboudeau J, & Baumann FC (1986). Automated kinetic assay of angiotensin-converting enzyme in serum. *Clin Chem* 32: 884-886.
- Benjamin N, Cockcroft JR, Collier JG, Dollery CT, Ritter JM, & Webb DJ (1989). Local inhibition of converting enzyme and vascular responses to angiotensin and bradykinin in the human forearm. *J Physiol* 412: 543-555.
- Berk BC (2003). Angiotensin type 2 receptor (AT2R): a challenging twin. *Sci STKE* 2003: PE16.
- Betschel S, Badiou J, Binkley K, Borici-Mazi R, Hebert J, Kanani A, Keith P, Lacuesta G, Wasserman S, Yang B, Aygoren-Pursun E, Bernstein J, Bork K, Caballero T, Cicardi M, Craig T, Farkas H, Grumach A, Katelaris C, Longhurst H, Riedl M, Zuraw B, Berger M, Boursiquot JN, Boysen H, Castaldo A, Chapdelaine H, Connors L, Fu L, Goodyear D, Haynes A, Kamra P, Kim H, Lang-Robertson K, Leith E, McCusker C, Moote B, O'Keefe A, Othman I, Poon MC, Ritchie B, St-Pierre C, Stark D, & Tsai E (2019). The International/Canadian Hereditary Angioedema Guideline. *Allergy Asthma Clin Immunol* 15: 72.
- Bisha M, Dao VT, Gholamreza-Fahimi E, Vogt M, van Zandvoort M, Weber S, Bas M, Khosravani F, Kojda G, & Suvorava T (2018). The role of bradykinin receptor type 2 in spontaneous extravasation in mice skin: implications for non-allergic angio-oedema. *Br J Pharmacol* 175: 1607-1620.
- Bosnyak S, Jones ES, Christopoulos A, Aguilar MI, Thomas WG, & Widdop RE (2011). Relative affinity of angiotensin peptides and novel ligands at AT1 and AT2 receptors. *Clin Sci (Lond)* 121: 297-303.

- Bosnyak S, Welungoda IK, Hallberg A, Alterman M, Widdop RE, & Jones ES (2010). Stimulation of angiotensin AT2 receptors by the non-peptide agonist, Compound 21, evokes vasodepressor effects in conscious spontaneously hypertensive rats. *Br J Pharmacol* 159: 709-716.
- Bouzekri N, Zhu X, Jiang Y, McKenzie CA, Luke A, Forrester T, Adeyemo A, Kan D, Farrall M, Anderson S, Cooper RS, & Ward R (2004). Angiotensin I-converting enzyme polymorphisms, ACE level and blood pressure among Nigerians, Jamaicans and African-Americans. *Eur J Hum Genet* 12: 460-468.
- Bradford MM (1976). A rapid and sensitive method for the quantitation of microgram quantities of protein utilizing the principle of protein-dye binding. *Anal Biochem* 72: 248-254.
- Brown NJ, Byiers S, Carr D, Maldonado M, & Warner BA (2009). Dipeptidyl peptidase-IV inhibitor use associated with increased risk of ACE inhibitor-associated angioedema. *Hypertension* 54: 516-523.
- Brown NJ, Ray WA, Snowden M, & Griffin MR (1996). Black Americans have an increased rate of angiotensin converting enzyme inhibitor-associated angioedema. *Clin Pharmacol Ther* 60: 8-13.
- Busse PJ, Christiansen SC, Riedl MA, Banerji A, Bernstein JA, Castaldo AJ, Craig T, Davis-Lorton M, Frank MM, Li HH, Lumry WR, & Zuraw BL (2021). US HAEA Medical Advisory Board 2020 Guidelines for the Management of Hereditary Angioedema. *J Allergy Clin Immunol Pract* 9: 132-150 e133.
- Caballero T (2021). Treatment of Hereditary Angioedema. *J Investig Allergol Clin Immunol* 31: 1-16.
- Calder PC (2020). Eicosanoids. *Essays Biochem* 64: 423-441.
- Campbell DJ (1987). Circulating and tissue angiotensin systems. *J Clin Invest* 79: 1-6.
- Campbell DJ (1996). Endogenous angiotensin II levels and the mechanism of action of angiotensin-converting enzyme inhibitors and angiotensin receptor type 1 antagonists. *Clin Exp Pharmacol Physiol* 23 Suppl 3: S125-131.
- Campbell DJ (2003). The renin-angiotensin and the kallikrein-kinin systems. *Int J Biochem Cell Biol* 35: 784-791.
- Campbell DJ (2018). Nephilysin Inhibitors and Bradykinin. *Front Med (Lausanne)* 5: 257.
- Campbell DJ, Duncan AM, Kladis A, & Harrap SB (1995). Angiotensin peptides in spontaneously hypertensive and normotensive Donryu rats. *Hypertension* 25: 928-934.
- Campbell DJ, Krum H, & Esler MD (2005). Losartan increases bradykinin levels in hypertensive humans. *Circulation* 111: 315-320.
- Capone ML, Tacconelli S, Di Francesco L, Sacchetti A, Sciulli MG, & Patrignani P (2007). Pharmacodynamic of cyclooxygenase inhibitors in humans. *Prostaglandins Other Lipid Mediat* 82: 85-94.

Carey RM (2017). Update on angiotensin AT2 receptors. *Curr Opin Nephrol Hypertens* 26: 91-96.

Chappell MC (2012). Nonclassical renin-angiotensin system and renal function. *Compr Physiol* 2: 2733-2752.

Chattopadhyay S, Santhamma KR, Sengupta S, McCue B, Kinter M, Sen GC, & Sen I (2005). Calmodulin binds to the cytoplasmic domain of angiotensin-converting enzyme and regulates its phosphorylation and cleavage secretion. *J Biol Chem* 280: 33847-33855.

Christiansen SC, Davis DK, Castaldo AJ, & Zuraw BL (2016). Pediatric Hereditary Angioedema: Onset, Diagnostic Delay, and Disease Severity. *Clin Pediatr (Phila)* 55: 935-942.

Cicardi M, Aberer W, Banerji A, Bas M, Bernstein JA, Bork K, Caballero T, Farkas H, Grumach A, Kaplan AP, Riedl MA, Triggiani M, Zanichelli A, Zuraw B, & EAACI Hutpo (2014). Classification, diagnosis, and approach to treatment for angioedema: consensus report from the Hereditary Angioedema International Working Group. *Allergy* 69: 602-616.

Cicardi M, Banerji A, Bracho F, Malbran A, Rosenkranz B, Riedl M, Bork K, Lumry W, Aberer W, Bier H, Bas M, Greve J, Hoffmann TK, Farkas H, Reshef A, Ritchie B, Yang W, Grabbe J, Kivity S, Kreuz W, Levy RJ, Luger T, Obtulowicz K, Schmid-Grendelmeier P, Bull C, Sitkauskiene B, Smith WB, Toubi E, Werner S, Anne S, Bjorkander J, Bouillet L, Cillari E, Hurewitz D, Jacobson KW, Katelaris CH, Maurer M, Merk H, Bernstein JA, Feighery C, Floccard B, Gleich G, Hebert J, Kaatz M, Keith P, Kirkpatrick CH, Langton D, Martin L, Pichler C, Resnick D, Wombolt D, Fernandez Romero DS, Zanichelli A, Arcoletto F, Knolle J, Kravec I, Dong L, Zimmermann J, Rosen K, & Fan WT (2010). Icatibant, a new bradykinin-receptor antagonist, in hereditary angioedema. *N Engl J Med* 363: 532-541.

Claesson-Welsh L (2015). Vascular permeability--the essentials. *Ups J Med Sci* 120: 135-143.

Cockcroft JR, Chowienczyk PJ, Brett SE, & Ritter JM (1994). Effect of NG-monomethyl-L-arginine on kinin-induced vasodilation in the human forearm. *Br J Clin Pharmacol* 38: 307-310.

Collet JP, Thiele H, Barbato E, Barthelémy O, Bauersachs J, Bhatt DL, Dendale P, Dorobantu M, Edvardsen T, Folliguet T, Gale CP, Gilard M, Jobs A, Juni P, Lambrinou E, Lewis BS, Mehilli J, Meliga E, Merkely B, Mueller C, Roffi M, Rutten FH, Sibbing D, Siontis GCM, & Group ESCSD (2021). 2020 ESC Guidelines for the management of acute coronary syndromes in patients presenting without persistent ST-segment elevation. *Eur Heart J* 42: 1289-1367.

Cosarderehoglu C, Nidadavolu LS, George CJ, Oh ES, Bennett DA, Walston JD, & Abadir PM (2020). Brain Renin-Angiotensin System at the Intersect of Physical and Cognitive Frailty. *Front Neurosci* 14: 586314.

Couture R, Harrison M, Vianna RM, & Cloutier F (2001). Kinin receptors in pain and inflammation. *Eur J Pharmacol* 429: 161-176.

Cui T, Nakagami H, Iwai M, Takeda Y, Shiuchi T, Tamura K, Daviet L, & Horiuchi M (2000). ATRAP, novel AT1 receptor associated protein, enhances internalization of AT1 receptor and inhibits vascular smooth muscle cell growth. *Biochem Biophys Res Commun* 279: 938-941.

- Curry FR, & Noll T (2010). Spotlight on microvascular permeability. *Cardiovasc Res* 87: 195-197.
- Cyr M, Lepage Y, Blais C, Jr., Gervais N, Cugno M, Rouleau JL, & Adam A (2001). Bradykinin and des-Arg(9)-bradykinin metabolic pathways and kinetics of activation of human plasma. *Am J Physiol Heart Circ Physiol* 281: H275-283.
- Danilov SM, Lunsdorf H, Akinbi HT, Nesterovitch AB, Epshtein Y, Letsiou E, Kryukova OV, Piegeler T, Golukhova EZ, Schwartz DE, Dull RO, Minshall RD, Kost OA, & Garcia JG (2016). Lysozyme and bilirubin bind to ACE and regulate its conformation and shedding. *Sci Rep* 6: 34913.
- Danilov SM, Tovsky SI, Schwartz DE, & Dull RO (2017). ACE Phenotyping as a Guide Toward Personalized Therapy With ACE Inhibitors. *J Cardiovasc Pharmacol Ther* 22: 374-386.
- Dao VT, Medini S, Bisha M, Balz V, Suvorava T, Bas M, & Kojda G (2016). Nitric oxide up-regulates endothelial expression of angiotensin II type 2 receptors. *Biochem Pharmacol* 112: 24-36.
- Davis AE, 3rd (2008). Hereditary angioedema: a current state-of-the-art review, III: mechanisms of hereditary angioedema. *Ann Allergy Asthma Immunol* 100: S7-12.
- Davis MJ (2012). Perspective: physiological role(s) of the vascular myogenic response. *Microcirculation* 19: 99-114.
- de Gasparo M, Catt KJ, Inagami T, Wright JW, & Unger T (2000). International union of pharmacology. XXIII. The angiotensin II receptors. *Pharmacol Rev* 52: 415-472.
- Del Borgo M, Wang Y, Bosnyak S, Khan M, Walters P, Spizzo I, Perlmutter P, Hilliard L, Denton K, Aguilar MI, Widdop RE, & Jones ES (2015). beta-Pro7Ang III is a novel highly selective angiotensin II type 2 receptor (AT2R) agonist, which acts as a vasodepressor agent via the AT2R in conscious spontaneously hypertensive rats. *Clin Sci (Lond)* 129: 505-513.
- Denk W, Delaney KR, Gelperin A, Kleinfeld D, Strowbridge BW, Tank DW, & Yuste R (1994). Anatomical and Functional Imaging of Neurons Using 2-Photon Laser-Scanning Microscopy. *Journal of Neuroscience Methods* 54: 151-162.
- Dinh DT, Frauman AG, Johnston CI, & Fabiani ME (2001). Angiotensin receptors: distribution, signalling and function. *Clin Sci (Lond)* 100: 481-492.
- Donoghue M, Hsieh F, Baronas E, Godbout K, Gosselin M, Stagliano N, Donovan M, Woolf B, Robison K, Jeyaseelan R, Breitbart RE, & Acton S (2000). A novel angiotensin-converting enzyme-related carboxypeptidase (ACE2) converts angiotensin I to angiotensin 1-9. *Circ Res* 87: E1-9.
- Duran WN, Breslin JW, & Sanchez FA (2010). The NO cascade, eNOS location, and microvascular permeability. *Cardiovasc Res* 87: 254-261.
- Egawa G, Nakamizo S, Natsuaki Y, Doi H, Miyachi Y, & Kabashima K (2013). Intravital analysis of vascular permeability in mice using two-photon microscopy. *Sci Rep* 3: 1932.

- Emerich DF, Dean RL, Osborn C, & Bartus RT (2001). The development of the bradykinin agonist labradimil as a means to increase the permeability of the blood-brain barrier: from concept to clinical evaluation. *Clin Pharmacokinet* 40: 105-123.
- Engvall E, & Perlmann P (1971). Enzyme-linked immunosorbent assay (ELISA). Quantitative assay of immunoglobulin G. *Immunochemistry* 8: 871-874.
- Fagyas M, Uri K, Siket IM, Fulop GA, Csato V, Darago A, Boczan J, Banyai E, Szentkiralyi IE, Maros TM, Szerafin T, Edes I, Papp Z, & Toth A (2014). New perspectives in the renin-angiotensin-aldosterone system (RAAS) II: albumin suppresses angiotensin converting enzyme (ACE) activity in human. *PLoS One* 9: e87844.
- Felipe SA, Rodrigues ES, Martin RP, Paiva AC, Pesquero JB, & Shimuta SI (2007). Functional expression of kinin B1 and B2 receptors in mouse abdominal aorta. *Braz J Med Biol Res* 40: 649-655.
- Feng D, Nagy JA, Hipp J, Dvorak HF, & Dvorak AM (1996). Vesiculo-vacuolar organelles and the regulation of venule permeability to macromolecules by vascular permeability factor, histamine, and serotonin. *J Exp Med* 183: 1981-1986.
- Feng YH, Sun Y, & Douglas JG (2002). Gbeta gamma -independent constitutive association of Galphas with SHP-1 and angiotensin II receptor AT2 is essential in AT2-mediated ITIM-independent activation of SHP-1. *Proc Natl Acad Sci U S A* 99: 12049-12054.
- Ferreira SH (1965). A Bradykinin-Potentiating Factor (Bpf) Present in the Venom of Bothrops Jararaca. *Br J Pharmacol Chemother* 24: 163-169.
- Fisslthaler B, Popp R, Kiss L, Potente M, Harder DR, Fleming I, & Busse R (1999). Cytochrome P450 2C is an EDHF synthase in coronary arteries. *Nature* 401: 493-497.
- Forrester SJ, Booz GW, Sigmund CD, Coffman TM, Kawai T, Rizzo V, Scalia R, & Eguchi S (2018). Angiotensin II Signal Transduction: An Update on Mechanisms of Physiology and Pathophysiology. *Physiol Rev* 98: 1627-1738.
- Forrester SJ, Kawai T, O'Brien S, Thomas W, Harris RC, & Eguchi S (2016). Epidermal Growth Factor Receptor Transactivation: Mechanisms, Pathophysiology, and Potential Therapies in the Cardiovascular System. *Annu Rev Pharmacol Toxicol* 56: 627-653.
- Foulquier S, Steckelings UM, & Unger T (2012). Impact of the AT(2) receptor agonist C21 on blood pressure and beyond. *Curr Hypertens Rep* 14: 403-409.
- Gainer JV, Morrow JD, Loveland A, King DJ, & Brown NJ (1998). Effect of bradykinin-receptor blockade on the response to angiotensin-converting-enzyme inhibitor in normotensive and hypertensive subjects. *N Engl J Med* 339: 1285-1292.
- Gainer JV, Nadeau JH, Ryder D, & Brown NJ (1996). Increased sensitivity to bradykinin among African Americans. *J Allergy Clin Immunol* 98: 283-287.

- Georgiadis D, Beau F, Czarny B, Cotton J, Yiotakis A, & Dive V (2003). Roles of the two active sites of somatic angiotensin-converting enzyme in the cleavage of angiotensin I and bradykinin: insights from selective inhibitors. *Circ Res* 93: 148-154.
- Gholamreza-Fahimi E, Bisha M, Hahn J, Strassen U, Krybus M, Khosravani F, Hoffmann TK, Hohlfeld T, Greve J, Bas M, Twarock S, & Kojda G (2020). Cyclooxygenase activity in bradykinin-induced dermal extravasation. A study in mice and humans. *Biomed Pharmacother* 123: 109797.
- Gibbs CR, Lip GY, & Beevers DG (1999). Angioedema due to ACE inhibitors: increased risk in patients of African origin. *Br J Clin Pharmacol* 48: 861-865.
- Gohlke P, Pees C, & Unger T (1998). AT<sub>2</sub> receptor stimulation increases aortic cyclic GMP in SHRSP by a kinin-dependent mechanism. *Hypertension* 31: 349-355.
- Gonzalez-Hernandez Mde L, Godinez-Hernandez D, Bobadilla-Lugo RA, & Lopez-Sanchez P (2010). Angiotensin-II type 1 receptor (AT1R) and alpha-1D adrenoceptor form a heterodimer during pregnancy-induced hypertension. *Auton Autacoid Pharmacol* 30: 167-172.
- Guang C, Phillips RD, Jiang B, & Milani F (2012). Three key proteases--angiotensin-I-converting enzyme (ACE), ACE2 and renin--within and beyond the renin-angiotensin system. *Arch Cardiovasc Dis* 105: 373-385.
- Guo DC, Papke CL, He R, & Milewicz DM (2006). Pathogenesis of thoracic and abdominal aortic aneurysms. *Ann N Y Acad Sci* 1085: 339-352.
- Hamid S, Rhaleb IA, Kassem KM, & Rhaleb NE (2020). Role of Kinins in Hypertension and Heart Failure. *Pharmaceuticals (Basel)* 13.
- Hansen JL, Servant G, Baranski TJ, Fujita T, Iiri T, & Sheikh SP (2000). Functional reconstitution of the angiotensin II type 2 receptor and G(i) activation. *Circ Res* 87: 753-759.
- Harrison C, & Acharya KR (2014). ACE for all - a molecular perspective. *J Cell Commun Signal* 8: 195-210.
- Hata AN, & Breyer RM (2004). Pharmacology and signaling of prostaglandin receptors: multiple roles in inflammation and immune modulation. *Pharmacol Ther* 103: 147-166.
- Haudenschild DR, Eldridge A, Lein PJ, & Chromy BA (2014). High abundant protein removal from rodent blood for biomarker discovery. *Biochem Biophys Res Commun* 455: 84-89.
- He H, Venema VJ, Gu X, Venema RC, Marrero MB, & Caldwell RB (1999). Vascular endothelial growth factor signals endothelial cell production of nitric oxide and prostacyclin through flk-1/KDR activation of c-Src. *J Biol Chem* 274: 25130-25135.
- Hein L, Barsh GS, Pratt RE, Dzau VJ, & Kobilka BK (1995). Behavioural and cardiovascular effects of disrupting the angiotensin II type-2 receptor in mice. *Nature* 377: 744-747.

- Hofman Z, de Maat S, Hack CE, & Maas C (2016). Bradykinin: Inflammatory Product of the Coagulation System. *Clin Rev Allergy Immunol* 51: 152-161.
- Holmquist B, Bunning P, & Riordan JF (1979). A continuous spectrophotometric assay for angiotensin converting enzyme. *Anal Biochem* 95: 540-548.
- Horiuchi M, Hayashida W, Kambe T, Yamada T, & Dzau VJ (1997). Angiotensin type 2 receptor dephosphorylates Bcl-2 by activating mitogen-activated protein kinase phosphatase-1 and induces apoptosis. *J Biol Chem* 272: 19022-19026.
- Hornig B, Kohler C, Schlink D, Tatge H, & Drexler H (2003). AT1-receptor antagonism improves endothelial function in coronary artery disease by a bradykinin/B2-receptor-dependent mechanism. *Hypertension* 41: 1092-1095.
- Huang XC, Richards EM, & Summers C (1995). Angiotensin II type 2 receptor-mediated stimulation of protein phosphatase 2A in rat hypothalamic/brainstem neuronal cocultures. *J Neurochem* 65: 2131-2137.
- Hunley TE, Tamura M, Stoneking BJ, Nishimura H, Ichiki T, Inagami T, & Kon V (2000). The angiotensin type II receptor tonically inhibits angiotensin-converting enzyme in AT2 null mutant mice. *Kidney Int* 57: 570-577.
- Ibanez B, James S, Agewall S, Antunes MJ, Bucciarelli-Ducci C, Bueno H, Caforio ALP, Crea F, Goudevanos JA, Halvorsen S, Hindricks G, Kastrati A, Lenzen MJ, Prescott E, Roffi M, Valgimigli M, Varenhorst C, Vranckx P, Widimsky P, & Group ESCSD (2018). 2017 ESC Guidelines for the management of acute myocardial infarction in patients presenting with ST-segment elevation: The Task Force for the management of acute myocardial infarction in patients presenting with ST-segment elevation of the European Society of Cardiology (ESC). *Eur Heart J* 39: 119-177.
- Ichiki T, Labosky PA, Shiota C, Okuyama S, Imagawa Y, Fogo A, Niimura F, Ichikawa I, Hogan BL, & Inagami T (1995). Effects on blood pressure and exploratory behaviour of mice lacking angiotensin II type-2 receptor. *Nature* 377: 748-750.
- Iwata M, & H. Greenberg B (2011). Ectodomain Shedding of ACE and ACE2 as Regulators of Their Protein Functions. *Current Enzyme Inhibition* 7: 42-55.
- Jackson L, Eldahshan W, Fagan SC, & Ergul A (2018). Within the Brain: The Renin Angiotensin System. *Int J Mol Sci* 19.
- Jalowy A, Schulz R, Dorge H, Behrends M, & Heusch G (1998). Infarct size reduction by AT1-receptor blockade through a signal cascade of AT2-receptor activation, bradykinin and prostaglandins in pigs. *J Am Coll Cardiol* 32: 1787-1796.
- Jaspard E, Wei L, & Alhenc-Gelas F (1993). Differences in the properties and enzymatic specificities of the two active sites of angiotensin I-converting enzyme (kininase II). Studies with bradykinin and other natural peptides. *J Biol Chem* 268: 9496-9503.

- Johren O, Dendorfer A, & Dominiak P (2004). Cardiovascular and renal function of angiotensin II type-2 receptors. *Cardiovasc Res* 62: 460-467.
- Kakoki M, & Smithies O (2009). The kallikrein-kinin system in health and in diseases of the kidney. *Kidney Int* 75: 1019-1030.
- Karpe PA, Gupta J, Marthong RF, Ramarao P, & Tikoo K (2012). Insulin resistance induces a segmental difference in thoracic and abdominal aorta: differential expression of AT1 and AT2 receptors. *J Hypertens* 30: 132-146.
- Katada J, & Majima M (2002). AT(2) receptor-dependent vasodilation is mediated by activation of vascular kinin generation under flow conditions. *Br J Pharmacol* 136: 484-491.
- Keane TM, Goodstadt L, Danecek P, White MA, Wong K, Yalcin B, Heger A, Agam A, Slater G, Goodson M, Furlotte NA, Eskin E, Nellaker C, Whitley H, Cleak J, Janowitz D, Hernandez-Pliego P, Edwards A, Belgard TG, Oliver PL, McIntyre RE, Bhomra A, Nicod J, Gan X, Yuan W, van der Weyden L, Steward CA, Bala S, Stalker J, Mott R, Durbin R, Jackson IJ, Czechanski A, Guerra-Assuncao JA, Donahue LR, Reinholdt LG, Payseur BA, Ponting CP, Birney E, Flint J, & Adams DJ (2011). Mouse genomic variation and its effect on phenotypes and gene regulation. *Nature* 477: 289-294.
- Kessler SP, de SSP, Scheidemantel TS, Gomos JB, Rowe TM, & Sen GC (2003). Maintenance of normal blood pressure and renal functions are independent effects of angiotensin-converting enzyme. *J Biol Chem* 278: 21105-21112.
- Kessler SP, Hashimoto S, Senanayake PS, Gaughan C, Sen GC, & Schnermann J (2005). Nephron function in transgenic mice with selective vascular or tubular expression of Angiotensin-converting enzyme. *J Am Soc Nephrol* 16: 3535-3542.
- Khosravani F, Suvorava T, Dao VT, Brockmann N, Kocgirli O, Herbst FF, Valcaccia S, Kassack MU, Bas M, & Kojda G (2015). Stability of murine bradykinin type 2 receptor despite treatment with NO, bradykinin, icatibant, or C1-INH. *Allergy* 70: 285-294.
- Kjeldsen SE, von Lueder TG, Smiseth OA, Wachtell K, Mistry N, Westheim AS, Hopper I, Julius S, Pitt B, Reid CM, Devereux RB, & Zannad F (2020). Medical Therapies for Heart Failure With Preserved Ejection Fraction. *Hypertension* 75: 23-32.
- Knuuti J, Wijns W, Saraste A, Capodanno D, Barbato E, Funck-Brentano C, Prescott E, Storey RF, Deaton C, Cuisset T, Agewall S, Dickstein K, Edvardsen T, Escaned J, Gersh BJ, Svitil P, Gilard M, Hasdai D, Hatala R, Mahfoud F, Masip J, Muneretto C, Valgimigli M, Achenbach S, Bax JJ, & Group ESCSD (2020). 2019 ESC Guidelines for the diagnosis and management of chronic coronary syndromes. *Eur Heart J* 41: 407-477.
- Kohlstedt K, Shoghi F, Muller-Esterl W, Busse R, & Fleming I (2002). CK2 phosphorylates the angiotensin-converting enzyme and regulates its retention in the endothelial cell plasma membrane. *Circ Res* 91: 749-756.
- Kohout TA, & Rogers TB (1995). Angiotensin II activates the Na<sup>+</sup>/HCO<sub>3</sub><sup>-</sup> symport through a phosphoinositide-independent mechanism in cardiac cells. *J Biol Chem* 270: 20432-20438.

Koskelo P, Kekki M, & Wager O (1967). Kinetic behaviour of <sup>131</sup>I-labelled myoglobin in human beings. *Clin Chim Acta* 17: 339-347.

Kostenis E, Milligan G, Christopoulos A, Sanchez-Ferrer CF, Heringer-Walther S, Sexton PM, Gembardt F, Kellett E, Martini L, Vanderheyden P, Schultheiss HP, & Walther T (2005). G-protein-coupled receptor Mas is a physiological antagonist of the angiotensin II type 1 receptor. *Circulation* 111: 1806-1813.

Koumandou VL, & Scorilas A (2013). Evolution of the plasma and tissue kallikreins, and their alternative splicing isoforms. *PLoS One* 8: e68074.

Krege JH, Hodgin JB, Hagaman JR, & Smithies O (1995). A noninvasive computerized tail-cuff system for measuring blood pressure in mice. *Hypertension* 25: 1111-1115.

Kruger-Genge A, Blocki A, Franke RP, & Jung F (2019). Vascular Endothelial Cell Biology: An Update. *Int J Mol Sci* 20.

Kuo IY, & Ehrlich BE (2015). Signaling in muscle contraction. *Cold Spring Harb Perspect Biol* 7: a006023.

Laemmli UK (1970). Cleavage of structural proteins during the assembly of the head of bacteriophage T4. *Nature* 227: 680-685.

Lazard D, Briend-Sutren MM, Villageois P, Mattei MG, Strosberg AD, & Nahmias C (1994). Molecular characterization and chromosome localization of a human angiotensin II AT2 receptor gene highly expressed in fetal tissues. *Recept Channels* 2: 271-280.

Leeb-Lundberg LM, Marceau F, Muller-Esterl W, Pettibone DJ, & Zuraw BL (2005). International union of pharmacology. XLV. Classification of the kinin receptor family: from molecular mechanisms to pathophysiological consequences. *Pharmacol Rev* 57: 27-77.

Lenschow M, Bas M, Johnson F, Wirth M, & Strassen U (2018). A score for the differential diagnosis of bradykinin- and histamine-induced head and neck swellings. *Eur Arch Otorhinolaryngol* 275: 1767-1773.

Leonhardt J, Villela DC, Teichmann A, Munter LM, Mayer MC, Mardahl M, Kirsch S, Namsolleck P, Lucht K, Benz V, Alenina N, Daniell N, Horiuchi M, Iwai M, Multhaup G, Schulein R, Bader M, Santos RA, Unger T, & Steckelings UM (2017). Evidence for Heterodimerization and Functional Interaction of the Angiotensin Type 2 Receptor and the Receptor MAS. *Hypertension* 69: 1128-1135.

Lerch M (2012). Drug-induced angioedema. *Chem Immunol Allergy* 97: 98-105.

Li JM, Mogi M, Tsukuda K, Tomochika H, Iwanami J, Min LJ, Nahmias C, Iwai M, & Horiuchi M (2007). Angiotensin II-induced neural differentiation via angiotensin II type 2 (AT2) receptor-MMS2 cascade involving interaction between AT2 receptor-interacting protein and Src homology 2 domain-containing protein-tyrosine phosphatase 1. *Mol Endocrinol* 21: 499-511.

- Lira R, Oliveira M, Martins M, Silva C, Carvalho S, Stumbo AC, Cortez E, Verdoorn K, Einicker-Lamas M, Thole A, & de Carvalho L (2017). Transplantation of bone marrow-derived MSCs improves renal function and Na(+)+K(+)-ATPase activity in rats with renovascular hypertension. *Cell Tissue Res* 369: 287-301.
- Long BJ, Koefman A, & Gottlieb M (2019). Evaluation and Management of Angioedema in the Emergency Department. *West J Emerg Med* 20: 587-600.
- Lopez-Sublet M, Caratti di Lanzacco L, Danser AHJ, Lambert M, Elourimi G, & Persu A (2018). Focus on increased serum angiotensin-converting enzyme level: From granulomatous diseases to genetic mutations. *Clin Biochem* 59: 1-8.
- Macari D, Bottari S, Whitebread S, De Gasparo M, & Levens N (1993). Renal actions of the selective angiotensin AT2 receptor ligands CGP 42112B and PD 123319 in the sodium-depleted rat. *Eur J Pharmacol* 249: 85-93.
- Macari D, Whitebread S, Cumin F, De Gasparo M, & Levens N (1994). Renal actions of the angiotensin AT2 receptor ligands CGP 42112 and PD 123319 after blockade of the renin-angiotensin system. *Eur J Pharmacol* 259: 27-36.
- Madeddu P, Emanuelli C, Gaspa L, Salis B, Milia AF, Chao L, & Chao J (1999). Role of the bradykinin B2 receptor in the maturation of blood pressure phenotype: lesson from transgenic and knockout mice. *Immunopharmacology* 44: 9-13.
- Magder S (2018). The meaning of blood pressure. *Crit Care* 22: 257.
- Mahmoudpour SH, Asselbergs FW, Terreehorst I, Souverein PC, de Boer A, & Maitland-van der Zee AH (2015). Continuation of angiotensin converting enzyme inhibitor therapy, in spite of occurrence of angioedema. *Int J Cardiol* 201: 644-645.
- Makani H, Messerli FH, Romero J, Wever-Pinzon O, Korniyenko A, Berrios RS, & Bangalore S (2012). Meta-analysis of randomized trials of angioedema as an adverse event of renin-angiotensin system inhibitors. *Am J Cardiol* 110: 383-391.
- Marceau F, Bachelard H, Bouthillier J, Fortin JP, Morissette G, Bawolak MT, Charest-Morin X, & Gera L (2020). Bradykinin receptors: Agonists, antagonists, expression, signaling, and adaptation to sustained stimulation. *Int Immunopharmacol* 82: 106305.
- Matavelli LC, & Siragy HM (2015). AT2 receptor activities and pathophysiological implications. *J Cardiovasc Pharmacol* 65: 226-232.
- Maurer M, Bader M, Bas M, Bossi F, Cicardi M, Cugno M, Howarth P, Kaplan A, Kojda G, Leeb-Lundberg F, Lotvall J, & Magerl M (2011). New topics in bradykinin research. *Allergy* 66: 1397-1406.
- Maurer M, & Magerl M (2021). Differences and Similarities in the Mechanisms and Clinical Expression of Bradykinin-Mediated vs. Mast Cell-Mediated Angioedema. *Clin Rev Allergy Immunol*.

- McFall A, Nicklin SA, & Work LM (2020). The counter regulatory axis of the renin angiotensin system in the brain and ischaemic stroke: Insight from preclinical stroke studies and therapeutic potential. *Cell Signal* 76: 109809.
- McMurray JJ, Packer M, Desai AS, Gong J, Lefkowitz MP, Rizkala AR, Rouleau JL, Shi VC, Solomon SD, Swedberg K, Zile MR, Investigators P-H, & Committees (2014). Angiotensin-neprilysin inhibition versus enalapril in heart failure. *N Engl J Med* 371: 993-1004.
- Memon RJ, & Tiwari V (2020). Angioedema. In *StatPearls*. Treasure Island (FL).
- Menke JG, Borkowski JA, Bierilo KK, MacNeil T, Derrick AW, Schneck KA, Ransom RW, Strader CD, Linemeyer DL, & Hess JF (1994). Expression cloning of a human B1 bradykinin receptor. *J Biol Chem* 269: 21583-21586.
- Miles AA, & Miles EM (1952). Vascular reactions to histamine, histamine-liberator and leukotaxine in the skin of guinea-pigs. *J Physiol* 118: 228-257.
- Miura S, Karnik SS, & Saku K (2005). Constitutively active homo-oligomeric angiotensin II type 2 receptor induces cell signaling independent of receptor conformation and ligand stimulation. *J Biol Chem* 280: 18237-18244.
- Montinaro V, & Cicardi M (2020). ACE inhibitor-mediated angioedema. *Int Immunopharmacol* 78: 106081.
- Moreau ME, Garbacki N, Molinaro G, Brown NJ, Marceau F, & Adam A (2005). The kallikrein-kinin system: current and future pharmacological targets. *J Pharmacol Sci* 99: 6-38.
- Morgado M, Cairrao E, Santos-Silva AJ, & Verde I (2012). Cyclic nucleotide-dependent relaxation pathways in vascular smooth muscle. *Cell Mol Life Sci* 69: 247-266.
- Morwood K, Gillis D, Smith W, & Kette F (2005). Aspirin-sensitive asthma. *Intern Med J* 35: 240-246.
- Mulvany MJ, & Halpern W (1976). Mechanical properties of vascular smooth muscle cells in situ. *Nature* 260: 617-619.
- Murata T, Ushikubi F, Matsuoka T, Hirata M, Yamasaki A, Sugimoto Y, Ichikawa A, Aze Y, Tanaka T, Yoshida N, Ueno A, Oh-ishi S, & Narumiya S (1997). Altered pain perception and inflammatory response in mice lacking prostacyclin receptor. *Nature* 388: 678-682.
- Murphey LJ, Hachey DL, Oates JA, Morrow JD, & Brown NJ (2000). Metabolism of bradykinin in vivo in humans: Identification of BK1-5 as a stable plasma peptide metabolite. *Journal of Pharmacology and Experimental Therapeutics* 294: 263-269.
- Nagy JA, Benjamin L, Zeng H, Dvorak AM, & Dvorak HF (2008). Vascular permeability, vascular hyperpermeability and angiogenesis. *Angiogenesis* 11: 109-119.

- Narumiya S, Sugimoto Y, & Ushikubi F (1999). Prostanoid receptors: structures, properties, and functions. *Physiol Rev* 79: 1193-1226.
- Navar LG (2014). Physiology: hemodynamics, endothelial function, renin-angiotensin-aldosterone system, sympathetic nervous system. *J Am Soc Hypertens* 8: 519-524.
- Ng KK, & Vane JR (1968). Fate of angiotensin I in the circulation. *Nature* 218: 144-150.
- Nussberger J, Cugno M, Amstutz C, Cicardi M, Pellacani A, & Agostoni A (1998). Plasma bradykinin in angio-oedema. *Lancet* 351: 1693-1697.
- Nussberger J, Cugno M, Cicardi M, & Agostoni A (1999). Local bradykinin generation in hereditary angioedema. *J Allergy Clin Immunol* 104: 1321-1322.
- Ocaranza MP, Moya J, Barrientos V, Alzamora R, Hevia D, Morales C, Pinto M, Escudero N, Garcia L, Novoa U, Ayala P, Diaz-Araya G, Godoy I, Chiong M, Lavandero S, Jalil JE, & Michea L (2014). Angiotensin-(1-9) reverses experimental hypertension and cardiovascular damage by inhibition of the angiotensin converting enzyme/Ang II axis. *J Hypertens* 32: 771-783.
- Omori K, Kida T, Hori M, Ozaki H, & Murata T (2014). Multiple roles of the PGE2 -EP receptor signal in vascular permeability. *Br J Pharmacol* 171: 4879-4889.
- Ondetti MA, Rubin B, & Cushman DW (1977). Design of specific inhibitors of angiotensin-converting enzyme: new class of orally active antihypertensive agents. *Science* 196: 441-444.
- Oppong SY, & Hooper NM (1993). Characterization of a secretase activity which releases angiotensin-converting enzyme from the membrane. *Biochem J* 292 ( Pt 2): 597-603.
- Oudit GY, & Penninger JM (2011). Recombinant human angiotensin-converting enzyme 2 as a new renin-angiotensin system peptidase for heart failure therapy. *Curr Heart Fail Rep* 8: 176-183.
- Park-Windhol C, & D'Amore PA (2016). Disorders of Vascular Permeability. *Annu Rev Pathol* 11: 251-281.
- Parkin ET, Turner AJ, & Hooper NM (2004). Secretase-mediated cell surface shedding of the angiotensin-converting enzyme. *Protein Pept Lett* 11: 423-432.
- Patel S, Rauf A, Khan H, & Abu-Izneid T (2017). Renin-angiotensin-aldosterone (RAAS): The ubiquitous system for homeostasis and pathologies. *Biomed Pharmacother* 94: 317-325.
- Patel SN, Fatima N, Ali R, & Hussain T (2020). Emerging Role of Angiotensin AT2 Receptor in Anti-Inflammation: An Update. *Curr Pharm Des* 26: 492-500.
- Paul M, Poyan Mehr A, & Kreutz R (2006). Physiology of local renin-angiotensin systems. *Physiol Rev* 86: 747-803.

Paz Ocaranza M, Riquelme JA, Garcia L, Jalil JE, Chiong M, Santos RAS, & Lavandero S (2020). Counter-regulatory renin-angiotensin system in cardiovascular disease. *Nat Rev Cardiol* 17: 116-129.

Pellacani A, Brunner HR, & Nussberger J (1994). Plasma kinins increase after angiotensin-converting enzyme inhibition in human subjects. *Clin Sci (Lond)* 87: 567-574.

Peluso AA, Bertelsen JB, Andersen K, Mortensen TP, Hansen PB, Summers C, Bader M, Santos RA, & Steckelings UM (2018). Identification of protein phosphatase involvement in the AT2 receptor-induced activation of endothelial nitric oxide synthase. *Clin Sci (Lond)* 132: 777-790.

Persu A, Lambert M, Deinum J, Cossu M, de Visscher N, Ireng L, Ambroise J, Minon JM, Nesterovitch AB, Churbanov A, Popova IA, Danilov SM, Danser AH, & Gala JL (2013). A novel splice-site mutation in angiotensin I-converting enzyme (ACE) gene, c.3691+1G>A (IVS25+1G>A), causes a dramatic increase in circulating ACE through deletion of the transmembrane anchor. *PLoS One* 8: e59537.

Pfeffer MA, McMurray JJ, Velazquez EJ, Rouleau JL, Kober L, Maggioni AP, Solomon SD, Swedberg K, Van de Werf F, White H, Leimberger JD, Henis M, Edwards S, Zelenkofske S, Sellers MA, Califf RM, & Valsartan in Acute Myocardial Infarction Trial I (2003). Valsartan, captopril, or both in myocardial infarction complicated by heart failure, left ventricular dysfunction, or both. *N Engl J Med* 349: 1893-1906.

Pillinger NL, & Kam P (2017). Endothelial glycocalyx: basic science and clinical implications. *Anaesth Intensive Care* 45: 295-307.

Ponikowski P, Voors AA, Anker SD, Bueno H, Cleland JGF, Coats AJS, Falk V, Gonzalez-Juanatey JR, Harjola VP, Jankowska EA, Jessup M, Linde C, Nihoyannopoulos P, Parissis JT, Pieske B, Riley JP, Rosano GMC, Ruilope LM, Ruschitzka F, Rutten FH, van der Meer P, & Group ESCSD (2016). 2016 ESC Guidelines for the diagnosis and treatment of acute and chronic heart failure: The Task Force for the diagnosis and treatment of acute and chronic heart failure of the European Society of Cardiology (ESC) Developed with the special contribution of the Heart Failure Association (HFA) of the ESC. *Eur Heart J* 37: 2129-2200.

Rampart M, & Williams TJ (1986). Suppression of inflammatory oedema by ibuprofen involving a mechanism independent of cyclo-oxygenase inhibition. *Biochem Pharmacol* 35: 581-586.

Renart J, Reiser J, & Stark GR (1979). Transfer of proteins from gels to diazobenzoyloxymethyl-paper and detection with antisera: a method for studying antibody specificity and antigen structure. *Proc Natl Acad Sci U S A* 76: 3116-3120.

Reshef A, Kidon M, & Leibovich I (2016). The Story of Angioedema: from Quincke to Bradykinin. *Clin Rev Allergy Immunol* 51: 121-139.

Riordan JF (2003). Angiotensin-I-converting enzyme and its relatives. *Genome Biol* 4: 225.

Rocha ESM, Beraldo WT, & Rosenfeld G (1949). Bradykinin, a hypotensive and smooth muscle stimulating factor released from plasma globulin by snake venoms and by trypsin. *Am J Physiol* 156: 261-273.

- Saameli K, & Eskes TK (1962). Bradykinin and cardiovascular system: estimation of half-life. *Am J Physiol* 203: 261-265.
- Sachs B, Meier T, Nothen MM, Stieber C, & Stingl J (2018). [Drug-induced angioedema : Focus on bradykinin]. *Hautarzt* 69: 298-305.
- Salama RAM, El Gayar NH, Georgy SS, & Hamza M (2016). Equivalent intraperitoneal doses of ibuprofen supplemented in drinking water or in diet: a behavioral and biochemical assay using antinociceptive and thromboxane inhibitory dose-response curves in mice. *PeerJ* 4: e2239.
- Sandmann S, Yu M, Kaschina E, Blume A, Bouzinova E, Aalkjaer C, & Unger T (2001). Differential effects of angiotensin AT1 and AT2 receptors on the expression, translation and function of the Na<sup>+</sup>-H<sup>+</sup> exchanger and Na<sup>+</sup>-HCO<sub>3</sub><sup>-</sup> symporter in the rat heart after myocardial infarction. *J Am Coll Cardiol* 37: 2154-2165.
- Sarma JV, & Ward PA (2011). The complement system. *Cell Tissue Res* 343: 227-235.
- Sauer SK, Schafer D, Kress M, & Reeh PW (1998). Stimulated prostaglandin E2 release from rat skin, in vitro. *Life Sci* 62: 2045-2055.
- Schmaier AH (2016). The contact activation and kallikrein/kinin systems: pathophysiologic and physiologic activities. *J Thromb Haemost* 14: 28-39.
- Schmieder RE, Hilgers KF, Schlaich MP, & Schmidt BMW (2007). Renin-angiotensin system and cardiovascular risk. *The Lancet* 369: 1208-1219.
- Schmitz R, Jordan S, Muters S, & Neuhauser H (2012). Population-wide use of behavioural prevention and counselling programmes for lifestyle-related cardiovascular risk factors in Germany. *Eur J Prev Cardiol* 19: 849-856.
- Seshiah PN, Weber DS, Rocic P, Valppu L, Taniyama Y, & Griendling KK (2002). Angiotensin II stimulation of NAD(P)H oxidase activity: upstream mediators. *Circ Res* 91: 406-413.
- Shariat-Madar Z, Mahdi F, & Schmaier AH (2002). Identification and characterization of prolylcarboxypeptidase as an endothelial cell prekallikrein activator. *J Biol Chem* 277: 17962-17969.
- Sharpe M, Jarvis B, & Goa KL (2001). Telmisartan: a review of its use in hypertension. *Drugs* 61: 1501-1529.
- Sheikh IA, & Kaplan AP (1989). The mechanism of degradation of bradykinin (lysyl-bradykinin) in human serum. *Adv Exp Med Biol* 247A: 331-336.
- Shimuta SI, Barbosa AM, Borges AC, & Paiva TB (1999). Pharmacological characterization of RMP-7, a novel bradykinin agonist in smooth muscle. *Immunopharmacology* 45: 63-67.
- Shukla AK, Xiao K, & Lefkowitz RJ (2011). Emerging paradigms of beta-arrestin-dependent seven transmembrane receptor signaling. *Trends Biochem Sci* 36: 457-469.

Sica DA, & Black HR (2002). Angioedema in heart failure: occurrence with ACE inhibitors and safety of angiotensin receptor blocker therapy. *Congest Heart Fail* 8: 334-341, 345.

Sinert R, Levy P, Bernstein JA, Body R, Sivilotti MLA, Moellman J, Schranz J, Baptista J, Kimura A, Nothaft W, & group Cs (2017). Randomized Trial of Icatibant for Angiotensin-Converting Enzyme Inhibitor-Induced Upper Airway Angioedema. *J Allergy Clin Immunol Pract* 5: 1402-1409 e1403.

Skeggs LT, Dorer FE, Kahn JR, Lentz KE, & Levine M (1976). The biochemistry of the renin-angiotensin system and its role in hypertension. *Am J Med* 60: 737-748.

Sparks MA, Crowley SD, Gurley SB, Mirotso M, & Coffman TM (2014). Classical Renin-Angiotensin system in kidney physiology. *Compr Physiol* 4: 1201-1228.

Stauss HM (2007). Identification of blood pressure control mechanisms by power spectral analysis. *Clin Exp Pharmacol Physiol* 34: 362-368.

Steckelings UM, Wollschlager T, Peters J, Henz BM, Hermes B, & Artuc M (2004). Human skin: source of and target organ for angiotensin II. *Exp Dermatol* 13: 148-154.

Stoll M, Steckelings UM, Paul M, Bottari SP, Metzger R, & Unger T (1995). The angiotensin AT2-receptor mediates inhibition of cell proliferation in coronary endothelial cells. *J Clin Invest* 95: 651-657.

Straka BT, Ramirez CE, Byrd JB, Stone E, Woodard-Grice A, Nian H, Yu C, Banerji A, & Brown NJ (2017). Effect of bradykinin receptor antagonism on ACE inhibitor-associated angioedema. *J Allergy Clin Immunol* 140: 242-248 e242.

Strassen U, Bas M, Hoffmann TK, Knopf A, & Greve J (2015). Treatment of angiotensin receptor blocker-induced angioedema: A case series. *Laryngoscope* 125: 1619-1623.

Sturrock ED, Danilov SM, & Riordan JF (1997). Limited proteolysis of human kidney angiotensin-converting enzyme and generation of catalytically active N- and C-terminal domains. *Biochem Biophys Res Commun* 236: 16-19.

Suffritti C, Zanichelli A, Maggioni L, Bonanni E, Cugno M, & Cicardi M (2014). High-molecular-weight kininogen cleavage correlates with disease states in the bradykinin-mediated angioedema due to hereditary C1-inhibitor deficiency. *Clin Exp Allergy* 44: 1503-1514.

Swanson TJ, & Patel BC (2020). Acquired Angioedema. In *StatPearls*. Treasure Island (FL).

Takeuchi K, Watanabe H, Tran QK, Ozeki M, Sumi D, Hayashi T, Iguchi A, Ignarro LJ, Ohashi K, & Hayashi H (2004). Nitric oxide: inhibitory effects on endothelial cell calcium signaling, prostaglandin I<sub>2</sub> production and nitric oxide synthase expression. *Cardiovasc Res* 62: 194-201.

Tigerstedt R, & Bergman PQ (1898). Niere und Kreislauf. *Skandinavisches Archiv Für Physiologie* 8: 223-271.

Tipnis SR, Hooper NM, Hyde R, Karran E, Christie G, & Turner AJ (2000). A human homolog of angiotensin-converting enzyme. Cloning and functional expression as a captopril-insensitive carboxypeptidase. *J Biol Chem* 275: 33238-33243.

Towbin H, Staehelin T, & Gordon J (1979). Electrophoretic transfer of proteins from polyacrylamide gels to nitrocellulose sheets: procedure and some applications. *Proc Natl Acad Sci U S A* 76: 4350-4354.

Tsutsumi Y, Matsubara H, Masaki H, Kurihara H, Murasawa S, Takai S, Miyazaki M, Nozawa Y, Ozono R, Nakagawa K, Miwa T, Kawada N, Mori Y, Shibasaki Y, Tanaka Y, Fujiyama S, Koyama Y, Fujiyama A, Takahashi H, & Iwasaka T (1999). Angiotensin II type 2 receptor overexpression activates the vascular kinin system and causes vasodilation. *J Clin Invest* 104: 925-935.

Turner AJ, & Hooper NM (2002). The angiotensin-converting enzyme gene family: genomics and pharmacology. *Trends Pharmacol Sci* 23: 177-183.

Unger T, Borghi C, Charchar F, Khan NA, Poulter NR, Prabhakaran D, Ramirez A, Schlaich M, Stergiou GS, Tomaszewski M, Wainford RD, Williams B, & Schutte AE (2020). 2020 International Society of Hypertension Global Hypertension Practice Guidelines. *Hypertension* 75: 1334-1357.

UniProt C (2019). UniProt: a worldwide hub of protein knowledge. *Nucleic Acids Res* 47: D506-D515.

Vandenbroucke E, Mehta D, Minshall R, & Malik AB (2008). Regulation of endothelial junctional permeability. *Ann N Y Acad Sci* 1123: 134-145.

Vasile S, Hallberg A, Sallander J, Hallberg M, Aqvist J, & Gutierrez-de-Teran H (2020). Evolution of Angiotensin Peptides and Peptidomimetics as Angiotensin II Receptor Type 2 (AT2) Receptor Agonists. *Biomolecules* 10.

Venema RC, Ju H, Venema VJ, Schieffer B, Harp JB, Ling BN, Eaton DC, & Marrero MB (1998). Angiotensin II-induced association of phospholipase C $\gamma$ 1 with the G-protein-coupled AT1 receptor. *J Biol Chem* 273: 7703-7708.

Verdonk K, Durik M, Abd-Alla N, Batenburg WW, van den Bogaerdt AJ, van Veghel R, Roks AJ, Danser AH, & van Esch JH (2012). Compound 21 induces vasorelaxation via an endothelium- and angiotensin II type 2 receptor-independent mechanism. *Hypertension* 60: 722-729.

Wagner J, Drab M, Bohlender J, Amann K, Wiene W, & Ganten D (1998). Effects of AT1 receptor blockade on blood pressure and the renin-angiotensin system in spontaneously hypertensive rats of the stroke prone strain. *Clin Exp Hypertens* 20: 205-221.

Walloe L (2016). Arterio-venous anastomoses in the human skin and their role in temperature control. *Temperature (Austin)* 3: 92-103.

Wan Y, Wallinder C, Plouffe B, Beaudry H, Mahalingam AK, Wu X, Johansson B, Holm M, Botoros M, Karlen A, Pettersson A, Nyberg F, Fandriks L, Gallo-Payet N, Hallberg A, & Alterman M (2004).

Design, synthesis, and biological evaluation of the first selective nonpeptide AT<sub>2</sub> receptor agonist. *J Med Chem* 47: 5995-6008.

Weber F, & Anlauf M (2020). Hemmstoffe des Renin-Angiotensin-Systems. In *Arzneiverordnungs-Report 2020*. eds Schwabe U., & Ludwig W.-D. Springer Berlin Heidelberg: Berlin, Heidelberg, pp 231-259.

Wettschureck N, Strilic B, & Offermanns S (2019). Passing the Vascular Barrier: Endothelial Signaling Processes Controlling Extravasation. *Physiol Rev* 99: 1467-1525.

White WB, Bresalier R, Kaplan AP, Palmer BF, Riddell RH, Lesogor A, Chang W, & Keefe DL (2010). Safety and tolerability of the direct renin inhibitor aliskiren: a pooled analysis of clinical experience in more than 12,000 patients with hypertension. *J Clin Hypertens (Greenwich)* 12: 765-775.

Wide L, Axen R, & Porath J (1967). Radioimmunosorbent Assay for Proteins . Chemical Couplings of Antibodies to Insoluble Dextran. *Immunochemistry* 4: 381-&.

Wiese OJ, Allwood BW, & Zemlin AE (2020). COVID-19 and the renin-angiotensin system (RAS): A spark that sets the forest alight? *Med Hypotheses* 144: 110231.

Williams TJ, & Morley J (1973). Prostaglandins as potentiators of increased vascular permeability in inflammation. *Nature* 246: 215-217.

Williams TJ, & Peck MJ (1977). Role of prostaglandin-mediated vasodilatation in inflammation. *Nature* 270: 530-532.

Woodard-Grice AV, Lucisano AC, Byrd JB, Stone ER, Simmons WH, & Brown NJ (2010). Sex-dependent and race-dependent association of XPNPEP2 C-2399A polymorphism with angiotensin-converting enzyme inhibitor-associated angioedema. *Pharmacogenet Genomics* 20: 532-536.

Wu MA, Perego F, Zanichelli A, & Cicardi M (2016). Angioedema Phenotypes: Disease Expression and Classification. *Clin Rev Allergy Immunol* 51: 162-169.

Yamada H, Akishita M, Ito M, Tamura K, Daviet L, Lehtonen JY, Dzau VJ, & Horiuchi M (1999). AT<sub>2</sub> receptor and vascular smooth muscle cell differentiation in vascular development. *Hypertension* 33: 1414-1419.

Yamasaki E, Thakore P, Krishnan V, & Earley S (2020). Differential expression of angiotensin II type 1 receptor subtypes within the cerebral microvasculature. *Am J Physiol Heart Circ Physiol* 318: H461-H469.

Yang HY, Erdos EG, & Levin Y (1970). A dipeptidyl carboxypeptidase that converts angiotensin I and inactivates bradykinin. *Biochim Biophys Acta* 214: 374-376.

Yang J, Feng X, Zhou Q, Cheng W, Shang C, Han P, Lin CH, Chen HS, Quertermous T, & Chang CP (2016). Pathological Ace2-to-Ace enzyme switch in the stressed heart is transcriptionally controlled by the endothelial Brg1-FoxM1 complex. *Proc Natl Acad Sci U S A* 113: E5628-5635.

Yao L, Xue X, Yu P, Ni Y, & Chen F (2018). Evans Blue Dye: A Revisit of Its Applications in Biomedicine. *Contrast Media Mol Imaging* 2018: 7628037.

Yoon HE, Kim EN, Kim MY, Lim JH, Jang IA, Ban TH, Shin SJ, Park CW, Chang YS, & Choi BS (2016). Age-Associated Changes in the Vascular Renin-Angiotensin System in Mice. *Oxid Med Cell Longev* 2016: 6731093.

Yousif MH, Makki B, El-Hashim AZ, Akhtar S, & Benter IF (2014). Chronic treatment with Ang-(1-7) reverses abnormal reactivity in the corpus cavernosum and normalizes diabetes-induced changes in the protein levels of ACE, ACE2, ROCK1, ROCK2 and omega-hydroxylase in a rat model of type 1 diabetes. *J Diabetes Res* 2014: 142154.

Yusuf S, Sleight P, Pogue J, Bosch J, Davies R, & Dagenais G (2000). Effects of an angiotensin-converting-enzyme inhibitor, ramipril, on cardiovascular events in high-risk patients. *N Engl J Med* 342: 145-153.

Yusuf S, Teo K, Anderson C, Pogue J, Dyal L, Copland I, Schumacher H, Dagenais G, & Sleight P (2008a). Effects of the angiotensin-receptor blocker telmisartan on cardiovascular events in high-risk patients intolerant to angiotensin-converting enzyme inhibitors: a randomised controlled trial. *Lancet* 372: 1174-1183.

Yusuf S, Teo KK, Pogue J, Dyal L, Copland I, Schumacher H, Dagenais G, Sleight P, & Anderson C (2008b). Telmisartan, ramipril, or both in patients at high risk for vascular events. *N Engl J Med* 358: 1547-1559.

Zanichelli A, Longhurst HJ, Maurer M, Bouillet L, Aberer W, Fabien V, Andresen I, Caballero T, & Group IOSS (2016). Misdiagnosis trends in patients with hereditary angioedema from the real-world clinical setting. *Ann Allergy Asthma Immunol* 117: 394-398.

Zeerleder S, & Levi M (2016). Hereditary and acquired C1-inhibitor-dependent angioedema: from pathophysiology to treatment. *Ann Med* 48: 256-267.

Zhang H, Han GW, Batyuk A, Ishchenko A, White KL, Patel N, Sadybekov A, Zamlynyy B, Rudd MT, Hollenstein K, Tolstikova A, White TA, Hunter MS, Weierstall U, Liu W, Babaoglu K, Moore EL, Katz RD, Shipman JM, Garcia-Calvo M, Sharma S, Sheth P, Soisson SM, Stevens RC, Katritch V, & Cherezov V (2017). Structural basis for selectivity and diversity in angiotensin II receptors. *Nature* 544: 327-332.

Zhou L, Li Y, Hao S, Zhou D, Tan RJ, Nie J, Hou FF, Kahn M, & Liu Y (2015). Multiple genes of the renin-angiotensin system are novel targets of Wnt/beta-catenin signaling. *J Am Soc Nephrol* 26: 107-120.

## **Publications**

### **PEER-REVIEWED PUBLICATIONS**

**Gholamreza-Fahimi E.**, Bisha M., Hahn J., Straßen U., Krybus M., Khosravani F., Hoffmann T.K., Hohlfeld T., Greve J., Bas M., Twarock S., Kojda G. (2020). Cyclooxygenase activity in bradykinin-induced dermal extravasation. A study in mice and humans. *Biomed Pharmacother.* 123:109797. doi: 10.1016/j.biopha.2019.109797.

Contribution:

Miles assay experiments, assisting in the planning of the clinical trial, preparing and distributing the injection solutions to the other study sites, recruiting volunteers, carrying out and documenting the clinical experiments in collaboration with the study physician in Düsseldorf, collecting and compiling all data, writing the results section.

Bisha M., Dao V.T., **Gholamreza-Fahimi E.**, Vogt M., van Zandvoort M., Weber S., Bas M., Khosravani F., Kojda G., Suvorava T. (2018). The role of bradykinin receptor type 2 in spontaneous extravasation in mice skin: implications for non-allergic angio-oedema. *Br J Pharmacol.* 175(10):1607-1620. doi: 10.1111/bph.14166.

Contribution:

Miles assay and two-photon laser experiments.

Lange-Asschenfeldt C., Schäble S., Suvorava T., **Gholamreza-Fahimi E.**, Bisha M., Stermann T., Henning U., Kojda G. (2016). Effects of varenicline on alpha4-containing nicotinic acetylcholine receptor expression and cognitive performance in mice. *Neuropharmacology.* 107:100-110. doi: 10.1016/j.neuropharm.2016.03.025.

Contribution:

Western blot analysis, antibody validation.

### **PEER-REVIEWED PUBLICATIONS SUBMITTED**

Fehsel K., Schwanke K., Kappel B.A., **Gohlamreza-Fahimi E.**, Meisenzahl-Lechner E., Esser C., Hemmrich K., Haarmann-Stemmann T., Kojda G., Lange-Asschenfeldt C. (2021). Activation of the aryl hydrocarbon receptor by clozapine induces preadipocyte differentiation and endothelial dysfunction. *J. Psychopharmacol – status: revised manuscript submitted.*

Contribution:

Organ bath studies.

**CONFERENCE PRESENTATIONS**

**Gholamreza-Fahimi E.**, Krybus M., Bisha M., Kurz T., Hansen F.K. and Kojda G. AT2 activation reduces ACE activity. Poster presentation delivered at the 86th Annual Meeting of the German Society for Experimental and Clinical Pharmacology and Toxicology – DGPT, 2.-5. March 2020, Leipzig, Germany. Published: Naunyn-Schmiedeberg's Arch Pharmacol (2020) 393 (Suppl 1): Page 64 Poster 150.

Krybus M., **Gholamreza-Fahimi E.**, Khosravani F., Bisha M., Kojda G. Relative importance of NO and prostaglandins as mediators of bradykinin-induced skin edema in mice. Poster presentation delivered at the 86th Annual Meeting of the German Society for Experimental and Clinical Pharmacology and Toxicology – DGPT, 2.-5. March 2020, Leipzig, Germany. Published: Naunyn-Schmiedeberg's Arch Pharmacol (2020) 393 (Suppl 1): Page 65 Poster 151.

**Gholamreza-Fahimi E.**, Bisha M., Hahn J., Straßen U., Krybus M., Khosravani F., Hoffmann T., Hohlfeld T., Greve J., Bas M., Twarock S. and Kojda G. A bradykinin in skin edema trial (ABRASE) – implications for non-allergic angioedema. Poster presentation delivered at the Annual Meeting of the German Pharmaceutical Society – DPhG, 1.-4. September 2019, Heidelberg, Germany.

**Gholamreza-Fahimi E.**, Bisha M., Krybus M., Kurz T., Hansen F.K. and Kojda G. Activation of AT2 potentiates bradykinin-induced extravasation – role of ACE. Poster presentation delivered at the Annual Meeting of the German Pharmaceutical Society – DPhG, 1.-4. September 2019, Heidelberg, Germany.

Krybus M., **Gholamreza-Fahimi E.**, Khosravani F., Bisha M. and Kojda G. Role of prostaglandins in bradykinin-induced skin edema in mice. Poster presentation delivered at the Annual Meeting of the German Pharmaceutical Society – DPhG, 1.-4. September 2019, Heidelberg, Germany.

**Gholamreza-Fahimi E.**, Bisha M. and Kojda G. Involvement of Prostaglandins in Bradykinin induced skin edema in mice. Poster presentation at: Bradykinin symposium, 5.-6. September 2018, Berlin, Germany.

**Gholamreza-Fahimi E.**, Bisha M., Twarock S., Hohlfeld T. and Kojda G. A Bradykinin in Skin Edema Trial (ABRASE) – first results. Oral Presentation at the Bradykinin symposium, 5.-6. September 2018, Berlin, Germany.

**Gholamreza-Fahimi E.**, Bisha M., Kurz T., Hansen F.K. and Kojda G. Angiotensin-converting enzyme activity is attenuated by selective stimulation of angiotensin II type two receptor. Poster presentation delivered at the Annual Meeting of the German Pharmaceutical Society – DPhG, 26.-29. September 2017 – DPhG, Saarbrücken, Germany.

Bisha M., **Gholamreza-Fahimi E.**, Dao V.T. and Kojda G. Bradykinin receptor type two mediated dermal extravasation in mice is potentiated by moexipril. Poster presentation delivered at the European Society of Cardiology Congress – ESC, 26.-30. August 2017, Barcelona, Spain. Published: European Heart Journal, Volume 38, Issue suppl\_1, August 2017, ehx504.P4487.

Bisha M., **Gholamreza-Fahimi E.**, Dao V.T. and Kojda G. Bradykinin induced skin edema in mice is dependent on cyclooxygenase activity. Poster presentation delivered at the European Society of Cardiology Congress – ESC, 26.-30. August 2017, Barcelona, Spain. Published: European Heart Journal, Volume 38, Issue suppl\_1, August 2017, ehx504.P4488.

**Gholamreza-Fahimi E.**, Bisha M., Hansen F.K., Kurz T. and Kojda G. Inhibition of angiotensin-converting enzyme by selective stimulation of angiotensin II type 2 receptor. Poster presentation delivered at the 83rd German Pharm-Tox Summit, 6.-9. March 2017. Published: Naunyn-Schmiedeberg's Arch Pharmacol (2017) 390 (Suppl 1): Page 38 Poster 64.

Bisha M., **Gholamreza-Fahimi E.**, Khosravani F. and Kojda G. Role of prostaglandins for bradykinin induced skin edema in mice. Poster presentation delivered at the 83rd Annual Meeting of the German Society for Experimental and Clinical Pharmacology and Toxicology – DGPT, 6.-9. March 2017, Heidelberg, Germany. Published: Naunyn-Schmiedeberg's Arch Pharmacol (2017) 390 (Suppl 1): Page 38 Poster 65.

Bisha M., **Gholamreza-Fahimi E.**, Dao V.T. and Kojda G. Role of moexipril for bradykinin receptor type two mediated dermal extravasation in mice. Poster presentation delivered at the 83rd Annual Meeting of the German Society for Experimental and Clinical Pharmacology and Toxicology – DGPT, 6.-9. March 2017, Heidelberg, Germany. Published: Naunyn-Schmiedeberg's Arch Pharmacol (2017) 390 (Suppl 1): Page 38 Poster 66.

**Gholamreza-Fahimi E.**, Khosravani F., Bisha M., Dao V.T., Suvorava T., van Zandvoort M., Kojda G. Evaluation of non-invasive Two-photon laser microscopy to study endothelial permeability in-vivo. Poster presentation delivered at the 82nd German Pharm-Tox Summit, 29. February-3. March 2016, Berlin, Germany. Published: Naunyn-Schmiedeberg's Arch Pharmacol (2016) 389 (Suppl 1): Page 75 Poster 321.

## **Funding and Acknowledgement**

This work was financially supported by the Strategic Research Fund of Heinrich Heine University [grant number 701301635], the Research Committee of the Faculty of Medicine [grant number 9772681], and funds from the Institute of Pharmacology and Clinical Pharmacology under the direction of Prof. Dr. Jens W. Fischer.

First and foremost, I would like to thank my supervisor, Prof. Dr. George Kojda, who entrusted me with this exciting project and gave me the opportunity for professional as well as personal growth. He always supported me with great commitment and good advice, which was very important for my success. Moreover, I would like to thank Prof. Dr. Holger Stark for his co-supervision, Prof. Dr. Thomas Kurz and Prof. Dr. Finn Kristian Hansen who made the whole project possible by synthesizing compound 21, the main pharmacological tool of the study.

In particular, the clinical trial ABRASE could not have been conducted without the collaboration of the research groups of Prof. Dr. Thomas Hohlfeld, Prof. Dr. med. Thomas Hoffmann, Prof. Dr. Jens Greve, and Prof. Dr. Murat Bas.

The collaboration with Prof. Dr. Lange-Asschenfeldt and Dr. Karin Fehsel was a great opportunity to get to know another interesting field of research, for which I am grateful.

Through collaboration with Prof. Dr. Marc van Zandvoort and Dr. Michael Vogt at the University Hospital Aachen, access to the TPEM enabled visualization of physiological extravasation of mouse skin vessels for the first time.

Special thanks to Dr Tatsiana Suvorova and Dr Farbod Khosravani who introduced me to the methodology of organ bath, blood pressure and Miles assay experiments.

Last but not least, my heartfelt thanks go to my colleagues Marion Bisha, Oktay Kocgirli, and Michael Krybus, as well as all other colleagues at the Institute not listed here, for their support and the wonderful time we spent together.

## **Declaration of Authorship**

I hereby declare that the dissertation is my own work, created without assistance from third parties and in accordance with the "Principles of Good Scientific Practice at the Heinrich Heine University Düsseldorf".

I further confirm that this dissertation has not been submitted in the same or similar form in any other examination procedure.

## **Eidesstattliche Erklärung**

Ich versichere an Eides Statt, dass die Dissertation von mir selbständig und ohne unzulässige fremde Hilfe unter Beachtung der „Grundsätze zur Sicherung guter wissenschaftlicher Praxis an der Heinrich-Heine-Universität Düsseldorf“ erstellt worden ist.

Ich bestätige ferner, dass diese Dissertation in gleicher oder ähnlicher Form noch in keinem anderen Prüfungsverfahren eingereicht wurde.

Ehsan Fahimi



Düsseldorf, den 04.08.2021